Bridges with Spatial Cable Systems

Vejrum, Tina

Publication date:
1997

Document Version
Publisher's PDF, also known as Version of record

INSTITUT FOR BÆRENDE KONSTRUKTIONER OG MATERIALER

DTU

Bridges with Spatial Cable Systems

theoretical and experimental studies with special emphasis on lateral buckling stability of the girder

TINA VEJRUM

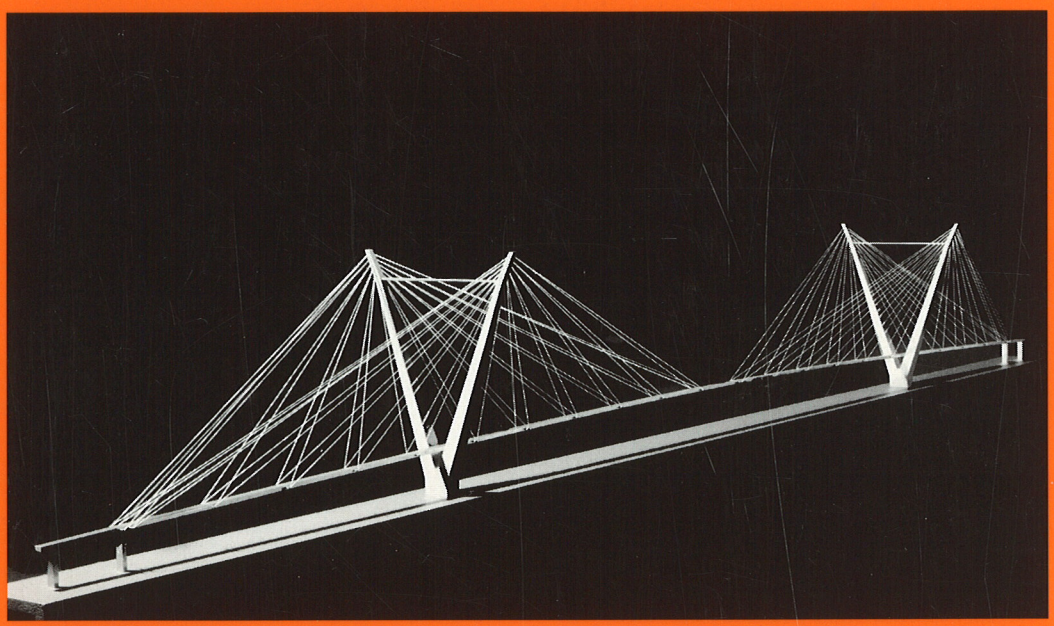

DEPARTMENT OF STRUCTURAL ENGINEERING AND MATERIALS
TECHNICAL UNIVERSITY OF DENMARK Series R No 19 1997

INSTITUT FOR BÆRENDE KONSTRUKTIONER OG MATERIALER

DTU

Bridges with Spatial Cable Systems

theoretical and experimental studies with special emphasis on lateral buckling stability of the girder

TINA VEJRUM

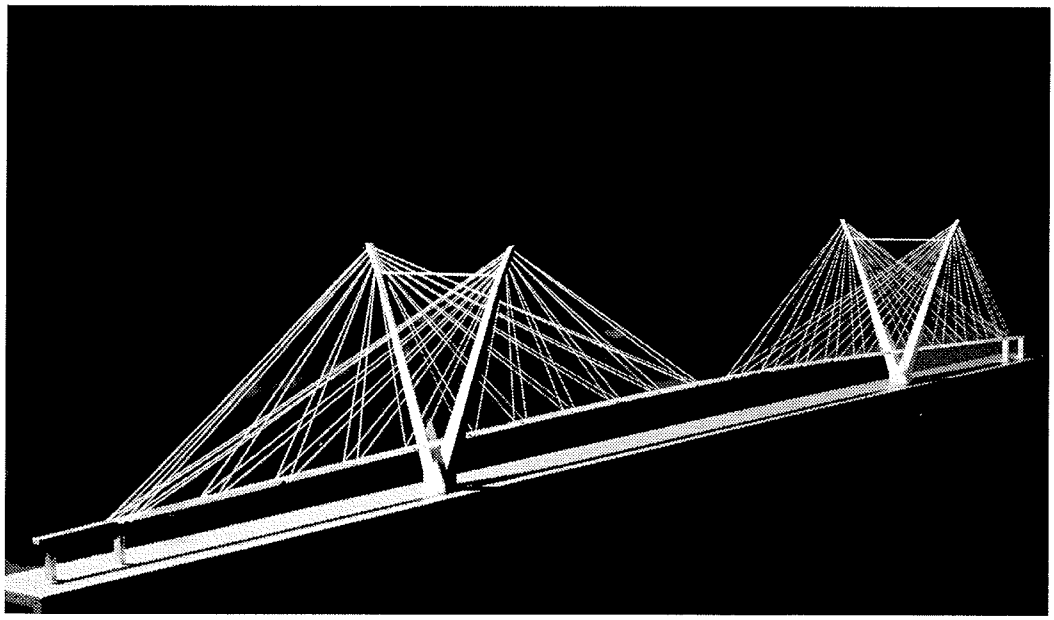

DEPARTMENT OF STRUCTURAL ENGINEERING AND MATERIALS
TECHNICAL UNIVERSITY OF DENMARK Series R No 19 1997

Bridges with Spatial Cable Systems

Printed by Tekst & Tryk A/S, Vedbæk, Denmark
ISBN 87-7740-201-4
ISSN 1396-2167

PREFACE

This thesis is submitted in partial fulfilment of the requirements for obtaining the degree of Ph. D. The research was carried out at the Department of Structural Engineering and Materials, Technical University of Denmark under the supervision of Professor Niels J. Gimsing (main supervisor) and Associate Professor, Ph. D. Henrik Stang.

I wish to express my gratitude to Professor Gimsing and to Henrik Stang for their guidance, interest and support throughout the study.

The Danish Research Councils (STVF) are recognized for their financial support of the project through Grant No. 16-4997-1 PG.

The present study succeeds the work of Søren V. Larsen, whom is gratefully acknowledged for his inspiration.

I also wish to thank Professor René Walther and his staff for their help during my stay at the Prestressed and Concrete Institute - IBAP, Swiss Federal Institute of Technology - Lausanne. Their suggestions for the model test are gratefully acknowledged.

The staff of the Department of Structural Engineering and Materials are thanked for their help and assistance, especially during the periods of model construction and tests. Many thanks are owed to Finn Sundeved for his help with design of the bridge model, and to Christian Bramsen for careful work and patience in relation to the photographic documentation of the model test. Furthermore Esther Martens is thanked for making one of the drawings.

Furthermore I wish to thank the Department of Planning, Technical University of Denmark for supplying the equipment for surveying operations during the model test. Special thanks are owed to Associate Professor Ole Mærsk-Møller for his persistent assistance in relation to the statistical treatment of test results.

Some of the tests were carried out by three students at the Technical University of Denmark: Allan Andreasen, Ulrik Winther Blindum and Lennart Østergaard. Their careful work is highly appreciated.

Special thanks are owed to MSc (Civ. Eng.) Johannes Sand Poulsen for his proof-reading of the present report, assistance with digital processing of the photos and for many inspiring discussions during the project.

Finally I wish to express my deepest gratitude to my parents for their invaluable support and understanding throughout the whole project.

Department of Structural Engineering and Materials,
Technical University of Denmark,
Lyngby, November 30th, 1996

Tina Vejrum

ABSTRACT

This thesis deals with the static behaviour and buckling stability of a long and narrow cable-stayed bridge.

The present trend within design of cable supported bridges moves towards increasing span-to-width ratios. As the girder becomes more narrow, transfer of lateral loads - such as wind load - in bending looses in efficiency. A possible solution to problems associated with lateral wind load on cable supported bridges with large span-to-width ratios could be to apply a so-called spatial cable system, that provides both vertical and lateral support for the girder.

The work presented in this thesis comprises studies on a prototype cable-stayed bridge with an 800 m main span and a girder width of 8 m giving a span-to-width ratio of 100:1. This is close to a factor of 2.5 compared to the span-to-width ratios found in cable-stayed bridges built until present. The investigations are divided into three parts: Analytical analyses and related parametric studies, FE-calculations and finally a model test.

In order to determine the range of inclination of cable planes that will be realistic to consider for spatial cable systems, parametric studies on the prototype bridge are carried out. These show that optimum height of a pylon supporting a spatial cable system does not differ from what is found for a pylon supporting a traditional cable system with vertical cable planes. An evaluation of material cost and of lateral deflections due to wind load indicates, that lateral inclination of cable planes should be between 1:4 and 1:2.

Four different layouts of the spatial cable system are presented and compared by means of numerical analyses. Focus is on the behaviour for wind load, especially with respect to deflections. Furthermore, the buckling stability of the girder is studied. FE-analyses show that the bridge type having an extremely narrow girder supported by a spatial cable system is not likely to exhibit any stability problems in its completed stage. However, as a distinctive feature related to a bridge having a narrow girder, the critical loads for lateral and vertical buckling are practically identical. This is in contrast to cable-stayed bridges built until present, where the critical load for lateral buckling is significantly higher than for vertical buckling.

A comparative experimental study on both lateral and vertical girder instability phenomena is carried out on a model of the bridge in the erection stage. The parameter to be varied is the lateral inclination of cable planes. Unfortunately some of the test results are disturbed by an adverse response of some of the structural elements used in the model. In spite of this it seems that the spatial cable system would have provided the requisite elastic support to the girder to prevent lateral buckling of being more critical than vertical buckling, when lateral inclination of cable planes is around 1:4. Thus the requisite inclination of cable planes to reduce lateral deflections due to wind to an acceptable level also stabilizes the narrow girder with respect to lateral buckling otherwise having a lower critical load than for vertical buckling.

Based on the investigations carried out in the present work it can be concluded, that arranging a spatial cable system is a promising way of solving problems related to applying a narrow girder.

SAMMENFATNING

Den foreliggende afhandling beskæftiger sig med den statiske opførsel herunder søjlestabiliteten af en skråstagsbro med en lang og smal brodrager.

Inden for design af skråstagsbroer sker der en udvikling i retning af at opføre broerne med større og større forhold mellem spændvidde og dragerbredde. Når brodrageren er meget smal bliver det imidlertid problematisk at overføre tværkræfter - som eksempelvis vind - vha. bøjning af drageren. En mulig løsning på disse problemer kunne være at anvende et såkaldt rumligt kabelsystem, der understøtter drageren både lodret og vandret.

Det foreliggende arbejde omfatter studier af en prototype skråstagsbro med et hovedfag på 800 m og en dragerbredde på 8 m, hvilket giver et forhold mellem spændvidde og dragerbredde på 100:1. Dette er næsten en faktor 2.5 større end de spændvidde-dragerbredde forhold som optræder i eksisterende skråstagsbroer. Undersøgelserne er delt i tre dele: Analytiske undersøgelser og tilknyttede parameterstudier, FE-beregninger og sluttelig et modelforsøg.

Parameterstudier af prototype broen bliver benyttet til at bestemme en realistisk tværhældning af kabelplanerne i det rumlige kabelsystem. Disse viser, at pylonhøjden bør vælges svarende til hvad der er almindelig praksis for pyloner, der understøtter traditionelle plane kabelsystemer. En vurdering af materialeomkostninger samt af udbøjninger for vindlast indikerer, at tværhældningen af kabelplanerne bør vælges i intervallet 1:4 og 1:2.

Fire forskellige forslag til udformningen af det rumlige kabelsystem præsenteres og sammenlignes vha. numeriske analyser. Der fokuseres på opførslen for vindlast, specielt mht. udbøjninger. Endvidere undersøges dragerens søjlestabilitet. FE-beregninger viser, at en bro med en ekstremt smal drager understøttet af et rumligt kabelsystem næppe vil udvise stabilitetsproblemer i den færdigmonterede situation. Dog er den kritiske last for hhv. lodret og vandret instabilitet praktisk taget ens, hvilket er et karakteristisk træk ved en bro udstyret med en smal drager. Dette er i modsætning til eksisterende skråstagsbroer, hvor den kritiske last for vandret instabilitet ligger væsentligt højere end for lodret instabilitet.

Der er blevet gennemført en sammenlignende eksperimentel undersøgelse af både vandret og lodret dragerinstabilitet. Forsøgene er udført på en model af broen i montagefasen, hvor tværhældningen af kabelplanerne varieres. Uheldigvis blev nogle af forsøgsresultaterne påvirket af en ugunstig opførsel af nogle af de konstruktionselementer, som modellen er opbygget af. På trods af dette lader det til, at det rumlige kabelsystem ville have givet drageren den nødvendige elastiske understøtning krævet for at forhindre vandret instabilitet i at være mere kritisk end lodret instabilitet, når tværhældningen af kabelplanerne er ca. 1:4. Det betyder, at den tværhældning af kabelplanerne, som kræves for at reducere udbøjningere pga. vind til et acceptabelt niveau, ligeledes vil stabilisere drageren mht. vandret søjleinstabilitet, som ellers ville have en lavere kritisk last end lodret søjleinstabilitet.

På baggrund af de undersøgelser som er blevet gennemført, kan det konkluderes, at rumlige kabelsystemer udgør en lovende løsning på de problemer, der er knyttet til at anvende en smal brodrager.

TABLE OF CONTENTS

Chapter 1

1. INTRODUCTION

1.1 Historical development in the 20th century

During the last century, modern cable supported bridges have taken over the role from arch-bridges and cantilever trusses as the record-holders for free spans.

For instance, the Firth of Forth Railway Bridge, which is a cantilever truss bridge, held the record in the beginning of this century with its 520 m spans. The Quebec Railway Bridge took over the record in 1917, but the 549 m truss span only slightly increased the applicability of this bridge type, and actually the Quebec Bridge is still the world's longest truss span.

During the period from 1885 to 1978 the span of the arch bridges increased from 172 m (the Luiz I Bridge over the Duoro in Portugal) to 510 m (New River Gorge, West Virginia), both steel trusses. This could indicate a natural limit in practice for the use of truss and arch bridges of approximately 600-800 m, based on *Gimsing* (1994).

In the present practice the box girder bridge finds its use for spans up to 150-200 m, or eventually up to 250-300 m, if the depth of the girder is varied. For spans above 200 m the pure box girder will need additional support from cables. The two basic types of cable

supported bridges are suspension and cable-stayed bridges. The first modern cable supported bridges were of the suspension type. It is generally accepted, that the Brooklyn Bridge across the East River in New York is the first modern suspension bridge. With its main span of 486 m and side spans of 286 m each, it has a total cable supported length of 1058 m. In order to increase the stiffness of the structure, the designer added stay cables to the suspension system.

The Brooklyn Bridge held the record for six years, when it was taken over by the Forth Railway Bridge as already mentioned. In 1929 the suspension bridge type got back the record of free span as the Ambassador Bridge (564 m) in Detroit was completed and from this point, the record-holder has always been a suspension bridge, Fig. 1.1.

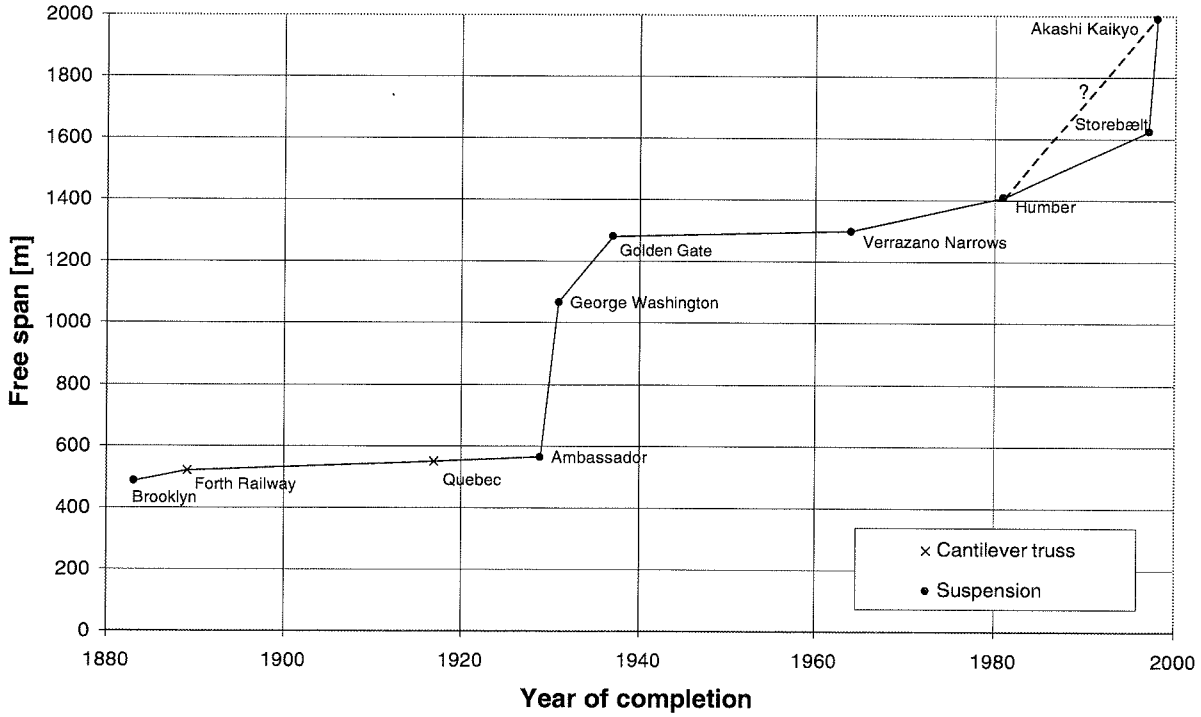

Figure 1.1 *Development of bridge span length. Adapted from* Tanaka *(1992).*

The giant leap from 564 m of the Ambassador Bridge to 1067 m of the George Washington Bridge was to a great extent made possible by use of the so-called 'deflection theory' developed in 1888 and used for the first major project in practice for the analysis of the

Manhattan Bridge in New York, opened to traffic in 1909.

The deflection theory is a second order theory taking into account the displacements of the main cable under traffic load when calculating the bending moments in the stiffening girder. As a cable with a small flexural rigidity will deflect towards the funicular curve under the action of live load, equilibrium is established more correctly for the deflected system rather than for the initial system with the dead load geometry. The bending moments in the stiffening girder are proportional to the vertical distance from the funicular curve to the distorted cable. Thus, by taking into account the second order effect related to the displacement of the cable, the bending moments in the stiffening girder will be significantly reduced, see for instance *Gimsing* (1993).

In 1932 the second order deflection theory was further developed to cover horizontal forces as well. The extended theory takes into account the inclination of the cable planes caused by lateral deflection of the stiffening girder. This is also known as the 'pendulum effect'. As it was the case when the two-dimensional deflection theory was applied, the calculated actions on the stiffening girder due to horizontal forces were reduced.

Despite the use of stay cables in the Brooklyn Bridge among others, no pure and modern type cable-stayed bridge was erected until 1956, when the Strömsund Bridge in Sweden opened to traffic with a main span of 183 m, *Gimsing* (1983).

However, it was in connection with the reconstruction of the bridges in Germany especially over the Rhine, that the cable-stayed bridge concept really started to develop. The first to be opened to traffic was the Theodor Heuss Bridge in Düsseldorf in 1957, with a main span of 260 m. The cable-stays are arranged in a harp configuration, whereas the Strömsund Bridge has a fan system, both systems having their advantages and disadvantages. In case of more than one cable plane, the harp system is generally believed to give a more pleasant appearance as the stays are parallel and therefore do not intersect each other at different angles, when the bridge is viewed from a skew angle. On the other hand, the fan system is more efficient from

a structural point of view, and both systems are applied in practice as well as different transitional forms.

In the initial stage, limitations in the calculational capacity dictated a limited number of stay cables and thereby a reasonably low degree of statical indetermination. This also means, that the stiffening girder only gets a discrete support from the stays in a limited number of points, so the stiffening girder still needs to have a certain bending stiffness.

In 1967, the erection of the first cable-stayed bridge having a multi-cable system was made possible thanks to the breakthrough in computer aided analysis. This bridge was the Friedrich Ebert Bridge across the Rhine near Bonn. The multi-cable system has the advantage of giving a more continuous elastic support of the stiffening girder. Furthermore, the cable forces to be transmitted from each anchor point of the stays are reduced, so local strengthening of the girder at the anchorages can be kept to a minimum, *Gimsing* (1983).

Today the world record for cable-stayed bridges belongs to the Normandy Bridge near Le Havre in France. This bridge has a modified multi-cable fan system and a main span of 856 m. It was completed in 1994. In 1999 the record will be taken over by the Tatara Bridge in Japan, basically having the same cable configuration as the Normandy Bridge, but a main span of 890 m.

1.2 Future problems

The use of cables as load carrying elements in the main structure of a bridge has proven highly efficient, as the high strength of the wire will decrease the escalation of the dead load otherwise related to longer spans. As indicated in the previous section, today cable supporting is applied for most spans above 250 m.

Traditional cable supported bridges are designed in a way so that the cable system mainly renders a vertical, or vertical and torsional support to the stiffening girder. However, cable supported bridges are being erected with larger and larger span-to-width ratios, either as a result of longer spans, or due to a narrow roadway.

In an earth-anchored system, the lateral wind load is transferred partly by the girder in transverse bending and partly by the cable system due to the inclination of the cable planes. In a traditional self-anchored system, the wind load has to be transferred entirely by the girder in transverse bending, as there will be no pendulum effect. Furthermore, the girder is submitted to a considerable compressive normal force introduced by vertical loads. With the present trend towards increasing the span-to-width ratio, the transfer of lateral loads by the girder in bending will loose in efficiency, *Gimsing* (1992). Adding to the horizontal load on the girder itself is also half of the wind load on the cable system, as each stay cable will transfer half of its wind load to the pylon and half to the girder, *Gimsing* (1994). As a consequence, the static and dynamic behaviour of the structure both during construction and in the completed stage might turn out to be unacceptable.

1.3 Background for this project

As pointed out in the previous Section, it is to be faced in a near future, that the question of transferring lateral forces becomes a decisive factor for the design of cable supported bridges, just like earlier the transfer of vertical loads had demanded the use of vertical cable support for the longer spans. A study on the development in lateral slenderness for suspension and cable-stayed bridges has been carried out by *Larsen* (1995), Fig. 1.2 and Fig. 1.3.

This lateral slenderness could either be the result of a very long span with a standard deck width of say 20-40 m, or it could be due to an extremely narrow girder used in connection with a moderate span. The first situation becomes relevant, because an increased span does

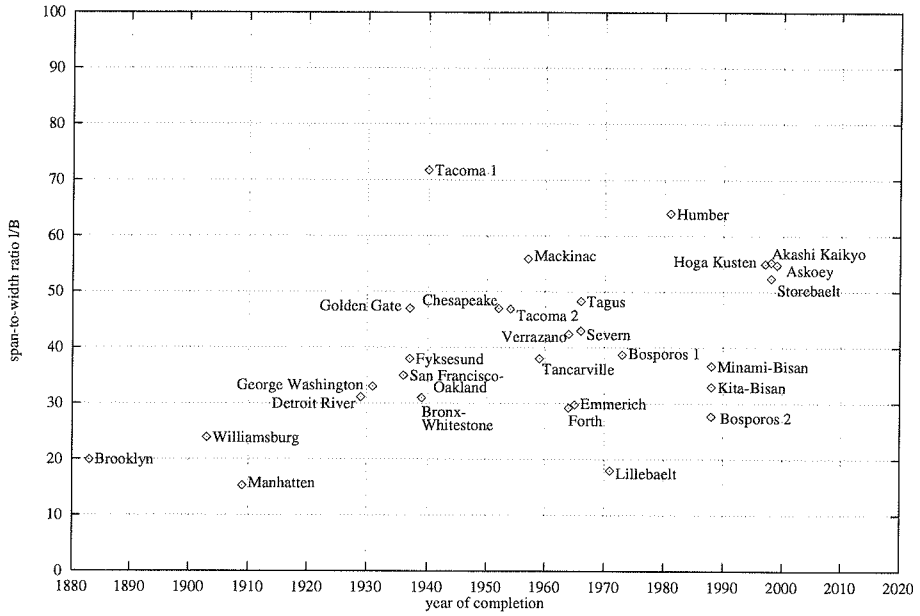

Figure 1.2 *Development in lateral slenderness (span-to-width ratio) for suspension bridges, where the width is taken as the centre-to-centre distance between the main cables. From* Larsen *(1995).*

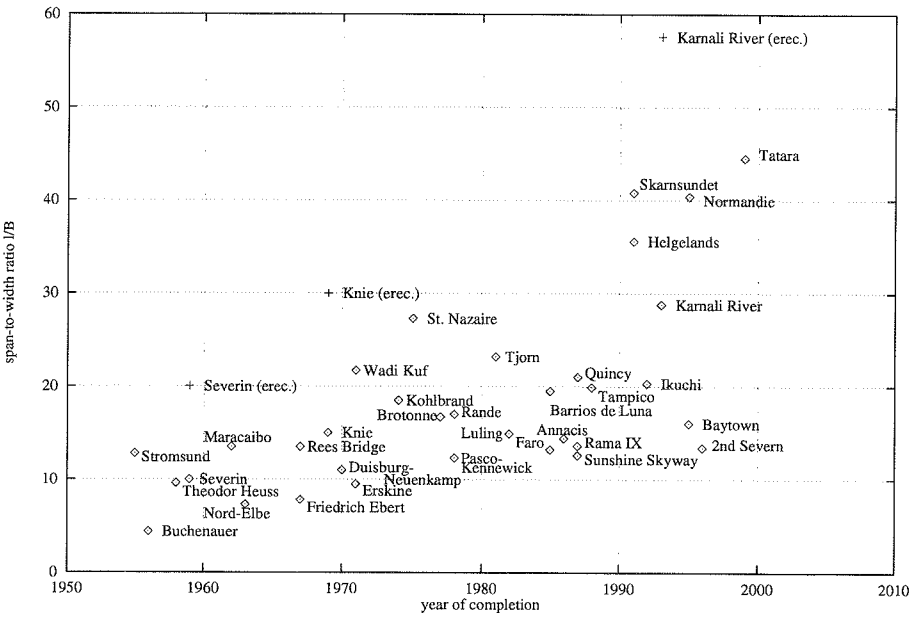

Figure 1.3 *Development in lateral slenderness (span-to-width ratio) for cable-stayed bridges. + indicates mono-tower bridges in erection stage. From* Larsen *(1995).*

not necessarily call for a wider deck, since the deck width is more a question of requirements for road and rail traffic. While the latter could occur in areas with small traffic intensity and thus limited demands concerning deck width. Taking into account the developments in construction techniques and cost, it becomes feasible from an economical point of view to build these bridges despite the low traffic volume.

A possible solution to the problems associated with lateral wind load on cable supported bridges with large span-to-width ratios could be to apply a spatial cable system, that provides both vertical and lateral support for the deck. A full three-dimensional support of the girder will require a cable system composed of at least three mutually inclined cable planes forming a spatial network of cables. However, to achieve symmetry four cable planes will generally be preferable. Fig. 1.4 shows a photo of an architectural model of a cable-stayed bridge having a spatial cable system.

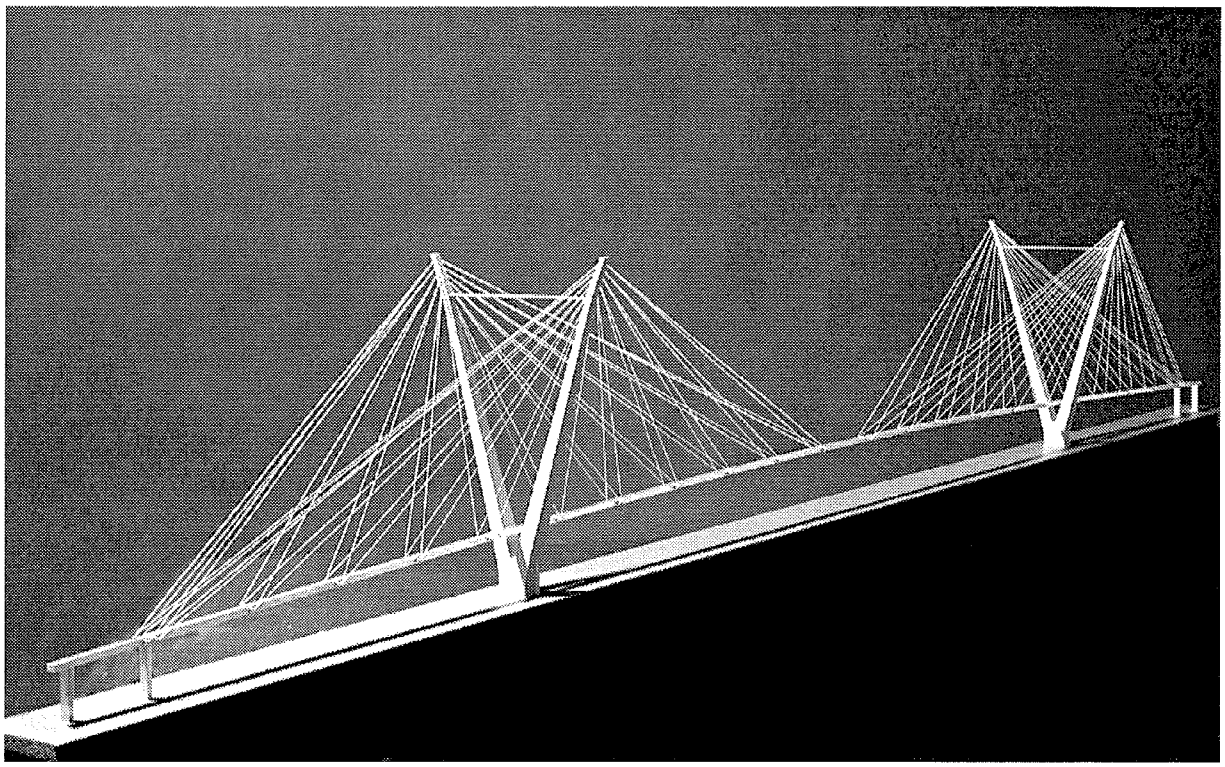

Figure 1.4 *Architectural model of a cable-stayed bridge having a spatial cable system.*

1.4 Aim of this project

In this project entitled "Bridges with Spatial Cable Systems" the static behaviour and buckling stability of cable-stayed bridges with three-dimensional cable systems are studied. We restrict the investigations to what we refer to as "fully spatial (three-dimensional) cable systems". We define the term "fully spatial cable systems" as cable systems where lateral loads are transferred by the same cables as used for carrying vertical loads. Thus the dead load is used to prestress the cables to allow transfer of lateral forces.

In the present study we focus on the cable system and on the interaction between cable system and girder. The work comprises parametric studies on a cable-stayed road bridge with an 800 m main span and a girder width of 8 m, giving a span-to-width ratio of 100. This choice of prototype bridge is based on the investigations performed by *Larsen* (1995), who carried out an extensive study on the aerodynamic behaviour of long and narrow bridges with both traditional and spatial cable systems. A span-to-width ratio of 100:1 is close to a factor of 2.5 compared to the maximum span-to-width ratios found in the cable-stayed bridges build at present, see Fig. 1.3. By choosing this relatively extreme value, the problems of lateral stability will become even more pronounced, than they have been till now and therefore well suited for a closer investigation. Only the static behaviour and buckling stability of bridges with spatial cable systems are dealt with in the present study. Dynamic problems related to the aerodynamic behaviour are covered by the work of *Larsen* (1995).

The investigations described in this report begin with an analytical parametric study on the overall geometry of a spatial cable system for a bridge with certain given requirements as for instance span length and girder cross-section corresponding to the above mentioned prototype bridge. By minimizing the total cost of the structure a reasonable choice for the overall geometry of the spatial cable system is obtained. This is used in the following numerical analysis.

The static behaviour and stability of four different layouts of the spatial cable system are

studied by means of finite element calculations (abbreviated: FE-calculations). In a bridge with a lateral slenderness as extreme as 100:1, a primary concern is, of course, the deflections under the action of wind load. Also, an important feature is the torsional characteristics of the girder in combination with the cable system. As a part of the finite element calculations a new way of controlling the dead load geometry has been tested. This method has the advantage of rendering the usual iteration process superfluous.

Sketches of the four spatial cable systems studied are shown in Fig. 1.5 and 1.6, where an alternative layout of the pylon, compared to the one used in the architectural model, is chosen to illustrate some of the different structural expressions related to applying a three-dimensional cable system.

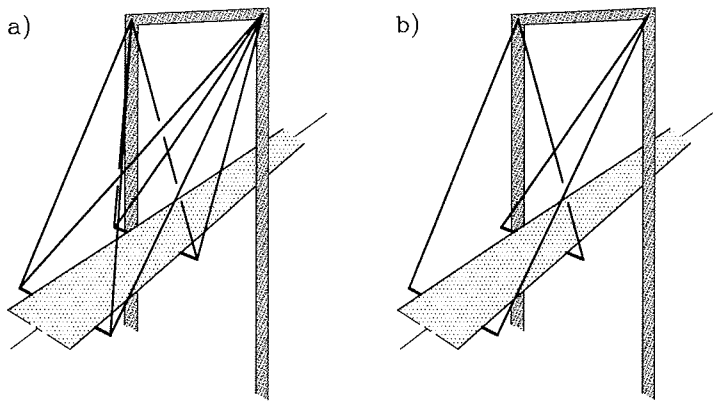

Figure 1.5 *Spatial cable systems a) and b).*

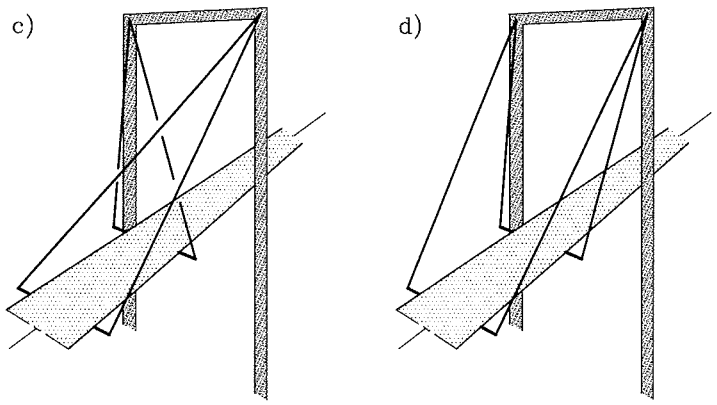

Figure 1.6 *Spatial cable systems c) and d).*

A main objective of the project has been to carry out a comparative experimental study on the buckling stability of a narrow, cable supported girder. The test series consists of a number of different geometries of the cable system: Vertical cable planes as well as inclined cable planes. The 5 m long model corresponds to the erection stage, where the maximum cantilever reaches the centre of the main span. This is a critical phase both concerning wind load on the cantilever and its buckling stability. Fig. 1.7 shows a photo of the model used in these tests.

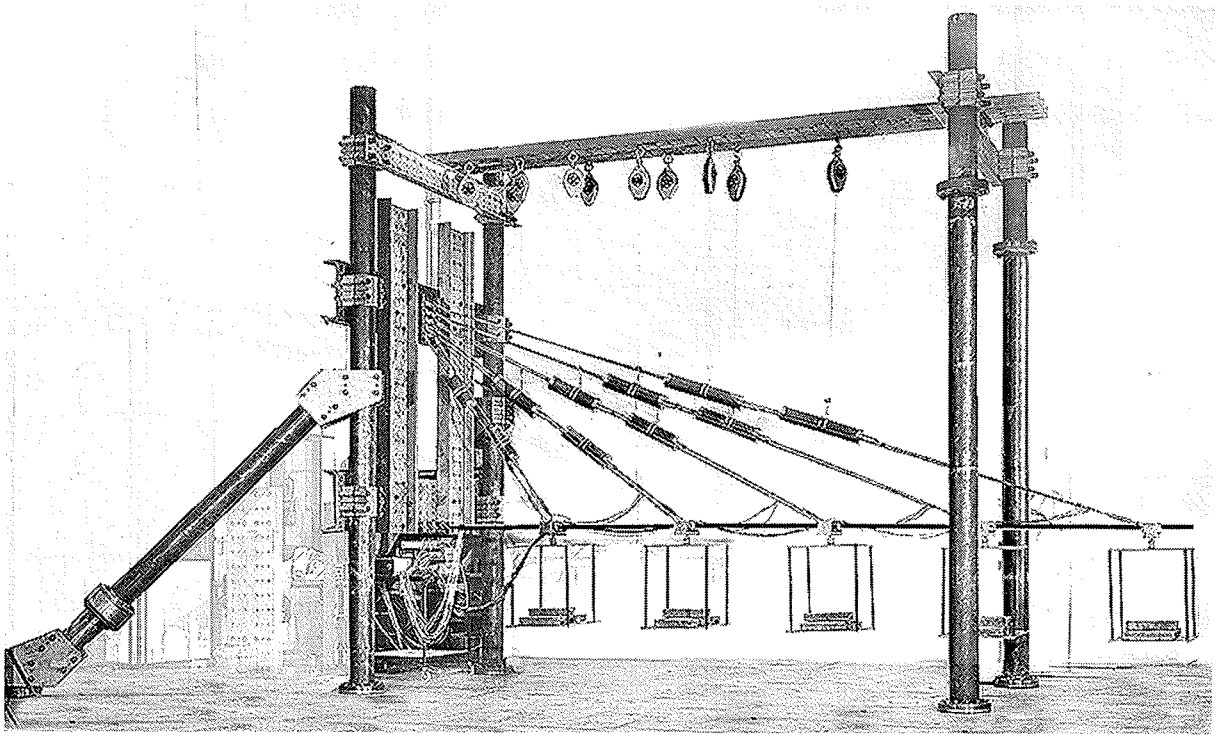

Figure 1.7 *Physical model used in tests of bridge with spatial cable system.*

Chapter 2

2. LAYOUT AND DESIGN OF PROTOTYPE BRIDGE

2.1 Introduction

In this Chapter 2 overall layout and basic dimensions of the prototype bridge are presented. The prototype bridge was briefly introduced in Chapter 1 and will be used throughout the present study. First the general layout of the cable-stayed bridge is given in Section 2.2. This includes span length, pylon height and overall structural system. In Section 2.3 four different layouts of the spatial cable system are presented. The properties of the bridge girder are given in Section 2.4. Various layouts of the pylon are presented in Section 2.5 and discussed in view of the different support conditions they offer for a spatial cable system, and consequently also for the girder. The loads considered in the design are described in Section 2.6.

In this study the cable system is in focus including the interaction between cable system and bridge girder. The overall layout of the cable system is the subject for parametric studies - both analytical and numerical - so consequently cable dimensions will be given in connection with the related parametric investigations in Chapter 3 and in Chapter 4. It should be stressed, that the layout of girder and pylons is not based on detailed designing. The intention has been

to obtain a realistic design upon which optimization of the cable system can be based. Consequently, no stress analysis in a more strict sense is carried out for neither girder nor pylons. The main purpose of this Chapter 2 is therefore to present the structural basis for the analytical parametric study of Chapter 3 and the numerical investigations in Chapter 4 and Chapter 5.

2.2 Overall layout of cable-stayed bridge

As indicated in Chapter 1 "Introduction" the present project succeeds the work of *Larsen* (1995). Therefore it is chosen to investigate a prototype bridge with the same overall layout as the one *Larsen* (1995) investigated with respect to aerodynamic stability. This prototype cable-stayed bridge has an 800 m main span and side spans of 250 m, resulting in a total cable supported length of 1300 m. With a girder width of 8 m the span-to-width ratio equals 100:1. Thus the prototype bridge is characterized by having a long span but still within the limits of what has been built until today, whereas the span-to-width ratio is extreme compared with present practice, see Fig. 1.3.

Because of the span length, which is within the limits of structures recently built or under construction, it is chosen to restrict investigations to a self-anchored system according with the common layout for cable-stayed bridges, thus the girder is subjected to compression over its entire length. The girder is placed 30 m above ground, and for simplicity it is assumed to be mounted without any camber. As a first approach the optimum pylon height above bridge deck for a traditional cable-stayed bridge with vertical cable planes is applied. For a main span of 800 m a reasonable estimate on the pylon height above deck is 120 m. The influence of this parameter on the cost of the structure is further investigated in Chapter 3.

At the abutments the girder is restrained against lateral and vertical displacements as well as torsion, whereas it is free to rotate about the two other axes and to displace in the longitudinal direction. Support conditions at the pylons depend on the layout of these, and this point is

treated in Section 2.5.

A sketch of the prototype bridge is shown in Fig. 2.1.

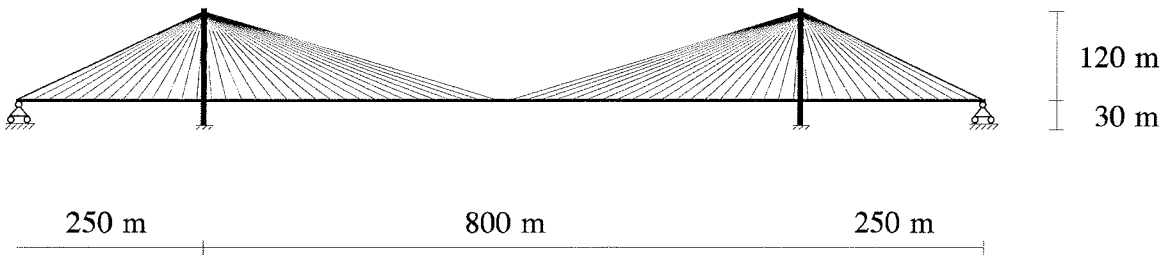

Figure 2.1 *Elevation of prototype cable-stayed bridge.*

2.3 General presentation of four layouts of the spatial cable system

In Chapter 1 the four different layouts of the spatial cable system investigated in the present work were briefly introduced. These can be seen in Fig. 2.2.

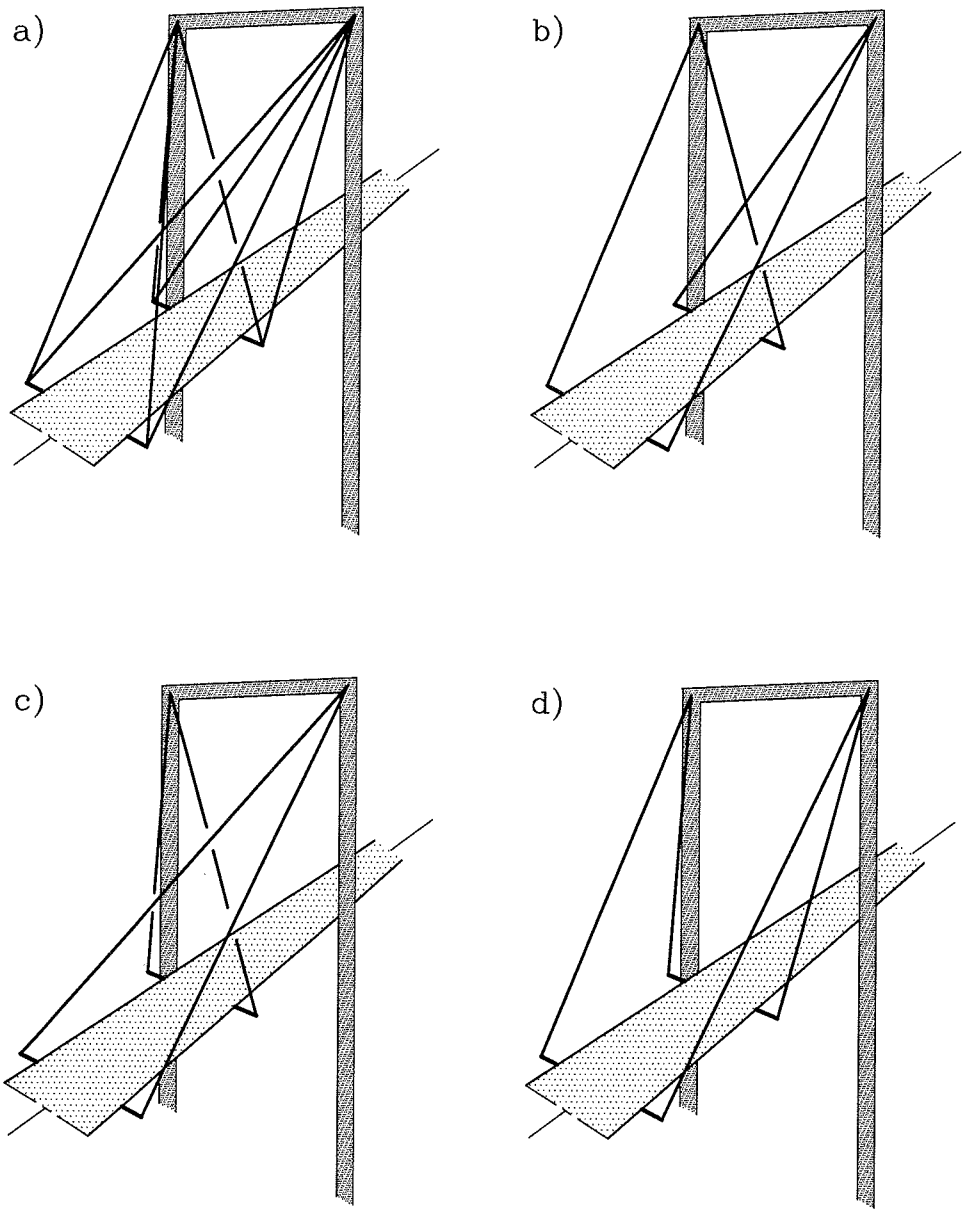

Figure 2.2 *Four different layouts of the spatial cable system.*

In the present study we consider what we refer to as "fully spatial (three-dimensional) cable systems". We define the term "fully spatial cable systems" as cable systems where lateral loads are transferred by the same cables as used for carrying vertical loads. This way, the dead load of the girder and the cables themselves is used to prestress the cables and thus make transfer of lateral forces possible by increasing or decreasing the prestress.

In Fig. 2.3 transfer of a lateral force is shown for the four spatial cable systems.

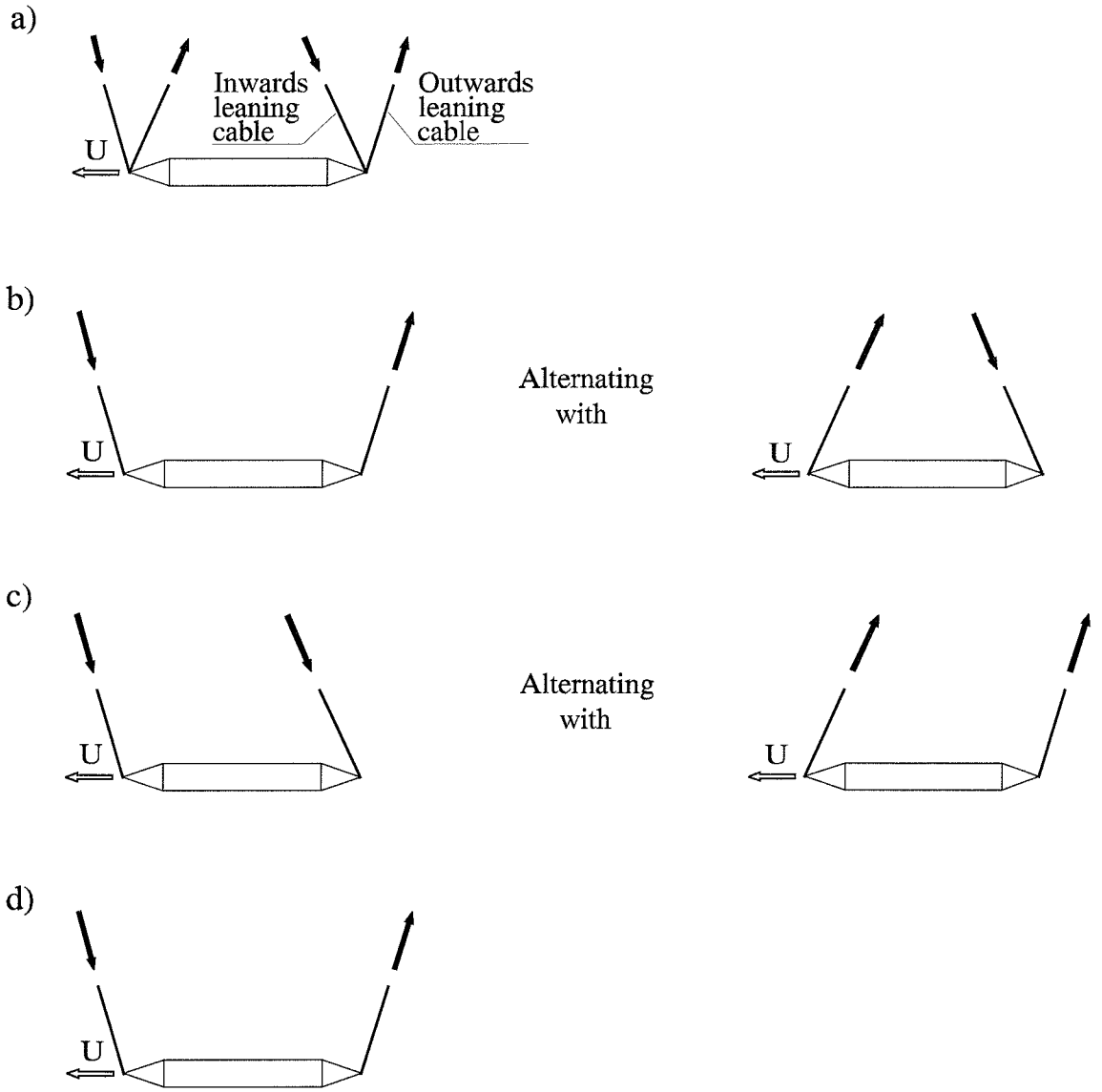

Figure 2.3 *Basic static behaviour of four layouts of spatial cable system subjected to lateral load.*

With system a) the lateral force can be transferred by the cable system without any aid from the girder. In system b) the girder needs to have a certain torsional stiffness, because the two cables per section of cable anchorage do not intersect at the centre of gravity of the girder and thus torsion arises. Consequently the girder has to transfer torsion from one section of cable

anchorage to the next, where the sign of the torsional moment is reversed. With cable system c) transfer of lateral forces by the cable system results in local vertical bending of the girder. This is not expected to cause any difficulties, since the girder will have a certain vertical bending stiffness to allow transfer of vertical loads from the loading point to the sections of cable anchorage. Finally, in cable system d) the girder needs to have a considerable torsional stiffness, if lateral forces are to be transferred by the cable system. In this cable system d) the sign of torsional moments is not reversed at the next section of cable anchorage as it was the case for cable system b), so with cable system d) transfer of lateral forces by the cable system gives rise to global torsional moments to be transferred by the girder. Actually, the box girders commonly used have a considerable torsional stiffness. The FE-calculations in Chapter 5 will show whether the torsional stiffness of our prototype girder is sufficient.

With respect to a torsional moment acting on the girder (e.g. due to eccentric traffic load), the situation is similar to what has been described above for lateral load: With cable system a) the torsional moment can be transferred by the cable system without any aid from the girder. In system b) transfer of a torsional moment by the cable system gives rise to local lateral forces acting on the girder. The sign of these is reversed at every section of cable anchorage. With cable system c) no additional load on the girder is related to transfer of torsional moments by the cable system. Finally, with cable system d) transfer of a torsional moment by the cable system is only possible if the girder can carry the lateral forces that arise in bending. This is investigated by means of FE-calculations in Chapter 5.

Transfer of vertical loads symmetric to the bridge axis does not give rise to significant differences between the four layouts of the spatial cable system.

Previously in the present Section the term "fully spatial" was introduced. We will now go further into details with the term "fully spatial" in relation to the four layouts of the spatial cable system.

Cable system a), consisting of four mutually inclined cable planes, is truly fully spatial since

all types of loading (vertical and lateral forces and torsional moments) can be transferred by the cable system without requiring aid from the girder. In cable system b) and c) a certain aid from the girder to transfer local actions is required in order to transfer all types of loading by means of the cable system. Thus, cable systems b) and c) can be considered as partially spatial. However, the cable systems b) and c) are still three-dimensional in the sense, that lateral loads are transferred by the same cables as used for carrying vertical loads. Cable system d) must be regarded as pseudo-spatial, since it consists of only two mutually inclined cable planes, so lateral forces can only be transferred by the cable system if the girder can carry the related global eccentricity moments in torsion. Thus a considerable rigidity of the girder is required to allow the cable system to act as spatial. For simplicity we will continue to use the term "spatial" in connection with all four systems.

As described above, cable system a) is the only system of the four that can be considered as truly fully spatial. However, it has some disadvantages compared to the other three. Most importantly, in system a) the number of cables is twice the number required for the other three systems. This fact gives rise to two adverse effects: Firstly, the wind load on the cable system is higher due to the larger surface of the cables. This will affect not only the cables but also the pylons, since all wind load is transferred to the pylon top, see Section 2.5. Secondly, the process of adjusting cables when mounted, will become more complicated and time-consuming when the number of cables is doubled. The adjusting of cables is not expected to cause difficulties using cable system b) or d). With system c) cables in a section of cable anchorage are not arranged symmetrically with respect to the bridge axis. Adjusting of cables consequently causes lateral displacements of the girder tip during cantilevering. Finally, cable system a) and b) have the disadvantage of two inwards leaning cables placed at the same section of cable anchorage, thus the two cables are crossing each other. This might lead to a relatively complicated structural detail at the intersection of the two cables. Out of the four proposed layouts for the spatial cable system, the pseudo spatial system d) is the most similar to a traditional system with two vertical cable planes. The advantages and disadvantages of the four spatial cable systems are listed in Tab. 2.1.

Cable system	Advantages	Disadvantages
a)	Fully spatial.	Larger wind load on the cable system. Adjusting of cables more complicated. Crossing cables.
b)	Only half the number of cables compared to a).	Only partially spatial. Crossing cables.
c)	Only half the number of cables compared to a). No crossing cables.	Only partially spatial. Unsymmetrical with respect to bridge axis.
d)	Only half the number of cables compared to a). No crossing cables.	Only pseudo-spatial.

Table 2.1 *Comparison of advantages and disadvantages related to the four spatial cable systems.*

2.4 Bridge girder

For the bridge deck a steel box girder is chosen. As mentioned previously the girder width is 8 m, while the depth is 2 m. The practice for moderate to long span bridges has moved towards applying an aerodynamic design of the girder to reduce the drag coefficient and hence the static wind load. Furthermore a streamlined cross-section improves the aerodynamic stability. Consequently the steel box girder is supplied with fairings ("wind noses") that are here considered to be non-structural members. The drag coefficient determined from wind tunnel tests performed by *Larsen* (1995) has been applied throughout the investigations.

Due to the inwards leaning cable planes of the spatial cable systems a), b) and c) presented in Fig. 2.2 and 2.3, cable attachments at the girder need to be moved away from the limits of the traffic area in order to meet the requirements for clearance. The requisite distance from the edge of the bridge deck to the attachments of cables depends on the inclination of cable planes. A reasonable estimate is to locate the attachments 2 m from the edge of the bridge deck, thus leading to a lateral distance of 12 m between cable planes at girder level. In longitudinal direction of the bridge the distance between cable supports is 20 m.

A realistic cross-section for the girder is shown in Fig. 2.4 and in Fig. 2.5 the idealized cross-section used throughout the present study is shown. The contribution to the structural features originating from longitudinal stiffening ribs is taken into account by assigning a fictitious or equivalent thickness to the deck plate as well as to the bottom and side panels. This equivalent thickness is 20 mm for the deck plate and 16 mm for the other panels. In Tab. 2.2 the main structural features are listed.

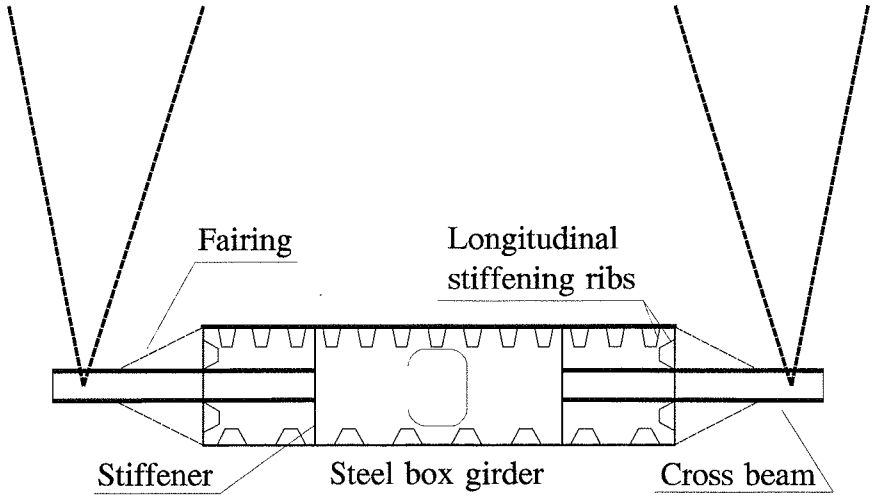

Figure 2.4 *Cross-section of girder.*

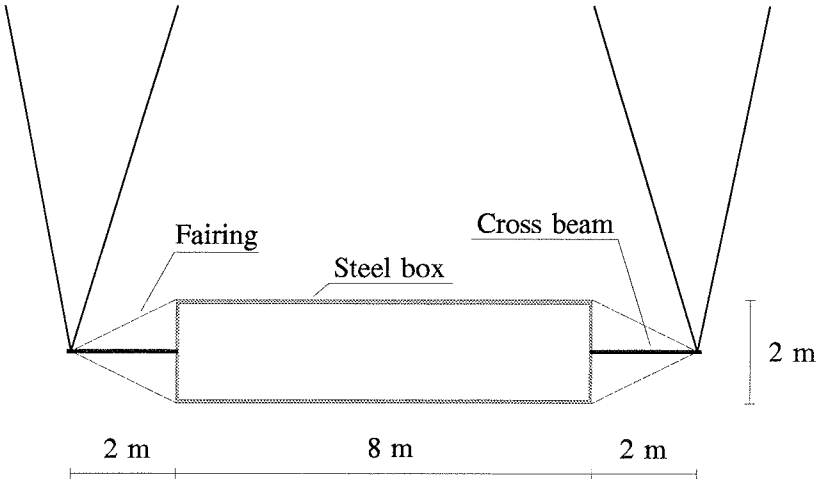

Figure 2.5 *Idealized cross-section of girder.*

Cross-sectional area, A	0.35 m^2
Moment of inertia, lateral bending, I_{lat}	2.6 m^4
Moment of inertia, vertical bending, I_{vert}	0.31 m^4
Moment of inertia, torsion, I_{tor}	0.92 m^4

Table 2.2 *Structural features of girder.*

The self weight of the steel box girder attains 27.7 kN/m. To this value adds the weight of bridge equipment. The main contributions originate from railings (6 kN/m) and a 50 mm thick layer of asphalt over the entire deck width (6 kN/m). To accommodate for other contributions, such as transverse bulkheads, further 3 kN/m are added. Thus the total dead load of the bridge girder including equipment is set to 42.7 kN/m.

2.5 Pylon structures and interaction with cable system

A fully spatial cable system offers a three-dimensional support of the girder allowing both vertical, lateral and twisting forces to be transferred by the cable system. As a consequence, no direct support of the girder at the pylons is required, and it is possible to let the girder pass freely from one abutment to the other only supported elastically by the cable system. One could therefore argue, that the true span of the girder is from abutment to abutment, thus 1300 m in our case, leading to a span-to-width ratio of approximately 160:1.

It is obvious that the requirements for supporting a spatial cable system will lead to a pylon configuration that differs from pylons supporting a traditional plane cable system. Most importantly the inclined cable planes demand for a considerable lateral distance between the two anchor zones at the pylon top. To get a reasonable inclination of cables in the lateral directions, this "pylon width" needs to be several times the girder width. Furthermore, pylons supporting a spatial cable system are subjected to extra loading because the entire wind load on girder and cable system has to be transferred from the pylon top to the foundations. In a cable-stayed bridge with vertical cable planes only half of the wind load on the cables is transferred at the pylon top. The remaining part of the wind load on the cable system and all the wind load on the girder only have to be transferred from girder level, where a lateral support is usually arranged, and downwards to the foundations, see also *Gimsing* (1992).

The fact that the entire wind load has to be transferred from the pylon top to the foundations in spatial cable systems asks for increased lateral strength and stiffness of the pylons. Also the resistance against motions of the pylon top parallel to the bridge axis plays a role. The transfer of wind load to the pylon top will force the two sides to move in opposite directions corresponding to an increase in tension in one anchor cable and a reduction in the other. This relative displacement of the two anchor zones in the pylon top will be amplified relative to half the length of the main span and thus contributes considerably to lateral deflections of the girder. This point is treated further in Chapter 3.

The general trend within design of cable-stayed bridges moves towards a preference for the modified fan configuration, see for instance *Gimsing* (1992). This seems also to be a reasonable choice for a spatial cable system. Only fan configurations - pure or modified - are considered in the present study.

In order to avoid significant bending in the pylon for permanent load it would be favourable to arrange the anchor zone so that it lies in the same inclined plane as the cables. This can be achieved by having a pylon configuration with inclined legs as shown on the photo in Fig. 1.4 (a V-pylon) or by supplying a frame type pylon (as shown in Fig. 2.2) with inclined "horns". The layout of different pylon structures supporting spatial cable systems have been discussed in *Gimsing* (1991) and *Gimsing* (1992). In this study, where focus is on the cable system and its interaction with the bridge girder, calculations will be restricted to concern only a frame type pylon.

The vertical legs of a frame type pylon can be erected in both steel and concrete using well known techniques. The cross beam at the top could be more troublesome to construct in concrete. As it will turn out in Chapter 3 the length of this cross beam is between half the pylon height and the full pylon height (60 m - 120 m), thus the cross beam is actually itself a medium span bridge. Furthermore, the cross beam is subjected to compression arising from forces transferred by the inclined cable planes. A solution might be to assemble the cross beam in steel on ground and lift it into position using erection techniques as for instance known from erection of steel pylons in Japan. In the present study only a steel pylon is considered. A sketch of the pylon structure used throughout the present study is shown in Fig. 2.6.

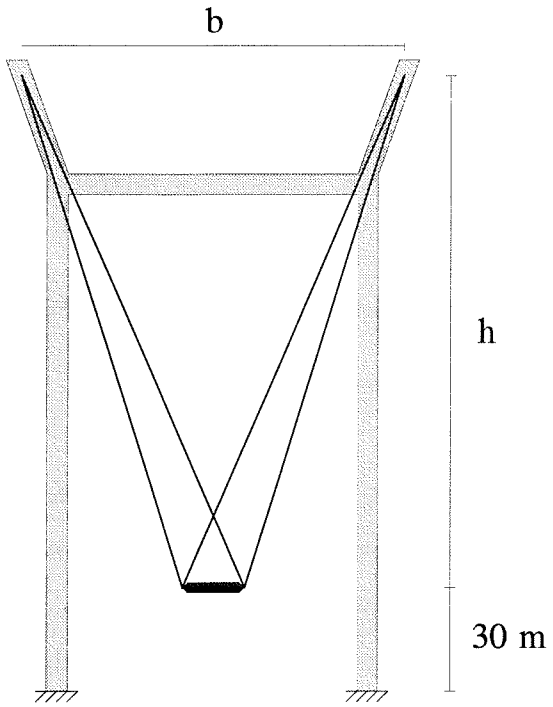

Figure 2.6 *Frame type pylon used for the analyses described in Chapter 3 through 5.*

The values of h and b will be determined by means of material cost minimization and evaluation of deflections described in Chapter 3 "Overall geometry of spatial cable system". In the parametric studies presented in Section 3.4 it is shown that the quantity of structural material in the pylons plays an important role for optimum geometry of the spatial cable system determined according to a criterion of material cost minimization. Consequently, pylons with varying cross-sections are considered in that context.

In the numerical analyses (Chapter 4 and 5) pylons are not subjects for a careful design like it is the case for the cable system. Thus in order to avoid a complicated geometry such as varying cross-section, both pylon legs and the cross beam are assumed to have a constant cross-section corresponding to a 4×9 m rectangular steel box with an equivalent plate thickness of 40 mm. This corresponds to the dimensions used in the work of *Larsen* (1995) and results in a realistic global stiffness of the pylon. The actual structural features of the pylon used in FE-calculations are listed in Tab. 2.3.

Cross-sectional area, A_{pylon}	1.04 m^2
Moment of inertia, bending in longitudinal direction of bridge, $I_{pylon, long}$	3.31 m^4
Moment of inertia, bending in lateral direction of bridge, $I_{pylon, lat}$	11.34 m^4
Moment of inertia, torsion, $I_{pylon, tor}$	7.98 m^4

Table 2.3 *Structural features of pylons.*

From Fig. 2.6 it is clearly seen that the pylon offers no direct support for the girder, so all actions on the girder have to be transferred by the cable system to pylon tops and abutments. In connection with a V-pylon as showed in Fig. 1.4 it is easier to arrange a lateral support for the girder, and eventually also a vertical and torsional restraint. We will return to the support of the girder at the pylon in Chapter 5 in relation to the discussion of the results of FE-calculations on the prototype bridge.

2.6 Loads

The main loads to consider in a general study on a cable-stayed bridge are the dead load, which is a permanent load, and the variable loads consisting of wind and traffic. Here only static loads are considered.

The primary concerns in the present study are related to deflections. Consequently a partial coefficient of 1.0 is applied to all loads, thus they are assumed to act with their characteristic values.

In the analytic and numerical studies on the static behaviour of bridges having spatial cable systems (Chapter 3, 4 and 5) only the completed stage is considered. The erection stage is treated in Chapter 6, 7 and 8 in relation to model tests.

2.6.1 Dead load

The dead load of the girder including bridge equipment equals g = 42.7 kN/m as mentioned in Section 2.4 "Bridge girder". The weight of the pylon is calculated on basis of the information given in Section 2.5 "Pylon structures and interaction with cable system". Finally, the dead weight of the cables is taken into account in connection with the design of these as described in Chapter 3 and 4.

2.6.2 Wind

The wind load is separated into two contributions: Wind on the structure and wind on the traffic. Here only static wind load is considered. Consequently, no dynamic actions due to wind such as gusts are taken into account. The aerodynamics of narrow cable supported bridges are treated in *Larsen* (1995).

The wind load is determined on basis of the Danish Code for Loads on Structures *DS410* (1982). From a reference wind speed of 27 m/s at an elevation of 10 m, the short term wind speed, v, at a certain height above ground can be determined. The wind speed depends on roughness of the surface and on the return period. Here the surface is assumed to be smooth corresponding to a crossing over water. Furthermore a 100-year lifetime of the structure is assumed.

Taking the girder as an example, it is positioned 30 m above ground leading to a 100-year design wind speed of v ~ 44 m/s.

For the girder the drag coefficient has been found through wind tunnel tests performed by *Larsen* (1995). Using the experimentally determined drag coefficient the static uniformly distributed wind load on the girder yields u = 1.85 kN/m. For simplicity wind load is assumed to be a fixed action, thus when wind load is present it acts with its full intensity over the entire structure.

For the pylons the wind speed is adjusted corresponding to the height above ground. In

average the uniformly distributed load on the pylon legs due to lateral wind equals 10 kN/m. The magnitude of wind load on the cable system is determined when actual cable dimensions are known.

The last contribution to the wind load to be considered in the present study is wind on vehicles. We assume that the maximum wind speed where the bridge is still open to traffic is v ~ 25 m/s. According to *DS410* (1982) the height of the traffic wind surface should be set to 2.5 m and the drag coefficient to 1.6. This results in a uniformly distributed load of 1.6 kN/m along the bridge girder associated with a torsional moment of 3.6 kNm/m. The torsion arises because the resultant of the wind load on vehicles is placed 2.25 m above the centre of gravity of the girder. At a wind speed of v ~ 25 m/s the uniformly distributed wind load on the girder is 0.63 kN/m.

2.6.3 Traffic

As recommended in *DS410* (1982) the traffic loads on the bridge are determined according to the Recommendations by the National Danish Road Authorities, *Vejdirektoratet* (1984). The traffic load has an intensity of 2.5 kN/m^2, and for simplicity the entire width of the box girder deck is regarded as traffic area. Thus the uniformly distributed traffic load along the bridge is set to p = 20 kN/m. Traffic load is considered as a free action and different positions of traffic load are dealt with. These are:

Traffic on the entire bridge
Traffic in the main span
Traffic in the side spans
Traffic in half the main span
Traffic over the entire bridge length, but in one direction only (eccentric traffic load)

No concentrated wheel loads are considered, since these have only a local effect, whereas the main interest in this study is the global structural behaviour.

Chapter 3

3. OVERALL GEOMETRY OF SPATIAL CABLE SYSTEM

3.1 Introduction

The purpose of the investigations in this Chapter is to obtain an indication of the range of inclination of cable planes that would be realistic to consider for spatial cable systems. This is obtained through analytical analyses and parametric studies on the overall geometry of spatial cable systems. The criteria for choosing a final overall geometry of the spatial cable system, that will be used throughout the remaining part of the present work, are material cost minimization of the entire structure and evaluation of vertical and lateral deflections due to traffic and wind load, respectively.

First some basic assumptions and idealizations are described in Section 3.2. Then the analytical analyses, forming basis for the parametric studies of Section 3.4, are carried out in Section 3.3. Finally conclusions on the analytical analyses and parametric studies are drawn in Section 3.5.

3.2 Basic assumptions and idealizations

In this Section basic assumptions and idealizations made prior to the analytical analyses are described.

The analytical expressions derived in *Gimsing* (1983) for the plane (i.e. two-dimensional), pure fan system form basis for the expansion of expressions to cover a spatial (i.e. three-dimensional) cable system. A main idealization made by *Gimsing* (1983) is to neglect the bending stiffness of the girder. This is well justified for in-plane actions (i.e. vertical loading and deflections), because the bending stiffness of the girder about the horizontal axis is usually insignificant for global actions. The girder just needs to have a minimum bending stiffness that allows actions to be transferred in bending from the loading point to the points where cables are anchored. Finally the fan, consisting of a finite number of cables, is idealized to a continuous system, thus summations of a finite number of cables can be substituted by integrations.

The assumptions described above are adapted for the expansion of expressions to cover spatial cable systems. Consequently, the bending stiffnesses of the girder in both the vertical and the lateral direction are neglected. As already mentioned this is well justified for bending in the vertical plane. The bending stiffness for lateral bending is significantly smaller for the narrow girder considered in the present work than found in actual cable-stayed bridges erected until today. However, even for the narrow girder considered here the bending stiffness for lateral bending is a factor of 8 higher than for vertical bending, see Tab. 2.2. The validity of the assumption that bending stiffnesses of the girder can be neglected, will be further discussed in Chapter 5 in connection with FE-calculations on the prototype bridge.

In accordance with the trend within design of cable-stayed bridges, a multi-cable system is assumed, thereby justifying the idealization from a finite number of cables to considering a continuous system. As pointed out in Section 2.5 "Pylon structures and interaction with cable system" the frame type pylon considered in this project does not offer any direct support for

the girder. However, both vertical and lateral displacements of the girder at the pylon are disregarded in connection with the idealization from a finite number of cables to continuous fans. This can to some extent be justified by the relatively stiff support of the girder offered by the short cables near the pylon in the prototype bridge. The point will be further treated by means of FE-calculations presented in Chapter 5.

The cables are assumed to be arranged in a pure fan system. The basic spatial cable system considered is of type a), see Fig. 2.2, i.e. there are four cables at each girder anchorage section.

In the present Chapter 3 a pylon with varying cross-section is considered in order to take into account the quantity of structural material in the pylon, when optimizing material cost of the entire structure. On the other hand cost of the girder is assumed to be independent of the cable system chosen.

The intensities of dead load, wind and traffic loads are indicated in Section 2.6 "Loads". The traffic load is assumed to act over the entire width of the bridge deck, thus eccentric traffic load is not considered here. Furthermore, only wind on the girder is considered, thus contributions from wind on the other structural elements as well as on vehicles are disregarded in the analytical analyses.

The limiting stress in the stay cables is set to σ_c = 700 MPa. When calculating deformations, an equivalent modulus of elasticity of E_{eq} = 180 GPa is applied for the cables, which is a typical value found for the commonly used helical strands. No sag effects are taken into account. The density of steel is set to 78.5 kN/m^3 for both structural steel in pylons and cable steel in stay and anchor cables, thus we do not account for the weight of the protection of cables.

3.3 Analytical analyses

3.3.1 Quantity of cable steel in stay cables

First the force in a single cable will be determined. Then the fans of discrete cables are idealized to continuous systems, where the quantity of cable steel is calculated.

A simplified approach to determine cable dimensions can be found in *Gimsing* (1991), where a spatial system with two cable planes anchored at the girder axis is considered:

$$A_c \approx \left(\frac{l_c}{h} \cdot P_{vert} + \frac{l_c}{b/2} \cdot P_{lat} \right) \cdot \frac{1}{\sigma_c} \tag{3.1}$$

where cable length, l_c, pylon height above bridge deck, h, pylon width, b, and the forces, P_{vert} and P_{lat}, are defined on Fig. 3.1. A_c is the cross sectional area of the cable and σ_c the limiting stress.

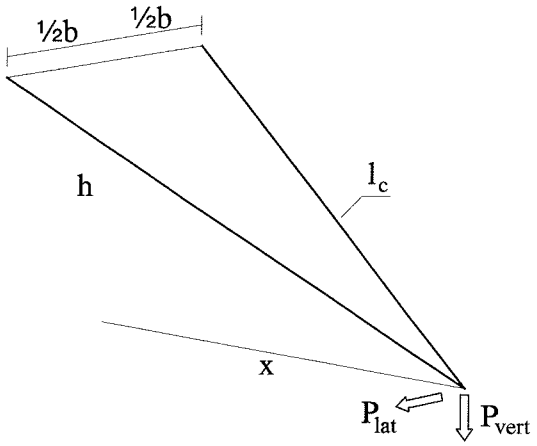

Figure 3.1 *Spatial system with two cable planes anchored at the girder axis.*

In the present Chapter we investigate the influence of overall geometry of the cable system on total cost of the structure. Since the pylon width minimizing the total cost is not yet known, it is decided to take into account the influence of distribution of forces originating from the different inclinations of the inwards or outwards leaning cable planes when calculating the quantity of cable steel. This factor might play a role in cases where pylon

width is only slightly larger than the distance between cable planes at girder level, λ. Due to the different inclinations of cable planes, the outwards leaning cables will transfer a relatively larger part of the vertical load, whereas the inwards leaning cables transfer relatively more of the lateral load. The terms "outwards" and "inwards leaning" cables as well as the parameter λ are defined on Fig. 3.2.

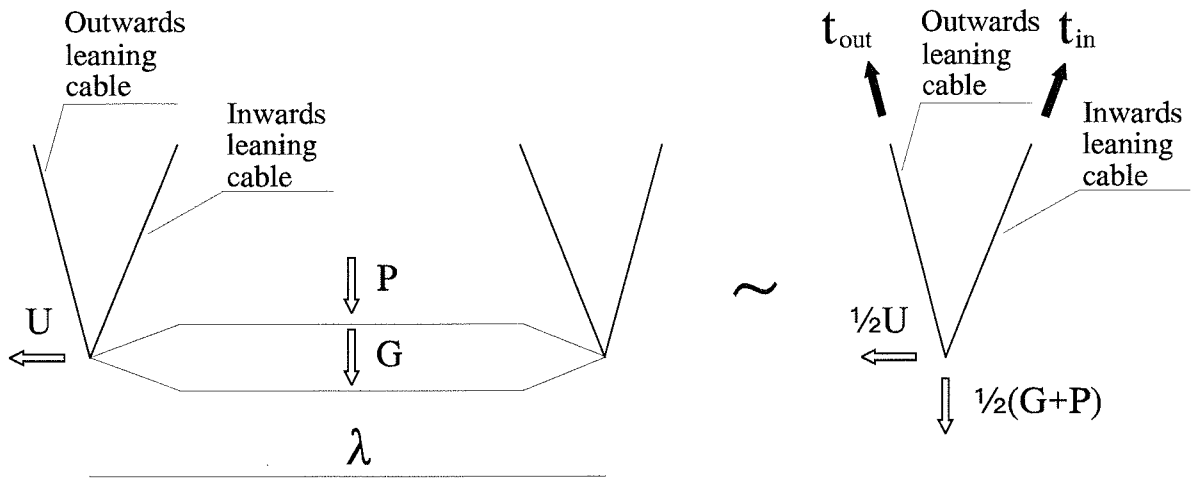

Figure 3.2 *Distribution of forces in spatial cable system. The forces t_{in} and t_{out} are projections of cable forces on a lateral plane to the girder axis.*

The load is assumed to be distributed equally between the cable planes anchored at the two sides of the girder, see Fig. 3.2.

The loads considered are the dead load of girder and bridge equipment, G, the uniformly distributed traffic load, P, and the wind load, U. In the first part of the present Section where we consider discrete cables instead of continuous fans, loads are taken as resultants of the uniformly distributed loads over a length equal to the distance between anchorage sections at the girder, (i.e. over a length of 20 m in our prototype bridge).

Some geometric parameters need to be defined, see Fig. 3.3:

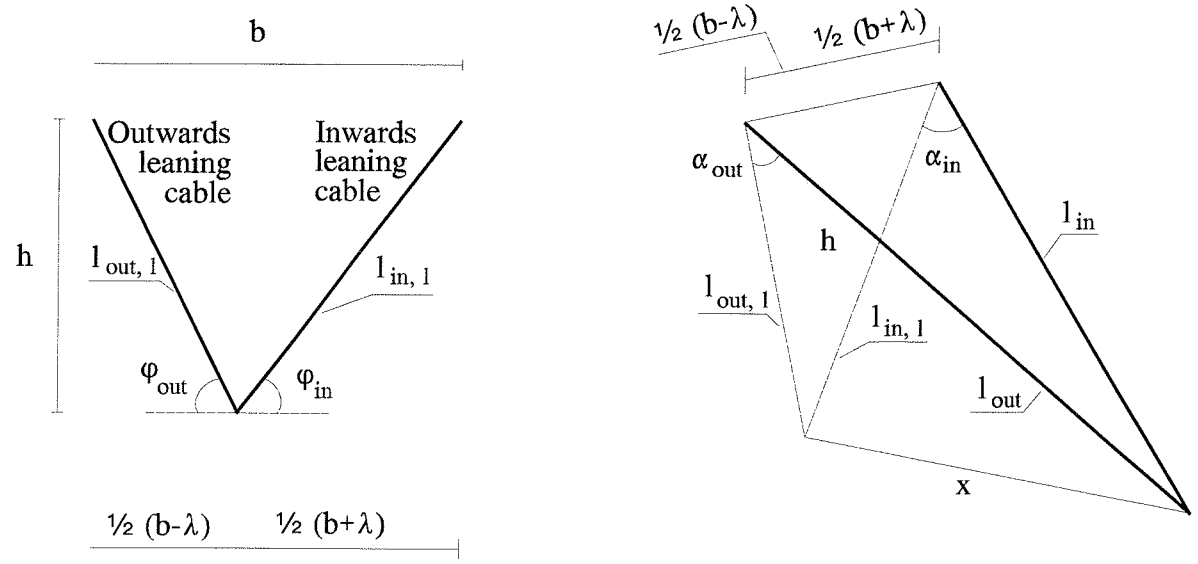

Figure 3.3 *Geometry of spatial cable system shown for the two cable planes attached to the same side of the girder. Left: Projection on lateral plane to girder axis. Right: Three-dimensional view.*

Let us begin with the projection of forces on the lateral plane to the girder axis (Fig. 3.3 left and Fig. 3.2 right). Ignoring the dead weight of cables themselves equilibrium for the vertical direction yields:

$$t_{out} \cdot \sin\varphi_{out} + t_{in} \cdot \sin\varphi_{in} - \frac{1}{2}(G+P) = 0 \tag{3.2}$$

While for the lateral direction we find:

$$t_{in} \cdot \cos\varphi_{in} - t_{out} \cdot \cos\varphi_{out} - \frac{1}{2}U = 0 \tag{3.3}$$

where t_{out} and t_{in} are projections of cable forces on the lateral plane. Solving Eq. (3.3) with respect to t_{in} and substituting this into Eq. (3.2) one gets:

$$t_{out} = \frac{1}{2} \frac{1}{\sin\varphi_{out} + \cos\varphi_{out} \cdot \tan\varphi_{in}} \cdot \left(G + P - \tan\varphi_{in} \cdot U \right) \tag{3.4}$$

and

$$t_{in} = \frac{1}{2} \frac{1}{\sin\varphi_{in} + \cos\varphi_{in} \cdot \tan\varphi_{out}} \cdot \left(G + P + \tan\varphi_{out} \cdot U \right) \tag{3.5}$$

In the following design of cables we need maximum cable forces. Consequently we consider the other outwards leaning cable where the cable force is increased due to wind load. This corresponds to reversing the sign of the last term in Eq. (3.4).

Taking the expression for the outwards leaning cable first, trigonometric functions are substituted by geometrical parameters:

$$\begin{aligned} \sin\varphi_{out} + \cos\varphi_{out} \cdot \tan\varphi_{in} &= \frac{h}{l_{out,\,l}} + \frac{\frac{1}{2}(b-\lambda)}{l_{out,\,l}} \cdot \frac{h}{\frac{1}{2}(b+\lambda)} \\ &= \frac{h}{l_{out,\,l}} \cdot \frac{b}{\frac{1}{2}(b+\lambda)} \end{aligned} \tag{3.6}$$

The cable force in three-dimensional space, T, is found by projection with respect to α_{out}, defined on Fig. 3.3 right.

The dead load of the cable is accounted for as follows, taking the outwards leaning cable as an example:

$$G_{out} = \gamma_c \cdot A_{out} \cdot l_{out} \tag{3.7}$$

where γ_c is the density of steel (in the unit: [force per length^3]). The cross-section of the cable, A_{out}, is found from:

$$A_{out} = \frac{T_{out}}{\sigma_c} \tag{3.8}$$

where T_{out} is the design cable force in the outwards leaning cable considered due to wind, traffic, dead weight of girder and cable.

T_{out} can now be determined:

$$T_{out} = t_{out}\,\frac{1}{\cos\alpha_{out}} + G_{out}\,\frac{1}{\sin\varphi_{out}}\,\frac{1}{\cos\alpha_{out}}$$

$$= \frac{1}{2}\,\frac{l_{out,\,l}}{h}\,\frac{\frac{1}{2}(b+\lambda)}{b}\left(G + P + \frac{h}{\frac{1}{2}(b+\lambda)}\,U\right)\frac{l_{out}}{l_{out,\,l}} + \frac{\gamma_c}{\sigma_c}\,\frac{l_{out}^{\,2}}{h}\,T_{out} \qquad (3.9)$$

Reducing Eq. (3.9) and solving with respect to T_{out} we find:

$$T_{out} = \frac{\frac{l_{out}}{h}\,\frac{\frac{1}{2}(b+\lambda)}{b}}{1 - \frac{\gamma_c}{\sigma_c}\,\frac{l_{out}^{\,2}}{h}} \cdot \frac{1}{2}\left(G + P + \frac{h}{\frac{1}{2}(b+\lambda)}\,U\right) \qquad (3.10)$$

Eq. (3.10) can be further reduced using the following approximation:

$$\frac{1}{1 - \frac{\gamma_c}{\sigma_c}\,\frac{l_{out}^{\,2}}{h}} = \frac{1 + \frac{\gamma_c}{\sigma_c}\,\frac{l_{out}^{\,2}}{h}}{1 - \left(\frac{\gamma_c}{\sigma_c}\,\frac{l_{out}^{\,2}}{h}\right)^2} \simeq 1 + \frac{\gamma_c}{\sigma_c}\,\frac{l_{out}^{\,2}}{h} \qquad (3.11)$$

because assuming as a reasonable average $l_{out} \sim 2h \sim 240$ m one gets:

$$\left(\frac{\gamma_c}{\sigma_c}\,\frac{l_{out}^{\,2}}{h}\right)^2 = \left(\frac{78.5\cdot 10^3\ N/m^3}{700\cdot 10^6\ N/m^2} \cdot 480\ m\right)^2 = 0.003 \qquad (3.12)$$

The expression for the cable force in the outwards leaning cable finally yields:

$$T_{out} \simeq \frac{l_{out}}{h}\,\frac{\frac{1}{2}(b+\lambda)}{b}\left(1 + \frac{\gamma_c}{\sigma_c}\,\frac{l_{out}^{\,2}}{h}\right) \cdot \frac{1}{2}\left(G + P + \frac{h}{\frac{1}{2}(b+\lambda)}\,U\right) \qquad (3.13)$$

In a similar way one gets for the cable force in the inwards leaning cable:

$$T_{in} \simeq \frac{l_{in}}{h}\,\frac{\frac{1}{2}(b-\lambda)}{b}\left(1 + \frac{\gamma_c}{\sigma_c}\,\frac{l_{in}^{\,2}}{h}\right) \cdot \frac{1}{2}\left(G + P + \frac{h}{\frac{1}{2}(b-\lambda)}\,U\right) \qquad (3.14)$$

Now, the quantity of steel in the stay cables will be determined. Instead of looking at single cables, a continuous system is now considered. The resultant forces G, P and U are substituted by the corresponding uniformly distributed loads over an infinitesimal length along the girder axis, dx. Eq. (3.13) is then written:

$$dT_{out} \simeq \frac{l_{out}}{h} \frac{\frac{1}{2}(b+\lambda)}{b} \left(1 + \frac{\gamma_c}{\sigma_c} \frac{l_{out}^2}{h}\right) \cdot \frac{1}{2}\left(g + p + \frac{h}{\frac{1}{2}(b+\lambda)} u\right) \cdot dx \qquad (3.15)$$

The quantity of cable steel in a single fan, Q_{out}, can now be determined from:

$$dQ_{out} = \gamma_c \cdot dV_{out} = \gamma_c \cdot l_{out} \cdot dA_{out} = \frac{\gamma_c}{\sigma_c} \cdot l_{out} \cdot dT_{out} \qquad (3.16)$$

where dV_{out} is an infinitesimal volume of the continuous fan.

Inserting the expression derived for dT_{out} we obtain:

$$dQ_{out} \simeq \frac{\gamma_c}{\sigma_c} \frac{1}{h} \frac{\frac{1}{2}(b+\lambda)}{b} \frac{1}{2}\left(g + p + \frac{h}{\frac{1}{2}(b+\lambda)} u\right) \cdot \left(l_{out}^2 + \frac{\gamma_c}{\sigma_c} \frac{l_{out}^4}{h}\right) \cdot dx \qquad (3.17)$$

The length of the cable depends on the distance x, counted from the pylon. For instance we have:

$$l_{out} = \sqrt{\left(\frac{1}{2}(b-\lambda)\right)^2 + h^2 + x^2} \qquad (3.18)$$

Inserting the appropriate cable lengths in Eq. (3.17) and integrating from the shortest cables at the pylon (x = 0) to the longest cables (x = a) one gets after some calculations:

$$Q_{out} \approx \frac{\gamma_c}{\sigma_c} \frac{\frac{1}{2}(b+\lambda)}{b} \frac{1}{2} \left(g + p + \frac{h}{\frac{1}{2}(b+\lambda)} u \right) \cdot \left[\frac{1}{5} \frac{\gamma_c}{\sigma_c} a \left(\frac{a}{h}\right)^4 \right.$$

$$+ \frac{1}{3} \left\{ 1 + 2 \frac{\gamma_c}{\sigma_c} \frac{1}{h} \left(h^2 + \left(\tfrac{1}{2}(b-\lambda)\right)^2 \right) \right\} \cdot \left(\frac{a}{h}\right)^3 + \left\{ \frac{\gamma_c}{\sigma_c} h + 1 + 2 \frac{\gamma_c}{\sigma_c} \frac{1}{h} \left(\tfrac{1}{2}(b-\lambda)\right)^2 \right.$$

$$\left. \left. + \frac{1}{h^2} \left(\tfrac{1}{2}(b-\lambda)\right)^2 + \frac{\gamma_c}{\sigma_c} \frac{1}{h^3} \left(\tfrac{1}{2}(b-\lambda)\right)^4 \right\} \cdot \left(\frac{a}{h}\right) \right] \cdot h^2 \qquad (3.19)$$

Eq. (3.19) gives us the quantity of cable steel in a single fan of outwards leaning stay cables out of totally eight such fans. The parameter a is either equal to the length of the side span, a_s , or to half the length of the main span, a_m .

The quantity of cable steel in a single fan of inwards leaning cables is derived in a similar way. The expression yields:

$$Q_{in} \approx \frac{\gamma_c}{\sigma_c} \frac{\frac{1}{2}(b-\lambda)}{b} \frac{1}{2} \left(g + p + \frac{h}{\frac{1}{2}(b-\lambda)} u \right) \cdot \left[\frac{1}{5} \frac{\gamma_c}{\sigma_c} a \left(\frac{a}{h}\right)^4 \right.$$

$$+ \frac{1}{3} \left\{ 1 + 2 \frac{\gamma_c}{\sigma_c} \frac{1}{h} \left(h^2 + \left(\tfrac{1}{2}(b+\lambda)\right)^2 \right) \right\} \cdot \left(\frac{a}{h}\right)^3 + \left\{ \frac{\gamma_c}{\sigma_c} h + 1 + 2 \frac{\gamma_c}{\sigma_c} \frac{1}{h} \left(\tfrac{1}{2}(b+\lambda)\right)^2 \right.$$

$$\left. \left. + \frac{1}{h^2} \left(\tfrac{1}{2}(b+\lambda)\right)^2 + \frac{\gamma_c}{\sigma_c} \frac{1}{h^3} \left(\tfrac{1}{2}(b+\lambda)\right)^4 \right\} \cdot \left(\frac{a}{h}\right) \right] \cdot h^2 \qquad (3.20)$$

3.3.2 Quantity of cable steel in anchor cables

The purpose of arranging anchor cables is to provide a support for the pylon top. Unsymmetrical loading on the girder with respect to the position of the pylon results in forces at the pylon top that will have to be counterbalanced by the anchor cables. Furthermore, as half the length of the main span exceeds the length of a side span, permanent loads results in forces at the pylon top parallel to the bridge axis. These forces have to be transferred to the abutments by

means of anchor cables, otherwise it would require an excessive bending stiffness of the pylon in the longitudinal direction to the bridge axis.

Maximum tension in the anchor cables arises in case of permanent load over the entire length of the bridge and traffic load in the main span only. Wind load is assumed to act with its full intensity over the entire length of the bridge.

The expressions for cable forces derived in the previous Section 3.3.1 "Quantity of cable steel in stay cables" (Eq. (3.15) for the outwards leaning cables and a corresponding expression for the inwards leaning cables) form basis for the design of anchor cables. Only components of stay cable forces parallel to the bridge axis are considered in the design of anchor cables. Vertical components of cable forces delivered at the pylon top are transferred to the base of the pylon by compression in pylon legs. Lateral components are mainly transferred in bending by the pylon. We return to the question of transferring lateral forces later in relation to the pylon and to deformations.

In order to simplify the expressions, the two anchor cables (outwards and inwards leaning) from each side of the pylon are substituted by a single cable anchored at the bridge axis.

Taking into account the dead weight, the cable force in an anchor cable, T_{ac} , can be determined from:

$$T_{ac} \simeq \int_{x=0}^{a_m} \left(\frac{x}{l_{out}} \, dT_{out} + \frac{x}{l_{in}} \, dT_{in} \right) - \int_{x=0}^{a_s} \left(\frac{x}{l_{out}} \, dT_{out,\, g+u} + \frac{x}{l_{in}} \, dT_{in,\, g+u} \right) + \frac{\gamma_c}{\sigma_c} \frac{l_{ac}^{\,2}}{h} T_{ac} \tag{3.21}$$

where dT_{out} is given by Eq. (3.15) and dT_{in} by a similar expression accounting for the geometry of the inwards leaning cables. The terms $dT_{out,\, g+u}$ and $dT_{in,\, g+u}$ account for the reduction of cable force in the anchor cable originating from permanent load and wind but no

traffic load in the side span. After some calculations the expression for T_{ac} yields:

$$
\begin{aligned}
T_{ac} \simeq \Bigg\{ & \frac{\frac{1}{2}(b+\lambda)}{b} \frac{1}{2} \left(g + p + \frac{h}{\frac{1}{2}(b+\lambda)} u \right) \cdot \\
& \left[\frac{1}{2} a_m^{\,2} \left\{ 1 + \frac{\gamma_c}{\sigma_c} \frac{1}{h} \left(\left(\tfrac{1}{2}(b-\lambda) \right)^2 + h^2 \right) \right\} + \frac{1}{4} a_m^{\,4} \frac{\gamma_c}{\sigma_c} \frac{1}{h} \right] \\
& + \frac{\frac{1}{2}(b-\lambda)}{b} \frac{1}{2} \left(g + p + \frac{h}{\frac{1}{2}(b-\lambda)} u \right) \cdot \\
& \left[\frac{1}{2} a_m^{\,2} \left\{ 1 + \frac{\gamma_c}{\sigma_c} \frac{1}{h} \left(\left(\tfrac{1}{2}(b+\lambda) \right)^2 + h^2 \right) \right\} + \frac{1}{4} a_m^{\,4} \frac{\gamma_c}{\sigma_c} \frac{1}{h} \right] \\
& - \frac{\frac{1}{2}(b+\lambda)}{b} \frac{1}{2} \left(g + \frac{h}{\frac{1}{2}(b+\lambda)} u \right) \cdot \\
& \left[\frac{1}{2} a_s^{\,2} \left\{ 1 + \frac{\gamma_c}{\sigma_c} \frac{1}{h} \left(\left(\tfrac{1}{2}(b-\lambda) \right)^2 + h^2 \right) \right\} + \frac{1}{4} a_s^{\,4} \frac{\gamma_c}{\sigma_c} \frac{1}{h} \right] \\
& - \frac{\frac{1}{2}(b-\lambda)}{b} \frac{1}{2} \left(g + \frac{h}{\frac{1}{2}(b-\lambda)} u \right) \cdot \\
& \left[\frac{1}{2} a_s^{\,2} \left\{ 1 + \frac{\gamma_c}{\sigma_c} \frac{1}{h} \left(\left(\tfrac{1}{2}(b+\lambda) \right)^2 + h^2 \right) \right\} + \frac{1}{4} a_s^{\,4} \frac{\gamma_c}{\sigma_c} \frac{1}{h} \right] \Bigg\} \cdot \\
& \frac{\sqrt{(b/2)^2 + h^2 + a_s^{\,2}}}{a_s} \frac{1}{h} \cdot \left(1 + \frac{\gamma_c}{\sigma_c} \frac{(b/2)^2 + h^2 + a_s^{\,2}}{h} \right)
\end{aligned}
\tag{3.22}
$$

The quantity of steel in an anchor cable can then be determined using a similar expression to Eq. (3.16):

$$
Q_{ac} = \gamma_c \cdot V_{ac} = \gamma_c \cdot l_{ac} \cdot A_{ac} = \frac{\gamma_c}{\sigma_c} \cdot l_{ac} \cdot T_{ac} \tag{3.23}
$$

3.3.3 Quantity of steel in pylons

The compressive forces in the vertical pylon legs are due to the vertical component of cable forces (stay and anchor cables) transferred at the pylon top. Maximum compression occurs for permanent as well as variable load on the entire bridge. Taking the vertical component of Eq. (3.15) for the outwards leaning cables and a corresponding expression for the inwards leaning cables and integrating over the length of main span and side span, respectively, and finally adding the vertical component of Eq. (3.22), compression in one pylon leg, C_p, yields:

$$C_p \simeq \int_{x=0}^{a_m} \left(\frac{h}{l_{out}} dT_{out} + \frac{h}{l_{in}} dT_{in} \right) + \int_{x=0}^{a_s} \left(\frac{h}{l_{out}} dT_{out} + \frac{h}{l_{in}} dT_{in} \right) + \frac{h}{l_{ac}} T_{ac} \tag{3.24}$$

Note that for simplicity it has been ignored, that Eq. (3.22) is derived for traffic load in the main span only in order to get maximum force in the anchor cables. Thus the expression for C_p is on the safe side. The explicit expression for C_p is given below, where the force in the anchor cables, T_{ac} , is determined by Eq. (3.22).

$$C_p \simeq \frac{\frac{1}{2}(b+\lambda)}{b} \frac{1}{2} \left(g + p + \frac{h}{\frac{1}{2}(b+\lambda)} u \right) \cdot \left[(a_m + a_s) \cdot \left\{ 1 + \frac{\gamma_c}{\sigma_c} \frac{1}{h} \left(\left(\frac{1}{2}(b-\lambda) \right)^2 + h^2 \right) \right\} + \frac{1}{3} \left(a_m^3 + a_s^3 \right) \frac{\gamma_c}{\sigma_c} \frac{1}{h} \right]$$

$$+ \frac{\frac{1}{2}(b-\lambda)}{b} \frac{1}{2} \left(g + p + \frac{h}{\frac{1}{2}(b-\lambda)} u \right) \cdot \left[(a_m + a_s) \cdot \left\{ 1 + \frac{\gamma_c}{\sigma_c} \frac{1}{h} \left(\left(\frac{1}{2}(b+\lambda) \right)^2 + h^2 \right) \right\} + \frac{1}{3} \left(a_m^3 + a_s^3 \right) \frac{\gamma_c}{\sigma_c} \frac{1}{h} \right]$$

$$+ \frac{h}{l_{ac}} T_{ac} \tag{3.25}$$

According to *Gimsing* (1983) the quantity of material in a vertical pylon leg, Q_p , can be estimated from the following expression, where the dead weight of the pylon itself is taken into account:

$$Q_p \simeq C_p \cdot \left(\exp\left(\frac{\gamma_p}{\sigma_p} h_p\right) - 1\right) \tag{3.26}$$

The total height of the pylon is $h_p = h + 30$ m, where h is the pylon height above bridge deck which is assumed to be placed 30 m above ground, cf. Section 2.2.

Here the pylon is assumed to be constructed in steel, thus $\gamma_p = \gamma_c$. According to *Gimsing* (1983) the limiting stress, σ_p , in the pylon legs subjected to compression generally ranges from 60% to 80% of the design yield stress. Which end of the range that should be chosen depends on transfer of unsymmetrical loading as it is described below.

The cross beam at the pylon top is subjected to compression due to the lateral component of cable forces transferred to the pylon top. Only symmetrical loading at the two sides of the pylon will contribute to compression in the cross beam. An unsymmetrical loading like wind load has to be transferred relaying on the lateral rigidity of the pylon, either in lateral bending of the pylon or by means of prestressed diagonal cables inside the frame, see Fig. 3.4.

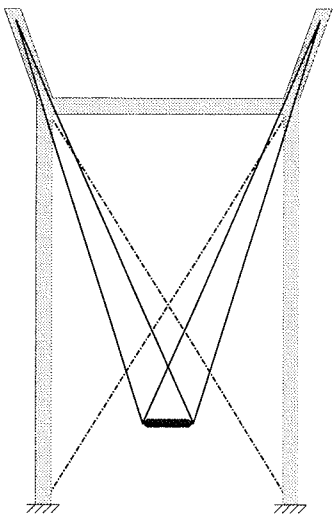

Figure 3.4 *Lateral rigidity of the pylon obtained by adding prestressed diagonals to the frame.*

If no diagonal cables are arranged the limiting stress in the pylon legs due to the compressive normal force, σ_p , should be around 60% of the design yield stress in order to account for stresses due to bending of the frame arising from transfer of unsymmetrical loading. If diagonal cables are added to the frame the limiting stress in the pylon legs due to the compressive normal force can be increased to around 80% of the design yield stress. On the safe side we here assume that the pylon transfers unsymmetrical loading in bending without aid from prestressed diagonal cables. Furthermore, assuming a characteristic yield stress of 350 MPa for the steel used in the pylons, a reasonable estimate on the allowable compressive stress is $\sigma_p \sim 165$ MPa based on the considerations described above.

As already mentioned the cross beam at the pylon top is subjected to compression due to the lateral component of cable forces, whereas unsymmetrical loading is transferred either in lateral bending of the pylon or by prestressed diagonal cables. However, adding prestressed diagonals will increase compression in the cross beam. To account for this possible contribution, the terms involving wind load in the expressions for cable forces are not disregarded when estimating maximum compression, C_{cb} , in the cross beam. The expression for C_{cb} yields:

$$C_{cb} \simeq \int_{x=0}^{a_m} \left(\frac{\frac{1}{2}(b-\lambda)}{l_{out}} dT_{out} + \frac{\frac{1}{2}(b+\lambda)}{l_{in}} dT_{in} \right) + \int_{x=0}^{a_s} \left(\frac{\frac{1}{2}(b-\lambda)}{l_{out}} dT_{out} + \frac{\frac{1}{2}(b+\lambda)}{l_{in}} dT_{in} \right) + \frac{\frac{1}{2}b}{l_{ac}} T_{ac} \tag{3.27}$$

The expression for C_{cb} is given explicitly in Eq. (3.28) below, where T_{ac} is determined from Eq. (3.22).

$$C_{cb} \simeq \frac{1}{h} \frac{\frac{1}{2}(b+\lambda)\ \frac{1}{2}(b-\lambda)}{b} \frac{1}{2} \left(g + p + \frac{h}{\frac{1}{2}(b+\lambda)} u\right) \cdot$$

$$\left[\left(a_m + a_s\right) \cdot \left\{1 + \frac{\gamma_c}{\sigma_c} \frac{1}{h} \left(\left(\tfrac{1}{2}(b-\lambda)\right)^2 + h^2\right)\right\} + \frac{1}{3}\left(a_m{}^3 + a_s{}^3\right) \frac{\gamma_c}{\sigma_c} \frac{1}{h}\right]$$

$$+ \frac{1}{h} \frac{\frac{1}{2}(b+\lambda)\ \frac{1}{2}(b-\lambda)}{b} \frac{1}{2} \left(g + p + \frac{h}{\frac{1}{2}(b-\lambda)} u\right) \cdot$$

$$\left[\left(a_m + a_s\right) \cdot \left\{1 + \frac{\gamma_c}{\sigma_c} \frac{1}{h} \left(\left(\tfrac{1}{2}(b+\lambda)\right)^2 + h^2\right)\right\} + \frac{1}{3}\left(a_m{}^3 + a_s{}^3\right) \frac{\gamma_c}{\sigma_c} \frac{1}{h}\right]$$

$$+ \frac{\frac{1}{2}b}{l_{ac}} T_{ac} \qquad (3.28)$$

The same expression used to estimate the quantity of steel in the pylon legs needed for transferring the compressive force, is applied here for the cross beam:

$$Q_{cb} \simeq C_{cb} \cdot \left(\exp\left(\frac{\gamma_p}{\sigma_p} b\right) - 1\right) \qquad (3.29)$$

where $\gamma_p = \gamma_c$ and $\sigma_p \sim 165$ MPa as previously indicated. The length of the cross beam is equal to the pylon width, b. The fact that the dead weight of the cross beam causes bending, is for simplicity not taken into account.

3.3.4 Deformations

Due to the extremely narrow girder studied in the present project, lateral deflections might become a decisive factor for the design and in determining the optimum inclination of cable planes. In order to fulfil requirements regarding maximum allowable lateral deflections, it might be necessary to choose a wider pylon than indicated by a simple overall structural cost minimization. On the other hand, by choosing a very wide pylon, vertical deflections increase because inclined cables are less suited for transferring vertical loads. In this Section girder deflections at the centre of the main span (i.e. at midspan) are evaluated ignoring bending

stiffnesses of the girder, as already mentioned in Section 3.2 "Basic assumptions and idealizations".

First the vertical deflection is treated. The maximum deflection occurs for traffic load in the main span only. There are two contributions to deflections: One originating from elongation of stay cables in the main span and one from elongation of the anchor cables. The latter can be regarded as a rigid body rotation of the cable system, see for instance *Gimsing* (1983). This is illustrated in Fig. 3.5.

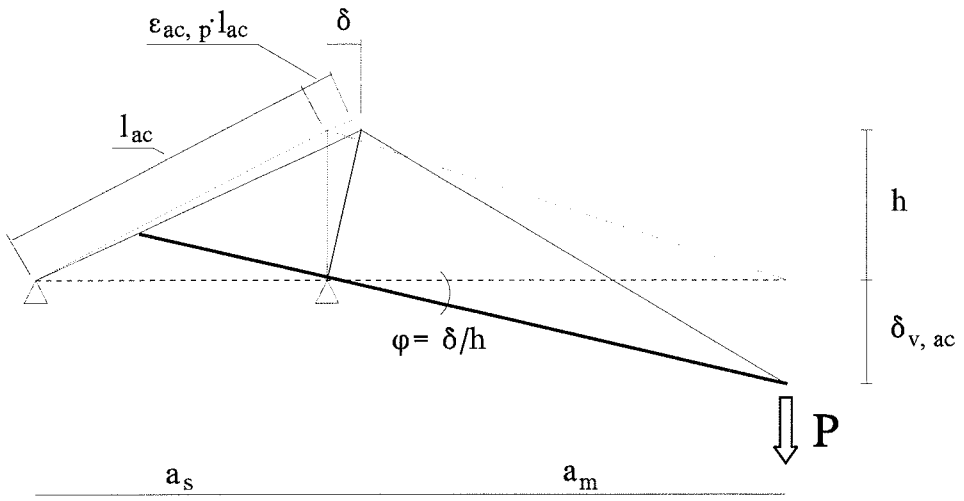

Figure 3.5 *Rotation of the cable system caused by elongation of the anchor cable. Adapted from* Gimsing *(1983).*

For small rotations, the rotation angle is given by:

$$\varphi = \frac{\delta}{h} = \frac{h^2 + a_s^2}{h \cdot a_s} \cdot \varepsilon_{ac,\,p} \tag{3.30}$$

At midspan the vertical deflection due to elongation of the anchor cables equals:

$$\delta_{v,\,ac} = a_m \cdot \varphi \tag{3.31}$$

The strain in the anchor cables is found using the following expression:

$$\varepsilon_{ac,\,p} = \frac{T_{ac,\,p}}{T_{ac}} \cdot \frac{\sigma_c}{E_{eq}} \tag{3.32}$$

where $T_{ac,\,p}$ is the tension in the anchor cable due to traffic in the main span, T_{ac} is the design cable force in the anchor cable as determined in Eq. (3.22), while E_{eq} is the equivalent modulus of elasticity and σ_c the limiting stress in the cables (see Section 3.2 "Basic assumptions and idealizations").

The term $T_{ac,\,p}$ equals:

$$T_{ac,\,p} \simeq \left\{ \frac{\frac{1}{2}(b+\lambda)}{b} \frac{1}{2} p \cdot \left[\frac{1}{2} a_m^{\,2} \left\{ 1 + \frac{\gamma_c}{\sigma_c} \frac{1}{h} \left(\left(\tfrac{1}{2}(b-\lambda) \right)^2 + h^2 \right) \right\} + \frac{1}{4} a_m^{\,4} \frac{\gamma_c}{\sigma_c} \frac{1}{h} \right] \right.$$

$$\left. + \frac{\frac{1}{2}(b-\lambda)}{b} \frac{1}{2} p \cdot \left[\frac{1}{2} a_m^{\,2} \left\{ 1 + \frac{\gamma_c}{\sigma_c} \frac{1}{h} \left(\left(\tfrac{1}{2}(b+\lambda) \right)^2 + h^2 \right) \right\} + \frac{1}{4} a_m^{\,4} \frac{\gamma_c}{\sigma_c} \frac{1}{h} \right] \right\} \cdot$$

$$\frac{\sqrt{(b/2)^2 + h^2 + a_s^{\,2}}}{a_s} \frac{1}{h} \cdot \left(1 + \frac{\gamma_c}{\sigma_c} \frac{(b/2)^2 + h^2 + a_s^{\,2}}{h} \right) \tag{3.33}$$

The vertical deflection due to elongation of stay cables in the main span, $\delta_{v,\,c}$, can be evaluated as follows:

To simplify we consider two cables instead of four per section of anchorage, and these two cables consequently carry half of the load on the girder. A further simplification is obtained by assuming the cables anchored at the girder axis instead of at the tip of the cross beams. The geometry is illustrated on Fig. 3.6.

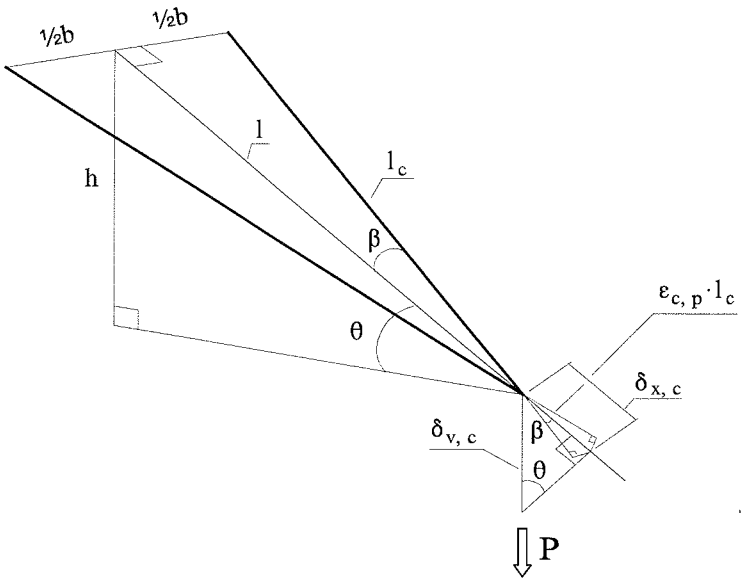

Figure 3.6 *Vertical deflection due to elongation of stay cables.*

The elongation of each stay cable is $\varepsilon_{c,p} \cdot l_c$, where $\varepsilon_{c,p}$ is the strain due to traffic load. This cable elongation is first projected on the direction formed by a line from the centre of the pylon top to the girder section in question. The length of this line is l. The projection, $\delta_{x,c}$ is indicated on Fig. 3.6. Finally the vertical deflection, $\delta_{v,c}$, is found by rotation about a lateral axis at the pylon top. Thus:

$$\cos\beta = \frac{\varepsilon_{c,p}\, l_c}{\delta_{x,c}} = \frac{l}{l_c} \tag{3.34}$$

$$\sin\theta = \frac{\delta_{x,c}}{\delta_{v,c}} = \frac{h}{l} \tag{3.35}$$

Solving Eq. (3.34) with respect to $\delta_{x,c}$ and inserting in Eq. (3.35) we find:

$$\delta_{v,c} = \frac{l_c^2}{h}\,\varepsilon_{c,p} \tag{3.36}$$

Taking the cable force as equal to the force found for the outwards leaning cables, the strain $\varepsilon_{c,p}$ can be written:

$$\varepsilon_{c,\,p} = \frac{dT_{out,\,p}}{dT_{out}} \frac{\sigma_c}{E_{eq}} \tag{3.37}$$

where dT_{out} is given by Eq. (3.15), while $dT_{out,\,p}$ are the terms in Eq. (3.15) involving traffic load only.

The contribution to vertical deflections due to elongation of stay cables finally yields:

$$\delta_{v,\,c} \simeq \frac{p}{g + p + \dfrac{h}{\frac{1}{2}(b+\lambda)}\,u} \frac{l_{out}^{\,2}}{h} \frac{\sigma_c}{E_{eq}} \tag{3.38}$$

where l_{out} is the length of cables at midspan.

The total vertical deflection at midspan due to traffic load thus equals:

$$\delta_v(a_m) = \delta_{v,\,ac} + \delta_{v,\,c} = \frac{a_m}{a_s} \frac{h^2 + a_s^{\,2}}{h} \frac{T_{ac,\,p}}{T_{ac}} \frac{\sigma_c}{E_{eq}} + \delta_{v,\,c} \tag{3.39}$$

where $T_{ac,\,p}$ is given by Eq. (3.33), T_{ac} by Eq. (3.22) and $\delta_{v,\,c}$ by Eq. (3.38).

Now lateral deflections at midspan are evaluated. Lateral deflections are also composed of two contributions: One from change of length of stay cables and one from a rigid body rotation of the cable system about the pylon top. The latter is related to change of forces in the anchor cables.

Because of the inclinations, wind load causes an increase of cable forces in the stay cables anchored at the pylon top in the windward side. Forces due to permanent load in stay cables anchored to the leeward pylon top are decreased. The situation is illustrated in Fig. 3.7.

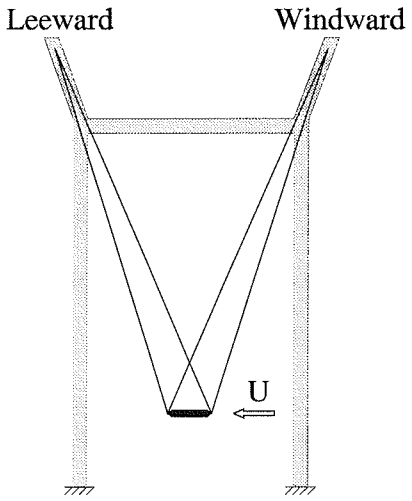

Figure 3.7 *Definition of windward and leeward side of the pylon.*

As a consequence the cable force in the anchor cable to the windward side is increased, while it is decreased in the other side. The increased cable force in the anchor cable causes an elongation and forces the windward side of the pylon top to move towards the main span. In the leeward side the pylon top is forced to displace towards the side span. The situation is illustrated in Fig. 3.8.

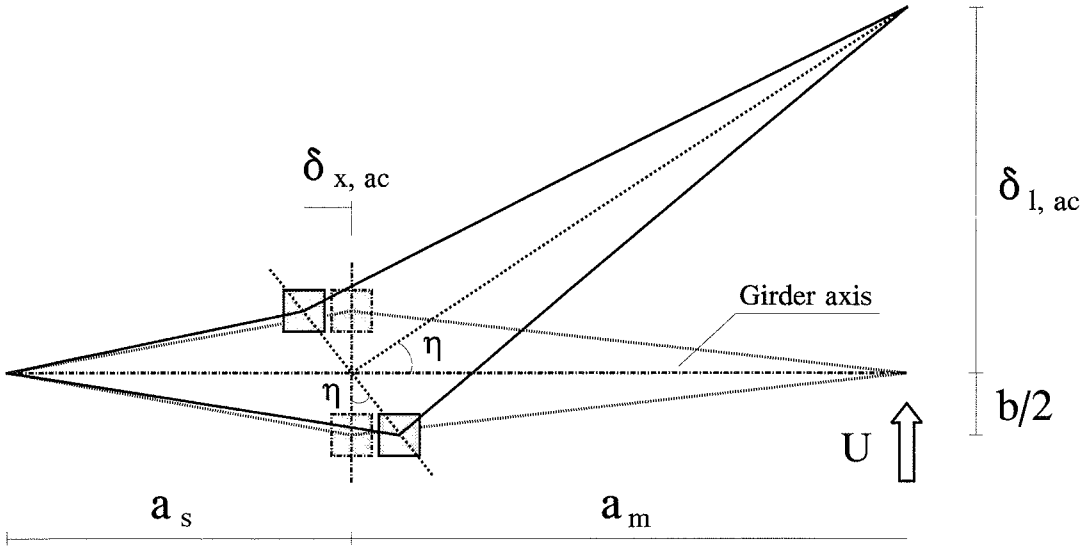

Figure 3.8 *Displacement of pylon top due to change in forces in anchor cables.*

The displacement parallel to the bridge axis of each side of the pylon top is $\delta_{x,\,ac}$, determined by:

$$\tan\eta = \frac{\delta_{x,\,ac}}{b/2} = \frac{\delta_{l,\,ac}}{a_m} \tag{3.40}$$

The change of length of an anchor cable due to wind load is $\varepsilon_{ac,\,u} \cdot l_{ac}$. By projection we find the component parallel to the bridge axis as follows:

$$\delta_{x,\,ac} = \varepsilon_{ac,\,u} \cdot l_{ac} \frac{a_s}{l_{ac}} = \varepsilon_{ac,\,u} \cdot a_s \tag{3.41}$$

The strain in the anchor cable due to wind load is found from:

$$\varepsilon_{ac,\,u} = \frac{T_{ac,\,u}}{T_{ac}} \frac{\sigma_c}{E_{eq}} \tag{3.42}$$

where $T_{ac,\,u}$ is the tension in the anchor cable due to wind load given by:

$$\begin{aligned} T_{ac,\,u} \simeq & \left\{ \frac{\frac{1}{2}(b+\lambda)}{b} \frac{1}{2} \frac{h}{\frac{1}{2}(b+\lambda)} u \cdot \right. \\ & \left[\frac{1}{2}\left(a_m^{\,2} - a_s^{\,2}\right) \cdot \left\{1 + \frac{\gamma_c}{\sigma_c} \frac{1}{h}\left(\left(\tfrac{1}{2}(b-\lambda)\right)^2 + h^2\right)\right\} + \frac{1}{4}\left(a_m^{\,4} - a_s^{\,4}\right) \frac{\gamma_c}{\sigma_c} \frac{1}{h} \right] \\ & + \frac{\frac{1}{2}(b-\lambda)}{b} \frac{1}{2} \frac{h}{\frac{1}{2}(b-\lambda)} u \cdot \\ & \left. \left[\frac{1}{2}\left(a_m^{\,2} - a_s^{\,2}\right) \cdot \left\{1 + \frac{\gamma_c}{\sigma_c} \frac{1}{h}\left(\left(\tfrac{1}{2}(b+\lambda)\right)^2 + h^2\right)\right\} + \frac{1}{4}\left(a_m^{\,4} - a_s^{\,4}\right) \frac{\gamma_c}{\sigma_c} \frac{1}{h} \right] \right\} \cdot \\ & \frac{\sqrt{(b/2)^2 + h^2 + a_s^{\,2}}}{a_s} \frac{1}{h} \cdot \left(1 + \frac{\gamma_c}{\sigma_c} \frac{(b/2)^2 + h^2 + a_s^{\,2}}{h}\right) \end{aligned} \tag{3.43}$$

The lateral deflection at midspan due to change of forces in the stay cables, $\delta_{l,\,c}$, can be evaluated using a similar procedure as applied for vertical deflections due to traffic. The situation is illustrated in Fig. 3.9.

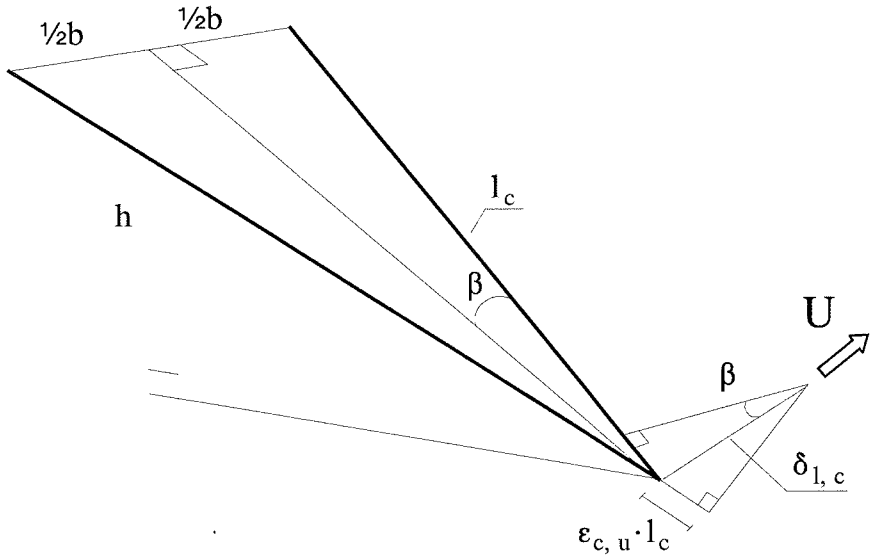

Figure 3.9 *Lateral deflection due to change of forces in stay cables.*

The lateral displacement due to elongation of one stay cable and shortening of the other equals:

$$\sin\beta = \frac{\varepsilon_{c,\,u} \cdot l_c}{\delta_{l,\,c}} = \frac{b/2}{l_c} \tag{3.44}$$

Thus

$$\delta_{l,\,c} = \varepsilon_{c,\,u} \cdot \frac{l_c^2}{b/2} \tag{3.45}$$

Taking the cable force equal to the force found for the inwards leaning cables, because these transfer the largest part of the wind load, $\varepsilon_{c,\,u}$ can be written:

$$\varepsilon_{c,\,u} = \frac{dT_{in,\,u}}{dT_{in}} \frac{\sigma_c}{E_{eq}} \tag{3.46}$$

The contribution to lateral deflections due to change of length of the stay cables finally yields:

$$\delta_{l,\,c} \simeq \frac{\frac{h}{\frac{1}{2}(b-\lambda)}\,u}{g + p + \frac{h}{\frac{1}{2}(b-\lambda)}\,u} \frac{l_{in}^{\,2}}{b/2} \frac{\sigma_c}{E_{eq}} \tag{3.47}$$

where l_{in} is the length of cables at midspan.

The total lateral deflection at midspan thus equals:

$$\delta_l\,(a_m) = \delta_{l,\,ac} + \delta_{l,\,c} = \frac{a_m}{b/2} \cdot a_s \cdot \frac{T_{ac,\,u}}{T_{ac}} \frac{\sigma_c}{E_{eq}} + \delta_{l,\,c} \tag{3.48}$$

where $T_{ac,\,u}$ is given by Eq. (3.43), T_{ac} by Eq. (3.22) and $\delta_{l,\,c}$ by Eq. (3.47).

3.4 Parametric studies

The expressions derived in the previous Section 3.3 "Analytical analyses" will now be used for parametric studies. These studies focus on the overall geometry of the spatial cable system, i.e. the inclination of cable planes described by the pylon height above deck, h, and the distance between the two anchor zones at the pylon top (referred to as "pylon width"), b.

3.4.1 Material cost

The first part of the parametric studies deals with the overall material cost of the structure. Consequently we need to add quantities of cable steel in stays and anchor cables to quantities of steel in pylons. In order to investigate if optimum geometry of the spatial cable system is sensitive to the ratio between unit price of cables (mounted and protected) and of pylon (erected), a parametric study on the influence of this ratio, r, is carried out.

When comparing material cost it is convenient to normalize with respect to a reference value. We choose a reference geometry of the cable system having a pylon height above deck of 120 m, corresponding to what is found as optimum for a traditional cable-stayed bridge with an 800 m main span. The reference pylon width is set to 60 m giving the cable planes a lateral inclination of 1:4 (in average of outwards and inwards leaning cables). As mentioned in Section 3.2, the contribution from the girder is assumed to be invariable to the cable system geometry and is thus not accounted for.

The parametric study on sensitivity with respect to the ratio of unit prices between cable steel and steel in pylon is shown in Fig. 3.10.

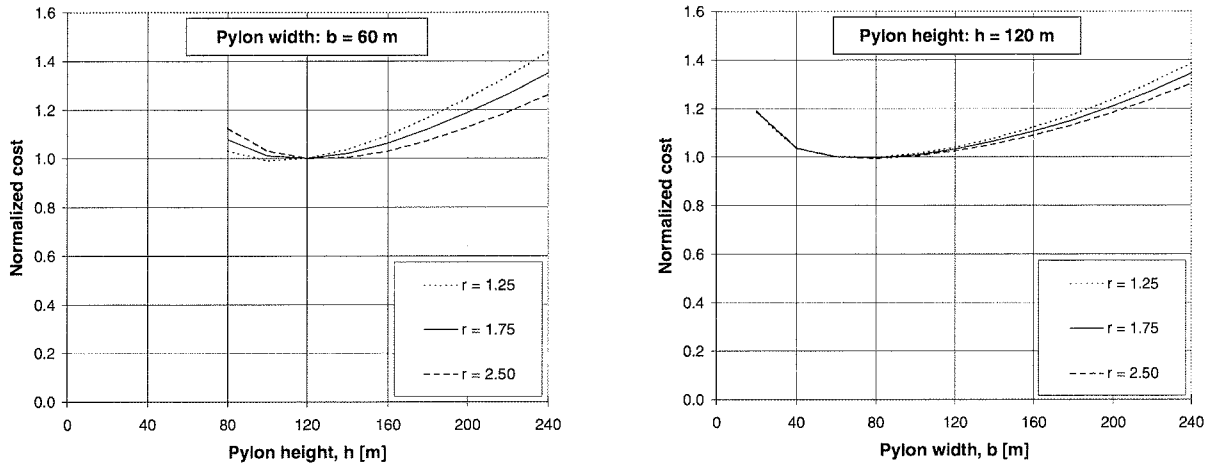

Figure 3.10 *Normalized structural cost as a function of pylon height (left) and pylon width (right) for three different ratios, r, between price of mounted cable and erected pylon.*

The parametric study illustrated in Fig. 3.10 comprises three ratios of price: r = 1.25, r = 1.75 and r = 2.50. These have been selected according to *Gimsing* (1983) and are believed to cover the price range found in practice. As it appears from Fig. 3.10 the price ratio only slightly influences the optimization, especially regarding the pylon width (Fig. 3.10 right). The pylon height is somewhat more sensitive towards choice of price ratio, but bearing in mind the simplifications and approximations made during the analytical analyses the apparent sensitivity

is within the accuracy of the analytical expressions. When evaluating material cost, a reasonable estimate on the accuracy is that differences in normalized cost should be in the order of 10%, if these are to be regarded as being of significance.

In this connection it should be recalled, that the pylon width is defined as the distance between the two anchor zones at the pylon top. When comparing pylon height with pylon width in order to evaluate inclination of cable planes it is thus half the pylon width that should be related to pylon height.

In the following parametric studies the price ratio is fixed to r = 1.75. The next parameter to evaluate is the pylon height, h. In Fig. 3.11 the normalized cost is shown as a function of pylon height for five different pylon widths. Inclination of cable planes in the lateral direction, b/2 : h, ranges from 1:12 to 1:0.67. Optimum pylon height appears to be fairly invariable towards pylon width. As it is expected optimum pylon height for a pylon supporting a spatial cable system does not differ from what is found for a pylon supporting a traditional plane cable system. This is due to the fact, that choice of pylon height is mainly governed by considerations related to transfer of vertical loads. Vertical loads on the bridge girder are of course the same no matter the cable system.

A reasonable choice for the pylon height above deck seems to be around h = 120 m. In Fig. 3.12 the normalized cost is shown as a function of pylon width for five different pylon heights. In this figure inclination of cable planes in the lateral direction, b/2 : h, ranges from 1:9 to 1:2.4. For a pylon height in the order of 100 m - 140 m, as determined above, optimum pylon width seems to range from 40 m to 120 m. This leads to an average lateral inclination of cable planes between 1:6 and 1:2. In this rather wide range normalized cost varies less than 10%. A final choice of pylon width will therefore be based on an evaluation of deflections.

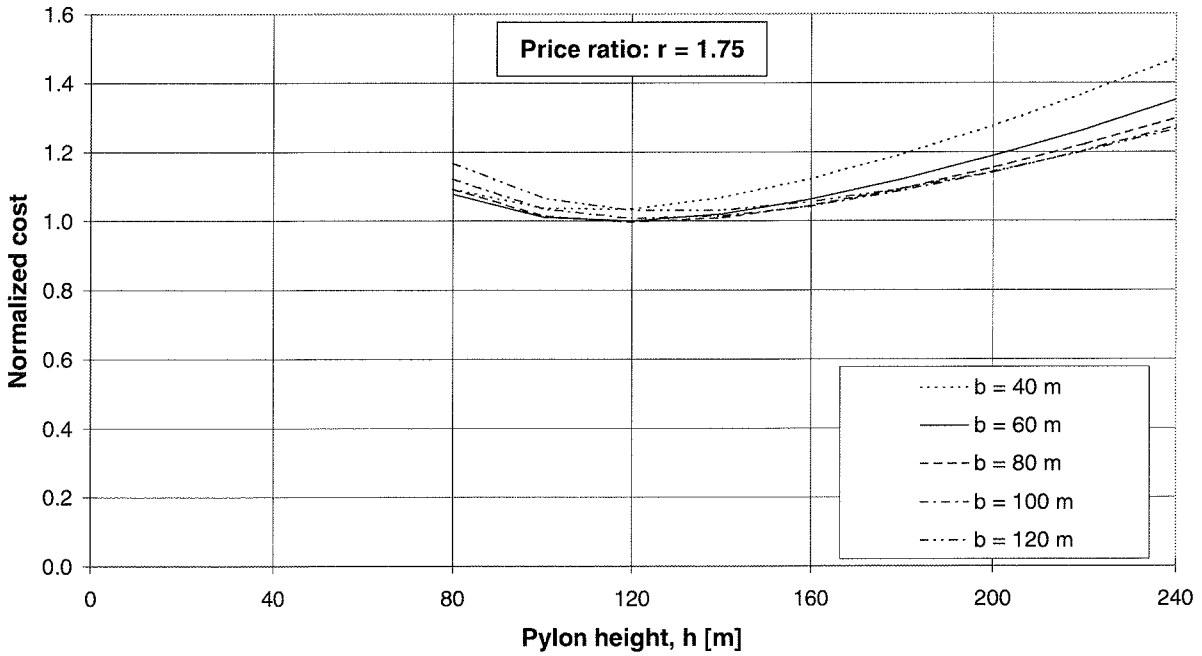

Figure 3.11 *Normalized structural cost as a function of pylon height.*

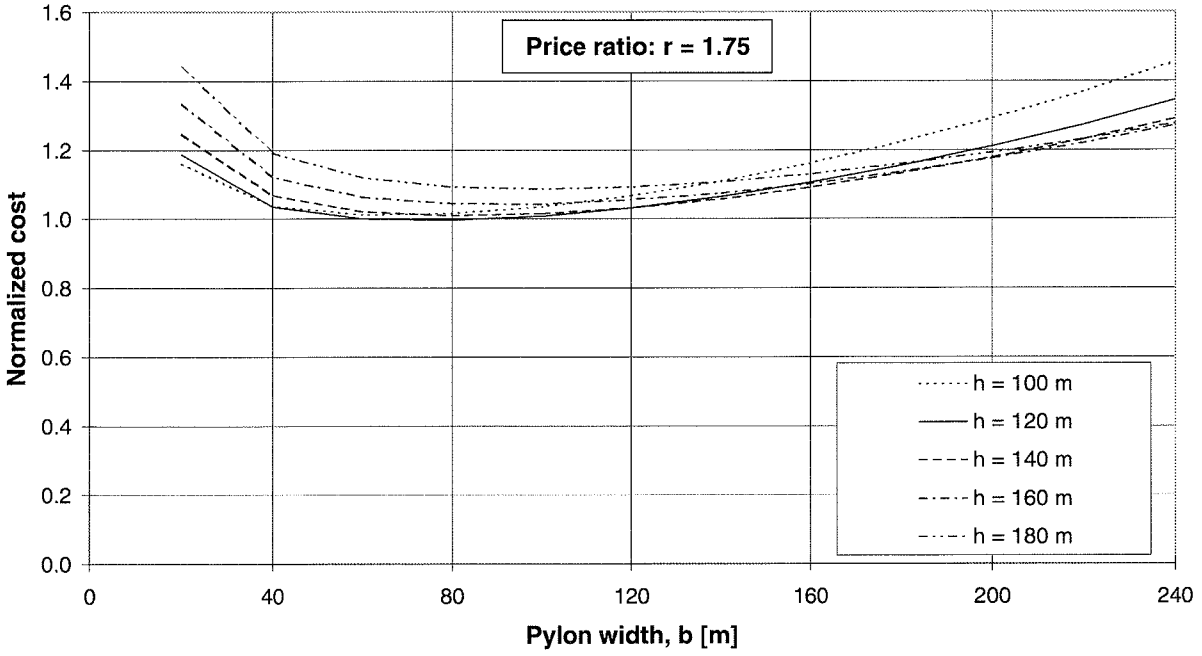

Figure 3.12 *Normalized structural cost as a function of pylon width.*

Before turning to the parametric studies on deflections attention should be drawn to Fig. 3.13 and 3.14. On these plots of normalized material cost both relative contributions from cables and pylon structures are shown as well as their sum. Near the reference geometry of the spatial cable system (h = 120 m, b = 60 m), which is minimizing structural cost fairly, stay and anchor cables count for 60% of the total cost of cable system and pylon structures. As pylon height is increased, the relative cost of pylon structures increases quite steeply (Fig. 3.13), thus the choice of pylon height from a criterion of material cost minimization for the total structure is very much governed by the cost of pylon structures. In contrast to this, the relative contributions from cable system and from pylons are fairly invariable to variations in pylon width, Fig. 3.14. Actually the pylon should be very wide (more than 210 m) before the material needed for the cross beam at the pylon top makes pylon structures more expensive than the cable system. For a fixed pylon height of 120 m, the cross beam account for less than 5% of the cost of the pylon structure when the pylon width ranges from 20 m to 60 m, whereas the cross beam accounts for more than 40% when the pylon width exceeds 210 m.

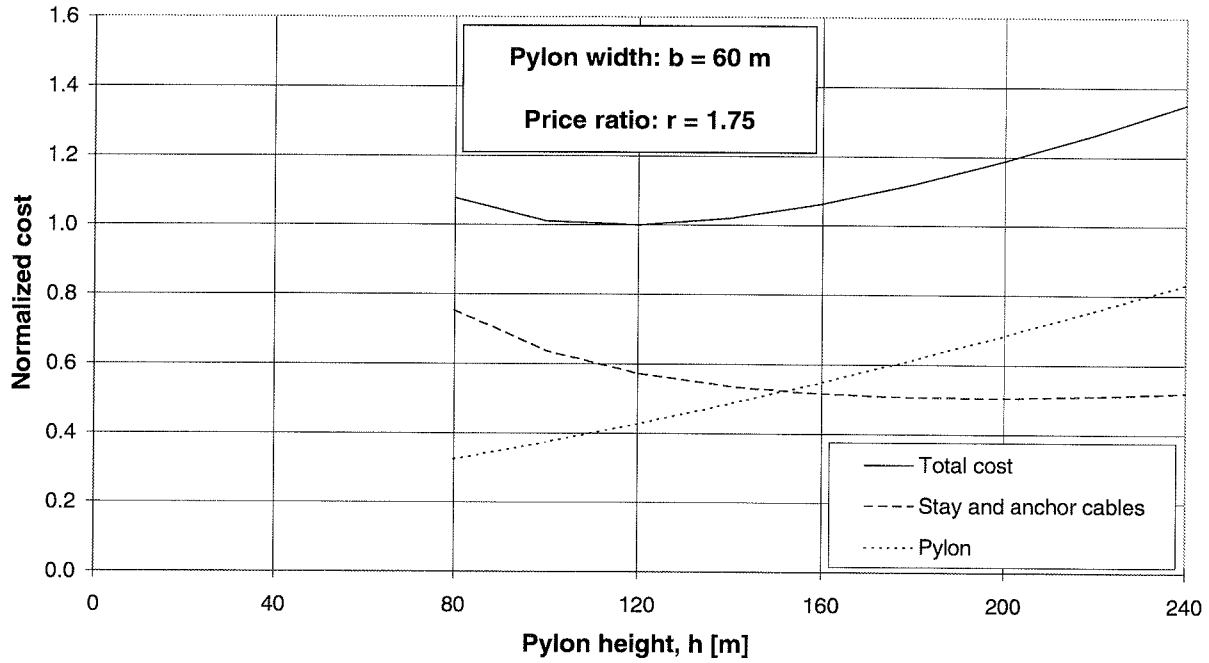

Figure 3.13 *Total cost of structure, relative contributions from stay and anchor cables as well as from pylon as a function of pylon height.*

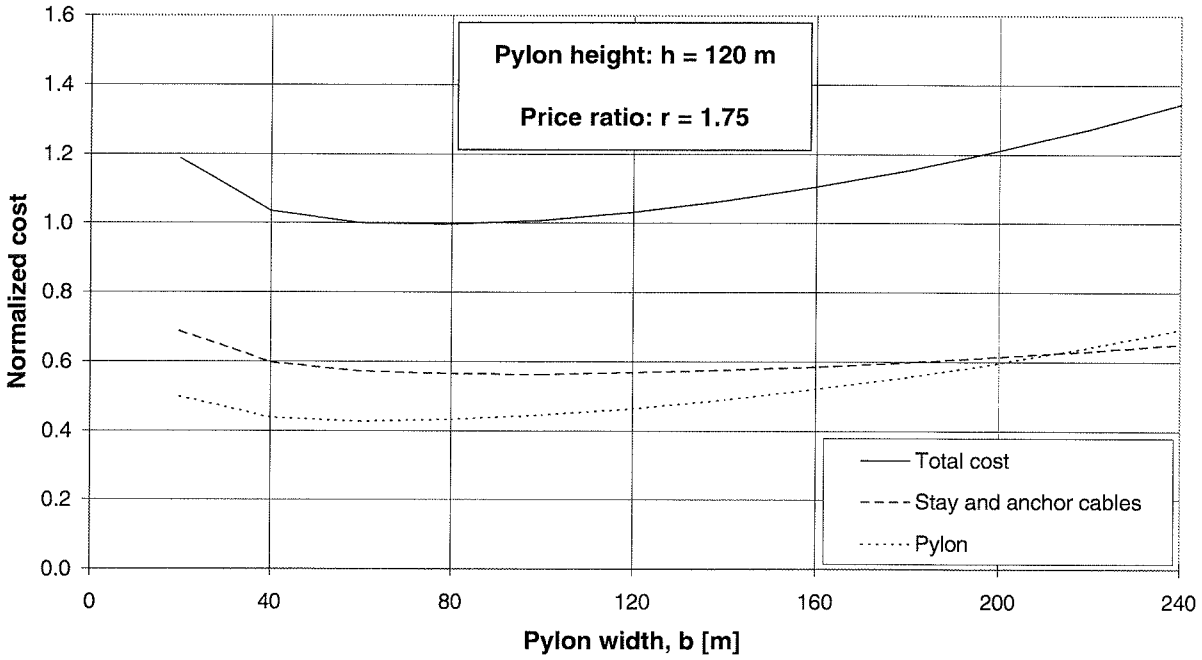

Figure 3.14 *Total cost of structure, relative contributions from stay and anchor cables as well as from pylon as a function of pylon width.*

3.4.2 Deflections

The second part of the parametric studies deals with lateral and vertical deflections as functions of pylon height, h, and pylon width, b. Throughout the parametric studies one of the two parameters pylon height or pylon width is fixed to its reference value, i.e. h = 120 m or b = 60 m. As found in the previous Section 3.4.1 this is a reasonable choice according to material cost optimization. On the following plots of deflections, contributions from stay cables and anchor cables are shown both separately and together with their sum.

In Fig. 3.15 lateral deflections due to wind load are shown as function of pylon width. The excessive deflections for small values of the pylon width are due to the way analytical expressions have been derived. In the analytical analyses it is assumed that cables actually have an inclination in the lateral direction to allow lateral forces to be transferred. If pylon width is small it takes a large cable force to obtain a certain lateral component and thus lateral deflections grow excessively. In case of a small value of b, the assumption of neglecting the

lateral bending stiffness of the girder leads to a very inaccurate description of lateral deflections, because the bending stiffness of the girder exceeds the stiffness of the lateral elastic support offered by the cable system. For large values of b the assumption of neglecting the bending stiffness of the girder is well justified, since the lateral stiffness of the structural system is dominated by the stiffness of the cable system. As it appears from Fig. 3.15 lateral deflections decrease rapidly when the pylon width is increased, and from a pylon width of b = 120 m no significant reduction of lateral deflections is obtained by increasing pylon width further. We will return to the lateral deflections as a function of pylon width in the end of this Section 3.4.2.

In Fig. 3.16 vertical deflections due to traffic are shown as function of pylon width for the reference pylon height of h = 120 m. Vertical deflections are only slightly increased when the pylon width is increased. The increase in vertical deflections is due to the fact that for a fixed pylon height it takes a larger cable force to transfer a certain vertical load, when cables are inclined in the lateral direction to the bridge axis. The contribution to vertical deflections from elongation of stay cables is of the same order of magnitude as from the rotation of the cable system due to an elongation of anchor cables.

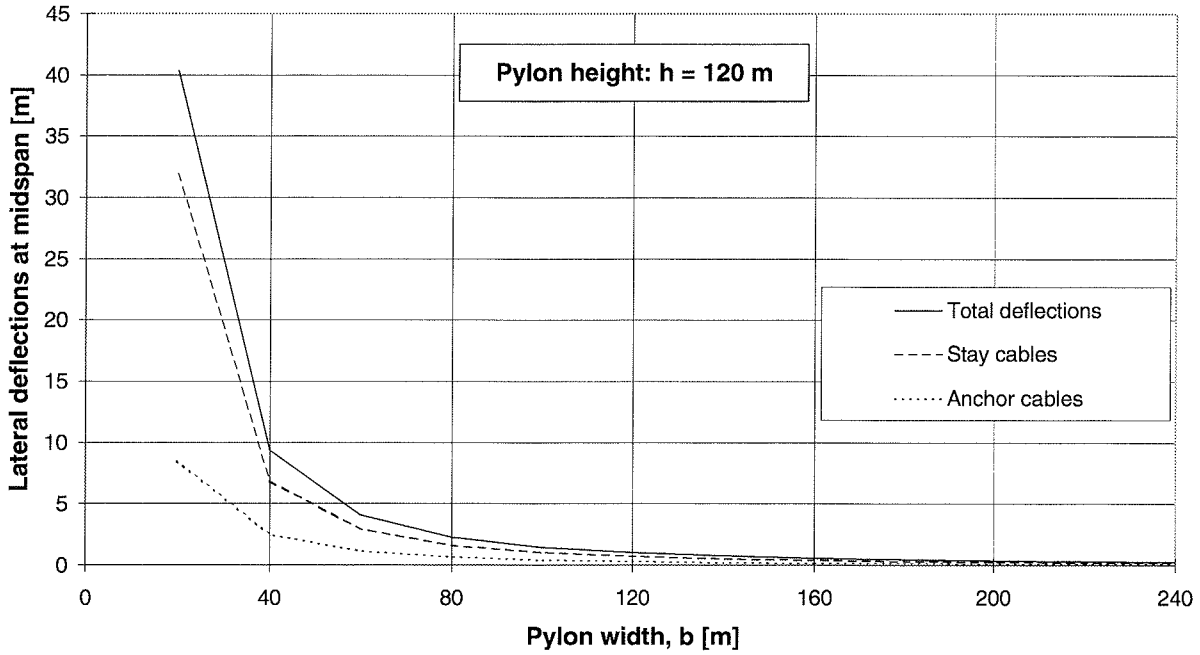

Figure 3.15 *Lateral deflections due to wind load as a function of pylon width. Pylon height fixed to h = 120 m.*

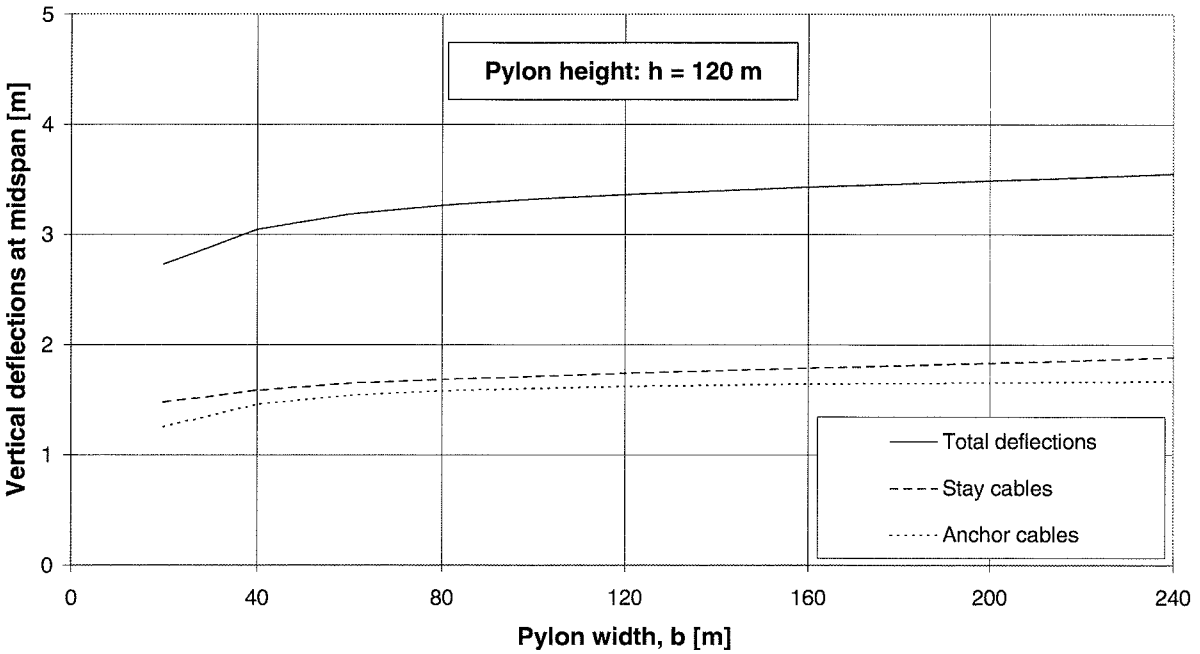

Figure 3.16 *Vertical deflections due to traffic in main span as a function of pylon width. Pylon height fixed to h = 120 m.*

In order to investigate the variation of deflections as a function of pylon height, lateral deflections due to wind are plotted in Fig. 3.17 while vertical deflections due to traffic are shown in Fig. 3.18 in both cases as functions of pylon height.

Both contributions to lateral deflections, i.e. from stay cables and from a rotation of the pylon top due to change of forces in anchor cables, vary almost linearly with the pylon height. The contribution from stay cables is two to three times the contribution from anchor cables.

With regard to vertical deflections due to traffic these of course decrease when pylon height is increased, since cables become more vertical and thus more suited for transferring vertical load. For a pylon height of h = 120 m the vertical deflection at midspan is approximately 3 m. In order to reduce the vertical deflection to 2 m, pylon height will have to be doubled. So a considerable deviation from optimum pylon height according to material cost minimization has to be accepted, if one wishes to reduce vertical deflections by increasing the pylon height.

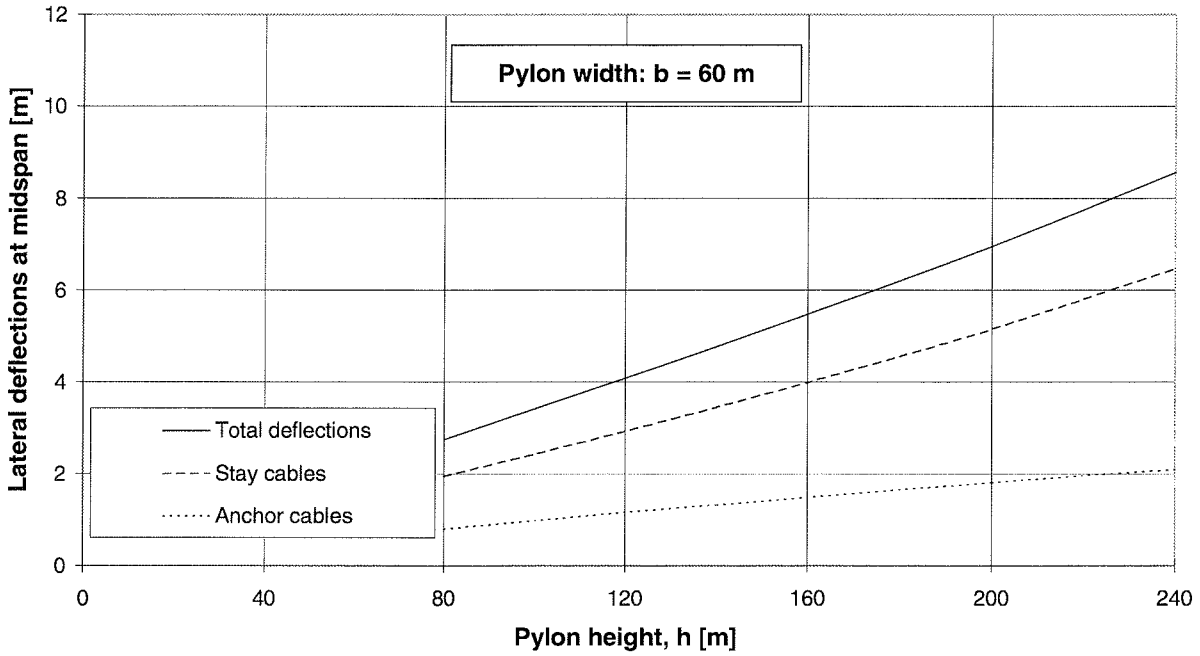

Figure 3.17 *Lateral deflections due to wind load as a function of pylon height. Pylon width fixed to b = 60 m.*

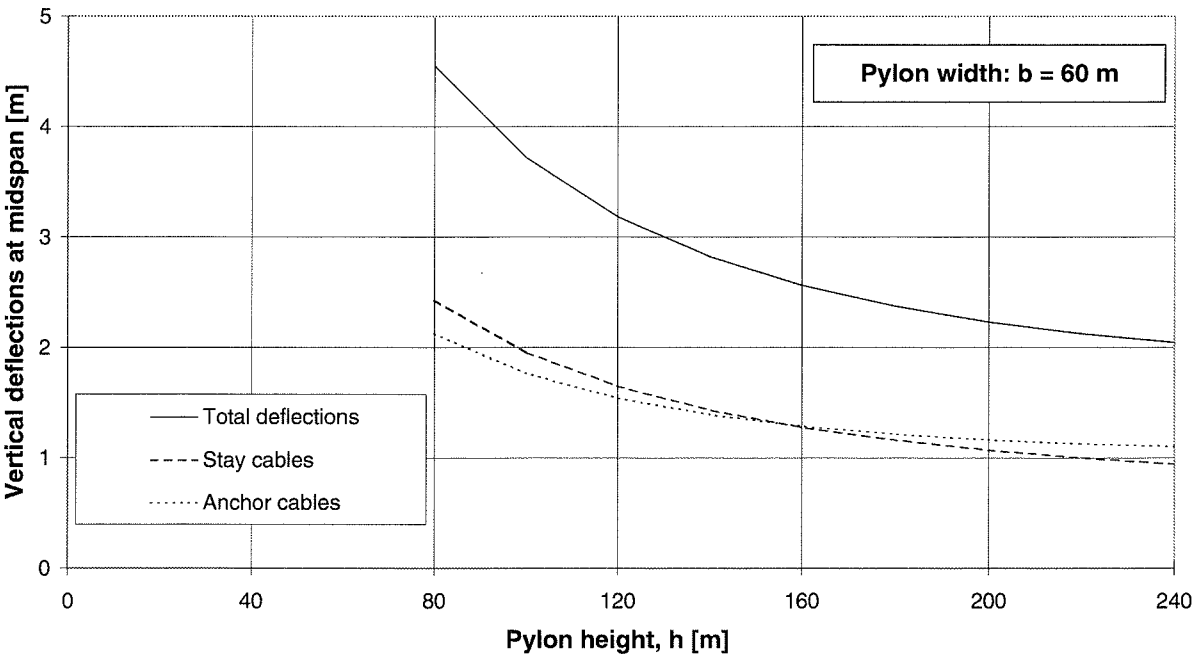

Figure 3.18 *Vertical deflections due to traffic in main span as a function of pylon height. Pylon width fixed to b = 60 m.*

Finally let us return to the lateral deflections due to wind load as a function of pylon width. These were shown in Fig. 3.15, and are plotted again in Fig. 3.19 this time omitting the smaller values of pylon width leading to excessive lateral deflections. As already mentioned the contribution from stay cables is approximately twice the contribution from anchor cables.

When doubling the pylon width from b = 40 m to b = 80 m lateral deflections are reduced by a factor of four from 9.5 m, which exceeds the width of the bridge deck, to 2.5 m approximately. For b = 120 m the total lateral deflection at midspan is 1 m. So according to this estimate on deflections a large gain concerning reduction of lateral deflections is obtained by choosing a pylon width in the range of b = 60 m to b = 120 m.

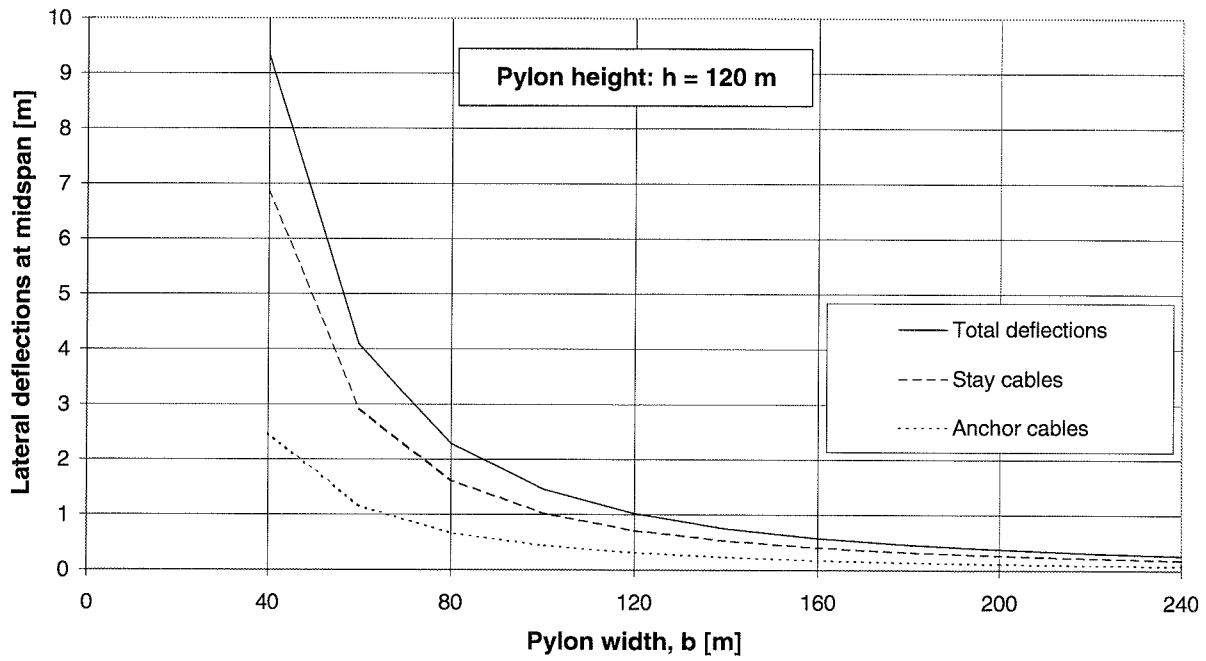

Figure 3.19 *Lateral deflections due to wind load as a function of pylon width. Pylon height fixed to h = 120 m.*

3.5 Conclusions on analytical analyses and parametric studies

In the previous Section 3.4 parametric studies were carried out on the structural cost and deflections at midspan as functions of the overall geometry of the cable system. Also the influence of the ratio between unit price of mounted cable steel and of erected pylon was investigated, but was found to be insignificant. In the present Section we conclude on the parametric studies and choose a final geometry of the spatial cable system to be used throughout the numerical analyses.

According to a material cost minimization pylon height should be around h = 120 m as would be expected for a corresponding traditional cable-stayed bridge with vertical cable planes. This leads to 3 m vertical deflection at midspan for traffic load. According to the recommendations by *Vejdirektoratet* (1984) vertical deflections should not exceed 1/400 of the span length, thus 2 m in our prototype taking the span length equal to the main span. Since the reduction of deflections due to the bending stiffnesses of girder and pylons have been omitted, the estimated vertical deflections for a pylon height of h = 120 m seem acceptable.

The material cost minimization indicated a pylon width within the range 40 m - 120 m. From an evaluation of lateral deflections it can be concluded that the pylon should be wider than 60 m, if a significant reduction of lateral deflections due to inclination of cable planes is to be achieved. The total lateral deflections due to wind load are approximately 4 m for a pylon width of b = 60 m. No guidelines concerning allowable lateral deflections are found in *Vejdirektoratet* (1984), so we adapt the restriction of 1/400 of the span length that is recommended for vertical deflections. In the present Chapter 3 when estimating deflections, the contribution from the bending stiffness of the girder has been neglected. Since bending stiffness of the girder for lateral bending is 8 times the bending stiffness for vertical bending, this is expected to reduce lateral deflections significantly when taken into account in the FE-analyses in Chapter 5. Consequently it is decided to choose a pylon width in the lower end of the range indicated by the parametric studies in order to keep pylon structures as close to common design of the present as possible. Throughout the remaining part of the studies on

the full-scale prototype bridge the pylon width is fixed to b = 60 m. The average lateral inclination of cable planes thus equals 1:4.

In the parametric studies of Section 3.4 the influence of three parameters has been investigated: Pylon height, pylon width and price ratio between cable system and pylon structure. The result in form of an optimized overall geometry of the spatial cable system depends on values assigned to other parameters not subjected to a parametric study but forming part of the expressions investigated in the present parametric studies. These are for instance the ratio between intensity of lateral and vertical loads, the ratio between intensity of permanent and variable loads, length of spans and ratio between main and side span length etc. From the analytical expressions derived in Section 3.3 it is a simple matter to investigate other prototype bridges with spatial cable systems and to investigate the influence of other parameters than the ones that have been in focus in the present project.

Chapter 4

4. FINITE ELEMENT MODELLING AND DEAD LOAD GEOMETRY

4.1 Introduction

In this Chapter FE-modelling of the chosen prototype bridge is described (Section 4.2). In the following Section 4.3 a new method for controlling the dead load geometry is presented. This method allows cable dimensions and dead load geometry to be determined in the same operation. Actual cable dimensions of the four spatial cable systems are determined in Section 4.4. Finally, in Section 4.5 possible stability problems related to compression in the girder are introduced.

4.2 FE-modelling

The FE-modelling carried out in the present project has been performed using the commercial LUSAS Finite Element System by FEA, Ltd. For further information see *LUSAS* (1993).

The geometry of the three-dimensional FE-model corresponds to the description of the

prototype bridge in Chapter 2. The structural features of girder and pylons are listed in Tab. 2.2 and Tab. 2.3, respectively. Cable dimensions are given in Section 4.4. In the main span there are 40 sections of cable anchorage while there are 12 in each side span plus the anchor cables, see Fig. 4.1. The cables are assumed to be arranged in a pure fan system.

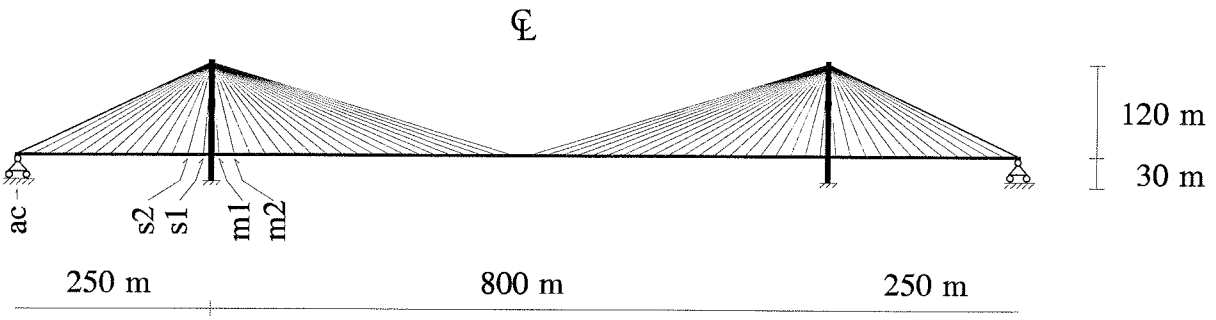

Figure 4.1 *Definition of dimensions and terms used for the FE-model of prototype bridge.*

The sections of cable anchorage are called m1, m2 etc. for the main span and s1, s2 etc. for the side spans counting from the pylon. The term "ac" refers to the anchor cables.

All structural members are modelled by the same type of beam elements, namely the BS4 element, see *LUSAS* (1993). These elements are three-dimensional beam elements for which shearing deformations are excluded. An internal node makes it possible to accommodate for an initially curved beam axis, though we here only apply straight beam members. The end nodes have six degrees of freedom: Three displacements and three rotations. The midlength node has two degrees of freedom: A relative displacement along the beam axis and a relative rotation about the beam axis. The variation of axial force, moments and torsion along the length of the beam element can be regarded as linear.

For the cables, modelled by one beam element each, these are assigned a very low bending stiffness compared to the other structural elements. In the FE-model cross beams at the girder are cantilevered 6 m from the girder axis, while in the prototype they are only cantilevered

2 m from the edge of the steel box. Consequently, the elements for the cross beams are assigned a fictitiously high bending stiffness in order to suppress deformations in these elements. The girder consists of one beam element between each section of cable anchorage. For the pylon legs five beam elements have been used, while there are three beam elements in the cross beam at the pylon top. For cable system a) the FE-model of the entire prototype bridge (i.e. without making use of the symmetric geometry of the bridge) consists of 487 beam elements and 713 element nodes plus 73 direction nodes defining local axes of the elements. Cable systems b), c) and d) only have half the number of cables compared to system a), thus in these cases FE-models consist of 355 beam elements and 581 element nodes plus the 73 direction nodes. A sketch of the connection between girder, cross beams and cables is shown in Fig. 4.2.

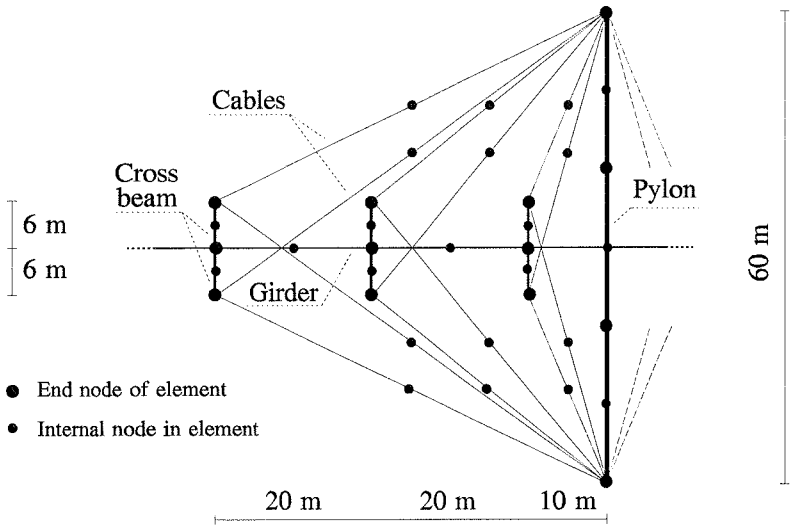

Figure 4.2 *Plan of connection between elements in FE-model.*

At the abutments the end nodes of the beam elements forming the girder are restrained against lateral and vertical displacement as well as torsion, whereas it is free to rotate about the two other axes and to displace in the longitudinal direction. Due to the very rigid cross beams it has not been necessary to supply the nodes in the FE-model, where anchor cables are attached to the cross beams, with supports. The girder passes freely at the pylons.

A linear elastic material model is used for all structural members. Sag effects are accounted for by assigning individual equivalent - tangent or secant - moduli of elasticity to the elements modelling cables. For the dead load situation tangent moduli corresponding to the chosen stress for permanent load are applied. For the other load cases involving variable load, appropriate secant moduli are utilized. Applying secant moduli implies an iteration before the correct stress level in the cables is found.

The loads considered in the present study have been described in Section 2.6. The different types of FE-calculations performed are: Linear static, eigenvalue buckling and geometrical nonlinear analyses. These will be described in detail in Chapter 5.

4.3 Dead load geometry

First of all we need some preliminary dimensions of the cables. These can be obtained from analytical analyses as the ones described in Section 3.3.

Then a dead load stress in the cables, σ_g, is chosen. The choice is based on the ratio between permanent and variable loads, and it usually ranges from 400 MPa to 550 MPa. In connection with a light steel girder a value near the lower end of the range is appropriate, while a heavier concrete girder demands for a higher dead load stress in the cables.

Now, the method to determine cable dimensions and dead load geometry will be described.

The basic principle is to make use of the fact, that for permanent load mainly axial forces act in the system. In order to suppress deformations and thus displacements for permanent load all axial stiffnesses of the structural members are increased by the same factor. Bending stiffnesses have to be correct otherwise the structural behaviour will be altered. The girder for instance would transfer dead load in bending instead of by tension in the cables. Since all

axial stiffnesses have been increased by the same factor, distribution of axial forces in the structural system is correct. In order to avoid numerical problems in the FE-calculations it has been found appropriate to increase axial stiffnesses by a factor of 10^2 to 10^3. This also results in an efficient support of the pylon top due to the very stiff anchor cables.

The initial geometry of the FE-model corresponds to the desired geometry for permanent loads. In our case this means that the girder is horizontal, but it is also possible to specify a camber. Due to the excessive axial stiffnesses there will be practically no deflections due to permanent load. Axial forces in the system as found by the FE-calculation are the correct forces, and we just need to divide by the correct cross sectional areas of the cables to find the dead load stress. If it does not equal the chosen σ_g, the cross sectional area of the cable in question (or, alternatively, of the neighbouring cables) has to be changed and a new calculation carried out. Otherwise the design of cables is completed. The dead load geometry corresponds to the initial geometry. This can be checked by assigning initial compressive strains corresponding to the dead load stress to the cables. All structural elements now have their correct axial stiffness. When permanent loads are applied to this system, practically no deflections from the initial geometry occur.

The procedure to determine cable dimensions and dead load geometry is summarized in Scheme 4.1 below:

1) Preliminary cable dimensions.

2) Choose target dead load stress σ_g.

3) Initial geometry equals desired geometry for permanent load.

4) Increase all axial stiffnesses by a factor of 10^2 - 10^3.

5) Apply permanent load.

6) Find actual dead load stresses from cable forces divided by the correct cross sectional areas.

7) Repeat steps 3) through 6) changing cross sectional areas of cables until an adequate agreement between actual and chosen target dead load stresses is obtained. When actual and target dead load stresses are in agreement, design of cables is completed.

8) Establish permanent load situation by assigning initial compressive strains corresponding to dead load stresses to the cables. Axial stiffnesses are correct. Apply permanent load.

Scheme 4.1 *Design of cables and controlling of dead load geometry, new method.*

In the new method described above, control of dead load geometry forms an integrated part of the process to determine cable dimensions. Thus only one iteration procedure is needed. In contrast to this traditional methods to design cables and control the dead load geometry involve two iterations. When cable dimensions have been found using a particular design criterion (first iteration procedure), permanent loads are applied to the system having the correct axial stiffnesses. This results in deflections. These deflections are subtracted from the node coordinates of the original system. In this way a new initial geometry of the system is defined. However, when permanent loads are applied to this new system, the girder will not return to the exact position found in the first calculation, because initial geometry and thus distribution of forces have been altered. Thus it is necessary to carry out an iteration (second iteration procedure) as listed in Scheme 4.2 below:

... Design of cables using a particular design criterion.

8a) Apply permanent load to system having correct axial stiffnesses and an initial geometry corresponding to the desired geometry for dead load.

8b) Subtract the obtained deflections from the geometry of the preceding system.

8c) Apply permanent load and carry out a new calculation of deflections.

8d) Repeat steps 8b) and 8c) until an adequate agreement between geometries of consecutive systems is obtained, i.e. the deflections found are negligible.

8e) Establish permanent load situation by applying permanent load to system having an initial geometry as in the last calculation of the iteration described above (steps 8b) and 8c)).

Scheme 4.2 *Controlling of dead load geometry, traditional method.*

The second iteration as it is described in Scheme 4.2 has been rendered superfluous using the new way of controlling dead load geometry, since it has become an integrated part of the design process, namely step 8) in Scheme 4.1.

A detailed analysis of erection procedures and the possibility to influence favourably the distribution of dead load in the system can be found in *Gimsing et al.* (1989).

4.4 Dimensions of cables

Using the procedure described in the previous Section 4.3, cable dimensions and dead load geometry have been determined for the four spatial cable systems. Cross sectional areas of the cables are listed in App. A, where also the total quantities of steel in the four cable systems are indicated.

As design criterion we have chosen a dead load stress of $\sigma_g \sim 450$ MPa in the cables. This way we obtain the same quantity of cable steel in all four layouts of the spatial cable system,

so these can be compared directly. However, this also means, that cable dimensions have not been determined from a stress analysis considering different load cases involving variable load (see Section 2.6 "Loads). Consequently, stress level as well as stress variations in the stay cables might for certain load cases exceed what would usually be considered allowable. The main purpose of the FE-calculations carried out in Chapter 5 is to compare the four layouts of the spatial cable system and to highlight differences in structural behaviour in order to make a choice of cable system for the remaining investigations of the present work. Thus, the purpose is not to design cables from a strict stress analysis.

In the present work it is chosen to design cables with an accuracy in the order of 1 mm^2 on the cross-sections with respect to the design criterion of a dead load stress equalling $\sigma_g \sim 450$ MPa. In practice, dimensions of available standard cables often dictate the final choice of cross-sections for the stay cables. Here we have chosen to determine cross-sections individually without considering available standard dimensions in order to get the same quantity of cable steel in all four spatial cable systems.

As mentioned in Section 4.3 "Dead load geometry" design of cables involves an iteration to determine cross-sections. When changing the cross-section of a cable it influences on the distribution of forces in the neighbouring cables due to the change in axial stiffness. However, when cable dimensions are reasonably close to fulfilling the design criterion it does not affect the total quantity of cable steel much. Apparent inconsistencies in App. A, where in certain cases some of the longer cables have smaller cross-sections than neighbouring shorter cables, are due to the above mentioned fact that the total quantity of cable steel is little sensitive towards minor changes in distribution of axial stiffnesses between neighbouring cables. Consequently it has not been attempted to eliminate all of these apparent inconsistencies regarding cable dimensions, since this has only a local effect and here we concentrate on global actions and responses.

4.5 Axial compression in girder

In a self-anchored system, as the one chosen for the present work, the girder is subjected to compression over its entire length giving rise to possible stability problems. In cable-stayed bridges erected until present the span-to-width ratio has been so small, that the safety factor against lateral buckling of the girder has well exceeded the safety factor against vertical buckling. However, if a narrow girder is used in connection with a traditional system with vertical cable planes lateral buckling might become a realistic mode of failure by instability even for only vertical loading. A solution to possible problems concerning lateral instability might be to apply a spatial cable system.

In this Section estimates on the safety factors against lateral and vertical buckling of the girder in our prototype bridge are given. In contrast to the analytical analysis presented in Chapter 3, the present investigation implies that the girder has a certain bending stiffness. Furthermore, in order to evaluate results of the numerical analysis on stability carried out in Chapter 5, calculations are based on actual cable dimensions as determined in Section 4.4. Spatial cable system a) is used as example, but regarding vertical instability the same results would be found for the other three layouts of the spatial cable system, because the total quantities of cable steel and thus the global elastic stiffnesses are practically identical, see App. A. Due to the differences between the fully, partially and pseudo-spatial systems with respect to the transfer of lateral loads, some differences regarding lateral girder instability must be expected. This point will be treated in Chapter 5. Inspiration to perform the following calculations has been found in *Klein* (1990).

The theory derived for an infinitely long beam on a continuous elastic support and subjected to a constant compressive normal force forms basis for the following calculations, see for instance *Timoshenko et al.* (1961). This is also known as the Winkler foundation, see Fig. 4.3.

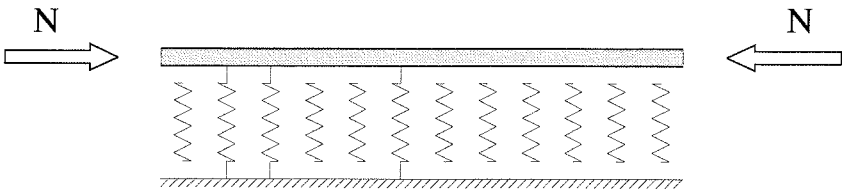

Figure 4.3 *Beam on continuous elastic support.*

For the two-dimensional case the compressive force to initiate buckling, N_{cr}, is determined by:

$$N_{cr} = 2 \cdot \sqrt{k \cdot EI} \tag{4.1}$$

where k is the spring stiffness of the continuous elastic support (unit: [force per length^2]), while EI is the bending stiffness of the beam. Both k and EI are assumed to be constant along the beam.

In order to estimate the safety factor against buckling of our prototype girder, we look at the two directions, vertical and lateral, separately. From the analytical analyses in Section 3.3 we derive expressions for the elastic support of the girder (vertical and lateral) offered by the spatial cable system. We restrict the analysis to compressive forces in the girder due to uniformly distributed vertical load along the girder, like for instance traffic load. Furthermore, we only look at the main span. Similar calculations can be carried out for the side span, but due to the shorter length and the fixed support at the abutments, the theory for an infinitely long beam on a continuous elastic support does not describe actual conditions quite so well as in the main span.

Compression in the girder arising from vertical loading is given by:

$$N_i = \sum_{j=i}^{n} \frac{q \cdot d}{\tan\theta_j} = \frac{q \cdot d}{h} \sum_{j=i}^{n} x_j \tag{4.2}$$

where N_i is the normal force between section of cable anchorage (i-1) and (i). There are totally n sections of cable anchorage in the fan. The resultant force per section of cable

anchorage of the uniformly distributed vertical load is qd, where d, the distance between sections of cable anchorage, is assumed constant. The distance from the pylon to the i'th section of cable anchorage is x_i, while h is the pylon height, see Fig. 4.4.

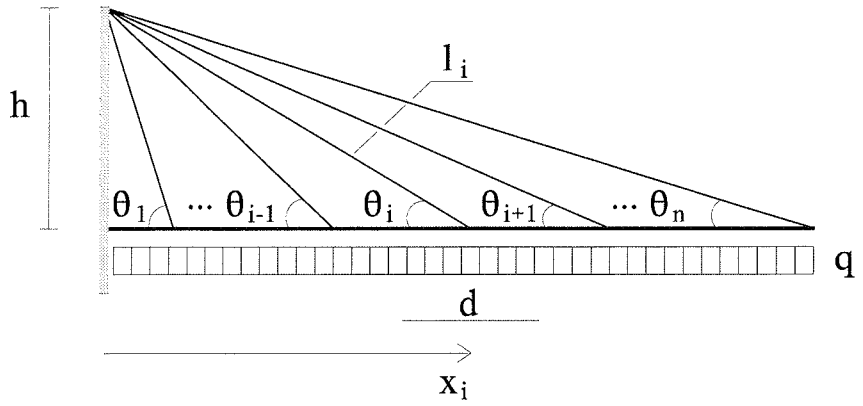

Figure 4.4 *Geometry in main span.*

Now spring stiffnesses of the elastic support offered by the cable system will be determined: Taking the vertical direction first and referring to Fig. 3.6 and Eq. (3.36), a vertical displacement, δ_v, due to the strain $\varepsilon_{q,i}$ in the stay cables at the i'th section is given by:

$$\delta_v = \frac{l_i^2}{h} \varepsilon_{q,i} \tag{4.3}$$

The strain $\varepsilon_{q,i}$ can be expressed by the stress, $\sigma_{q,i}$, (or the force, $F_{q,i}$) in the i'th cable:

$$\varepsilon_{q,i} = \frac{\sigma_{q,i}}{E_{eq,i}} = \frac{F_{q,i}}{E_{eq,i} \cdot A_i} = \frac{q \cdot d \cdot l_i}{E_{eq,i} \cdot A_i \cdot h} \tag{4.4}$$

where A_i is the total cross sectional area of cables at the i'th section, l_i the length of one cable at the i'th section and $E_{eq,i}$ the equivalent modulus of elasticity.

For a uniformly distributed vertical load, q, along the girder Hooke's law gives us:

$$k_v \cdot \delta_v = q \tag{4.5}$$

where k_v is the spring stiffness of the continuous elastic vertical support.

The spring stiffness at the i'th section, $k_{v,i}$, can now be found:

$$k_{v,i} = \frac{E_{eq,i} \cdot A_i}{l_i} \frac{1}{d} \frac{h^2}{l_i^2} \tag{4.6}$$

where the discrete support offered by the stay cables at the i'th section is assumed to be continuously distributed over the distance d, located d/2 to each side of the i'th section, see Fig. 4.4.

In a similar way we get for the continuous lateral spring stiffness due to the spatial cable system at the i'th section, $k_{l,i}$:

$$k_{l,i} = \frac{E_{eq,i} \cdot A_i}{l_i} \frac{1}{d} \frac{(b/2)^2}{l_i^2} \tag{4.7}$$

where again A_i is the total cross sectional area of stay cables at the i'th section. The expression in Eq. (4.7) is identical to Eq. (4.6) bearing in mind that half the pylon width in the lateral direction (b/2) corresponds to the pylon height (h) for the vertical direction, see Section 3.4 "Parametric studies".

For each section of cable anchorage we can now estimate the safety factors against lateral and vertical buckling by considering the discrete elastic support of varying stiffness along the girder offered by the cable system as constant and continuously distributed over a length equal to the distance between sections of cable anchorage. In this connection the distance, d, of 20 m is considered as "infinite" in order to apply the expression for an infinitely long beam on continuous elastic support, Eq. (4.1). We choose to normalize the safety factor with respect to the characteristic value of the uniformly distributed traffic load, thus in Eq. (4.2) we put

q = p = 20 kN/m.

The safety factor against lateral buckling at the i'th section, $S_{lat,\,i}$, can now be expressed as follows:

$$S_{lat,\,i} = \frac{2 \cdot \sqrt{k_{l,\,i} \cdot EI_{lat}}}{N_{p,\,i}} \tag{4.8}$$

where $k_{l,\,i}$ is given in Eq. (4.7). $N_{p,\,i}$ is found from Eq. (4.2) for q = p = 20 kN/m. The lateral bending stiffness of the girder is listed in Tab. 2.2.

In a similar way we have the safety factor against vertical buckling at the i'th section, $S_{vert,\,i}$:

$$S_{vert,\,i} = \frac{2 \cdot \sqrt{k_{v,\,i} \cdot EI_{vert}}}{N_{p,\,i}} \tag{4.9}$$

where $N_{p,\,i}$ is determined as described above, I_{vert} is found in Tab. 2.2 while $k_{v,\,i}$ is determined using Eq. (4.6).

The safety factors thus determined are compared in Fig. 4.5. Due to symmetry at midspan, only half the main span is shown.

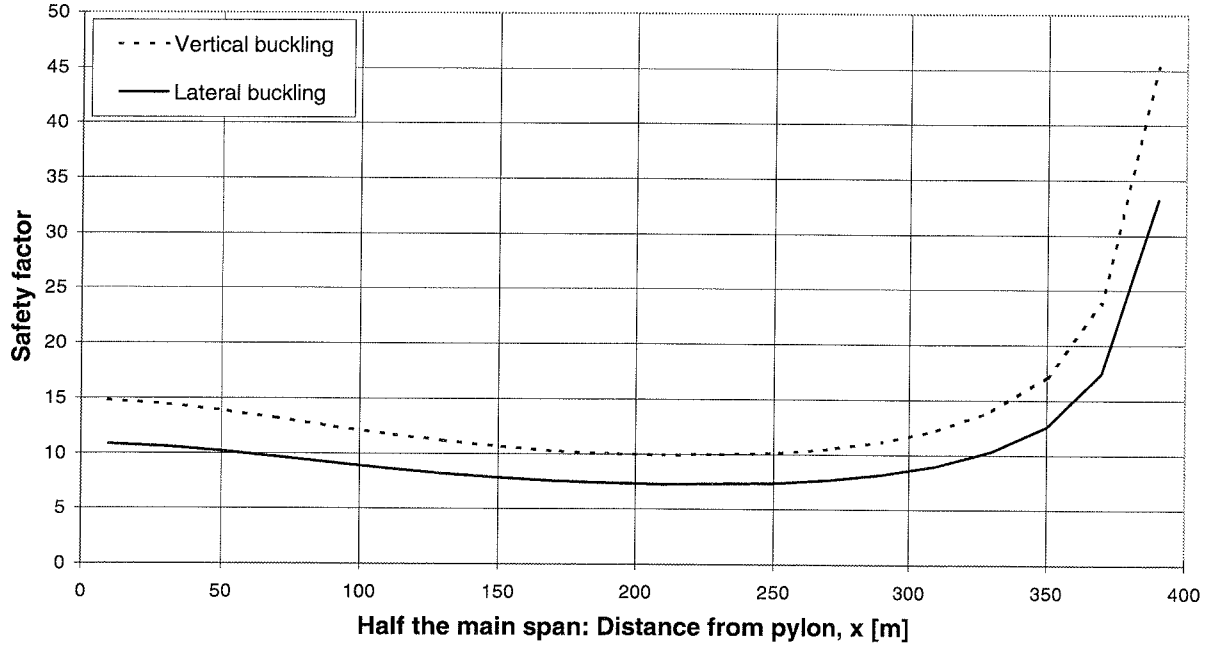

Figure 4.5 *Estimated safety factors against buckling of the prototype girder for a uniformly distributed vertical load. Normalized with respect to characteristic traffic load.*

At midspan (x = 400 m) the normal force equals 0, thus the safety factor will be infinite. An estimate on the critical loads to initiate buckling of the girder is obtained by identifying the areas having the lowest safety factors against buckling. The lowest safety factors against buckling are found near quarter span, x = 200 m. For lateral buckling we find a safety factor of $S_{lat} = 7.5$, thus it takes a uniformly distributed load of approximately 7.5 times traffic load to initiate lateral instability. The lowest safety factor against vertical buckling is estimated to $S_{vert} = 10$.

Using the method described in this Section 4.5 to estimate the safety factor against buckling of our prototype girder supported by a spatial cable system, we find that safety against lateral buckling is 25% lower than for vertical buckling. This indeed is a special point related to applying a narrow bridge girder. In this connection it should be stressed, that the safety found is sufficiently high compared to actual loading on the bridge to ensure, that this special prototype bridge having an extremely narrow girder supported by a spatial cable system is not

likely to exhibit any stability problems.

Furthermore it should be emphasized that the method used in the present Section is quite simplified due to the assumption of having a constant normal force when estimating the critical normal force to initiate buckling (Eq. (4.1)). A better approximation could be obtained by taking into account the parabolic variation of normal forces in the girder. The point of buckling stability of the prototype girder is further pursued by means of FE-calculations in Section 5.3.

Chapter 5

5. STATIC BEHAVIOUR AND STABILITY OF FOUR LAYOUTS OF THE SPATIAL CABLE SYSTEM

5.1 Introduction

In this Chapter results from the FE-analyses of the four layouts of the spatial cable system are presented. In Section 5.2 selected results from linear calculations on the static behaviour due to wind and traffic loads are presented and compared with the analytical analyses of Chapter 3. Then in Section 5.3 the question of buckling stability of the girder is dealt with by means of eigenvalue analyses and geometrical nonlinear calculations. Results are compared with the estimates on buckling load presented in Chapter 4. In Section 5.4 a parametric study on the torsional stiffness of the girder in connection with applying cable system d) is carried out. Finally, results of the FE-calculations are summarized in Section 5.5.

5.2 Static behaviour

In this Section we present selected results of linear FE-calculations of structural response to the loads listed in Section 2.6. We focus on cable forces and girder deflections, since these are decisive factors for evaluating applicability of the four different layouts of the spatial cable system. In the present study girder and pylons have not been subjected to a careful design, so actions on these structural elements are only given a few comments.

In Section 4.4 cable dimensions were determined from a design criterion of having a cable stress of 450 MPa for permanent loads. The load case of permanent loads will not be further treated here.

In the following the abbreviation "ac" refers to the anchor cables, "s" to the side span and "m" to the main span. The pylon is located between sections "s1" and "m1", using the numeration of cable anchorage sections introduced in Section 4.2.

5.2.1 Wind on structure

An important load case in relation to evaluating spatial cable systems is wind load on the structure. The total cable forces due to wind and permanent loads are shown in Fig. 5.1 - 5.4 for the four layouts of the cable system. As a supplement to the categories of outwards and inwards leaning cables it is furthermore indicated whether the cable is attached to the windward or the leeward side of the girder. Due to wind load, stresses in the outwards leaning cables attached to the windward side and in the inwards leaning cables attached to the leeward side are increased. In the other cables stresses are decreased, see also Fig. 2.3. Due to symmetry at midspan only results for half the bridge are shown.

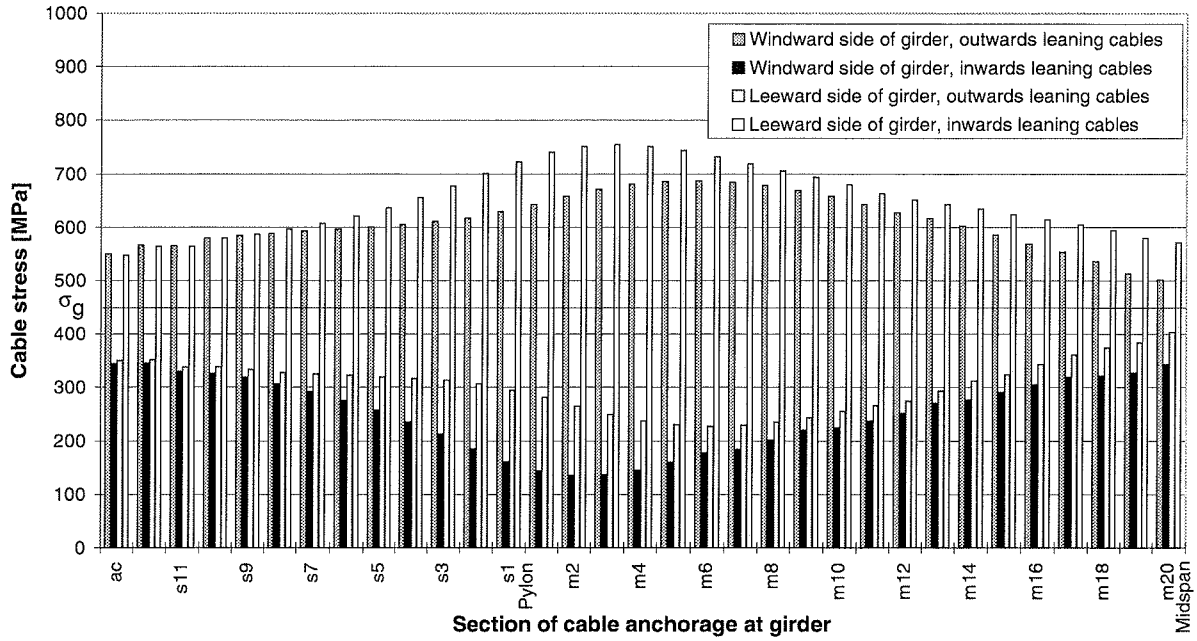

Figure 5.1 *Cable system a). Wind load on structure.*

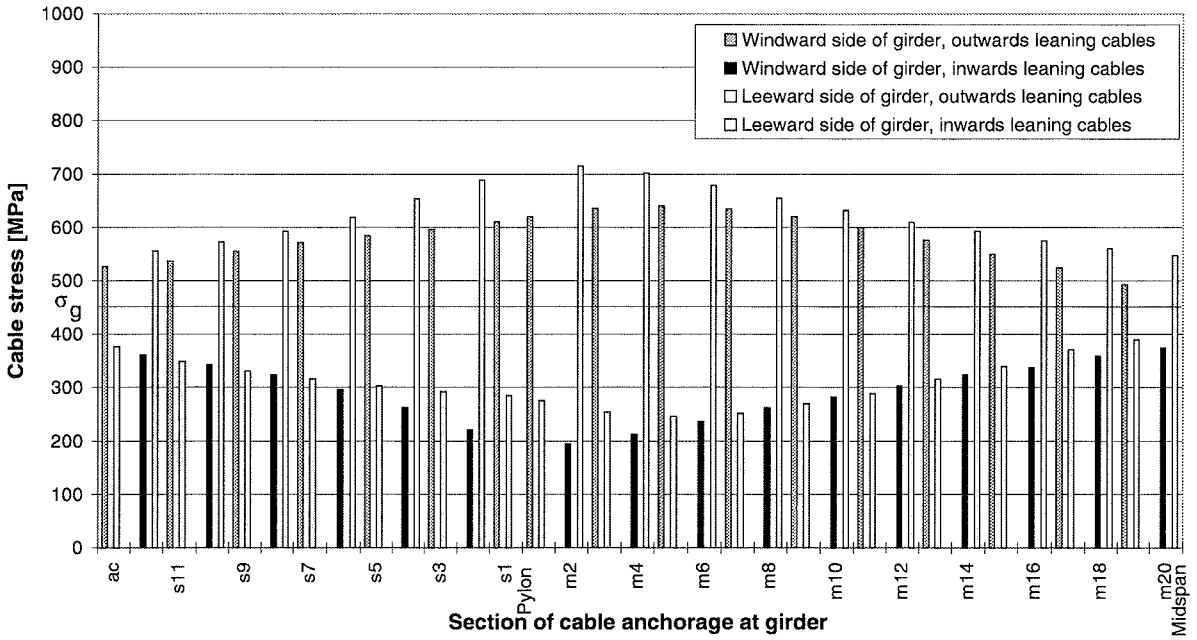

Figure 5.2 *Cable system b). Wind load on structure.*

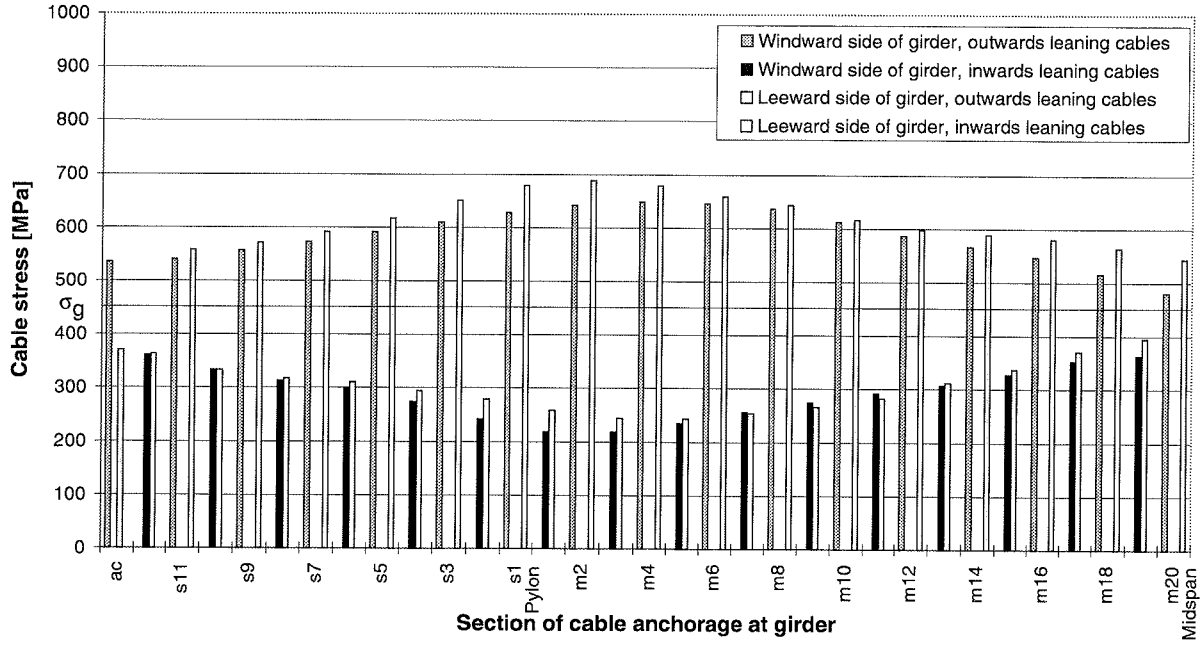

Figure 5.3 *Cable system c). Wind load on structure.*

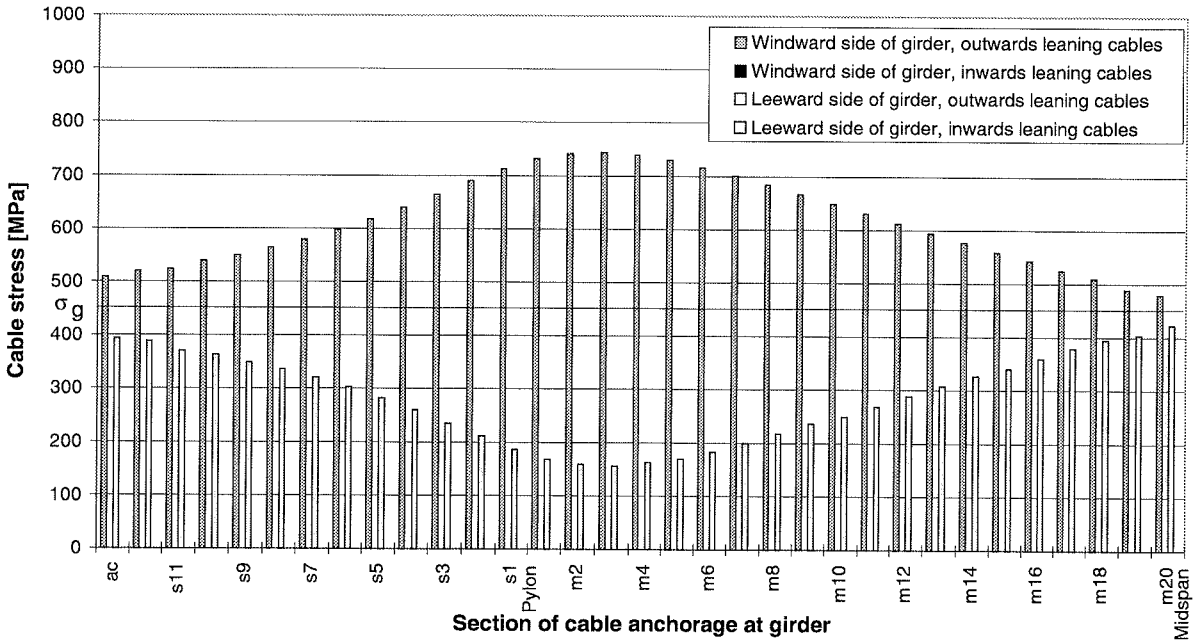

Figure 5.4 *Cable system d). Wind load on structure.*

The stay cables close to the pylon experiences the largest changes in stresses because these cables are the shortest and most stiff ones. This picture is common for all four layouts of the spatial cable system. Inwards leaning cables experiences larger stress variations than outwards leaning cables (cable system a), b) and c)).

The changes in stresses are highest for cable system a) and d), where stresses range from 150 MPa to 750 MPa approximately. For cable system b) and c) changes in stresses range from 200 MPa to 700 MPa. In case of system a) wind load on the cable system is higher because the number of cables is the double. Consequently changes in cable forces from the dead load situation are higher. In case of system d) the cable system cannot transfer wind load without aid from the girder (see Section 2.3). This leads to larger deflections than seen for the other three cable systems. Deflections will be dealt with below. Furthermore, cable system d) consists of only outwards leaning cables and no inwards leaning cables. Consequently, cable forces for wind load are higher in relation to cable system d), because the outwards leaning cables are not so well suited for transferring lateral forces as the inwards leaning cables.

In relation to wind load it should be recalled that wind can come from the opposite direction as well. Therefore, the same stay cable can experience stress variations equal to the total stress ranges mentioned above. The wind load applied corresponds to the 100-year wind, so for this particular wind load fatigue is not involved. However, turbulences as well as other load cases involving lower wind speeds and thus occurring more frequently might cause fatigue problems in the stay cables or their anchorages. In case of an actual bridge having a spatial cable system it is necessary to evaluate if the wind climate on site is likely to cause fatigue and furthermore if the decrease of cable forces due to wind is acceptable regarding the stiffness of the system.

In Fig. 5.5 lateral deflections from wind load are shown for the four layouts of the spatial cable system.

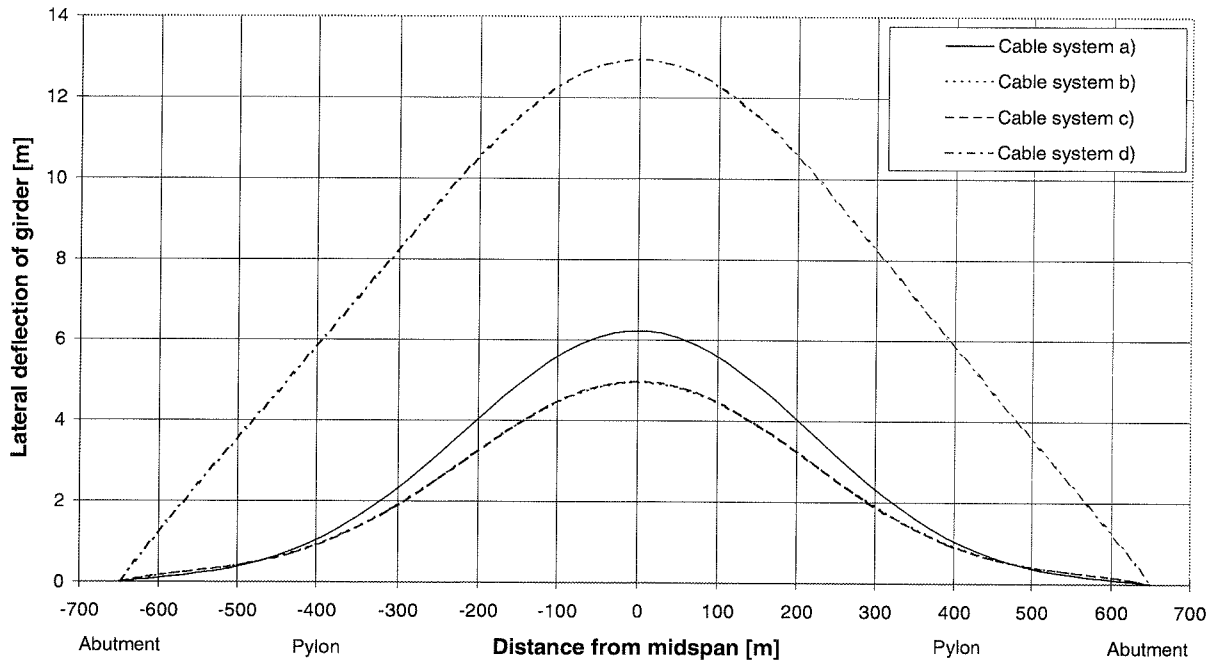

Figure 5.5 *Lateral deflections for wind load on structure. Comparison of the four layouts of the spatial cable system.*

Maximum lateral deflections at midspan attain 6.2 m for cable system a), for cable system b) and c) 5.0 m, while the midspan deflection is 13 m in case of cable system d). Deflection curves for system b) and c) are identical. The larger deflections of system a) are related to the higher wind load on the cable system, as already mentioned.

In the following we concentrate on cable system a), where 4.1 m or 66% of the midspan deflection is due to wind on the cable system. Wind on the girder accounts for 1.9 m or 31% of the total deflection. Only 3% of the lateral deflections are due to wind on the pylons. However, as described in Section 3.3 "Analytical analyses" pylon deflections are important because they lead to a rigid body rotation of the cable system. For wind load on the entire structure each side of the pylon top moves 22 cm parallel to the bridge axis and in opposite directions. This leads to a rigid body rotation accounting for 2.1 m of the total midspan deflection or 34%. In the lateral direction the pylon top is displaced 0.45 m, partly due to change of forces in cables and partly due to wind on the pylon. When the pylon top is fixed

in the lateral direction, midspan deflections are reduced by 0.8 m. This demonstrates that rigidity of the cable system support at the pylon top is quite important for the overall deformational characteristics of the structural system.

In the following, we compare results of the FE-calculations with the analytical analyses. For wind load on the girder the analytically predicted lateral deflection at midspan attains 4 m (see Fig. 3.17), where 70% are due to the stay cables and 30% due to the anchor cables causing a displacement of the pylon top. For wind load on the girder but not on cable system and pylons, FE-calculations taking into account the bending stiffness of the girder results in a 1.9 m lateral deflection at midspan. If bending stiffness of the girder is reduced by a factor of 10^3, lateral deflection at midspan for wind on the girder attains 3.3 m, compared to the 4 m found in the analytical analysis. For the chosen geometry of the spatial cable system, contribution to the lateral stiffness from the girder itself is quite important, since it reduces lateral deflections from 3.3 m to 1.9 m, thus by about 40%. Out of the 1.9 m total lateral deflection, 62% are due to the stay cables. This is in good agreement with analytical predictions.

Deviations can to some extent be explained by the fact, that in the analytical analysis we neglected deflections at the pylon as a result of the idealization from a finite number of cables to a continuous system, whereas in the FE-model the girder is free at the pylon. FE-calculations show, that lateral deflections at the pylon equal approximately 15% of the midspan deflections, cf. Fig. 5.5. Arranging a fixed support in the lateral direction at the pylons would only reduce midspan deflections by 7%. So a significant reduction of lateral deflections by arranging a support at the pylons would require a restraint of rotations. In this case lateral deflections are reduced by 20%.

Furthermore, an equivalent elastic modulus of 180 GPa has been assigned to all cables in the analytical analysis of lateral deflections, whereas individual equivalent moduli of elasticity accounting for actual sag effects have been applied in the FE-analyses. Finally, an explanation of deviations between analytical analysis and FE-calculations could be, that cable dimensions

are not exactly the same due to the different design criteria used. In the analytical analysis the quantity of cable steel has been determined from a combination of permanent, traffic and wind loads. For the FE-analysis cables have been designed to a dead load stress of $\sigma_g \sim 450$ MPa. This leads to some difference in axial stiffnesses of the cables in the two analyses.

Finally, we will give a few comments to the torsion arising from wind load. For cable system a), b) and c) the maximum inclination of the girder equals 0.3° to horizontal, which is the same as a 4 cm vertical difference between the two sides of the girder. For cable system d) the vertical difference between the two sides of the girder is 1.8 m or 13° inclination to horizontal. With respect to wind load, the behaviour of cable system d) must be considered as unacceptable.

5.2.2 Traffic load

Traffic load is assumed to be a free action, so different positions of the traffic load need to be considered. These have been introduced in Section 2.6 "Loads".

First we consider traffic load on the entire bridge. This results in stresses in the stay and anchor cables ranging from 600 MPa to 670 MPa. Due to the different lateral inclinations of the cable planes, stress level in the outwards leaning cables is slightly higher than in the inwards leaning cables because the outwards leaning cables are more suited for transferring vertical loads. Cable dimensions have been determined from a criterion of having a dead load stress $\sigma_g \sim 450$ MPa. The main contribution to dead load stresses in cables is dead weight of girder and bridge equipment, which is a uniformly distributed load. Traffic load is also uniformly distributed, so this explains why the stress level in the cables is so uniform for traffic load on the entire bridge.

Deflections due to traffic on the entire bridge are shown in Fig. 5.6 for all four layouts of the spatial cable system.

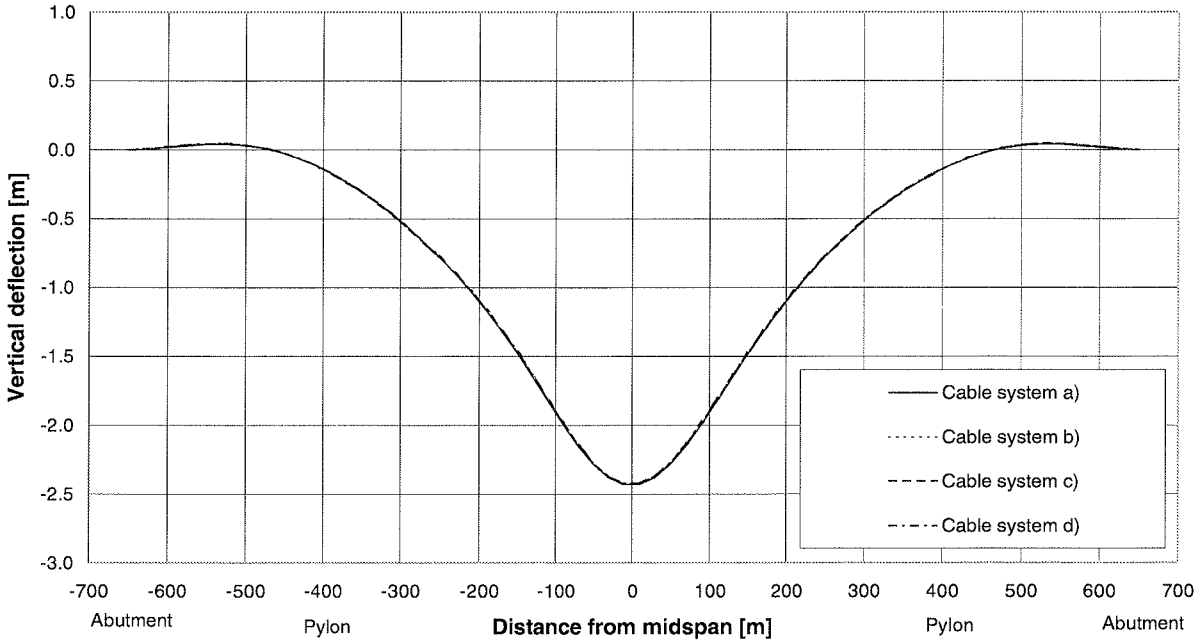

Figure 5.6 *Vertical deflections for traffic load on the entire bridge. Comparison of the four layouts of the spatial cable system. Note: All four curves* are *shown.*

For vertical load the four layouts of the cable system are seen to behave identically, so in the remaining part of this Section 5.2.2 we restrict investigations to cable system a).

The vertical deflection at midspan is 2.4 m. Out of these 2.4 m rotation of the cable system due to elongation of anchor cables and the related displacement of the pylon top accounts for 1.1 m or 45%. At the pylons vertical deflections equal 0.15 m or 6% of the midspan deflection, so with respect to vertical loading the short and stiff cables at the pylons supply an almost fixed support for the girder. This corresponds to the assumption made prior to the analytical analysis of vertical deflections. Ignoring the vertical bending stiffness of the girder the analytical analysis predicts a vertical deflection at midspan of 3 m, where 52% are due to elongation of stay cables and 48% to the anchor cables.

As already mentioned in relation to lateral deflections due to wind, deviations between midspan deflections according to the analytical and to the numerical analysis can to some

extent be explained by the fact, that an equivalent elastic modulus of 180 GPa has been assigned to all cables in the analytical analysis of vertical deflections. In the FE-analyses individual equivalent moduli of elasticity have been used. Furthermore cable dimensions are not exactly the same in the analytical and in the FE-analysis.

In Fig. 5.7 vertical deflections are shown for different positions of the traffic load. Cable system a) is used as example. The deflection curve for traffic on the entire bridge is shown in the same figure for comparison.

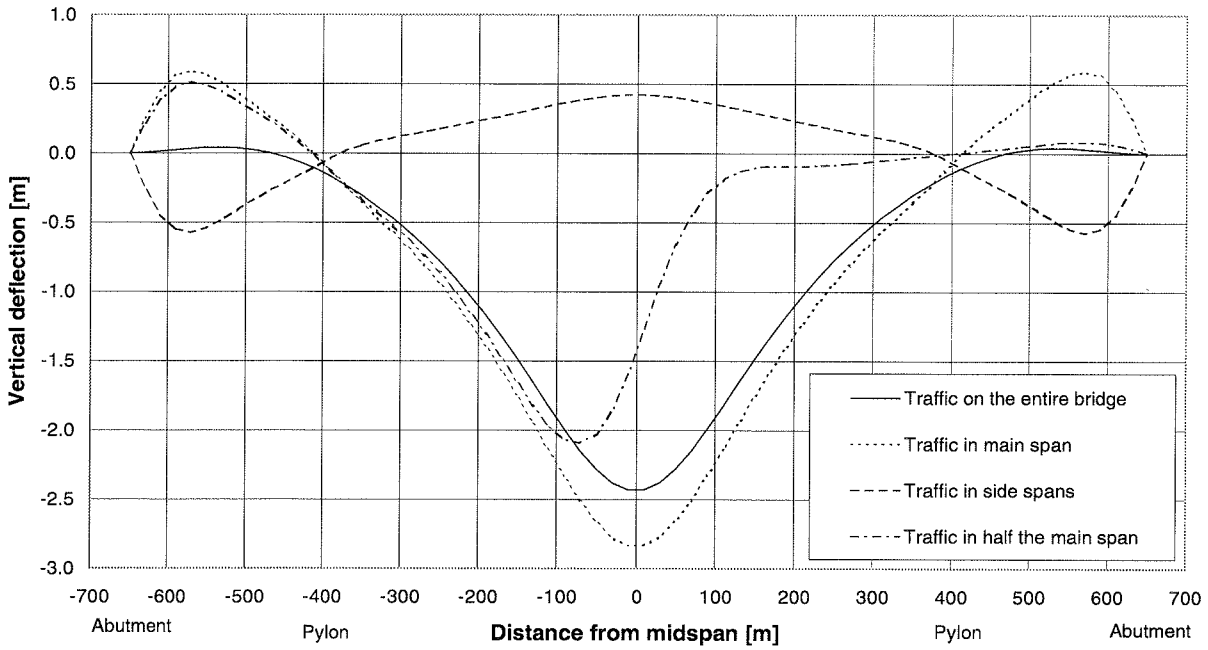

Figure 5.7 *Cable system a). Vertical deflections for different positions of traffic load.*

Traffic only in the main span causes the largest deflection at midspan (2.8 m). This also leads to the largest forces in the anchor cables, because pylon tops are displaced towards the main span. Stresses in the anchor cables reach approximately 700 MPa. At the centre of the side span forces in the stay cables are slightly decreased, whereas the stress level in main span stay cables corresponds to the load case with traffic load on the entire bridge.

Traffic in the side spans results in the lowest forces in the anchor cables because pylon tops

are forced towards the side spans. The stresses in the anchor cables are decreased to 380 MPa. Maximum stresses in side span stay cables correspond to when there is traffic load on the entire bridge, whereas stay cables in the main span are hardly affected by traffic load in the side spans. At the centre of the main span the girder is lifted about 0.5 m, and the maximum deflection in the side spans also attains approximately 0.5 m.

The final load case we will consider here involving only traffic load, is traffic in half the main span. Maximum deflections attain 2 m, but more important is the longitudinal displacement of the girder. Due to support conditions at the abutments the girder is actually "floating" in the longitudinal direction where it is only supported by the cables - especially the longer and flat cables. Consequently traffic load in half the main span results in a longitudinal displacement of 20 cm at the far abutment, while it is around 10 cm at the nearer abutment. The point of longitudinal displacements of the girder is further treated in Section 5.3.1 "Eigenvalue analyses".

With respect to vertical loading, the behaviour of the prototype bridge with the chosen geometry of the spatial cable system does not differ from what is known from traditional cable-stayed bridges with vertical cable planes.

5.2.3 Wind and eccentric traffic loads

The final load case we consider in the present study is a combination of eccentric traffic and wind loads. In order to get maximum torsional action on the girder we apply traffic load over the entire bridge length but in one lane only. This situation is common in relation to maintenance and repair. A wind load corresponding to a wind speed of 25 m/s is applied together with the eccentric traffic load. The wind load attains 34% of the load applied for the 100-year wind. Direction of the wind is chosen to give maximum torsion together with the eccentric traffic load. We restrict the investigation to cable system a).

In Fig. 5.8 cable stresses are shown.

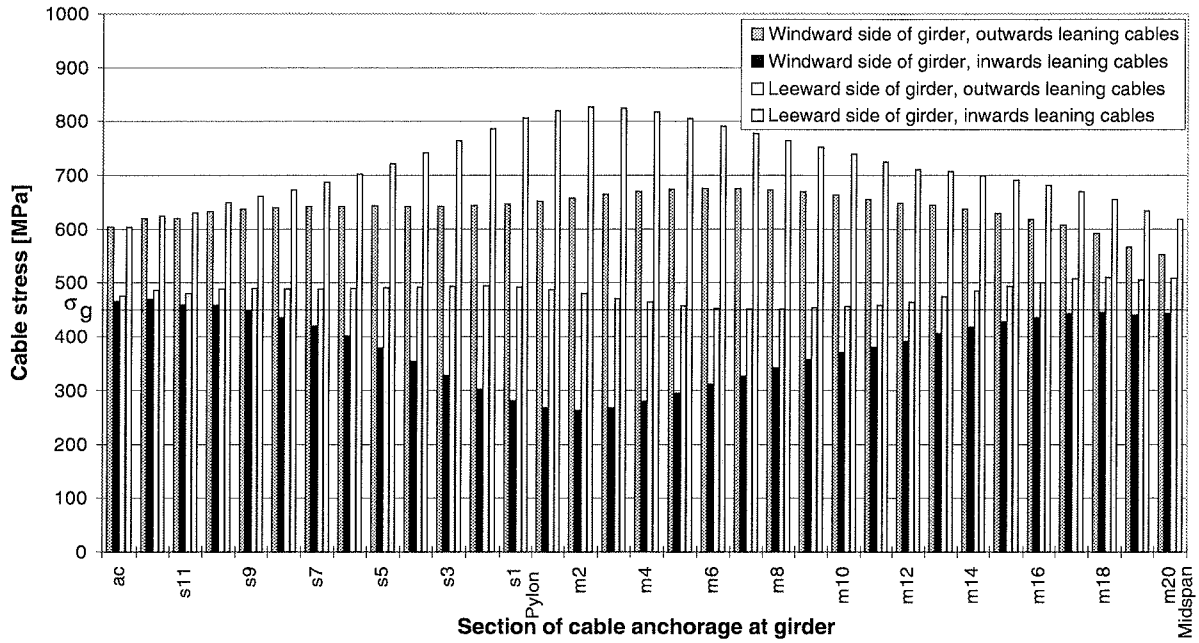

Figure 5.8 *Cable system a). Cable stresses for wind and eccentric traffic loads. Wind speed: 25 m/s.*

Stresses in the cables range from 270 MPa to 820 MPa in the inwards leaning cables and from 450 MPa to 680 MPa in the outwards leaning cables. The stress level in the inwards leaning cables seems too high, but it should be recalled, that a partial coefficient of 1.0 is assigned to both traffic and wind load. Again the question of fatigue problems in the stay cables arise.

Eventually, using cable system a) there is the possibility of changing the distribution of dead load stresses between outwards and inwards leaning cables and thus reduce the difference in stress variations in the two types of cables. Since the inwards leaning cables carry the largest portion of the wind load, the outwards leaning cables should carry relatively more of the dead load. However, when adjusting distribution of dead load stresses between outwards and inwards leaning cables one should of course assure that a complete relief of the inwards leaning cables due to wind load cannot occur.

Lateral deflections for wind and eccentric traffic loads are shown in Fig. 5.9. The maximum deflections equals 3.8 m or almost half the deck width. This will probably be considered as unacceptable with respect to requirements for traffic comfort.

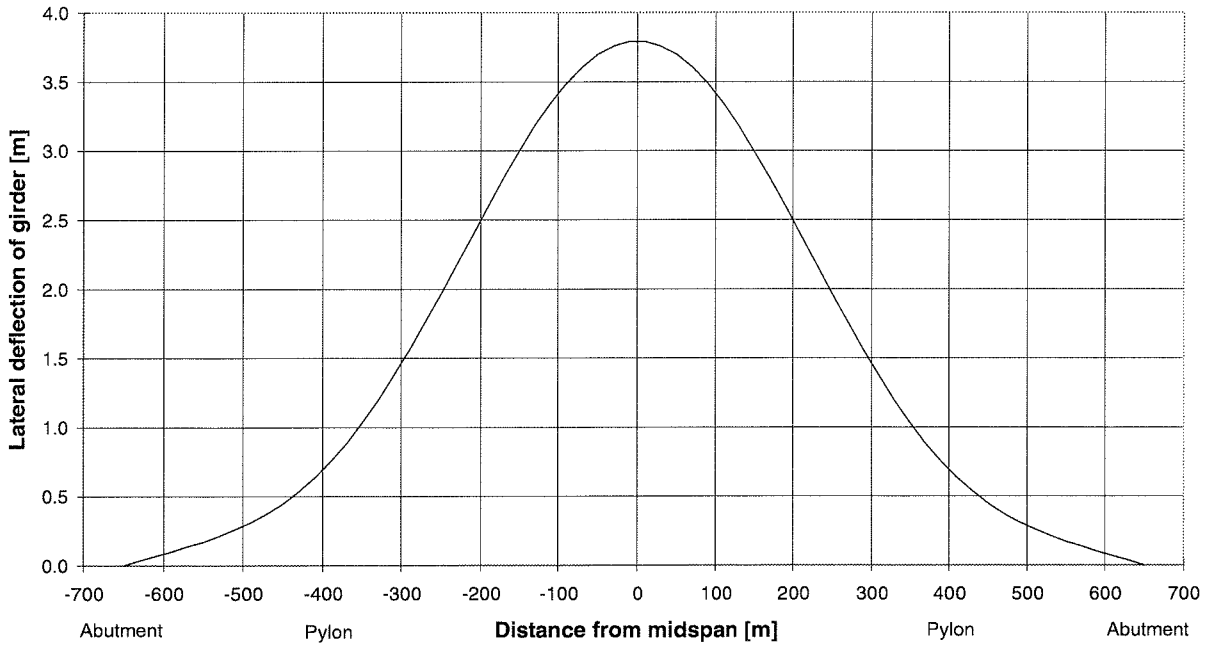

Figure 5.9 *Cable system a). Lateral deflections for wind and eccentric traffic loads. Wind speed: 25 m/s.*

Vertical deflections are shown in Fig. 5.10 for the girder axis and for the two sides of the girder. The maximum inclination of the girder occurs at midspan and equals 10° to horizontal, which again must be considered unacceptable for traffic comfort.

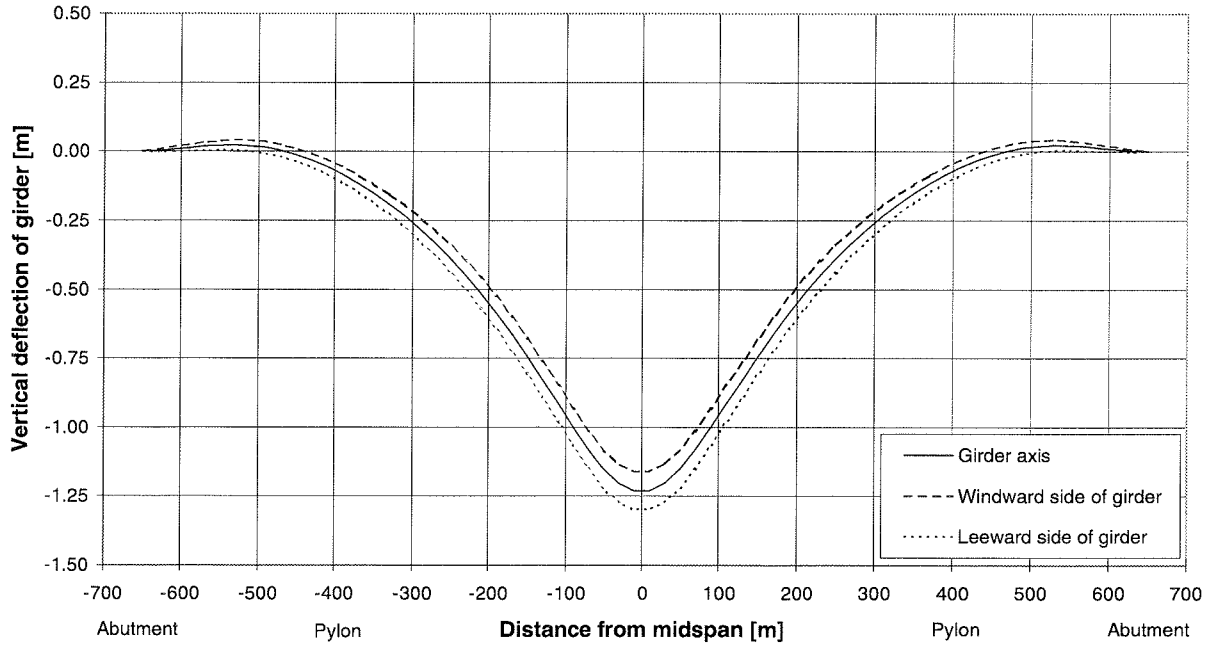

Figure 5.10 *Cable system a). Vertical deflections for wind and eccentric traffic loads. Wind speed: 25 m/s.*

5.3 Buckling stability

In Section 4.5 "Axial compression in girder" the question of buckling stability of the girder was introduced. This question will now be dealt with by means of FE-calculations. We restrict the investigation to comprise compression introduced by uniformly distributed vertical loading only.

5.3.1 Eigenvalue analyses

First an eigenvalue buckling analysis is carried out. This type of analysis is also known as "linear buckling analysis". Equilibrium is established in the deflected system. The term "linear" refers to the fact that deflections are not assumed to influence on the distribution of forces in the system as loading is increased. This demands for a linear material model

otherwise stiffnesses of the elements would change, when loading is increased. In relation to cables and sag effects a linear material model is well suited for describing conditions at a relatively high load level, because the equivalent elastic modulus approaches the elastic modulus of steel or a slightly lower value depending on the layout of the cables (helical strands, parallel-wire strands etc.). According to the estimates on buckling loads presented in Section 4.5, buckling load is in the order of 8 to 10 times the traffic load. It is therefore well justified to use a linear material description for the cables. The deformational characteristics of a cable-stayed bridge are mainly governed by the stay and anchor cables. Consequently it is assumed to be acceptable to use a linear elastic material model for the girder also.

An eigenvalue buckling analysis is well suited for describing the behaviour of a relatively stiff structure, where displacements prior to failure by instability are not a decisive factor for the structural response. As already mentioned we only consider vertical loading. Buckling load is expected to be relatively high compared to service loads leading to large vertical deflections. Consequently, the eigenvalue buckling analysis is expected to describe lateral buckling for vertical loading quite well. For the behaviour in the vertical direction a geometrical nonlinear description taking into account redistribution of forces due to deflections might be necessary.

In Fig. 5.11 four fundamental buckling modes of the prototype bridge are shown together with an elevation of the FE-model. These buckling modes are found for all four layouts of the spatial cable system, even though the corresponding buckling load is not always exactly the same. In Fig. 5.11 we have chosen to show cable system b) omitting most of the stay cables in order to get a more clear picture of girder deflections. Deflected geometry is indicated with the dashed line.

FE-model:

Longitudinal:

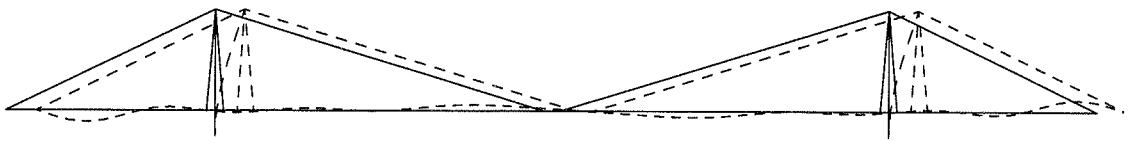

Lateral, asymmetric:

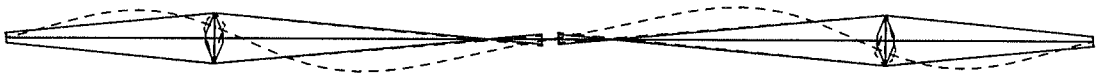

Lateral, symmetric:

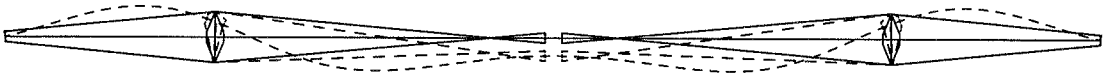

Vertical, symmetric:

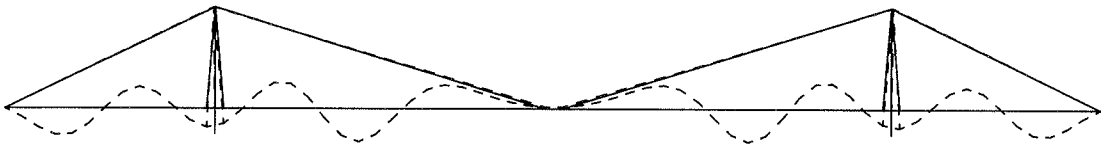

Figure 5.11 *Four fundamental buckling modes of the prototype bridge.*

In Tab. 5.1 we have listed the buckling loads corresponding to the four fundamental buckling modes shown in Fig. 5.11. The number in brackets indicates the order of the buckling mode in question. The buckling mode having the lowest critical load is #1 and so forth.

Cable system	Longitudinal	Lateral asymmetric	Lateral symmetric	Vertical symmetric
a)	266 kN/m (#3)	260 kN/m (#1)	265 kN/m (#2)	286 kN/m (#4)
b)	266 kN/m (#1)	267 kN/m (#2)	276 kN/m (#3)	288 kN/m (#4)
c)	266 kN/m (#1)	269 kN/m (#2)	277 kN/m (#3)	288 kN/m (#4)
d)	267 kN/m (#4)	231 kN/m (#2)	218 kN/m (#1) 258 kN/m (#3)	290 kN/m (#5)

Table 5.1 *Critical loads according to an eigenvalue buckling analysis.*

For cable systems a), b) and c) the four modes shown in Fig. 5.11 are the four modes having the lowest critical load. For cable system d) the mode indicated in Tab. 5.1 as "Lateral, symmetric (#1)" differs from the one shown in Fig. 5.11. This lateral symmetric mode of cable system d) is shown in Fig. 5.12. Due to this "extra" lateral symmetric mode in system d), the following modes have a number one higher than in the other three layouts of the spatial cable system. For instance mode #4 in cable system a), b) and c) corresponds to mode #5 in system d).

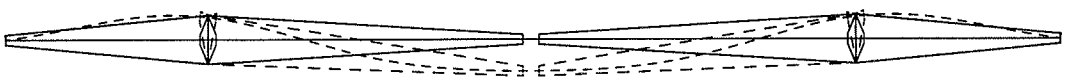

Figure 5.12 *Lateral symmetric buckling mode (#1) of cable system d).*

With respect to the four lowest modes, cable system b) and c) behave identically. Also cable system a) is behaving similarly, though the order of the buckling modes is altered. This is probably due to slight differences in cable dimensions and thus axial stiffnesses. Because the three lower modes are so close with respect to critical load, small differences between stiffness of the cable system might change the order of the buckling modes.

Note the buckling mode involving a longitudinal displacement of the girder and deflection of the pylon. This mode is due to the absence of a fixed support of the girder in the longitudinal direction. This mode of instability can be eliminated by supplying a fixed support in the longitudinal direction at one abutment. However, this has the disadvantage that the structural system is then no longer symmetric with respect to midspan. Consequently all dilatation will take place at the abutment where the girder is free to move. Another way of eliminating the instability involving longitudinal displacement of the girder is to increase the rigidity of the longitudinal support of the pylon top. However, this cannot be obtained by increasing the stiffness of the anchor cables, because the structural system is self-anchored. Consequently displacements of pylon top and girder end at the abutment are identical. An efficient support of the pylon tops by means of anchor cables thus demands for an earth-anchored system, which also decreases compression in the girder. If an earth-anchored system is not applied, increased rigidity of the cable system support at the pylon top can only be obtained by increasing bending stiffness of the pylon itself in the longitudinal direction to the bridge axis.

Turning to the lateral buckling modes and taking cable system a), b) and c) first, it should be recalled that the normal force at midspan is 0. This explains why the asymmetric mode has a lower critical load than the symmetric mode. Recalling the results from Section 4.5 the lowest safety factor against lateral buckling was found near quarter span corresponding to the area where the asymmetric lateral mode has its maximum deflections according to the FE-analysis, (see Fig. 5.11). The same phenomenon is reflected in the symmetric lateral mode. Due to the relatively low compressive normal force near midspan, the tendency to lateral instability is less pronounced in this area than at quarter span. Actually, deflections near

quarter span are larger than at midspan also for this symmetric lateral buckling mode.

For cable system d) the picture is slightly different because lateral deflections involves a twist of the girder as explained previously. The tendency of twisting is more pronounced at midspan leading to a lower critical load for the symmetric lateral mode than for the asymmetric, because twist at midspan is zero for the asymmetric mode. If we compare the critical load for the asymmetric lateral modes of system d) and b), the critical load of system d) is 13% lower. Comparing the critical load for the lowest symmetric modes found in system b) and d), the critical load of system d) is 21% lower. However, it should be recalled that the lowest order symmetric lateral mode of system d) is not identical with the lowest order symmetric mode of the other systems. If we compare identical symmetric modes of system b) and d), the critical load of system d) is only 7% lower.

In Section 4.5 the predicted critical load for lateral buckling was 7.5 times the traffic load or 150 kN/m for our prototype bridge. The FE-analysis predicts a critical load of 260 - 269 kN/m or approximately 13 times the traffic load. The difference is probably due to the following two main reasons: Firstly the method used in Section 4.5 assumes a constant normal force in the girder when estimating the critical compressive force to initiate buckling, while the FE-calculations account for the parabolic distribution of normal forces along the girder. Secondly the spatial cable system provides an elastic support of varying stiffness along the girder. The theory used in Section 4.5 assumes a continuous elastic support of constant stiffness. Furthermore the chosen geometry of the spatial cable system does not lead to a very stiff elastic support of the girder. This is reflected in the lower lateral buckling modes having only a few waves along the girder. Thus the behaviour is to a large extent governed by the bending stiffness of the girder itself rather than of the elastic support originating from the laterally inclined cable planes.

Furthermore, the estimates in Section 4.5 are based on a theory derived in two dimensions, where cable stiffnesses have been projected on to the plane in question (lateral or vertical).

Consequently the elastic stiffnesses of the two or four cable planes of the spatial cable systems have been summarized to form one cable plane, and the stability problem is reduced from three dimensions to two. In contrast to this, the numerical eigenvalue buckling analyses carried out are three-dimensional. This means that the actual geometry of the three-dimensional elastic support of the girder is modelled, including the lateral distance between cable planes. As mentioned in Section 2.3 a lateral displacement of the girder also implies a local twist in case of spatial cable systems b) and c), and a global twist of the girder in case of cable system d). The reason is that the two cables per section of cable anchorage do not intersect at the centre of gravity of the girder. This effect can only be modelled using a three-dimensional description. When the torsional rigidity of the girder is activated and contributes to the load transfer, a higher critical load must be expected. This is probably a part of the explanation why the estimates on critical loads based on a two-dimensional description are lower than the results of the three-dimensional numerical eigenvalue buckling analyses. Furthermore the contribution to load transfer originating from twist of the girder might explain why the critical loads for the lateral modes (asymmetric and symmetric) found in the eigenvalue buckling analyses are slightly higher for cable system b) and c) than for cable system a), see Tab. 5.1.

For vertical buckling all four layouts of the spatial cable system behave identically. According to the predictions in Section 4.5, maximum deflections occur near quarter span, but in contrast to the lower order lateral modes, the lowest vertical mode has many waves along the girder. This is because the behaviour is governed by the elastic support offered by the cable system and not by the bending stiffness of the girder itself. Consequently the critical load predicted in Section 4.5 is expected to show better agreement for vertical buckling than was found for lateral buckling. Actually this is the case. In Section 4.5 a critical load of 10 times the traffic load was found, equivalent to 200 kN/m. The eigenvalue buckling analysis yields 290 kN/m, thus a 45% higher critical load. Again the difference must be due to the assumptions of a constant normal force and of a continuous elastic support of constant stiffness made in Section 4.5. The FE-calculation takes into account both the parabolic distribution of normal forces and the varying stiffness of the discrete stay cables. Furthermore as mentioned above, the estimates

presented in Section 4.5 are based on a two-dimensional approach while the numerical analyses are carried out in three dimensions.

However, none of the two methods applied to predict vertical buckling take into account redistribution of forces in the system due to deflections arising from the vertical loading. This is done in the following Section describing geometrical nonlinear calculations.

5.3.2 Geometrical nonlinear calculations

As mentioned above a geometrical nonlinear analysis takes into account redistribution of forces due to deflections. This could be quite important in our investigation on stability since we use vertical loading to introduce compression in the girder. Consequently we carry out a geometrical nonlinear calculation accounting for large displacements, but assuming small rotations and small strains. This is known as the Total Lagrangian Formulation, see for instance *Cook* (1981) and *LUSAS* (1993).

Due to the relatively high stress level at buckling load we apply a linear material model for the stay cables. Furthermore we apply a linear material description for the steel girder.

The four layouts of the spatial cable system exhibit the same behaviour in the vertical direction, so we restrict the geometrical nonlinear investigation to one layout. We choose cable system b).

In a geometrical nonlinear calculation on a cable-stayed bridge instability is characterized by an excessive increase in deflections for a slight increase in loading. At a certain load level deflections grow so rapidly that it is no longer possible to find a state of equilibrium. This load level is identified as the critical load. For cable system b) we find a critical load of 233 kN/m or 11.7 times the characteristic traffic load. This is 19% below the critical load according to the eigenvalue buckling analysis. In Fig. 5.13 vertical deflections at midspan are shown as a function of load.

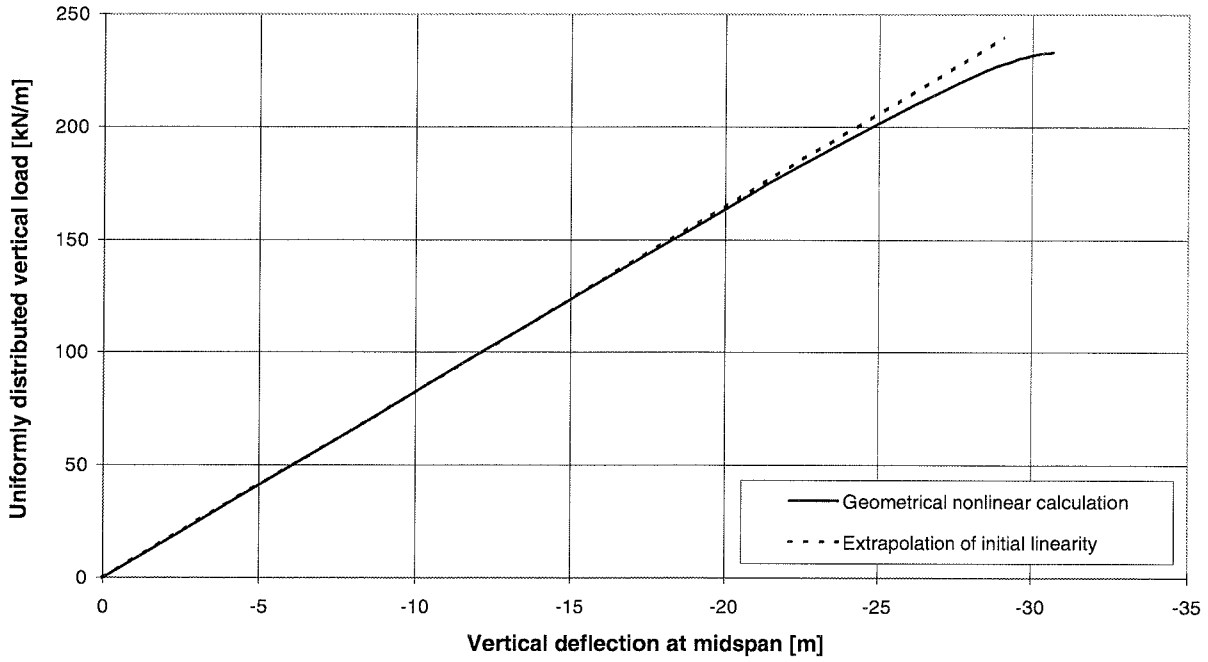

Figure 5.13 *Geometrical nonlinear calculation, vertical deflections at midspan.*

The load-deflection relationship is characterized by linearity until a load level very close to the critical load, where deflections grow excessively. This behaviour is typical for cable-stayed bridges, see for instance *Walther et al.* (1985) and *Klein* (1990).

Referring to Fig. 5.13 maximum deflections at midspan reach more than 30 m or almost 1/25 of the main span length. Deflections of this magnitude would without doubt result in yielding in some of the structural elements. So in order to obtain a more realistic description of the last part of vertical buckling by means of a nonlinear calculation, an elasto-plastic material model should be applied for cables and girder instead of the linear elastic model used here. However, we refrain from doing so here, since the critical loads found are sufficiently high to ensure that the prototype bridge investigated does not exhibit any stability problems.

5.4 Parametric study on torsional stiffness of girder

5.4.1 Static behaviour

In Section 5.2 we saw that the response to lateral load of cable system d) differs from the response of the other three layouts of the spatial cable system. As described in Section 2.3 cable system d) can only be considered as pseudo spatial since torsion has to be transferred by the girder. In connection with wind load this resulted in excessive lateral deflections, when applying the correct torsional stiffness of the prototype girder, see Fig. 5.5. Therefore we carry out a parametric study on the torsional stiffness of the girder.

In Fig. 5.14 the lateral midspan deflections are plotted as function of torsional stiffness for cable system d). For comparison lateral deflections for the other three layouts of the spatial cable system are indicated as well for the correct stiffness of the prototype girder.

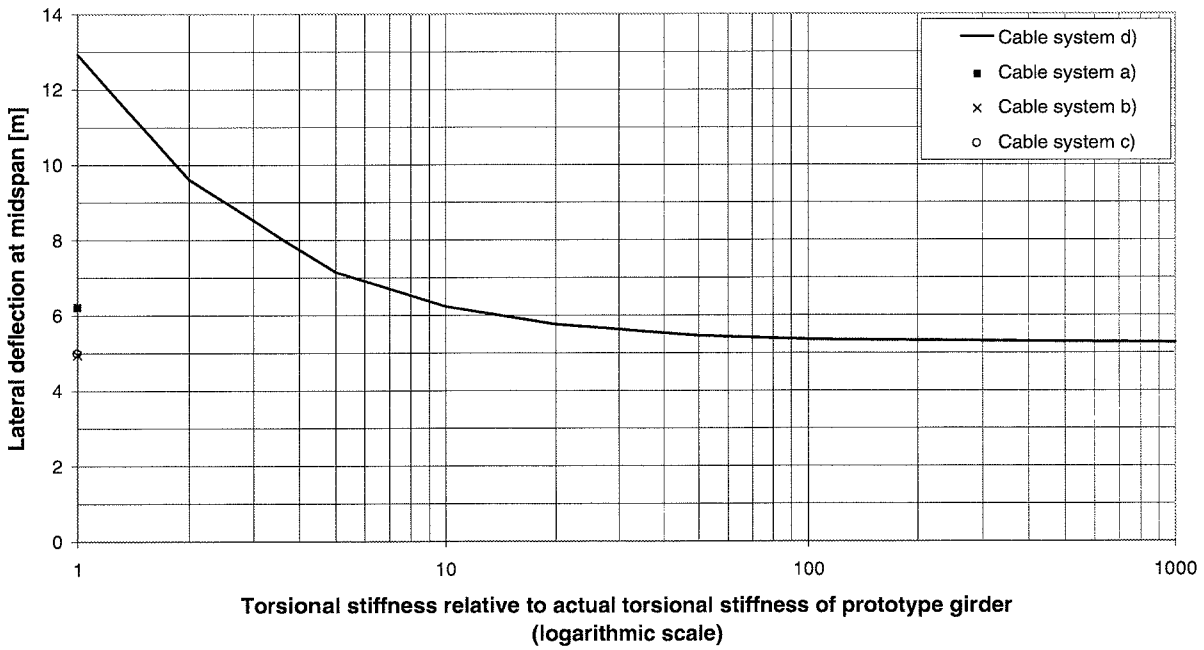

Figure 5.14 *Cable system d). Lateral deflection at midspan as function of torsional stiffness of girder. Compared to cable system a), b) and c).*

In connection with cable system d) torsional stiffness of the girder should be increased by a factor of 10 to reduce lateral deflections to correspond to cable system a). From a factor of 100 no further reduction of lateral deflections is gained by increasing torsional stiffness.

In Fig. 5.15 lateral deflections of system d) along the girder are shown for different values of the torsional stiffness. For comparison the deflection curve of cable system b) having the correct torsional stiffness is shown as well.

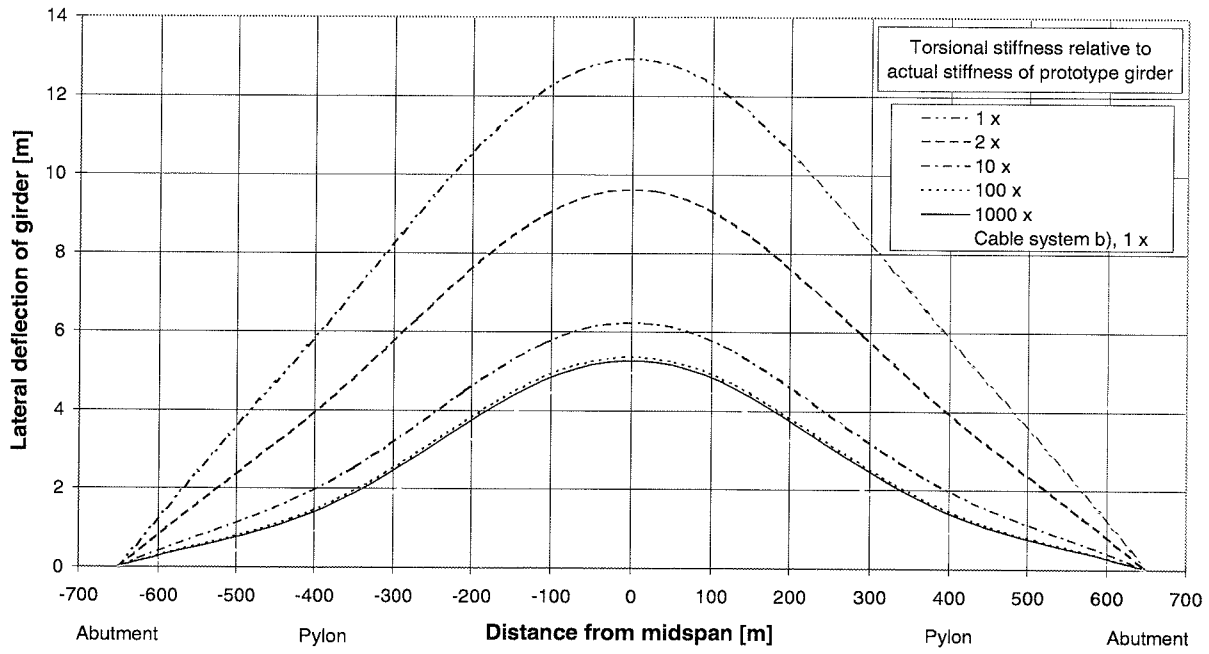

Figure 5.15 *Cable system d). Lateral deflections of girder as function of torsional stiffness. Compared to cable system b).*

When increasing torsional stiffness of the girder the deflection curve of cable system d) approaches the one of cable system b), but the deflections of cable system d) remain 0.2 m - 0.5 m larger than of cable system b).

Considering a box section and taking the thickness of the panels as constant, moment of inertia for torsion, I_{tor} , yields:

$$I_{tor} \simeq \frac{2 \cdot (w \cdot d)^2 \cdot t}{w + d} \tag{5.1}$$

where w is the width and d the depth of the box section. The torsional stiffness is proportional to thickness of the panels, t. Furthermore it is proportional to the area within the boundaries of the box to the power of 2 divided by the length of the boundaries. Increasing torsional stiffness by increasing plate thickness of the panels adds proportionally to the self weight of the girder. On the other hand increasing girder width and/or height does not add quite so much to the self weight. Consequently, a realistic increase of torsional stiffness would be a factor of about 2-3. The parametric study on lateral deflections due to wind load indicates that this is not enough to make the behaviour of cable system d) acceptable.

5.4.2 Buckling stability

In Section 5.3.1 we gave some comments on the behaviour of cable system d) with respect to buckling. In the present Section we carry out a parametric study on the influence of torsional stiffness on the buckling stability as described by an eigenvalue analysis. These results are shown in Fig. 5.16. The critical load for the four fundamental buckling modes described in Section 5.3.1 are plotted as function of torsional stiffness. For comparison the critical loads found for cable system b) are indicated as well. It should be recalled that the symmetric lateral modes are not identical for cable system b) and d), cf. Fig. 5.11 and 5.12.

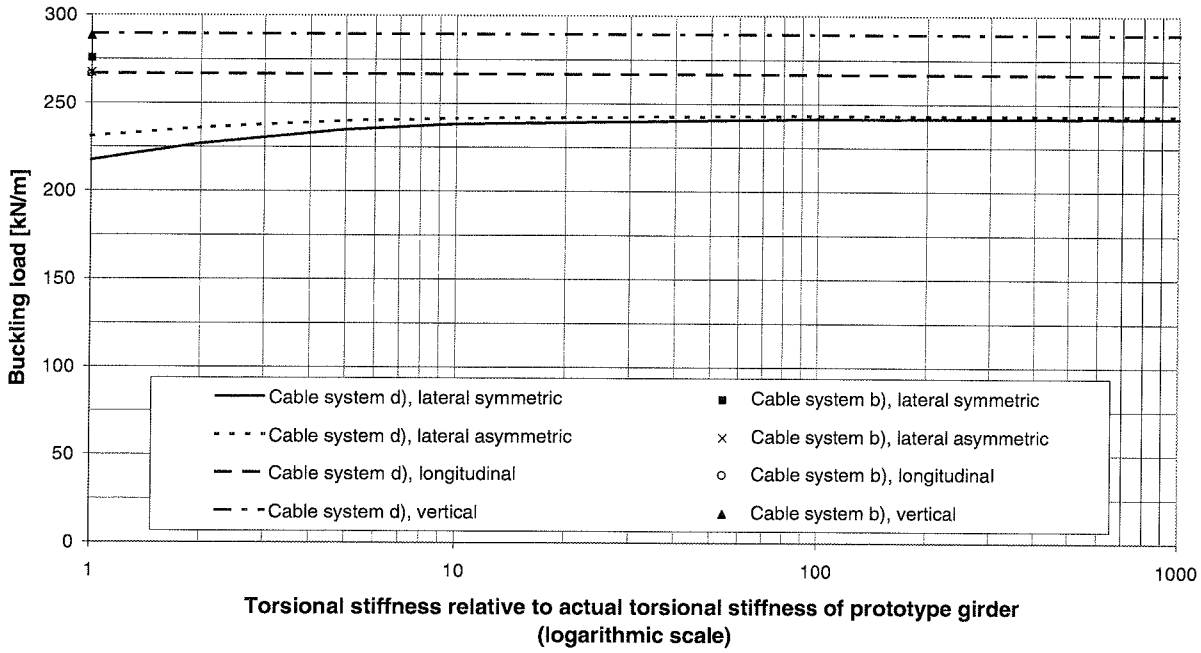

Figure 5.16 *Cable system d). Buckling load as function of torsional stiffness. Compared to cable system b).*

As it appears from Fig. 5.16 only the lateral modes are influenced by the torsional stiffness. Assuming constant bending stiffnesses critical loads for vertical and longitudinal buckling are invariable to changes in torsional stiffness. Increasing torsional stiffness by a factor of 1000 increases critical load for the symmetric lateral mode by 11% and for the asymmetric lateral mode by 5%. So the buckling behaviour of cable system d) is not very sensitive towards the torsional stiffness of the girder.

5.5 Conclusions on FE-analyses of prototype bridge

In this Section we conclude on the results of FE-analyses on the prototype bridge, and on comparisons of four layouts of the spatial cable system.

The main purpose for applying a spatial cable system is to reduce lateral deflections and increase the lateral stability. In the numerical study presented in this Chapter we have chosen to design cables to a dead load stress of $\sigma_g \sim 450$ MPa. In average cable planes are inclined 1:4 in the lateral direction to the bridge axis.

With respect to wind load the fully spatial system, a), and the two partially spatial systems, b) and c), behave similarly bearing in mind that wind load on the cable system itself is larger for cable system a). Deflections of cable system d) due to wind load are unacceptable, and it demands for an excessive increase of the torsional stiffness of the girder to reduce deflections to a level comparable to the other three layouts.

For the chosen geometry of the spatial cable system the lateral bending stiffness of the girder itself contributes perceptibly to the stiffness of the system in the lateral direction. In relation to a real prototype bridge it has to be evaluated if the lateral deflections found in the present study are acceptable compared to actual serviceability requirements. If the lateral deflections found for wind load, and for wind and eccentric traffic loads are too large, one solution is to incline cable planes further. The parametric study in Section 3.4 indicated that a realistic pylon width ranges from half the pylon height to the full pylon height. Consequently one could consider an overall geometry of the spatial cable system where cable planes are inclined 1:2 in the lateral direction corresponding to a pylon width equal to the pylon height. This would also reduce stress variations in the cables due to wind load, since a further inclination of cables in the lateral direction would make them more suited for transferring lateral loads.

Another way of solving the problem of large stress variations in the cables for variable load

could be to increase the permanent load. For instance one could consider a composite or a concrete girder instead of the light steel box girder used in the present study. When the permanent load is relatively high compared to variable loads, stress variations due to the latter are relatively small. One could also combine the advantages of a concrete girder and a steel girder by having the heavy concrete cross-section placed in the area close to the pylons, where stress variations in the cables are largest. Then a light steel girder could be used in the area near midspan (for instance from quarter span to quarter span), where transfer of vertical load is not so efficient because stay cables are relatively flat. This concept has for instance been applied for the Normandy Bridge.

For vertical loading the four layouts of the spatial cable system behave identically.

With respect to buckling stability there are only slight differences between cable system a), b) and c). Also cable system d) behaves in a similar way, so concerning buckling it turns out not to be so important that torsion has to be transferred by the girder instead of by the cable system. FE-analyses show that a bridge with an extremely narrow girder supported by a spatial cable system is not likely to exhibit any stability problems in the completed stage, since the critical loads for buckling instability equal approximately 12 times the characteristic traffic load. However, as a distinctive feature related to a bridge having a narrow girder, the critical loads for lateral and vertical buckling are practically identical. This is in contrast to cable-stayed bridges built until present, where the critical load for lateral buckling is significantly higher than for vertical buckling.

In the present Chapter we have only considered the bridge in its completed stage. In the remaining part of this work we focus on the erection stage in relation to buckling stability of the narrow, cantilevered girder.

Chapter 6

6. DESIGN OF PHYSICAL MODEL AND PLANNING OF TEST SERIES

6.1 Introduction

When dealing with structural problems of a more complicated kind, experiments are often very useful or even essential as a supplement to mathematical modelling. A mathematical model is based on a theory, which is a simplified description of the phenomenon one wishes to investigate. It is obvious, that for complicated systems the description needs to be simplified, otherwise it would be too complicated to use in practice. The more assumptions made, the simpler the theory will be to use. On the other hand, the cost of simplicity could be the accuracy or the realm of validity of the model.

A physical model, on the other hand, has the advantage that "Nature does not forget any parameters or any higher order effects", meaning that the behaviour of the physical model exposed to the defined actions corresponds to reality. The inaccuracies are introduced, when we want to interpret our observations on the model: Firstly, how do we make sure, that we actually measure, what we believe we measure? What is the accuracy of our observations, and to what degree can we be expected to disturb the equilibrium of the system by our measurements? Are we in control of all the important parameters in a way so that the test

results can be reproduced? Then again we need a theory to provide us with an interpretation of our observations on the model. And last but not least: Even though our physical model represents its own reality in model scale, to what extent does it actually describe the real problem in scale 1:1, that we originally wanted to investigate? See also *Askegaard* (1978) and *Brincker et al.* (1991).

As indicated above, useful information can be obtained from both mathematical and experimental methods when used with precaution. For more complicated problems the methods should not stand alone but rather as supplements, so that they can be checked out with each other by comparison. This is the background for our decision to make a series of experimental studies on the buckling stability of a narrow, cable supported girder.

6.2 Aim of the model test

In Section 5.3 we dealt with the buckling stability of the narrow girder of the prototype bridge in its completed stage. Two different approaches were introduced: Eigenvalue buckling analysis and geometrical nonlinear calculation. In the present study we focus on compression introduced by vertical loading. Based on the investigations presented in Section 5.3 we conclude, that a good description of the lateral girder instability is obtained through an eigenvalue analysis, while the best description of the behaviour in the vertical direction must be expected to be obtained through a geometrical nonlinear calculation. For the chosen geometry of the spatial cable system we found that the critical loads for lateral and vertical buckling are practically identical. This is indeed a distinctive feature related to a bridge having a narrow girder because in cable-stayed bridges built until present, the critical load for lateral buckling is significantly higher than for vertical buckling. When the critical loads for lateral and vertical buckling are almost identical, the question of a possible interaction between the two modes of instability arises. It was decided to investigate this field further by carrying out a comparative experimental study on both lateral and vertical girder instability phenomena. Furthermore, test results were expected to supply an experimental indication of the inclination

of cable planes needed for stabilizing tendencies to lateral buckling. This can of course be compared with FE-predictions.

The aim of studying both lateral and vertical instability with - basically - the same model, influenced fundamentally on the design of the model itself as well as on the test setup and procedures. The parameter to be varied is the overall geometry of the cable system. The experimental parametric study focuses on the spatial cable system, but with two geometries of a plane cable system (laterally free or restrained) as reference tests.

We believe this is the first time an experimental parametric study on the buckling stability of a narrow cable supported girder has been carried out.

6.3 Design of the model

As indicated in the previous Section, design of the physical model was to a large extent determined from the aim of studying both lateral and vertical instabilities and possible interactions, more than from a precise scaling down of a well defined prototype bridge. The starting point for design of the model has, of course, been the prototype bridge treated earlier in this study, and the basic dimensions of the model correspond to an approximate scaling down from this prototype. However, it has been necessary to make a number of idealizations in order to get an operational model. As a result, all calculations and all response predictions are made in model scale. This means, that the mathematical modelling is adapted to the actual layout of the model test, instead of attempting to let the prototype bridge dictate the design of the physical model down to the last detail, which would not even have been practicable. This of course, reduces the realm of validity of the test results when generalized to prototype scale. On the other hand, by focusing on modelling the behaviour of the physical model, a good evaluation of the quality of the mathematical description of the phenomena observed can be obtained.

Here, description of the design process will be restricted to dimensions of the actual model and to comparisons with the original prototype bridge. First of all some fundamental choices must be made concerning the overall structural system including the type of cable system, type of loading and scaling factors between prototype and model. Then basically, three structural elements must be designed: Cables, girder and pylon, as well as connections between the different structural elements. A more detailed description of the design of the bridge model can be found in *Vejrum* (1996). Nevertheless, some important choices and idealizations need a few comments.

6.3.1 Basic choices: Cable system

Based on the results presented earlier in this study (Chapter 5), it was decided to use cable system d) for the tests on the spatial system. This cable system has the advantage compared to the other three, that it can more easily be transformed from spatial to plane and visa versa simply by inclining the cable planes, as there are no inwards leaning cables. Even though system d) can only be considered as pseudo spatial since torsion has to be transferred by the girder, it was documented in Section 5.3 "Buckling stability", that this has no crucial influence on the buckling modes compared to the other spatial systems studied here. The critical load for lateral buckling is slightly lower than for the other three layouts of the spatial cable system, but this fact is assumed to be acceptable compared to the practical advantages obtained from applying cable system d) for the model test.

6.3.2 Basic choices: Structural system

An important phase to study in more details is the erection stage, where the maximum cantilever reaches the centre of the main span. In a number of cases special measures have been necessary to ensure stability during cantilevering of girders supported by a plane cable system, e.g. the Karnali River Bridge and the Normandy Bridge, see *Gimsing* (1994). The main concern in these cases have been wind load on the cantilever arm and the related deflections, but with a more pronounced lateral slenderness, it might also be a problem to ensure the buckling stability. As already mentioned, the aerodynamic stability of a narrow cable supported bridge both during construction and in the completed stage has thoroughly

been investigated by *Larsen* (1995).

Here the focus is on the buckling stability during cantilevering. Therefore the model corresponds to half the main span, and in order to simulate the support conditions during the construction phase, the girder has no translational freedoms at the pylon but is free to rotate about a horizontal axis in the lateral direction. Thus, the girder is laterally and torsionally restrained at the pylon during erection.

6.3.3 Basic choices: Geometrical length scale

The choice of a geometrical length scale was based on a number of considerations. A primary concern is to have as large a scale as possible for the obvious reason, that construction details are easier manufactured and measuring equipment easier to install, when the model is large. On the other hand the available standard equipment and free space in laboratories set a limit to the size of the model. Therefore, a reasonable choice for the geometrical length scale is found to be around 1:80 giving a cantilever of 5 m and a pylon height from girder to pylon top of approximately 1.5 m. This scaling is as far as possible used throughout the design of the model.

6.3.4 Basic choices: Loading

To simplify the test setup it was decided only to use vertical load to introduce compression in the girder. It should be recalled, that to ensure the possibility of both vertical and lateral instability phenomena to develop, no restraints - lateral nor vertical - arising from the loading arrangement can be allowed.

6.3.5 Similitude requirements

In cases where the geometry plays a dominant role for the load carrying capacity of the structure - as for a structural element subjected to compression - it is important that the scaling factor of strains is equal to 1, see *Askegaard* (1978). The relationship between stresses, σ, and strains, ε, is given by the well known expression, where E is the modulus of elasticity:

$$\sigma = E \cdot \varepsilon \tag{6.1}$$

Using this, the properties of the model are now scaled from the assumed prototype according to the Cauchy scaling, giving the following equation for the corresponding scaling factors

$$K_\sigma = K_E \cdot K_\varepsilon \tag{6.2}$$

where

$$K_\varepsilon \equiv 1 \tag{6.3}$$

Using the length scale, K_l, given by:

$$K_l = \frac{l_{prototype}}{l_{model}} \equiv 80 \tag{6.4}$$

some preliminary dimensions of the model are obtained. From this preliminary design a number of idealizations became necessary as already mentioned. A consistent application of the model laws in this particular case would therefore be to scale the test results from the actual dimensions of the physical model to an appropriate prototype bridge.

6.3.6 Ultimate strength

First of all it is important to notice, that in traditional cable-stayed bridges in the completed stage the safety factor against failure by vertical instability of the girder is in the order of 8-12 times the service load, or approximately 3-6 times the sum of permanent and service loads for the most common cases, where the traffic load equals 50-100% of the dead weight, (cf. the results presented in Chapter 5). The structural component with the lowest degree of safety is often the stay cables, where the safety factor against yielding is usually taken as 2.2. However, to achieve an economical structure the safety factor for most components should be of the same order of magnitude. See for instance *Gimsing* (1983) and *Walther et al.* (1985).

This means, that in order to be able to investigate instability phenomena, all parts of the model need to be overdimensioned by approximately a factor of two or three regarding strength

compared to the prototype dimensions. At the same time the model needs to keep the correct stiffnesses of all elements important for load distribution and deflections, otherwise its behaviour would differ from the intended.

This influences strongly on the design of cables, as their cross-section cannot be increased without increasing the axial stiffness at the same time, when the same material is to be used. Instead, it was decided to model the axial stiffness of the cables with tension springs. In this way the rest of the cable can be made of steel rods with an area, that makes it reasonable to consider this part of the cable completely rigid in comparison with the springs. So all the requisite elongation of the compound cable element should be due to the tension springs, and both the springs and the steel rod should have sufficient load carrying capacity for the cable force at stability load, as these two elements are connected in series.

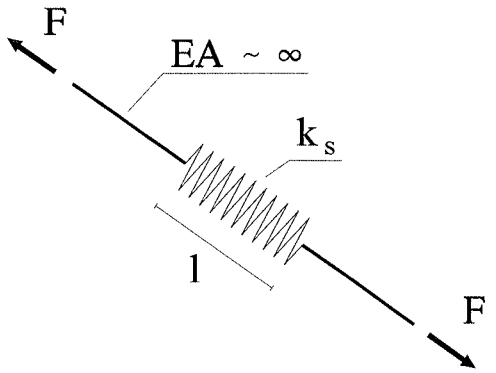

Figure 6.1 *Principle of cable element consisting of steel rod in series with a tension spring.*

6.3.7 Idealizations: Number of cable sets and their axial stiffness

In the prototype bridge, the distance between the cable sets is 20 m at the girder, so in half of the main span there are 20 sets. In the physical model in scale 1:80 this would give a distance of only 25 cm at the girder, causing some difficulties regarding fixation to the girder and also regarding vertical spacing between cable anchorages at the pylon top. Also the amount of work to fabricate 20 cable sets would be considerable. A more reasonable layout

of the cable system in the model would be 5 sets with a spacing of 1 m, so four cable sets in the prototype correspond to one in the model. This implies, that the cross-sections of the cables in four consecutive sets are added. Together with the matching tangent modulus, E_t, corresponding to a dead load stress of 450 MPa in the prototype cables and using the appropriate scaling factor for the spring stiffness of the cables, k, the latter given by:

$$k = \frac{E_t A_c}{l_c} \tag{6.5}$$

thus

$$K_k = \frac{K_l^2}{K_l} = K_l \tag{6.6}$$

this leads to a target axial spring stiffness of the cables in the model of approximately 75-80 N/mm. The cross-sections of prototype cables used here can be found in App. A.

6.3.8 Idealizations: Girder geometry and material

First of all it was decided to use aluminium instead of steel for the girder. The reason for this was the reduction of the load needed to reach the limit of stability. The lateral buckling load, N_{cr}, of the plane cable system is governed by the classical Euler formulation:

$$N_{cr} = \frac{\pi^2 EI}{l_s^2} \tag{6.7}$$

where l_s depends on normal force distribution and support conditions. EI is the bending stiffness. By replacing the steel girder by one in aluminium, the critical normal force and consequently the critical vertical load can be reduced to approximately 1/3.

A reasonable description of the vertical buckling can be obtained by using the expression for an infinitely long beam on a continuous elastic support also known as the Winkler foundation:

$$N_{cr} = 2 \cdot \sqrt{k_v \cdot EI} \tag{6.8}$$

where k_v is the vertical spring stiffness of the elastic support. The normal force is here assumed constant along the girder. Consequently, for the vertical instability it can be expected that the necessary load can be reduced to $1/\sqrt{3}$ (~58%) by choosing aluminium instead of steel.

It should be emphasized that for the plane system, where the girder gets no lateral support from the cable system, the change in modulus of elasticity causes a change in the ratio between critical load for the first lateral and the first vertical buckling mode. This is to some extent compensated by choosing appropriate moments of inertia for the aluminium profile.

The choice of cross-section is governed by several concerns: First of all it is important to notice, that even though the ultimate strength of certain aluminium alloys is comparable to mild steel, the stress-strain relationship is nonlinear in contrast to steel. Therefore, it is desirable to keep the stress level as low as possible. Furthermore, no permanent deformations are allowed in the girder, if this is to be reused in several tests.

As explained in Section 6.3.7 "Idealizations: Number of cable sets and their axial stiffness", the cable spacing in the model is four times the spacing in the prototype. Consequently a solid profile was chosen to avoid any local instability problems of the girder between the cable supports. This is also advantageous for the sections where the load is to be transferred, as a local strengthening is then superfluous. The girder material finally chosen was AlMgSi 0.5 with a cross-section of 30 mm × 50 mm.

6.3.9 Idealizations: Pylon stiffness

As already described in Section 3.3.4 "Deformations", a displacement of the pylon top is related to an elongation of the anchor cables, causing the total cable system to rotate, see Fig. 6.2 (and cf. Fig. 3.5):

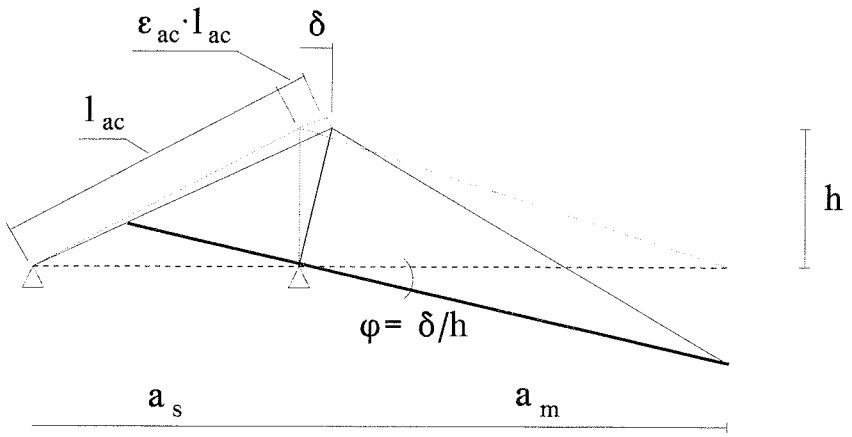

Figure 6.2 *Rigid body rotation of the cable system caused by elongation of the anchor cable. Adapted from* Gimsing *(1983).*

The rotation angle is given by:

$$\varphi = \frac{\delta}{h} = \frac{h^2 + a_s^2}{h \cdot a_s} \cdot \varepsilon_{ac} \tag{6.9}$$

giving the following elastic support of the pylon top in the longitudinal direction of the bridge, k_l:

$$k_l = \frac{EA_{ac}}{l_{ac}} \cdot \frac{a_s^2}{l_{ac}^2} = EA_{ac} \cdot \frac{a_s^2}{(h^2 + a_s^2)^{3/2}} \tag{6.10}$$

where $E \cdot A_{ac}$ is the axial stiffness of the anchor cable, l_{ac} is the original anchor cable length, while h and a_s are the pylon height and length of the side span, respectively.

In the following the effect of a rigid body rotation of the cable system about the base of the pylon will be evaluated with respect to stability of the girder.

As it is the case for the main span, cables in a model side span should correspond to four cables in the prototype, leading to three cable sets in model scale plus the anchor cables. Actually, when estimating the stiffness of the support of the pylon top, it would be realistic

also to take into account the cable set right after the anchor cables. As this cable set - the third counted from the pylon - would be anchored just 12.5 cm from the vertical support at the side span end, it would add most efficiently to the longitudinal support of the pylon top.

From the prototype cable dimensions listed in App. A, and using Eq. (6.10), the elastic support of the pylon top in model scale is found to lie in the interval 180 N/mm to 240 N/mm per anchor cable.

The next step is to estimate the size of the horizontal component of cable forces as this is to be transferred from the pylon top by the anchor cables. Only additional load in the main span will be considered, as this leads to the maximum horizontal force at the pylon top. Assuming an additional load corresponding to twelve times the service load (see Section 6.3.6 "Ultimate strength") to cause vertical instability, one reaches a load of 240 kN/m in the prototype equalling 3 kN/m in model scale. When this vertical load is projected according to the cable angles, a horizontal force of approximately 30 kN is found.

In model scale the result of the investigation is a displacement of the pylon top in the order of 60-85 mm towards the main span, corresponding to a 3° rotation of the cable system.

The change of the distribution of forces in the structure can be evaluated in the following way, where only axial forces in the structural members are taken into account:

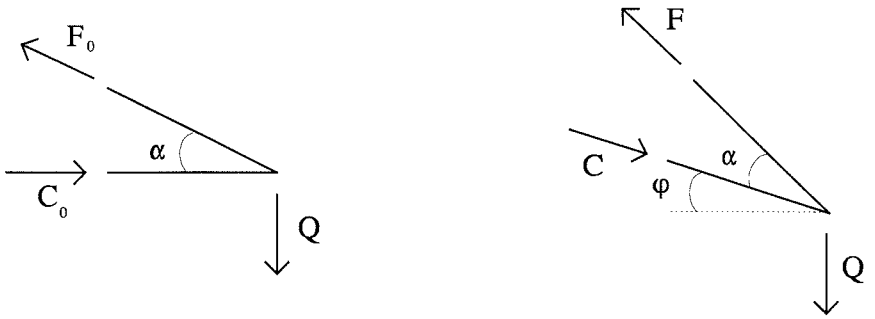

Figure 6.3 *Rigid body rotation of the cable system. Equilibrium in the initial and the rotated stage.*

to the normal force in the girder due to the vertical load applied at the cable set under consideration. The total normal force is of course accumulated along the girder.

$$F_0 = 1.206 \cdot Q \quad , \quad C_0 = 0.675 \cdot Q \tag{6.19}$$

$$F = 1.205 \cdot Q \quad , \quad C = 0.621 \cdot Q \tag{6.20}$$

In this case an 8% reduction of the contribution to the compression in the girder, but this is of minor influence on the total destabilizing compression in the girder, as the steeper cables do not contribute much. The change in cable force is still less than 2‰.

The fact, that cable forces and thereby compression in the girder are reduced seems quite logical, as cables become steeper and thus get more suited for transferring vertical load, when the cable system is given the rigid body rotation shown on Fig. 6.2.

However, no bending of the girder arises from the rigid body rotation of the cable system, and as the rotation only slightly changes the distribution of forces in the structure, no major influence on the behaviour with respect to vertical buckling is to be expected. This is confirmed by FE-calculations in model scale, where the pylon top is given an elastic support corresponding to the action from a side span. As demonstrated above this can be simulated by means of a longitudinal elastic support with a spring stiffness in the order of 180-240 N/mm in each side of the pylon. The results of these calculations are compared with a FE-model, where the displacement of the pylon top in the longitudinal direction of the bridge is restrained. No change in critical load can be detected at all for the lower vertical modes.

Due to the fact, that a displacement of the pylon top caused by an elongation of the anchor cables in both sides will only slightly change the distribution of forces in the system, there will be no effect on the behaviour with respect to lateral buckling either. However, a change in structural behaviour would occur, if the two sides of the pylon top are allowed to move in opposite directions, i.e. an increase in tension in one anchor cable and a reduction in the other. In order to check the effect of this phenomenon, which obviously only has influence on the

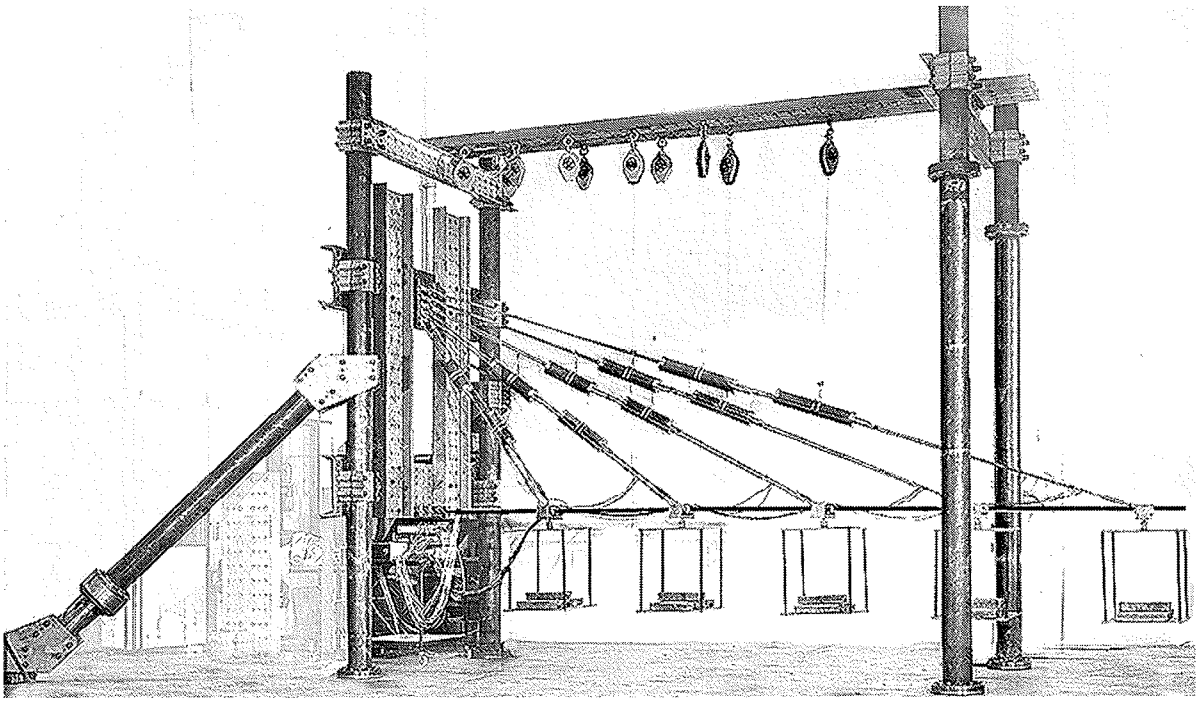

Figure 6.5 *General view of test setup.*

For the plane cable system the layout of the supporting arrangement at the pylon top is seen in Fig. 6.6.

The spherical bearings ensure the correct statical behaviour of the cable elements, that have a relatively large bending stiffness due to the overdimensioned cross-section. However, the maximum sideways rotation of the bearings is limited to 9°.

These spherical bearings are also used at the connection between the cables and the girder, see Fig. 6.7. The distance between the centre lines of the bearings is 162 mm corresponding to approximately 12 m in the prototype. It should be noticed that the axle, at which the cables are mounted, does not pass through the girder as this would lead to a nonallowable weakening of the section. Due to bending of the axle, this element needs a diameter of 20 mm even when Cr.Ni.Mo.6-steel, which has a yield strength superior to 640 MPa, is used. So, instead of transferring the force directly to the girder, it is led through the two spacers on each side of the girder to the steel plates on its top and bottom side and finally into the girder itself by the

two vertical fitted bolts. The actions on these bolts are much less than on the axle, and therefore Ø10 is sufficient, leading to a weakening of the section of only 20%, whereas the axle would have caused a weakening of 67%. To prevent the bearings from slipping sideways, the axle is provided with spacing bushs made from steel tubes, that fit precisely onto the axle. As certain geometrical requirements in the Danish Code *DS412* (1983) could not be met (distances from holes to free edges), the fitting was test loaded before mounting in the model.

FE-calculations have been carried out to check the effect of local strengthening of the girder due to the fittings for load transfer. When full composite action is taken into account over a length of 80 mm corresponding to the distance between the two rows of bolts, a 7% increase of the critical load for the first lateral mode is found. The increase of the critical load for the first vertical mode is 2%.

At the level of the pylon the appropriate end support conditions for the girder are obtained as can be seen in Fig. 6.8.

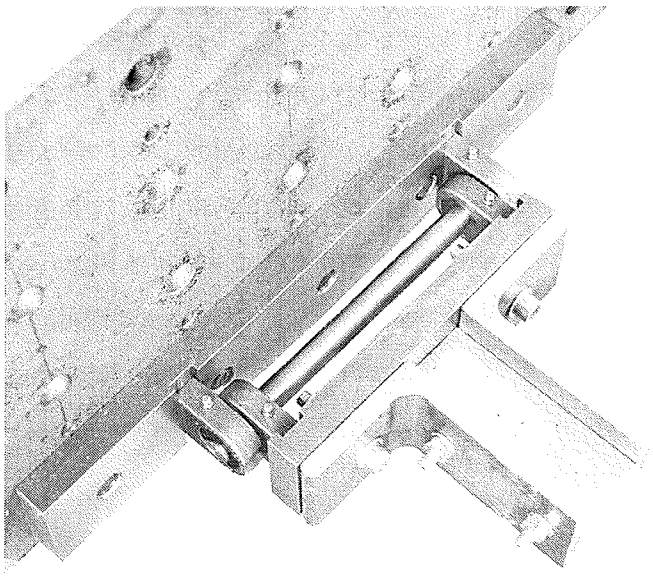

Figure 6.8 *End support for girder.*

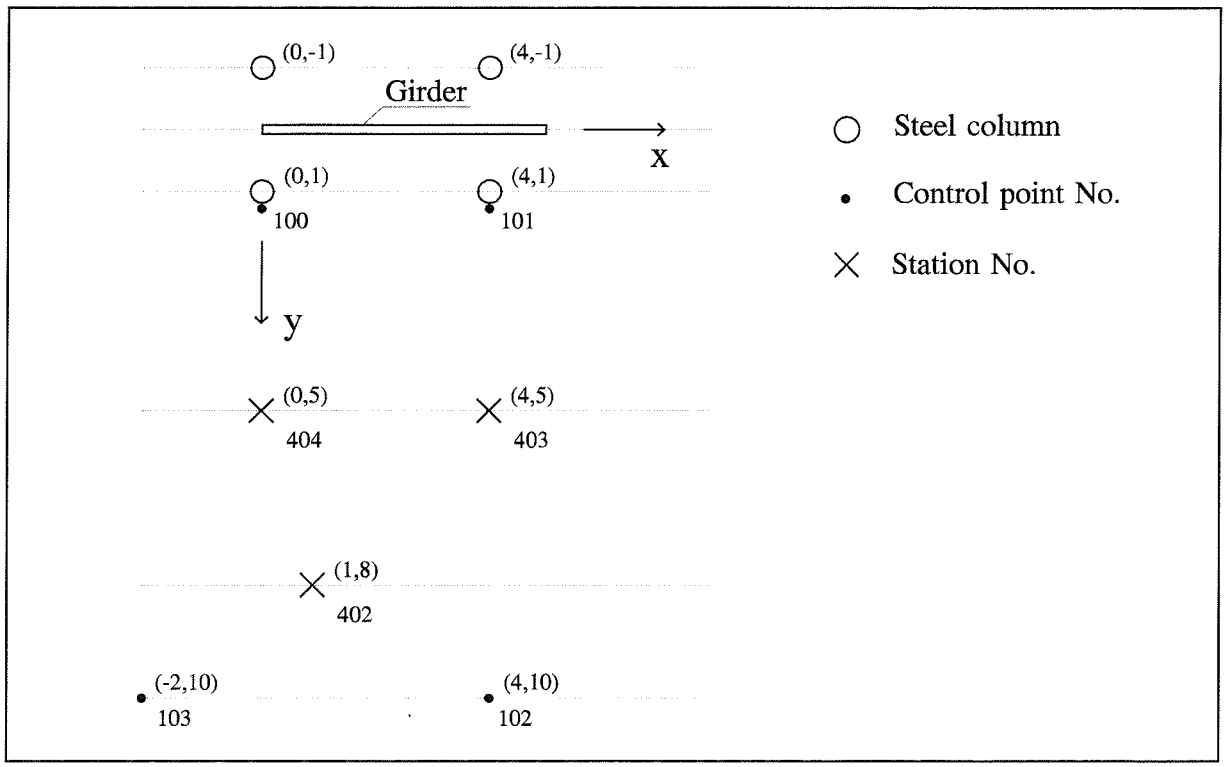

Figure 6.9 *Plan of test setup.*

6.4.2 Load

The model is loaded at five points, i.e. at the anchorage of each cable set. Loading is in the form of 5, 10 and 25 kg plummets placed on scales weighing 30 kg each. Load steps between deflection measurements are varied in the interval from 5 kg to 50 kg. In the following. external load is indicated in [kg]. This is transformed to [N], when forces (cable forces, sectional forces etc.) are determined. The critical load found in the tests is indicated in [kg] corresponding to the weight of scale and plummets at each point of load transfer.

6.4.3 In situ stiffness of cylindrical springs

Cable forces are determined by means of precalibrated transducers placed in series with the springs, while the elongation of the compound cable element - concentrated in the springs - is read on a metric scale on the axle, see Fig. 6.10.

6.4.5 Twist at free end of girder

A 1 m long measure is fixed at the free end of the girder. Rulers are placed at the ends of the cantilevered measure and at two of the steel columns supporting the model. By scanning the rulers in a horizontal plane - ensured by checking the fixed rulers on the steel columns - the twisting angle is determined, see Fig. 6.12.

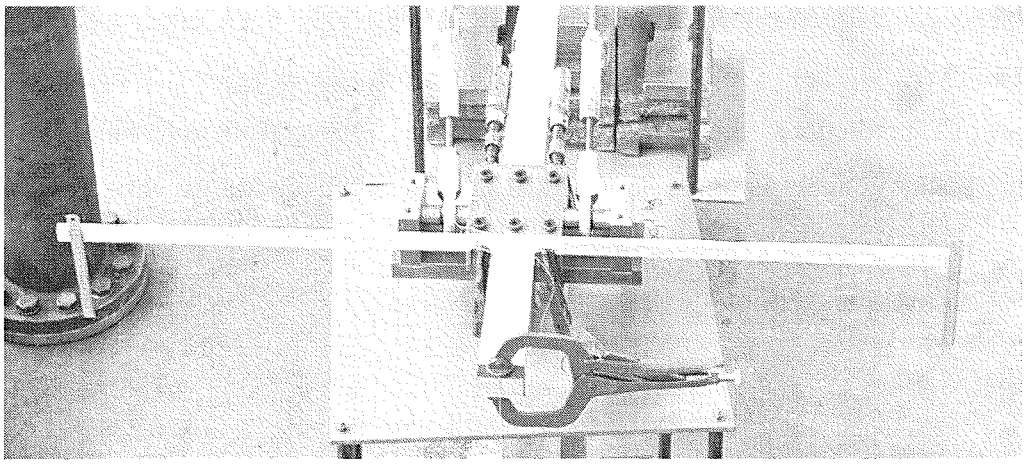

Figure 6.12 *Equipment to measure twist at the free end of the girder.*

6.5 Test programme

First of all two reference tests on the plane cable system are executed to provide the two end point values of the critical load, i.e. for pure lateral instability of the girder without any lateral elastic support and for pure vertical instability of the laterally restrained girder. Then results for all geometries of the spatial cable system must lie within this range, as the axial stiffness of cables is kept constant.

Next, the cable system is changed to spatial. Based on an eigenvalue buckling analysis geometry of the cable system is chosen, so the expected critical load (lateral mode) lies near the midpoint of the above-mentioned range. Subsequently the horizontal distance between

It should be emphasized, that the sideways rotation of the spherical bearings is restricted to 9°. As the inclination of the cable planes is simply obtained by increasing the distance between the anchorages at the pylon top and thereby rotating the bearings, this puts a limit to the maximum inclinations that can be achieved when lateral displacements are also to be allowed without restraints. This problem is solved by restricting further inclination to the longer cables when maximum capacity of the shortest is reached. FE-calculations are adapted to the actual geometry.

An extra girder was kept stand by in case the first one got permanent deformations during testing, which actually happened. To check the stiffness of the new girder mounted with the original cables and fittings, the reference test on the laterally restrained plane system was repeated.

The final programme of accomplished tests looks as follows:

Girder	Test	Cable system
1	I	Plane, laterally free
	II	Plane, laterally restrained
	III	Spatial, a = 35 cm
	IV	Spatial, a = 45 cm
	V	Spatial, a = 55 cm
2	VI	Plane, laterally restrained
	VII	Spatial, a = 75 cm

Table 6.1 *Test programme.* a *is the distance between cable anchorages at pylon top.*

Chapter 7

7. RESULTS OF MODEL TEST

7.1 Introduction

In this Chapter results of the model tests are presented. Due to the extensive amount of data, only selected parts are shown in the Chapter. The remaining test results are found in the appendices or in *Vejrum* (1996). In the beginning of this chapter results from preliminary tests on the girder material and calibrations of the cylindrical tension springs are presented. Then results of tests on the bridge models are described in chronological order, because results from the previous tests were used to plan the following layouts of the cable system. This means that the test programme was adjusted consecutively to the actual results obtained. Some possibilities for control of results are presented in Section 7.3.4, while comparisons of results from different tests and with FE-predictions can be found in Chapter 8.

Another material property of some possible influence on test results is the effect of creep, as duration of a test was often in the order of days. A creep test on a piece of the girder material was performed at a stress level of 35 MPa, i.e. approximately twice the maximum stress due to normal force at the end support of the girder. No sign of creep was observed, see *Vejrum* (1996). Nevertheless, some of the load was removed for the higher load cases, when the model was to be left for the night during a test.

The bending stiffness of the aluminium profile about both main axes was determined experimentally by means of a 4-point bending rig. In Fig. 7.2 and 7.3 the relationship between applied bending moment and measured curvature is shown for the strong and the weak axis, respectively. The experimentally determined bending stiffness attained 21.3 kNm^2 for the strong axis and 7.82 kNm^2 for the weak, which is 3% and 1% below the theoretical values of bending stiffness used during the design process.

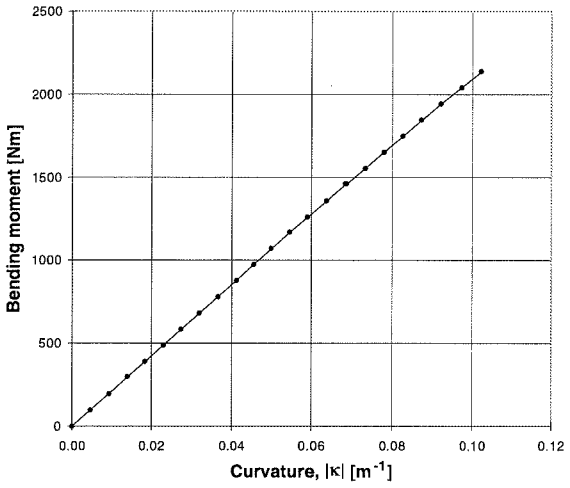

Figure 7.2 *Bending about strong axis.*

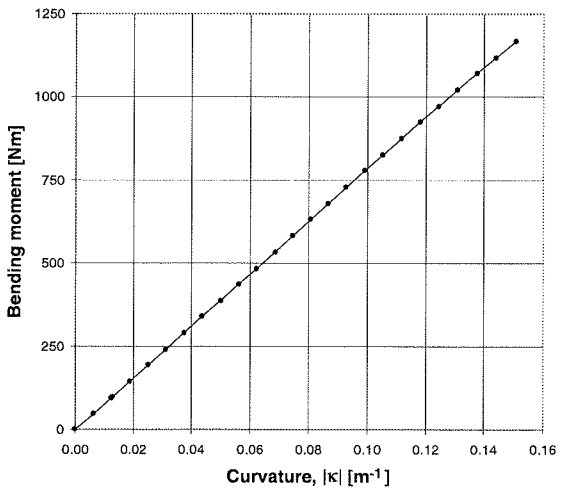

Figure 7.3 *Bending about weak axis.*

According to the experimentally determined stress-strain relationship the applied maximum moments correspond to maximum stresses of approximately 160 MPa for the strong axis and 145 MPa for the weak. The curves in Fig. 7.2 and 7.3 clearly show that it is reasonable to take the bending stiffness as constant in the whole range examined. The explanation of linearity in bending at this relatively high stress level is, that only a small part of the cross-

used for planning the test series.

7.2.2 Calibration of cylindrical tension springs

As mentioned in Section 6.3.7 "Idealizations: Number of cable sets and their axial stiffness" the target axial stiffness is identical for all cable springs, but the requirements for load carrying capacity differ. This led to four different sizes of cylindrical springs, as the same size could be used both for cable set #2 and #3. Three types of discs are available: A, B and C. The discs used are of type C, the most soft, as this reduced the number of discs needed for a specific requirement of elongation. According to information from the supplier the disc response should have been linear up to at least 75% of the deformation corresponding to a total flattening of the disc.

However, this turned out not to be the case. An extensive investigation including tests on individual springs and further information from the manufacturer revealed, that the linear spring response only counts for the hard type A springs, whereas the soft type C springs have a very nonlinear response where the spring stiffness corresponding to a deformation of 75% of total flattening is reduced to one eighth of the initial value.

The highly nonlinear response from the discs, and thereby from the cylindrical tension springs, has to some extent influenced on the bridge model behaviour. First of all, spring stiffness (tangent or secant) depends on the load level making comparison between target and actual stiffness more troublesome. Secondly, spring stiffness is reduced when the force is increased unlike real cables, where stiffness due to reduction of sag effects is increased and asymptotically approaches the elastic modulus of steel, or a slightly lower value depending on layout of the cable.

Another adverse feature about the cylindrical springs is, that their response is not completely stable. This is probably due to the relatively complicated layout of these spring elements, see Fig. 6.4, where some friction of unknown and probably variable size must be expected. Furthermore, this causes the two springs in a set to not act completely identically in the

7.3 Bridge model tests

7.3.1 Deflection and critical load

The most interesting results of the bridge model tests are deflections of the girder and critical loads. Deflection curves for different load levels in a test are presented in one figure to make instability appear more clearly. In Tab. 7.1 load levels at which full measurements have been carried out in the different tests are indicated. The geometries of the cable system are listed in Tab. 6.1 for the seven tests. In the following, when deflection curves are studied it should be kept in mind, that load levels are not equidistant, and that not all deflection curves are shown in the plots in order to improve clarity. Furthermore, the term "load" refers to the mass of scale and plummets per point of load transfer, i.e. the external loading has the unit [kg].

In the following Fig. 7.6 - 7.19 vertical and lateral deflections for each bridge model test are presented. Of special interest is the behaviour of the bridge model in the first two reference tests on the plane cable system (Test I on the laterally free system and Test II on the laterally restrained system), as the results of these tests formed the basis for planning the following tests on spatial systems.

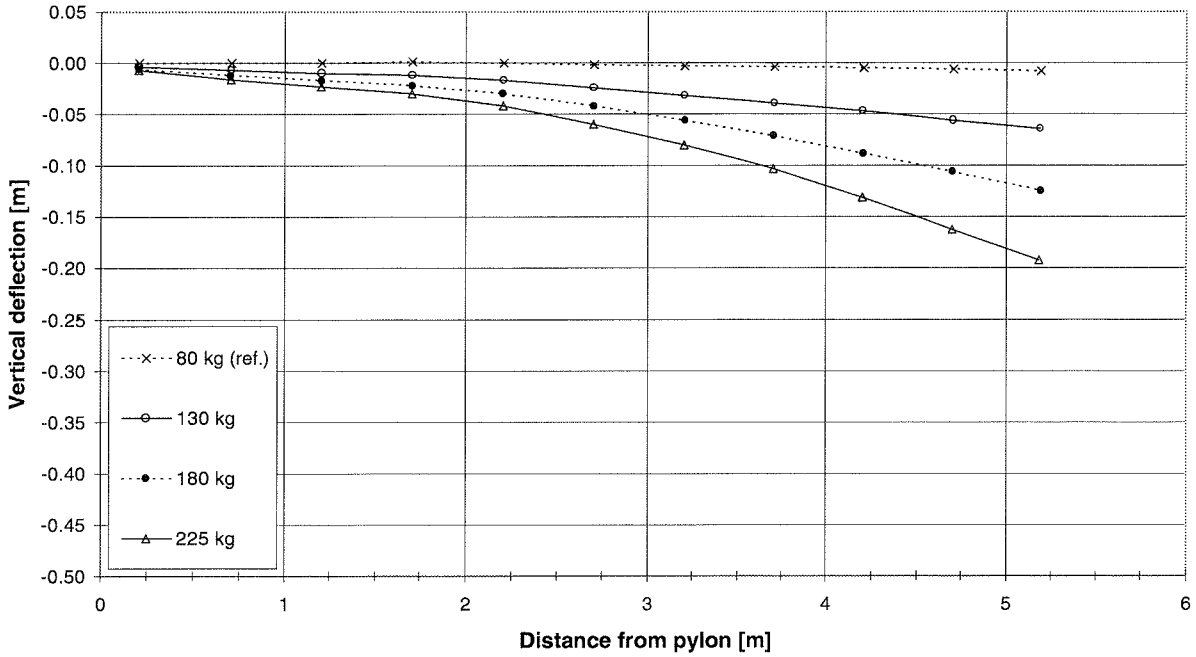

Figure 7.6 *Vertical deflections. Test I, plane system, laterally free.*

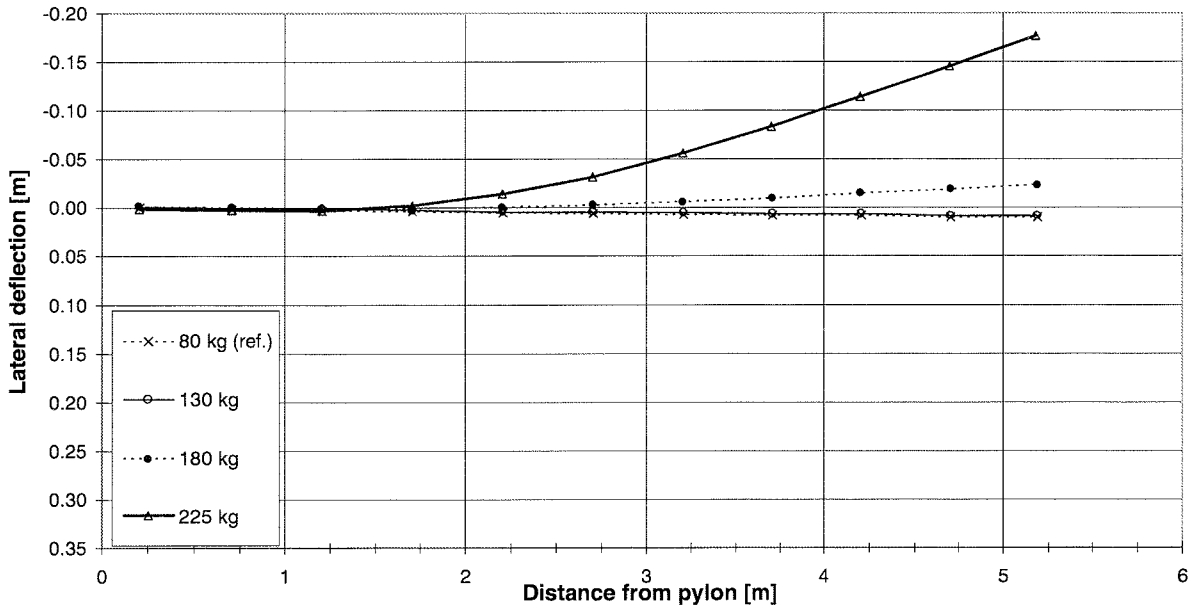

Figure 7.7 *Lateral deflections. Test I, plane system, laterally free.*

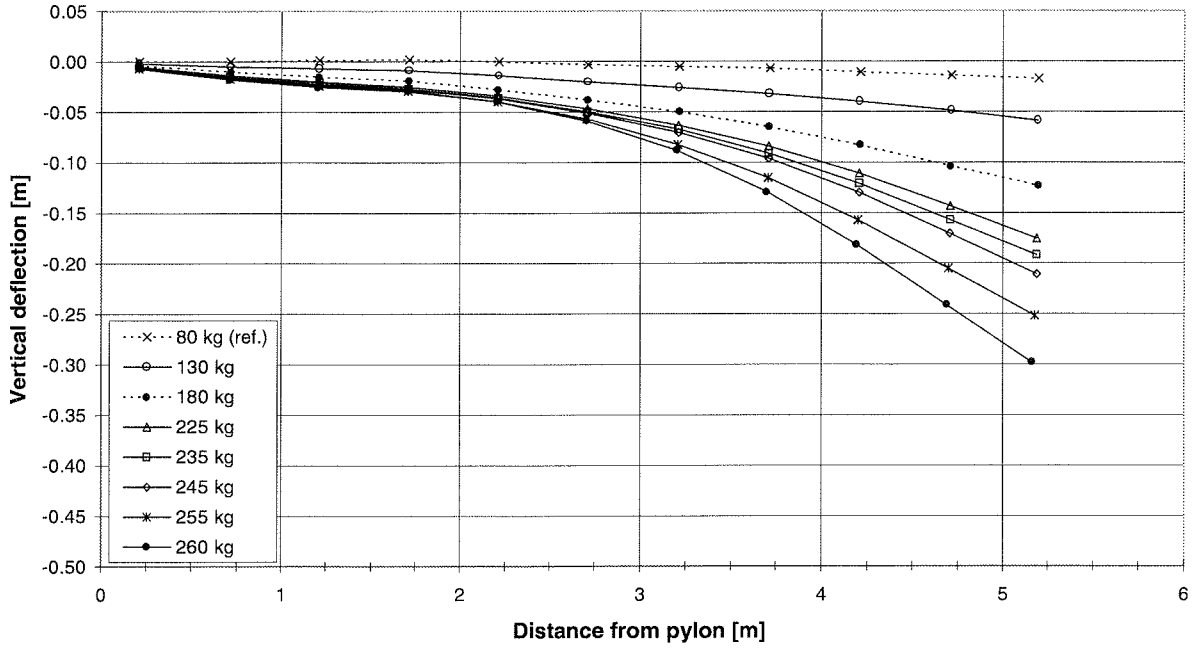

Figure 7.10 *Vertical deflections. Test III, spatial system, a = 35 cm.*

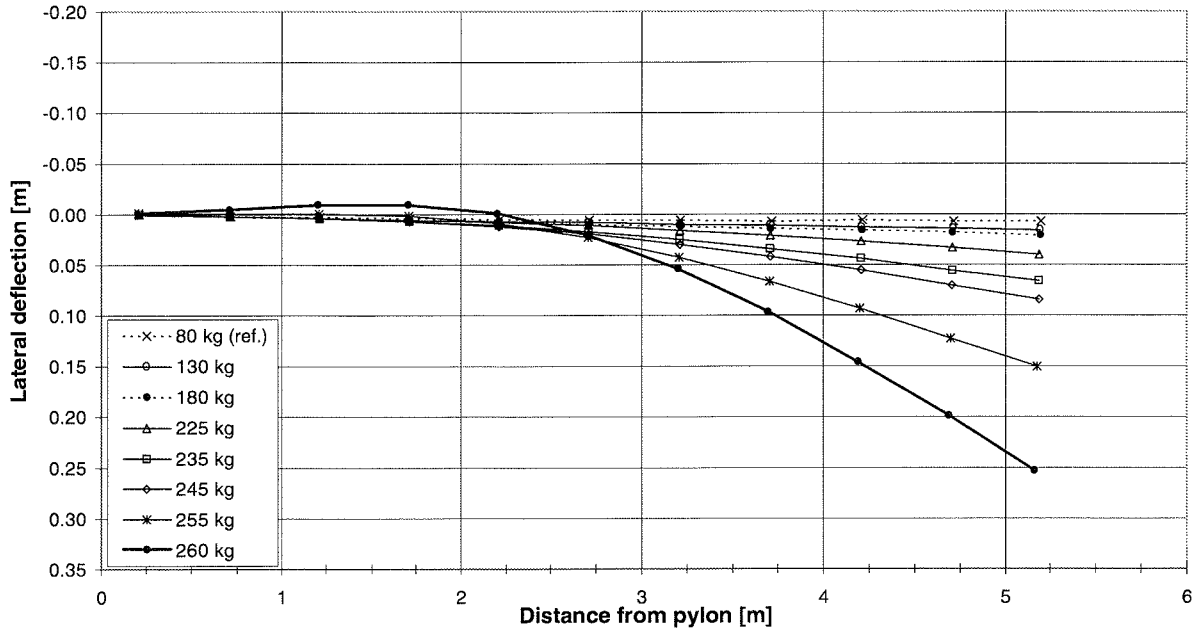

Figure 7.11 *Lateral deflections. Test III, spatial system, a = 35 cm.*

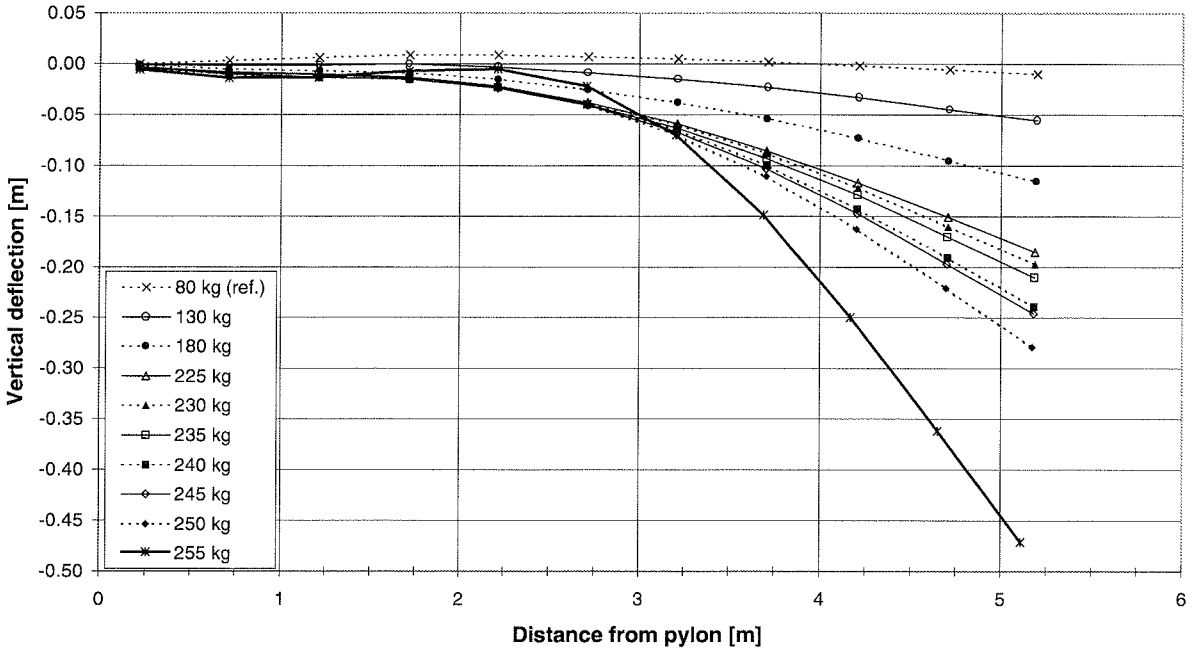

Figure 7.14 *Vertical deflections. Test V, spatial system, a = 55 cm.*

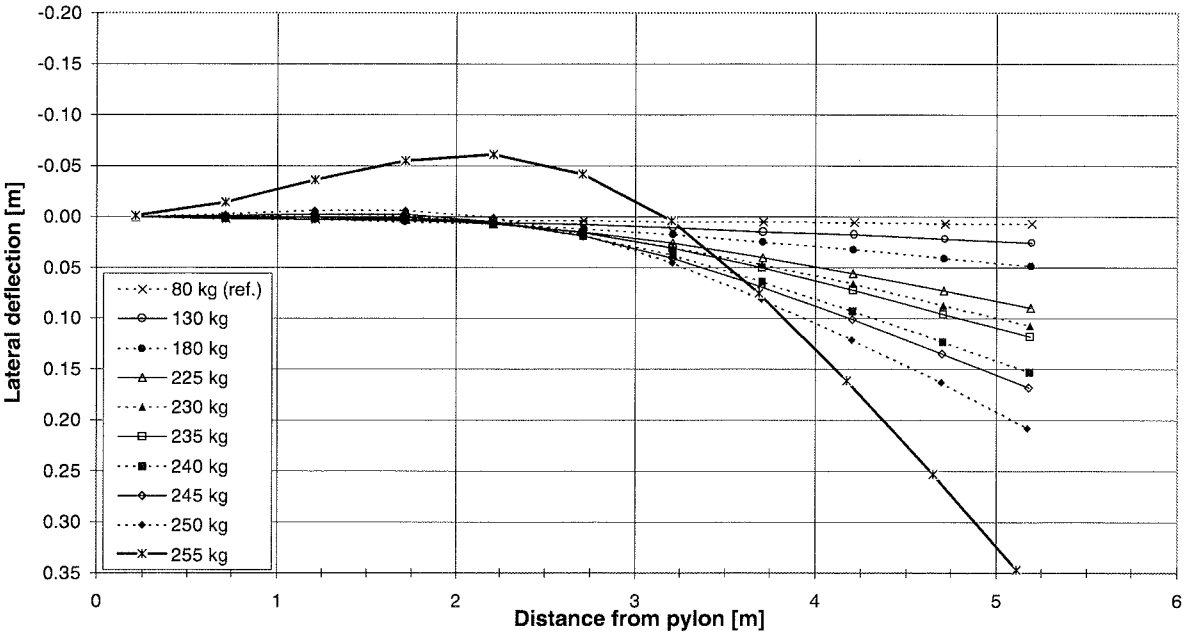

Figure 7.15 *Lateral deflections. Test V, spatial system, a = 55 cm.*

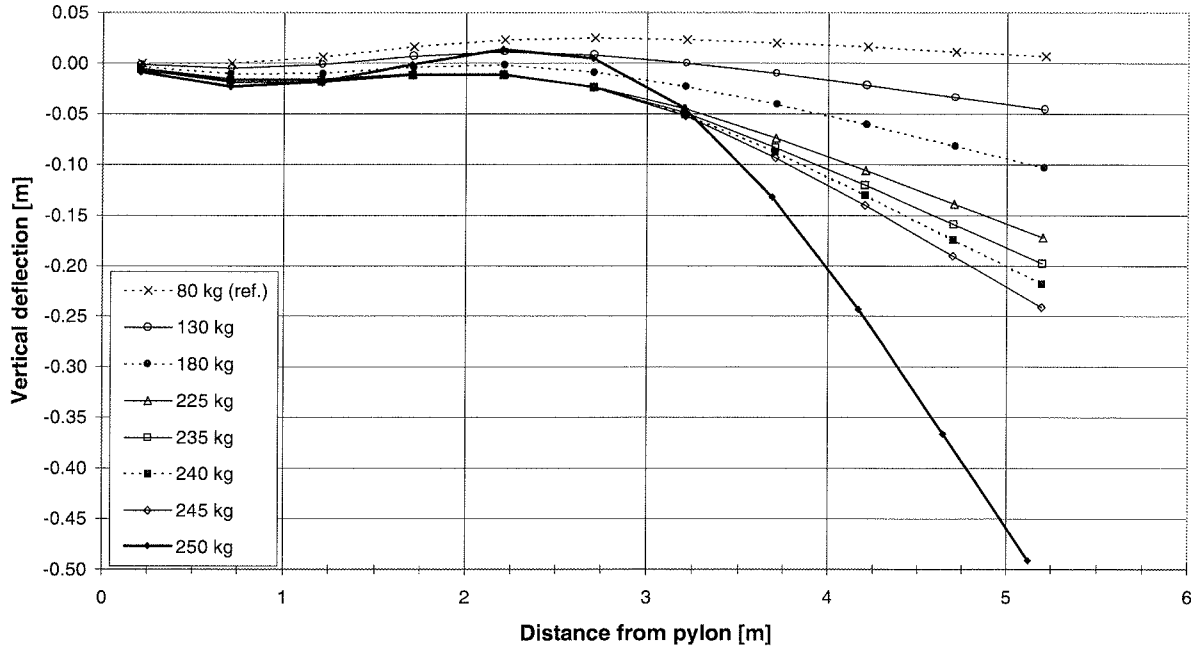

Figure 7.18 *Vertical deflections. Test VII, spatial system, a = 75 cm.*

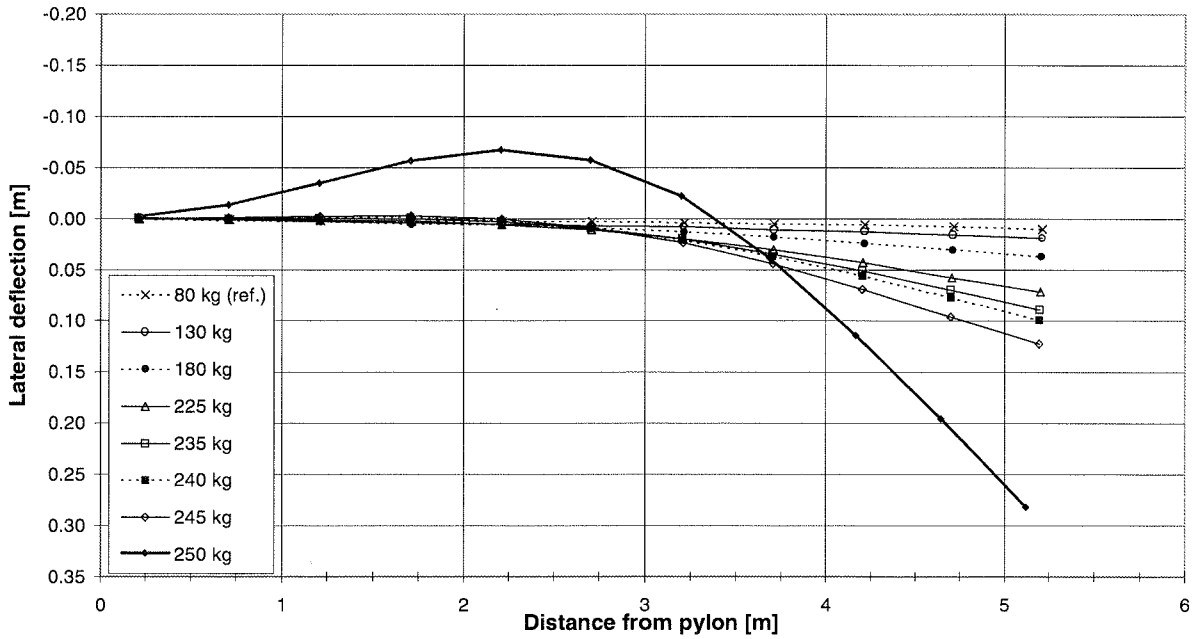

Figure 7.19 *Lateral deflections. Test VII, spatial system, a = 75 cm.*

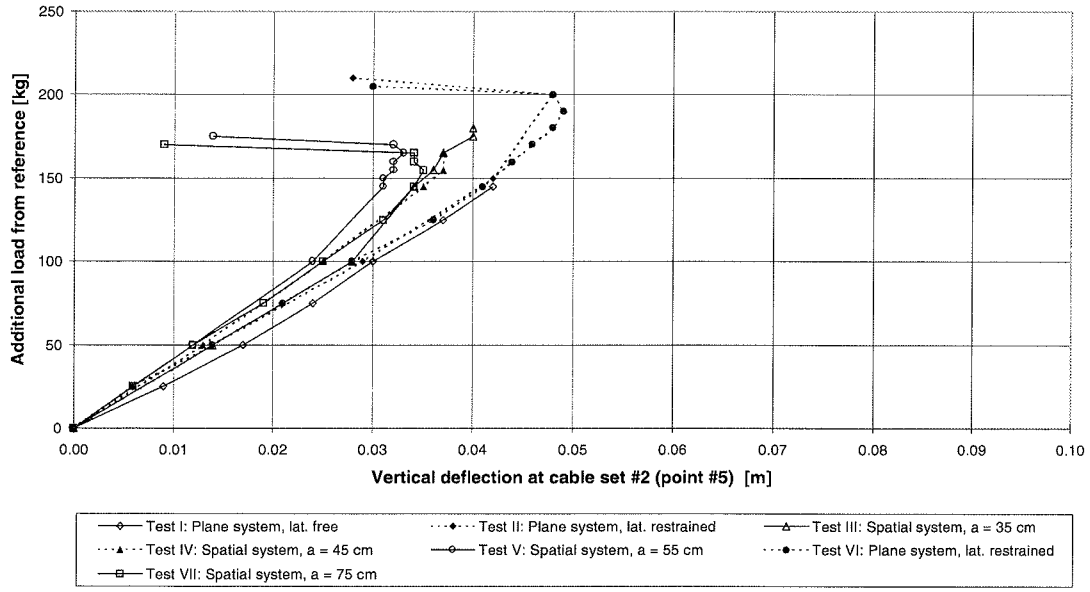

Figure 7.20 *Vertical deflections as a function of load.*

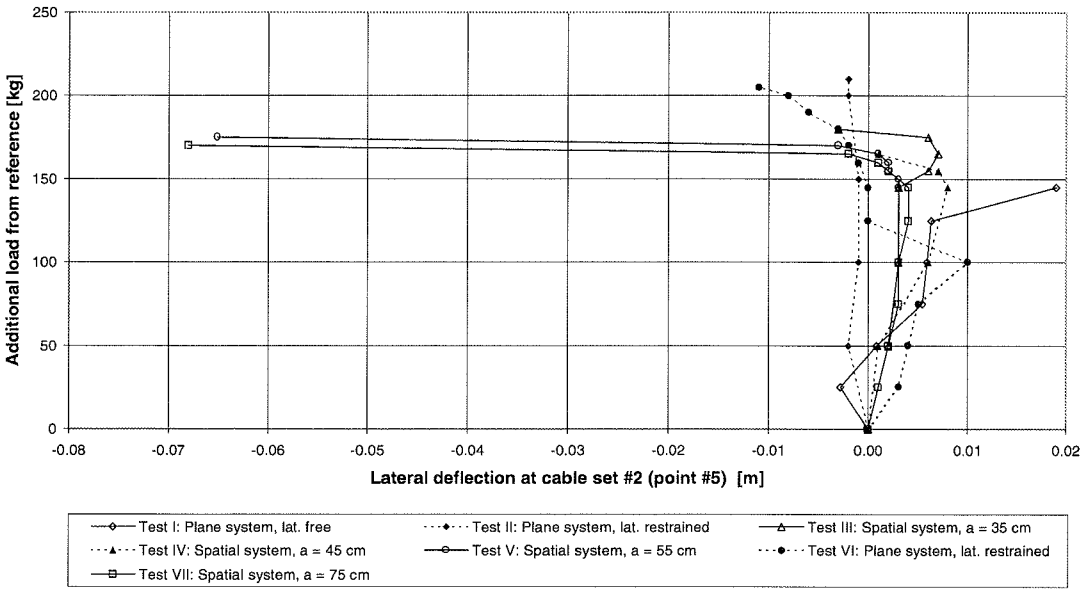

Figure 7.21 *Lateral deflections as a function of load.*

As can be seen from the plots of deflections, Fig. 7.20 - 7.23, it is more correct to indicate a range for the critical load rather than a single value, because the true value for the load that initiates instability lies between the preceding load, that did not cause any change in structural response and the load level for which the girder was forced into a buckled geometry, which clearly left practically none or only little capacity for further loading.

An overview of instability modes and corresponding loads is given in Tab. 7.2, and in Fig. 7.24 the same results are shown in graphic presentation. The loads indicated are the total weight of scale and lead per point of load transfer, i.e. per cable set. The lower end of the range indicates the initiation of the change in structural behaviour, while the upper end is the maximum load applied in the test. Preliminary conclusions of this kind were used in the consecutive planning of the test series.

Test	Cable system	Mode of instability	Critical load
I	Plane, laterally free	Lateral	[205 kg; 225 kg]
II	Plane, laterally restrained	Vertical	[280 kg; 290 kg]
III	Spatial, a = 35 cm	Lateral	[225 kg; 260 kg]
IV	Spatial, a = 45 cm	Lateral	[225 kg; 245 kg]
V	Spatial, a = 55 cm	Lateral / Combined	[230 kg; 255 kg]
VI	Plane, laterally restrained	Vertical	[270 kg; 285 kg]
VII	Spatial, a = 75 cm	Lateral / Combined	[225 kg; 250 kg]

Table 7.2 *Bridge model test results. Evaluated from girder deflections.*

The photos in Fig. 7.25 and 7.26 show a vertical instability mode and two different lateral modes, respectively. The photos have been taken at the last load level in Test II (the laterally restrained plane system), in Test I (the laterally free plane system) and finally in Test III (the

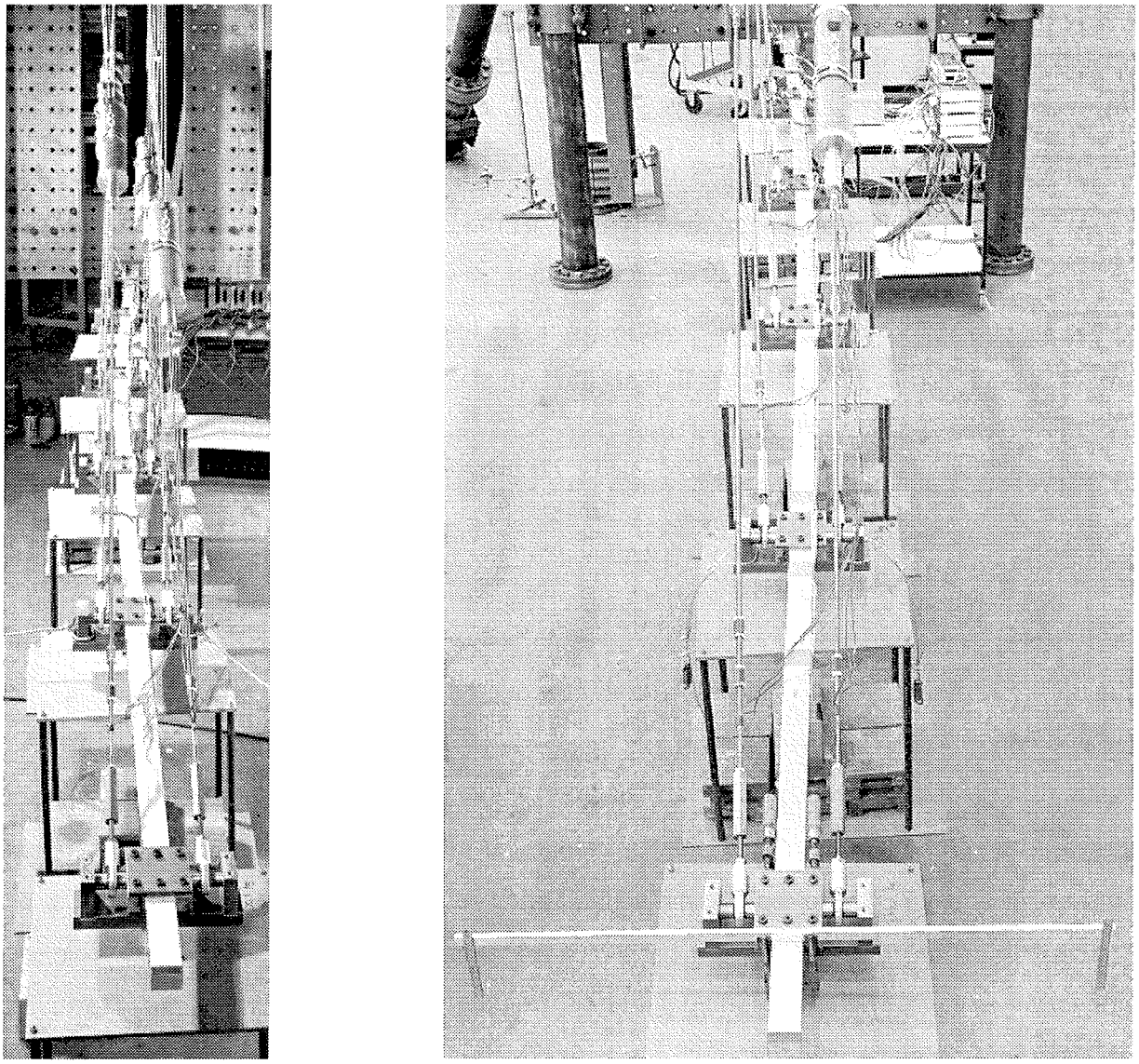

Figure 7.26 *Failure mode by lateral instability. Left: Test I, plane system, laterally free. Right: Test III, spatial system, a = 35 cm.*

7.3.2 Cable forces and in situ spring response

The behaviour of a cable-stayed bridge is primarily governed by the deformational characteristics of the stay cables. Therefore, it is important to follow the behaviour of the compound cable element closely during testing. As already mentioned in Section 6.4.3. "In situ stiffness of cylindrical springs" cable forces are calculated from the transducer signals,

Common for the graphs in the following is, that they all show changes with respect to the reference load situation of 80 kg external load per cable set, described in details in Section 6.6. The reason for this is related to experimental considerations, because the strain gage signals drift differently during time since the original unloaded state was established. This period of time is in the order of months. On the other hand, as test conditions (temperature, humidity etc.) in the laboratories are fairly stable over a period of a couple of days and the strain gages used are temperature compensated for the material in question (steel or aluminium, respectively), it is reasonable to use the 80 kg-load step of each test as reference state for that particular test. The disadvantage connected with the fact that strain gage signals drift is, that the reference load distribution of forces in the system is unknown. This is of course inconvenient in relation to an element with a nonlinear response (here: the springs), where the actual absolute load level also plays a role and not just the changes in loading. However, as already mentioned elongations of the springs are read during testing and thus there is no need for a calibration curve to provide the requisite information on spring response as a function of the force in the cables.

The cable sets are numbered according to their position relative to the girder end support at the pylon. Consequently, cable set #1 consists of the shortest cables closest to the pylon and so forth. The terms "front" and "back" refer to the two sides of the model: "Front" facing the free area in front of the model used for the surveying equipment, while "back" is the side close to the wall in the laboratory. This means, that points related to the front side of the model have positive y-coordinates, cf. Fig. 6.9.

Furthermore, the term "additional load from reference" refers to the mass of the additional plummets added at each point of load transfer to the 80 kg - reference load, i.e. the additional external loading has the unit [kg]. For the cable forces tension is taken as positive.

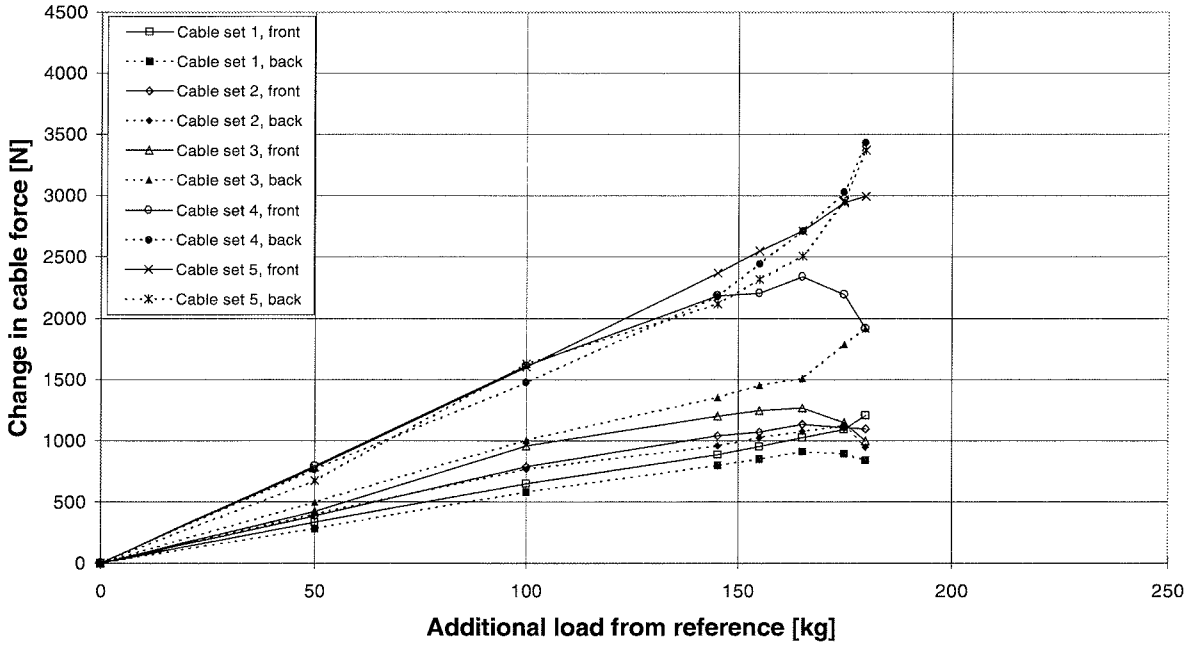

Figure 7.29 *Development in cable forces. Test III, spatial system, a = 35 cm.*

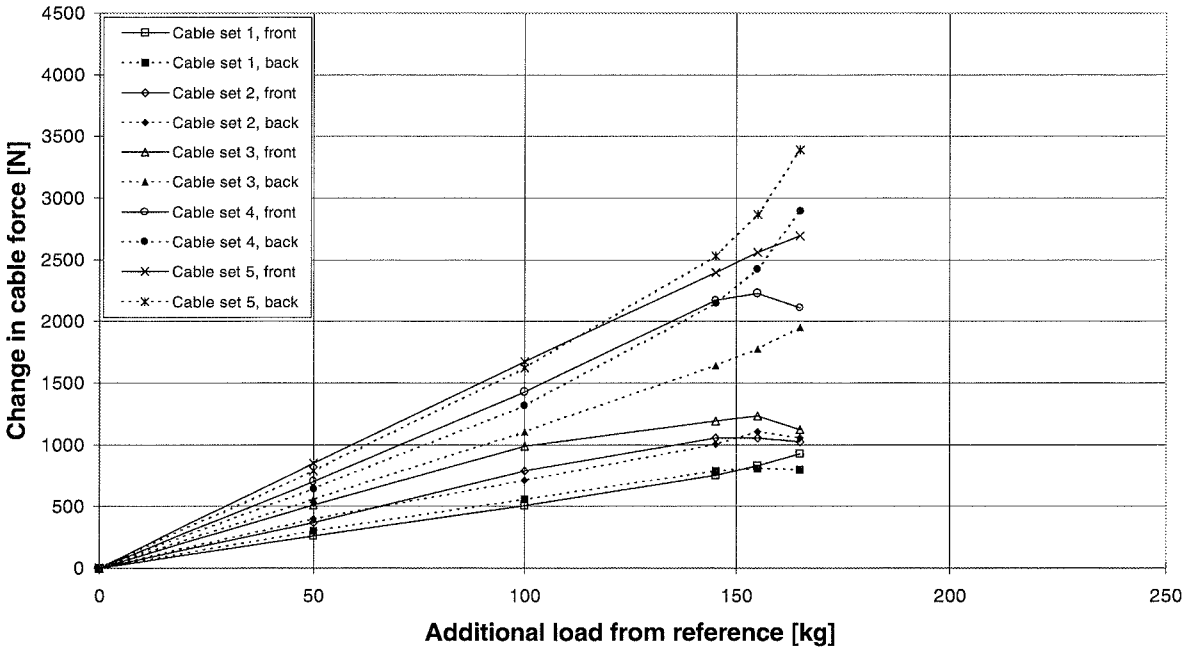

Figure 7.30 *Development in cable forces. Test IV, spatial system, a = 45 cm.*

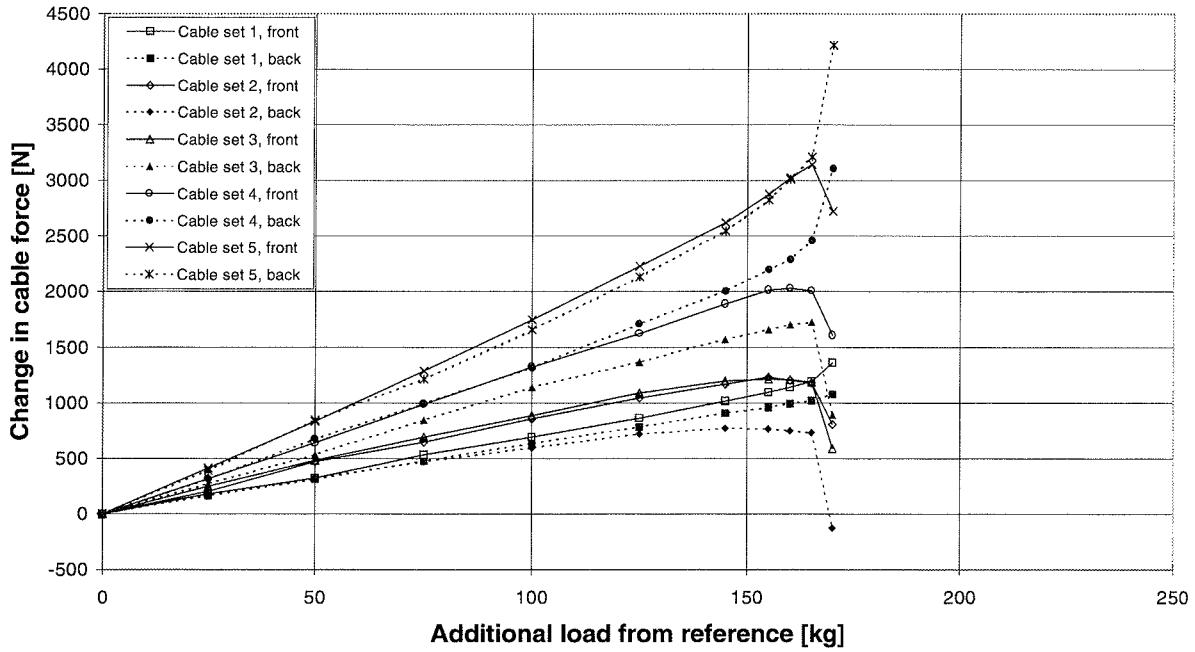

Figure 7.33 *Development in cable forces. Test VII, spatial system, a = 75 cm.*

The plots of cable forces need a few comments:

First of all it should be recalled, that the graphs show changes in cable forces from the reference load situation. This means, that negative values are due to a relief of the cable force below the level corresponding to the reference stage,- of course the resultant should always be tensile.

Furthermore the inclination of cable planes for the spatial systems causes, that cable forces are slightly higher for the same level of external loading. As already mentioned the sideways rotation of the spherical bearings is restricted. Consequently the maximum distance between cable anchorages at the pylon top is limited to 45 cm for cables in the first set. Up to Test IV (a = 45 cm) all cable sets had the same distance between anchorages at the pylon top. For Test V cable set #1 was left with a distance of 45 cm, while the others were further inclined to a = 55 cm. Test VI was the plane system, where a = 16.2 cm for all cables. Finally, for Test VII cable set #1 was left in the position of vertical cable planes, whereas the four outer cable sets were installed with a spacing of a = 75 cm at the pylon top.

Test	Cable sets, where both cable forces are increased	Cable sets, where both cable forces are decreased	Cable sets, where cable forces deviate
I			1, 2, 3, 4, 5
II	1, 4, 5	2, 3	
III		2	1, 3, 4, 5
IV		2	1, 3, 4, 5
V	(5)	2, (3)	1, (3), 4, (5)
VI	1, (4), 5	2, 3	(4)
VII	1, (5)	2, 3	4, (5)

Table 7.3 *Course of cable forces in the decisive phase of the tests. Brackets indicate that the picture is ambiguous for the cable set in question.*

Based on the description of cable force distribution in Tab. 7.3 a set of conclusions on instability mode and load can be made. These are listed in Tab. 7.4. Here the last load case, where the course of cable forces can still be considered to be linear, is denoted "Initiation". The stage, where a mode of instability has clearly developed, is denoted "Developed", and for completion the maximum load applied in the test is indicated as "Final".

outermost cable set (#5). In the tests on the restrained plane system loading was proceeded until a vertical mode of instability had clearly formed. As this requested a girder tip deflection of approximately 0.5 m, consequently the outermost scale touched ground. In Test V and VII both lateral and vertical deflections increased so steeply, that the scale was posed on the floor. The combined actions in these tests on spatial systems caused permanent deformations in the girder, which consequently had to be replaced.

The evaluations of buckling mode and load based on the cable forces correspond well to conclusions made from girder deflections. However, due to hysteresis in the springs (see Fig. 7.5), one could expect the response to actions of reversed sign to be delayed with respect to deflections, whereas the redistribution of forces is immediate. Actually, when the course of cable forces in Test VII is studied, it is only the distribution of forces in cable set #4 that indicates a lateral instability developing. The same counts for Test V, where it is not until the last load case, that the distribution of forces in cable set #1 and #5 correspond to a lateral mode, and the course of forces in set #2 actually more indicates a vertical mode. This point is further examined in the following, where the in situ responses of the springs are plotted Fig. 7.34 - 7.43.

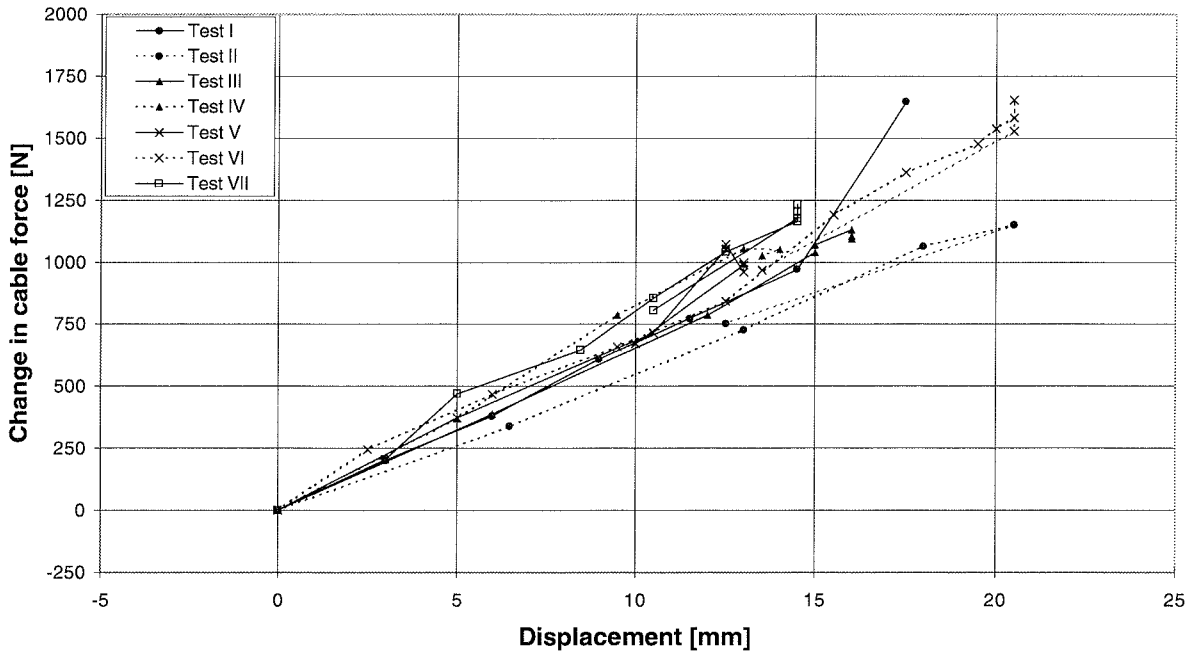

Figure 7.36 *In situ response of spring 2/3b (cable set 2, front).*

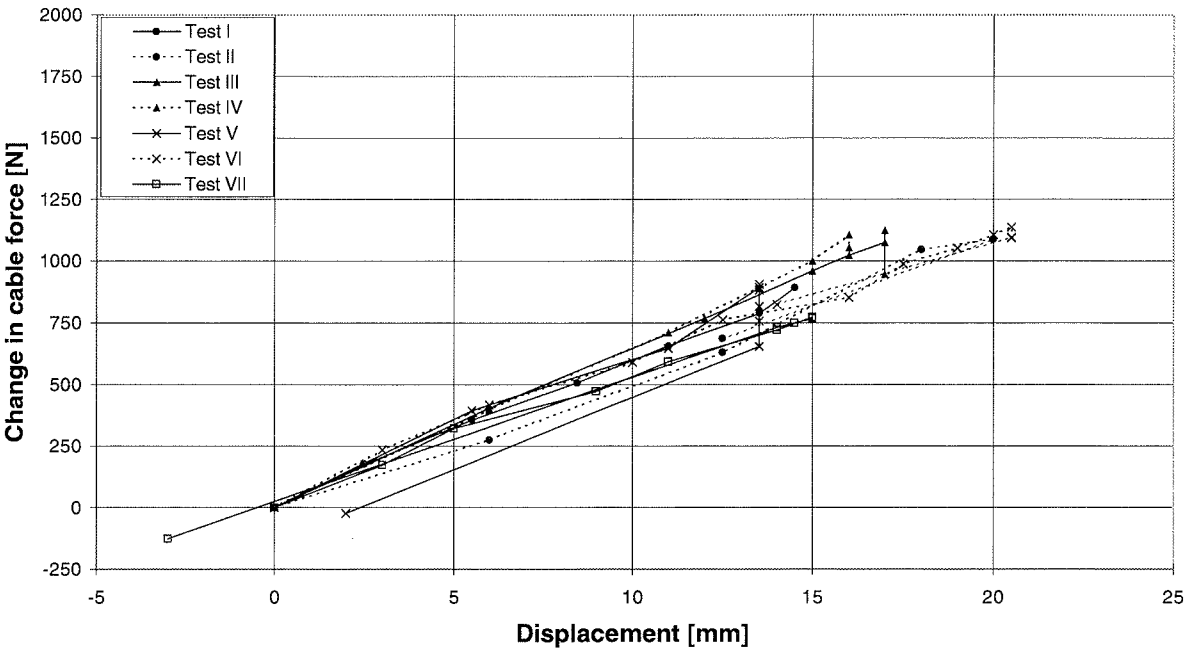

Figure 7.37 *In situ response of spring 2/3a (cable set 2, back).*

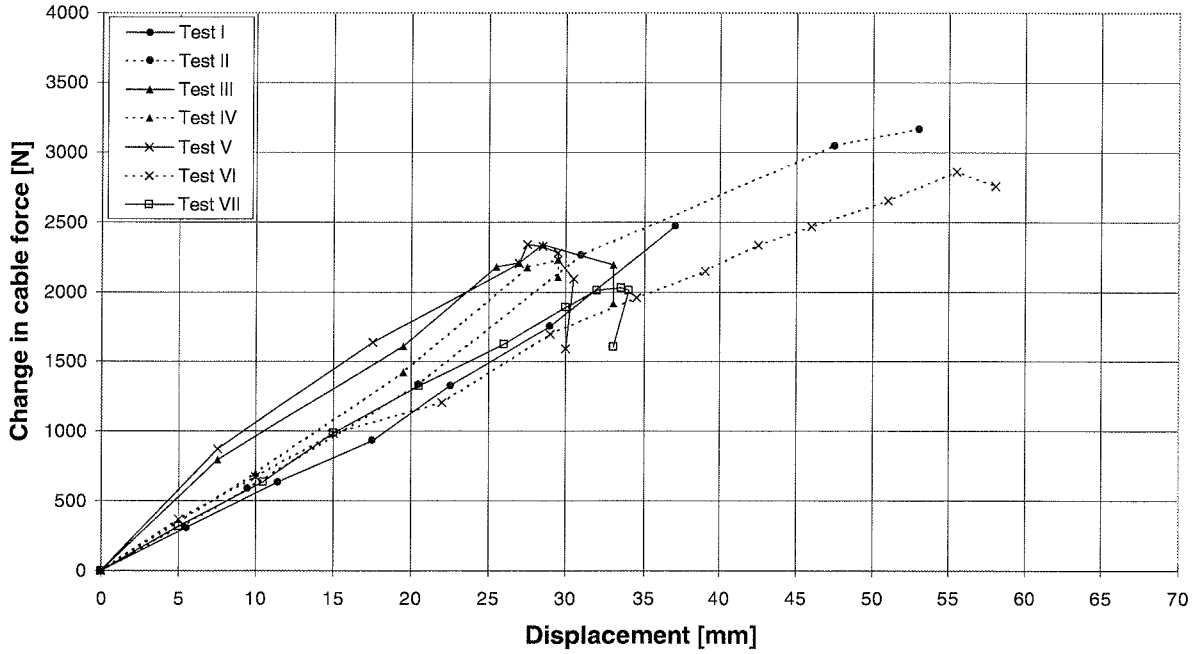

Figure 7.40 *In situ response of spring 4a (cable set 4, front).*

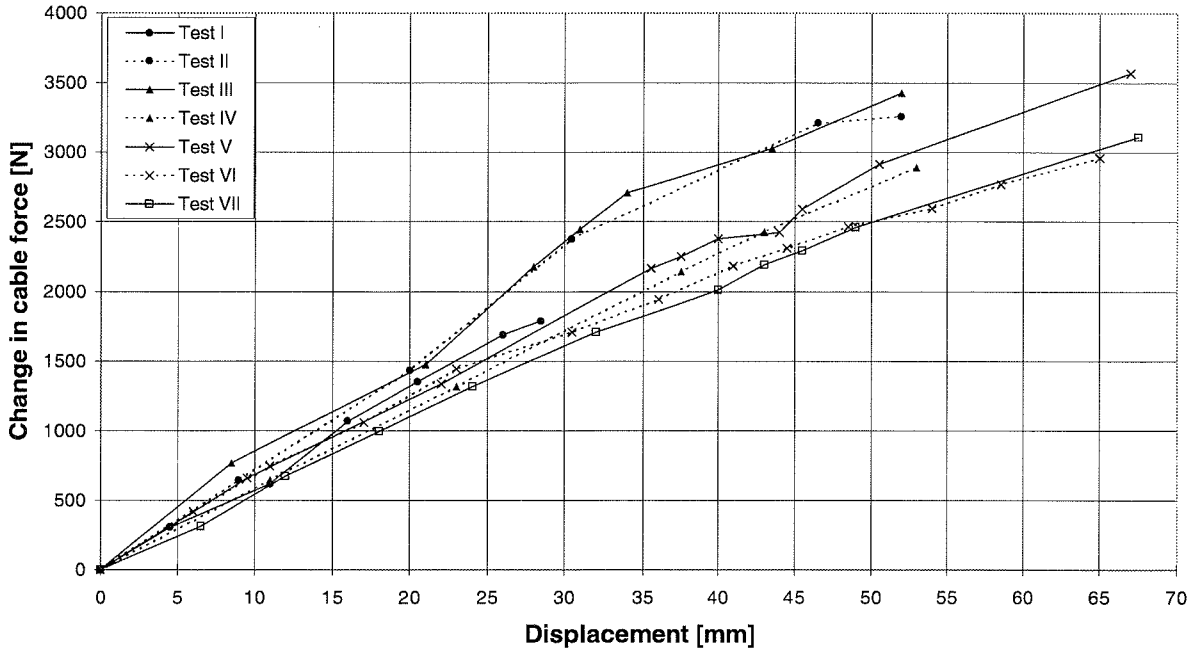

Figure 7.41 *In situ response of spring 4b (cable set 4, back).*

In the comments to the plots of cable forces it was mentioned, that the graphs show changes with respect to the reference load situation. The same counts for the in situ response of the springs. Therefore negative cable forces and elongations are due to a change below the level corresponding to the reference stage. Accuracy of cable forces is 0.5% as already stated, while the spring elongations is read within ±0.5 mm on the metric scale on the axles.

The first thing to be noticed concerning the in situ spring response is the scatter. To get a better idea of the size of scatter, the secant stiffness of the individual springs is plotted for three load levels: Namely a 50 kg and a 100 kg increase of external loading per scale, and finally for the maximum cable force registered in the test. All secant stiffnesses are calculated from the reference stage of 80 kg per scale, see Fig. 7.45 through 7.47. The in situ secant stiffnesses differ from 8% to 66% from the average based on all seven tests.

Now, focusing on the average in situ stiffness of the springs it is seen to be lower than intended. In Section 6.3.7 "Idealizations: Number of cable sets and their axial stiffness" the target axial stiffness of the cables in the model was found to be of the order of 75 - 80 N/mm. The initial stiffness for an increase in external loading of 50 kg per scale is 71 N/mm taking the average of all springs and through all tests. This average value drops to 67 N/mm for an increase in external loading of 100 kg per scale, and reaches 63 N/mm for the case of maximum cable force. The decreasing stiffness reflects the nonlinear nature of the discs used for the cylindrical tension springs. So in average, the in situ stiffness of the springs amounts to 80 - 90% of the target value.

To check if there is a tendency of increasing or decreasing stiffness as a function of load cycle number, the course of spring stiffness throughout the test series is plotted for the three load levels described above, see Fig. 7.48 to 7.50. Apparently this is not the case. The only situation, where there has been no change at all of neither position of cable anchorages nor of girder, is between Test I and II. Between Test II and III, and III and IV the position of cable anchorages at the pylon top has been altered. The same counts for Test IV and V except for cable set #1, that was left as it was. Between Test V and VI both the girder and the cable

Even though it was not possible to detect a characteristic development of the individual spring responses during the test series, there is actually a clear tendency in the evolution of the relative spring responses in the sets. As already mentioned, it was attempted to install a stiff and a slack spring alternately in the same side of the model. According to Fig. C1 and C2 (App. C), this aim has actually been fulfilled quite well in Test I and II. Then a shift starts to form in sets #1, #4 and #5, so that the spring placed in the front cable gets more stiff than the one in the backward cable. In Test V, VI and VII it is only in cable set #3, that the backward spring acts more stiffly of the two. The effect of having almost all the more stiff springs placed in the same side of the girder will of course favour a deflection towards this side, as the springs in the opposite side elongate more at a given load level. The size of the lateral forces and torsional moments thus arising depends on the inclination of the cable planes as well as on the actual difference in axial stiffness in the two cables forming each set. This effect is further pursued in Sections 8.2 "Comparisons of test results mutually" and 8.3 "Comparisons of test results with FE-predictions", where the in situ spring responses of each of the seven tests are used as input for the FE-calculations on the corresponding layout of the bridge model.

Returning to the plots of in situ response in Fig. 7.34 to 7.43 the hysteresis in the springs will now be discussed. Mainly, the cables subjected to a decreasing cable force when instability develops, are the cables in set #2 and #3 together with the front side cables in set #4 and #5. The size of hysteresis will be evaluated in the following way, see Fig. 7.44:

of the steel rods attaining only 0.5 - 1.5% of the elongation of the springs, it is reasonable to assume all the elongation to be concentrated in the springs and consequently ignoring the elastic deformation of the steel rods.

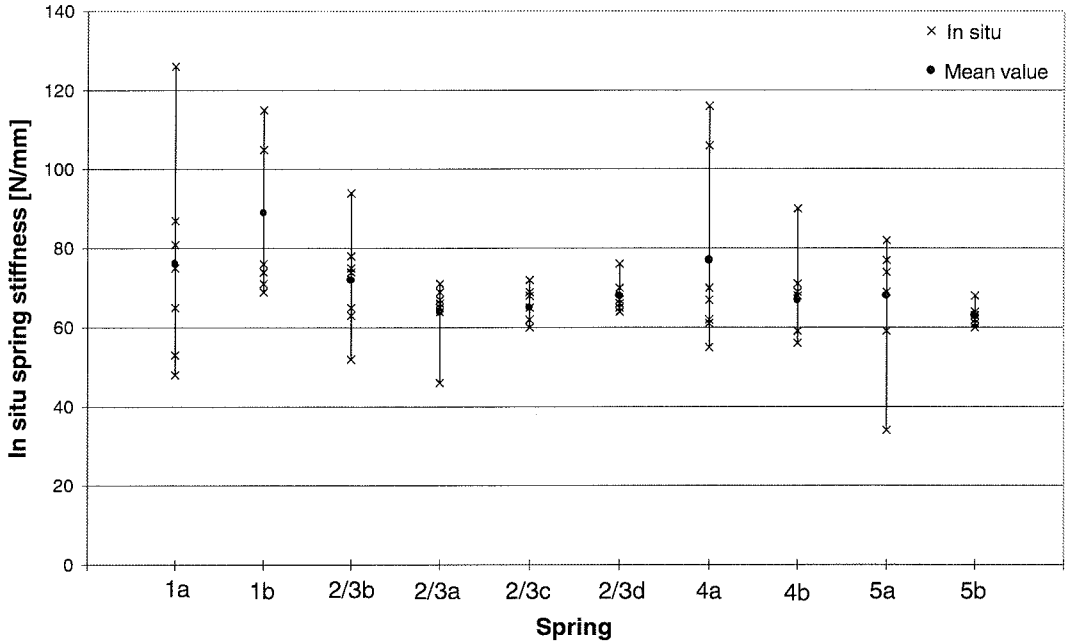

Figure 7.45 *Spring stiffness variation at a change in external loading of 50 kg per scale.*

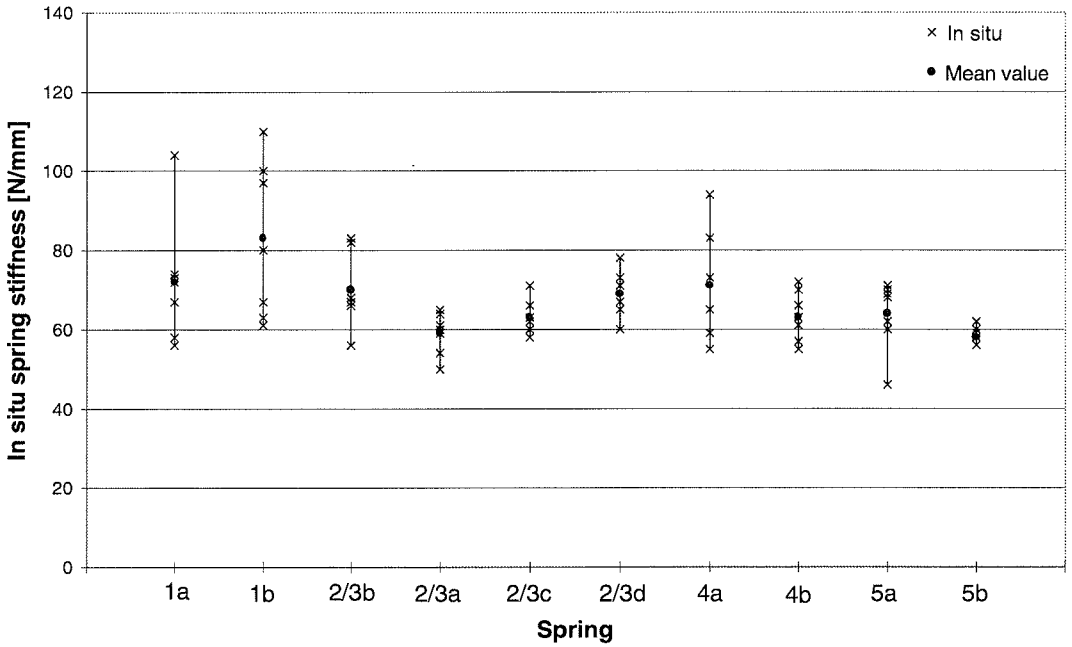

Figure 7.46 *Spring stiffness variation at a change in external loading of 100 kg per scale.*

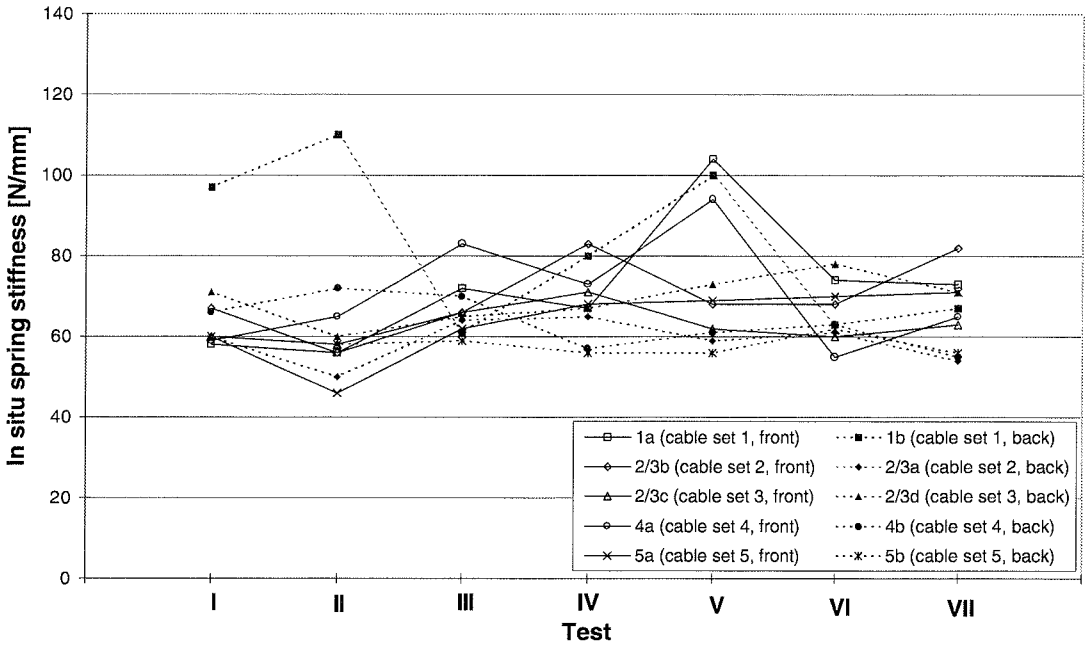

Figure 7.49 *Spring stiffness variation through test series at a change in external loading of 100 kg per scale.*

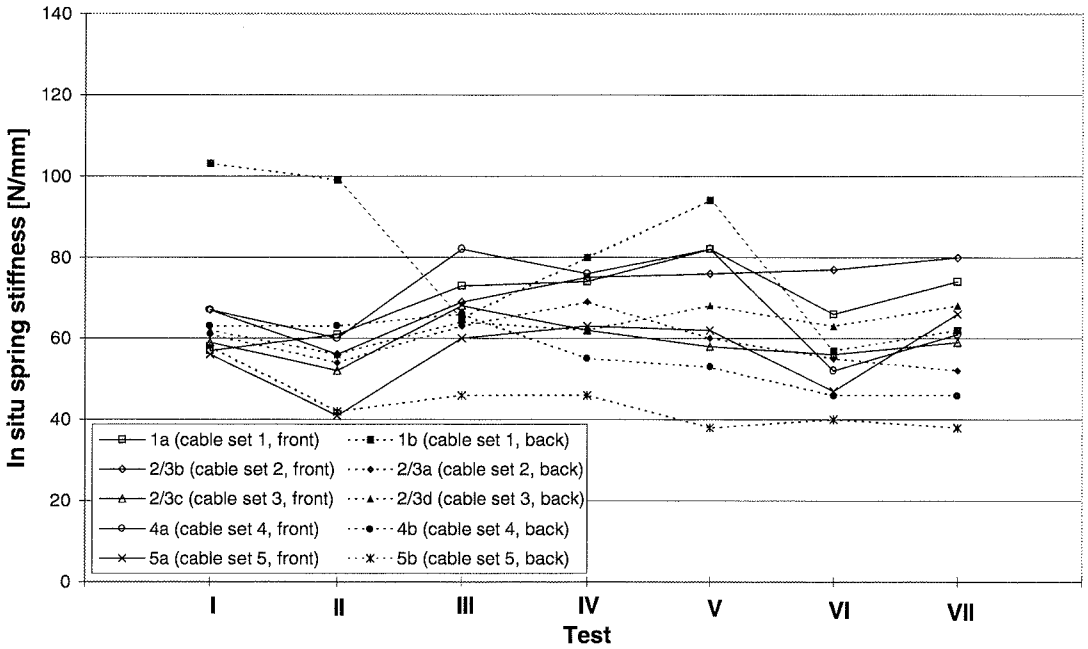

Figure 7.50 *Spring stiffness variation through test series at maximum cable force.*

7.3.3 Girder normal force and bending moments

In the following we describe the measured sectional forces in the girder. The main purpose of plotting the normal forces is to check the behaviour of the bridge model, including the control of equilibrium of forces described in the following Section. Plotting bending moments serves two purposes: Firstly, the development in bending moments discloses initiation of the instability phenomenon and secondly, the slope of the moment curves provides information on shear forces needed for checking the vertical equilibrium of forces.

In this Section, concerning sectional forces, all graphs show changes with respect to the reference state as was the case in Section 7.3.2 regarding cable forces. This means that due to drifting signals from the strain gages over a longer period of time, all graphs in the following presentation are based on changes in measured sectional forces from the reference load stage. As before the additional load has the unit [kg] corresponding to the mass of the extra plummets added to the reference load of 80 kg.

The accuracy of the gage factor and thus of the strain gage signals is within 1%. However, imprecise positioning of the strain gages on the girder might add further inaccuracy to the determination of sectional forces from the strain gage measurements. A rotation of the strain gage compared to the girder axis leads to a reduced signal, but the reduction will be less than 4‰ even for a rotation of 5°, so this possible inaccuracy has no practical importance. On the other hand, a displacement of the strain gage with respect to the centre line, will lead to errors that are not negligible. It is estimated, that the strain gages will be no more than 1 mm off the centre line on the side in question.

Taking the normal force first, an error will occur due to the presence of bending moments, if a gage is placed incorrectly, see Fig. 7.52. Depending on the sign of the bending moment, it will either reduce or increase the apparent normal force. The size of the error thus arising can be estimated as follows:

$N \sim 4 - 10$ kN $\Rightarrow$ $\varepsilon_N \sim 40 - 100$ με

$M_{lat} \sim 100 - 150$ Nm $\Rightarrow$ $\varepsilon_{N,\,err} \sim 5 - 7$ με

$M_{vert} \sim 80 - 100$ Nm $\Rightarrow$ $\varepsilon_{N,\,err} \sim 10 - 13$ με

If only one gage is displaced with respect to the centre line, the error will be divided by four as the normal force is the average of the results from four strain gages. From the ranges of strains indicated above, the inaccuracy on determination of the normal force is in the order of 1-8%, but for the higher load levels, the increase is relatively higher for the bending moments than for the normal force, so in these cases the inaccuracy could easily be higher. However, if two opposite gages (top/bottom or front/back) are displaced equally in opposite directions, the errors will be balanced out.

Now turning to the bending moments, errors arising from imprecise positioning of strain gages are due to the biaxial bending. A typical combination of moments will be $M_{lat} \sim 150$ Nm and $M_{vert} \sim 100$ Nm as stated above. The corresponding strains are $\varepsilon_{lat} \sim 175$ με and $\varepsilon_{vert} \sim 190$ με, thus the error on ε_{lat} due to a 1 mm displacement of a strain gage is in the order of $\varepsilon_{lat,\,err} = \varepsilon_{vert} \cdot d/(h/2) = \varepsilon_{vert}/15 \sim 13$ με, while the error on ε_{vert} is approximately $\varepsilon_{vert,\,err} = \varepsilon_{lat} \cdot d/(b/2) = \varepsilon_{lat}/25 \sim 7$ με. The depth, h, and the width, b, of the aluminium profile are defined in Fig. 7.52. As bending moments are determined from two strain gage readings the error on moments is in the order of 2-3%. If the difference between the two moments in biaxial bending is larger than in this example, the error on the smaller moment due to displacement of a strain gage would rise. However, if the two opposite gages are displaced equally in the same direction, the errors will be balanced out.

For the normal force in the girder it has been chosen to take compression as positive. Between the points of load transfer where the cables introduce compression in the girder, the normal force is constant. As previously mentioned, the sections provided with strain gages are situated at the midpoint between points of load transfer and are named accordingly. For instance the section between cable sets #2 and #3 is called "section 2 - 3", etc.

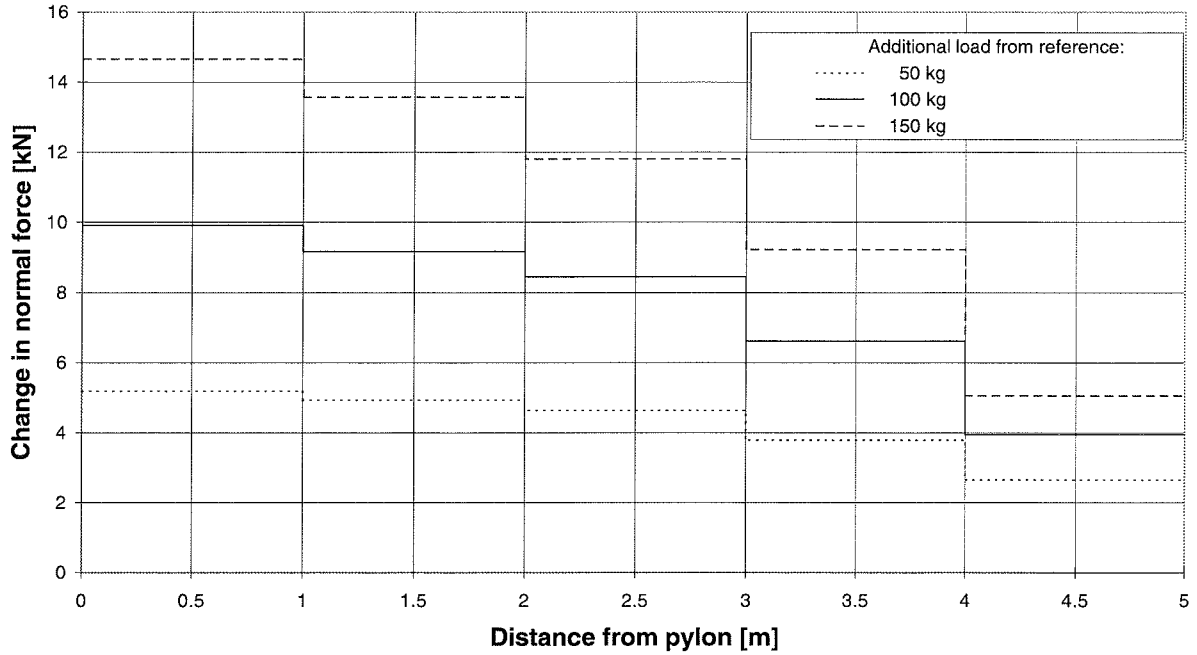

Figure 7.53 *Distribution of normal forces along the girder for three selected load levels. Test II, plane system, laterally restrained.*

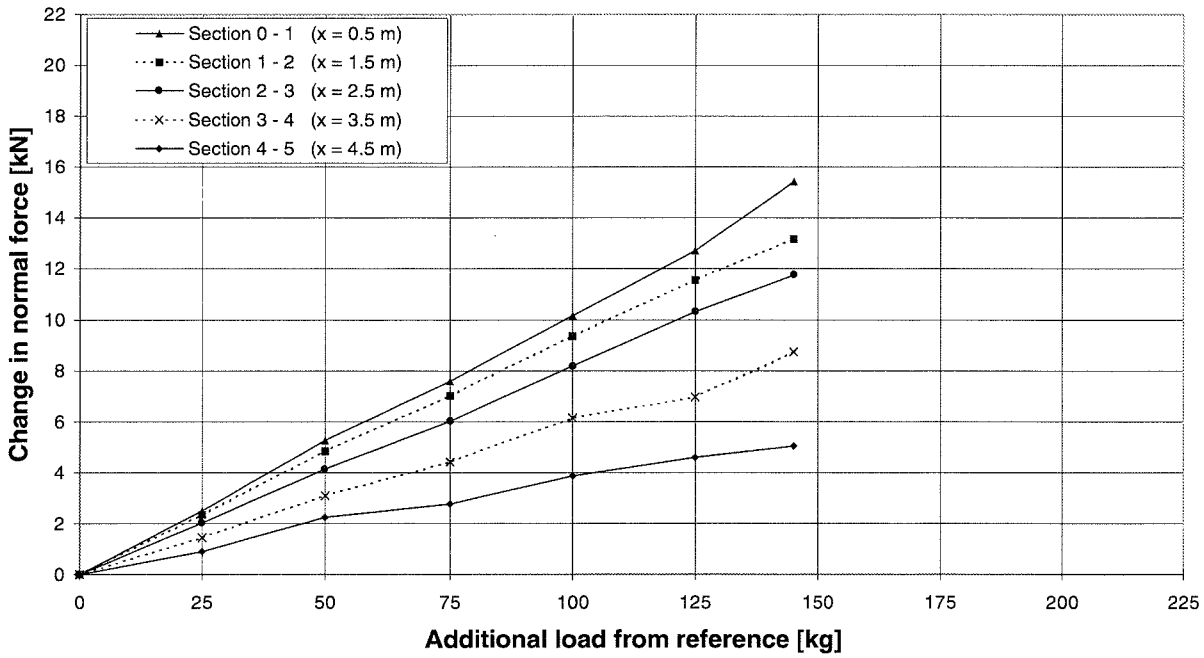

Figure 7.54 *Development in normal forces. Test I, plane system, laterally free.*

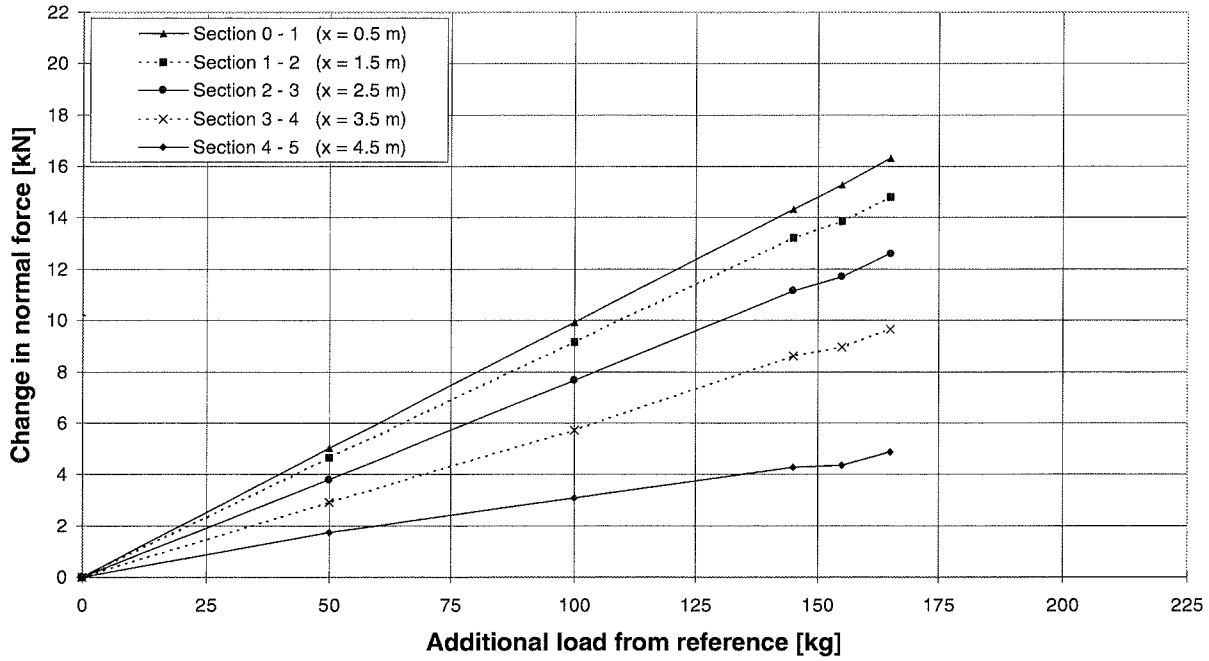

Figure 7.57 *Development in normal forces. Test IV, spatial system, a = 45 cm.*

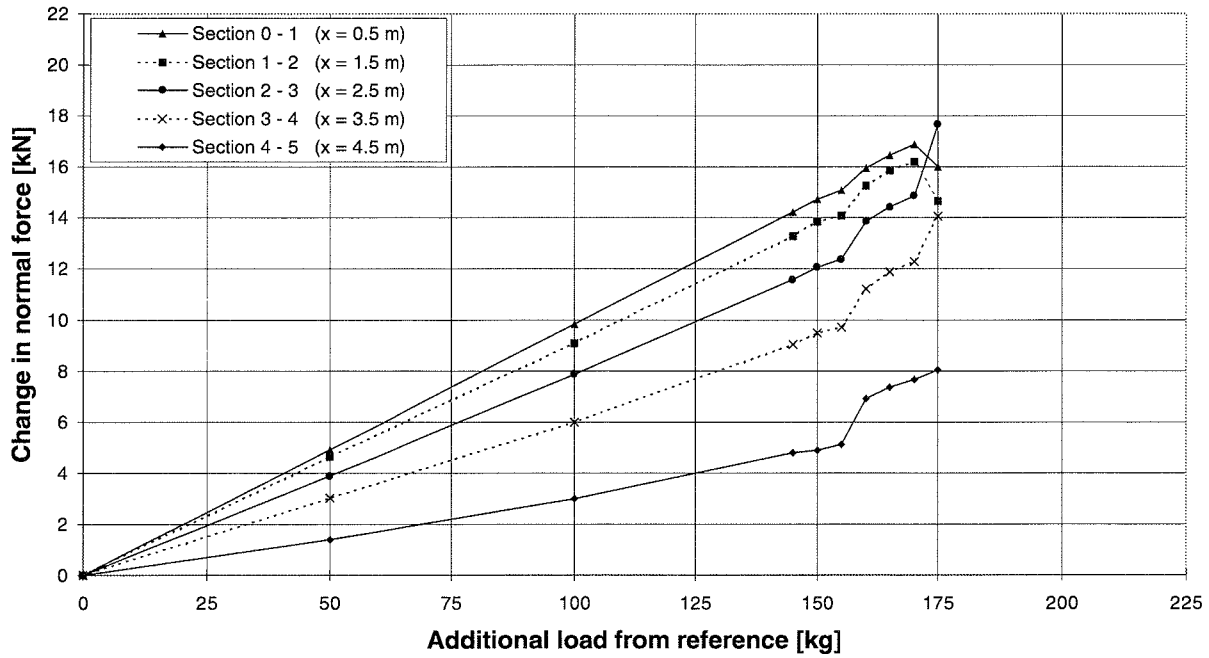

Figure 7.58 *Development in normal forces. Test V, spatial system, a = 55 cm.*

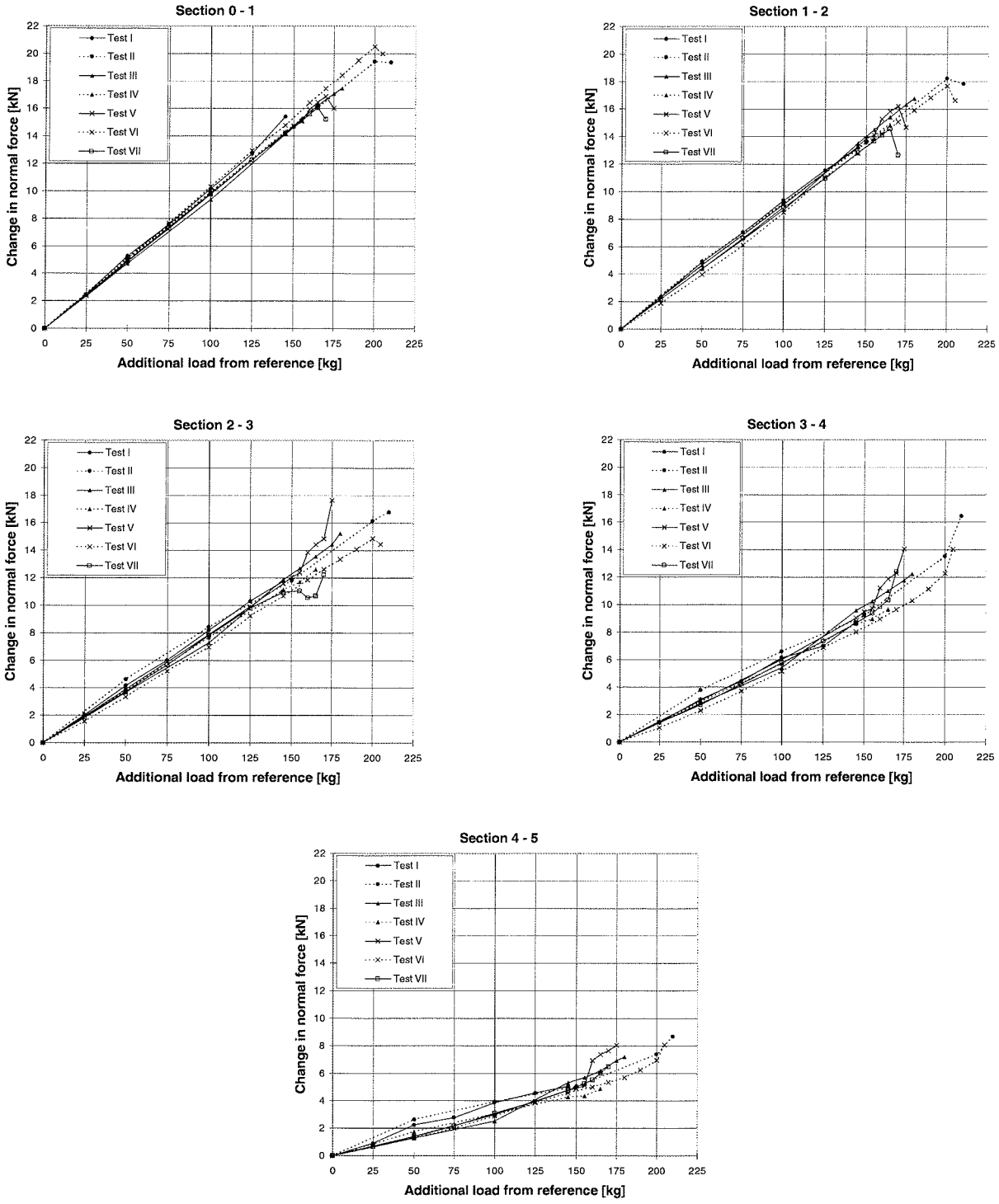

Figure 7.61 *Comparison of normal forces throughout the test series.*

In the following moment curves from the seven tests are shown. Fig. 7.62 - 7.75 show the development in bending moments in the five sections between cable supports equipped with strain gages, as a function of additional external loading. The curves for vertical and lateral bending are placed on the same page for each test to facilitate the comparisons that form the basis for conclusions on mode of instability. Furthermore, the range on the ordinate axis is the same for both moments. In this way the size of the two moments can easily be compared, but doing so one should bear in mind the difference in bending stiffnesses about the two axes, cf. Section 7.2.1 "Preliminary tests". Here, the bending stiffness about the strong axis was experimentally determined to be 2.7 times the bending stiffness about the weak axis.

For the bending moment about the horizontal axis, the standard sign convention for beams is applied, so that compression at the top and tension at the bottom of the section is taken as positive.

For bending about the vertical axis, moments giving compression at the back and tension at the front side of the girder are considered positive.

The distribution of bending moments along the girder is found in App. E for the three selected load levels used previously, i.e. 50 kg, 100 kg and 145 kg/150 kg additional weight per scale, respectively. The variation of bending moments is linear between the points of load transfer, and the moments are zero at the outermost point of load transfer, i.e. at the free end of the girder. Using this fact and the information on changes in bending moments obtained from strain gage measurements at the midpoint sections between the points of load transfer, the distribution of bending moments along the girder is determined. At the end support of the girder rotations about a vertical axis are restrained, and thus the value of the moment at this fixation appears from the moment curve for lateral bending. In contrast to this, rotations about a lateral axis are allowed at the girder end support, so the value of the moment curve for vertical bending at this position indicates the unintended restraint due to friction in the hinge.

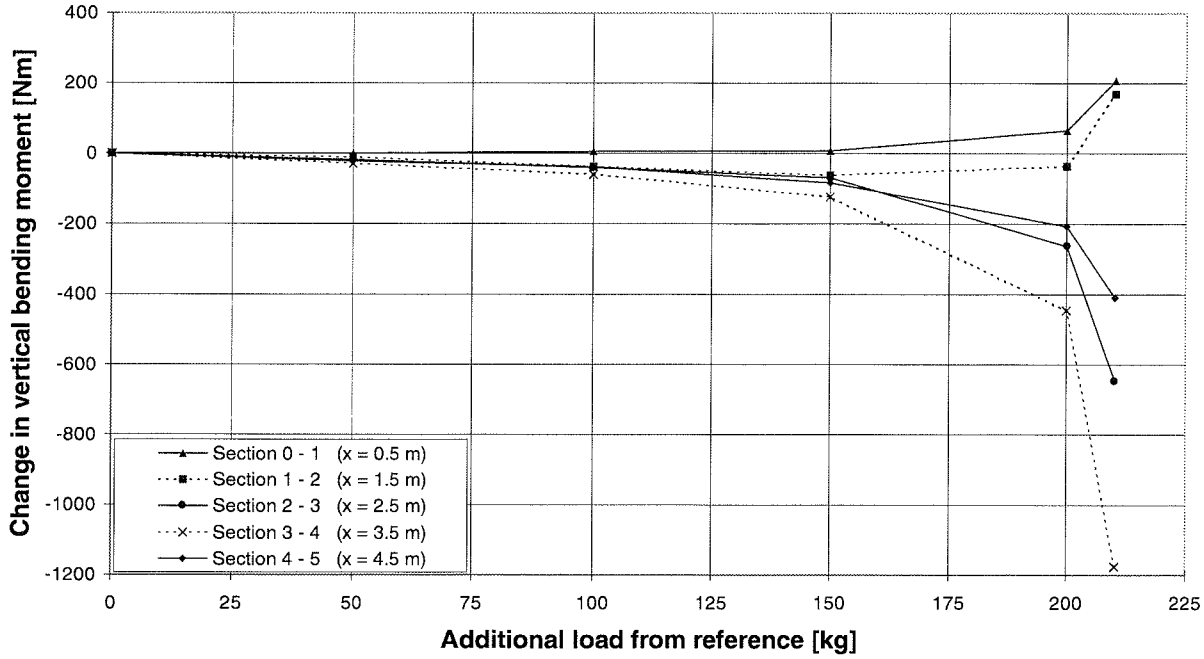

Figure 7.64 *Development in vertical bending moments. Test II: Plane system, laterally restrained.*

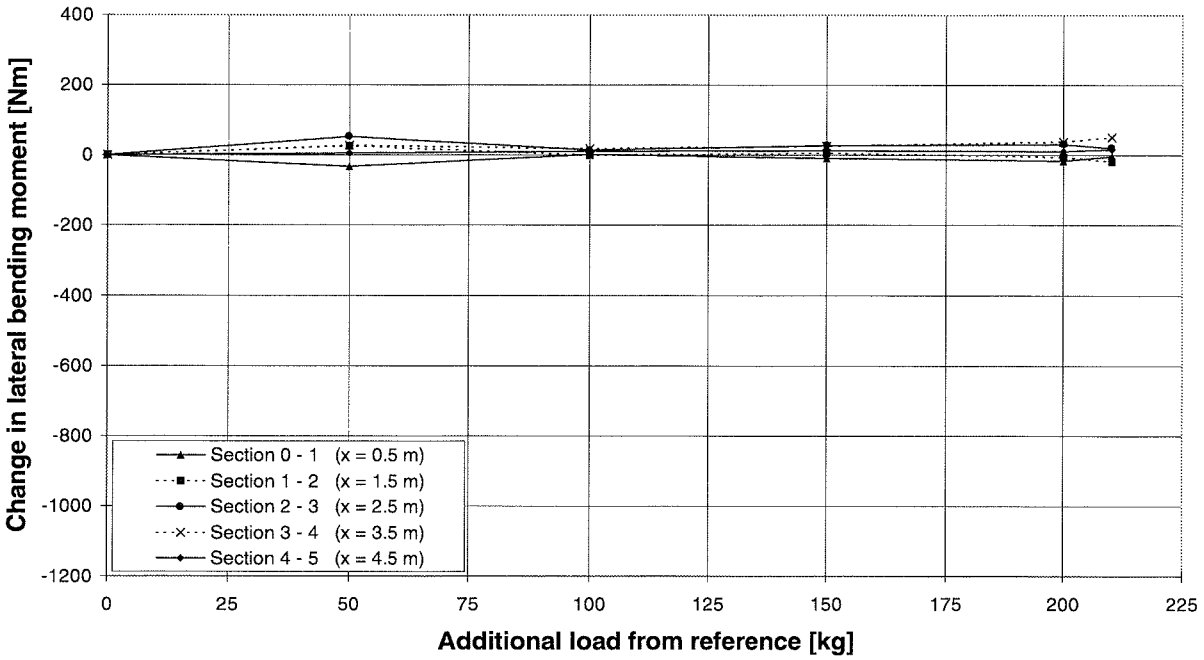

Figure 7.65 *Development in lateral bending moments. Test II: Plane system, laterally restrained.*

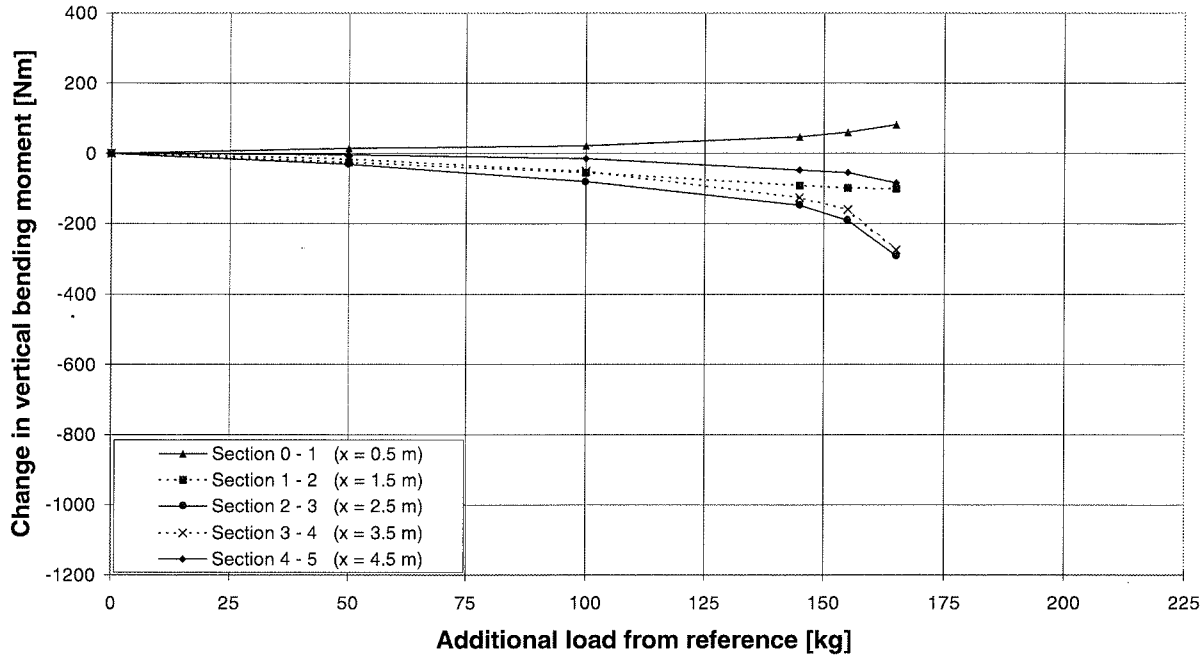

Figure 7.68 *Development in vertical bending moments. Test IV: Spatial system, a = 45 cm.*

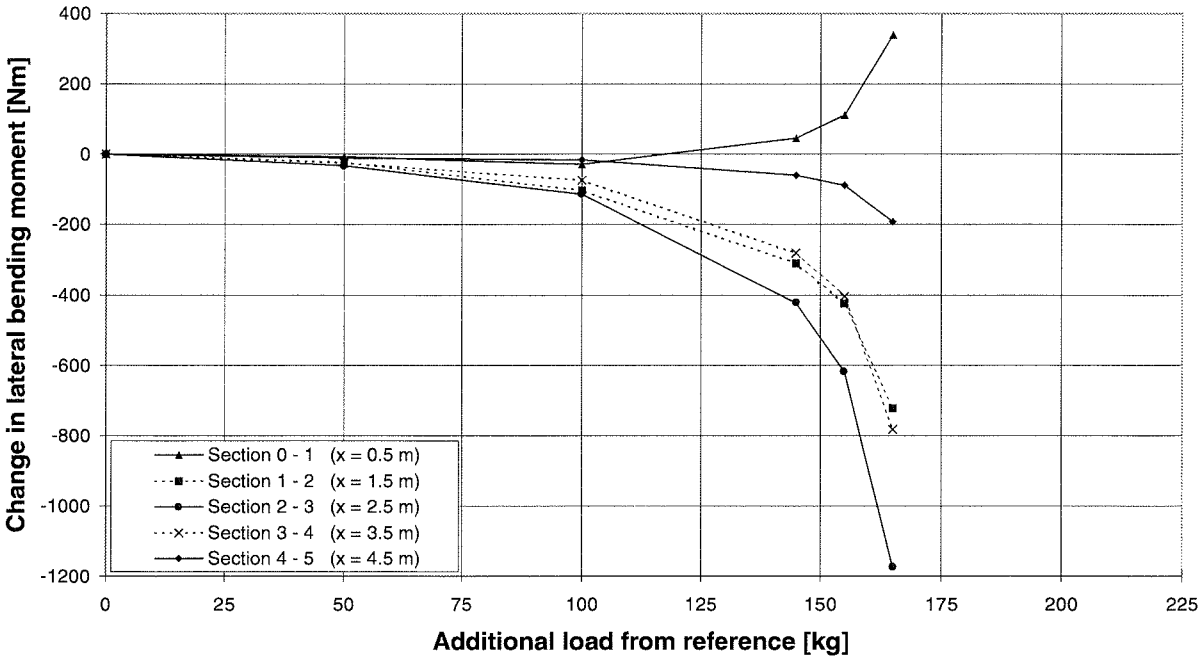

Figure 7.69 *Development in lateral bending moments. Test IV: Spatial system, a = 45 cm.*

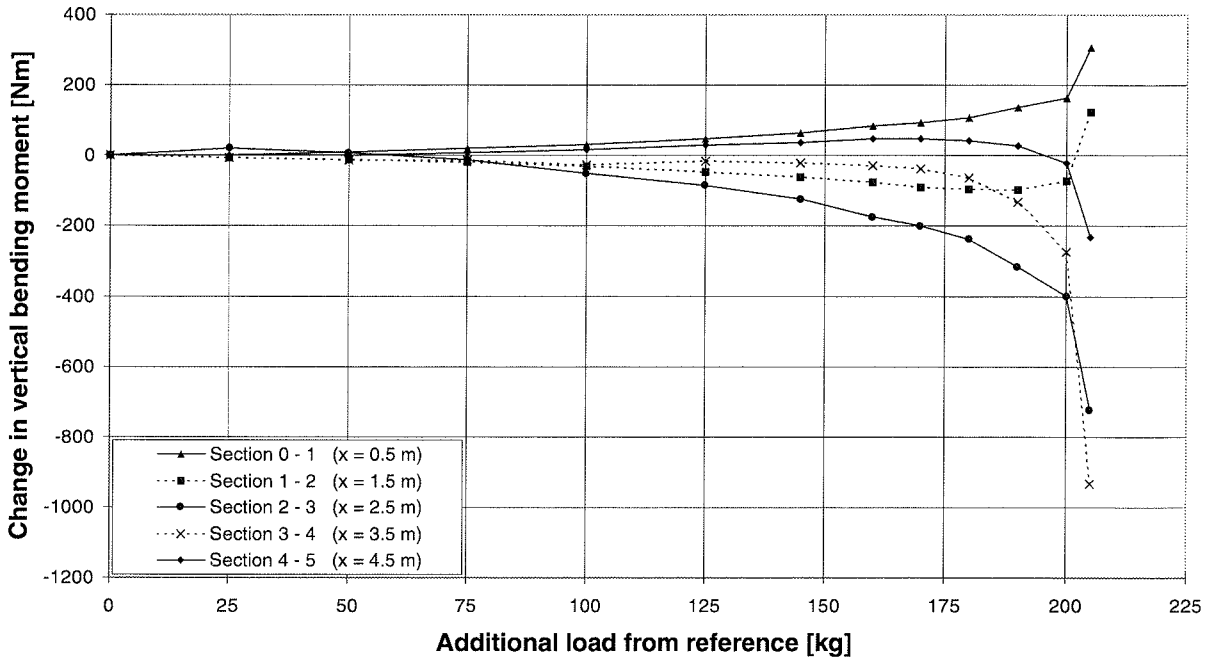

Figure 7.72 *Development in vertical bending moments. Test VI: Plane system, laterally restrained.*

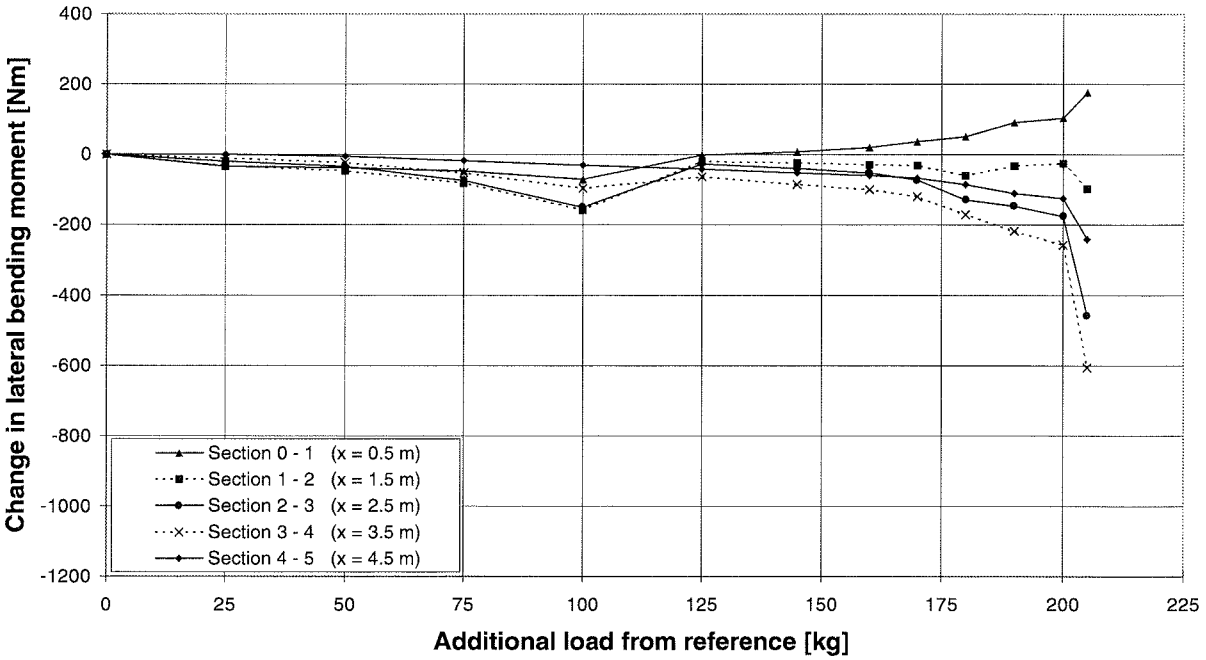

Figure 7.73 *Development in lateral bending moments. Test VI: Plane system, laterally restrained.*

The formation of the instability phenomenon is reflected in the development in bending moments. The moment amplification reveals itself as a deviation from proportionality between increase in external load and in bending moment. First, bending moments are increased due to extra loading and the corresponding additional deflections. Secondly, the presence of a compressive normal force adds further to the bending moment. This means, that moment curves will deviate from linearity right from the start, and thus it is more troublesome to indicate a specific load level where initiation of the instability phenomenon in question takes place. On the other hand, the mode of instability (lateral, vertical or combined) as well as its final stage appear clearly from the development in bending moments. In Tab. 7.5 the modes of instability in the seven tests are listed as evaluated from the development in bending moments. Critical load is indicated as the range between the two last load levels, because it is due to this final load step that increase in bending moments really accelerates.

Test	Cable system	Mode of instability	Critical load
I	Plane, laterally free	Lateral	[205 kg; 225 kg]
II	Plane, laterally restrained	Vertical	[280 kg; 290 kg]
III	Spatial, a = 35 cm	Lateral	[255 kg; 260 kg]
IV	Spatial, a = 45 cm	Lateral	[235 kg; 245 kg]
V	Spatial, a = 55 cm	Combined / (Lateral)	[250 kg; 255 kg]
VI	Plane, laterally restrained	Vertical	[280 kg; 285 kg]
VII	Spatial, a = 75 cm	Combined / (Vertical)	[245 kg; 250 kg]

Table 7.5 *Bridge model test results. Evaluated from bending moments in girder.*

First, attention will be drawn to the two sets of curves representing the pure modes of lateral and vertical instability of the plane cable system as they were obtained in this series of experiments. The figures in question are Fig. 7.62 - 7.63 (Test I) and Fig. 7.64 - 7.65 (Test

insufficient lateral restraint of the girder in Test VI is reflected in Fig. 7.73, where the lateral bending moment is plotted. However, this has apparently not influenced the development in vertical bending, compare Fig. 7.64 and 7.72.

7.3.4 Control of test results

As a result of the instrumentation of the bridge model, there are many redundancies in the system. These redundancies give the opportunity to check results and to estimate the accuracy of the measurements. In this Section determination of the distribution of forces in the system is in focus. The redundancies related to measurements of deflections have been commented in Section 6.4.1 "Position of girder", where the surveying methods applied are described.

For the behaviour of the cables, i.e. the spring response in our case, a redundancy is basically created when both force and elongation are measured, if a calibration (pre- or post-) of the response of the structural element takes place. However, the spring responses were not stable making calibration curves useless. Instead the directly measured responses are used throughout the investigations. The transducers measuring cable forces are equipped with two strain gages each in order to compensate for bending, thus this leaves no redundancies.

For measurements of sectional forces in the girder, on the other hand, there are redundancies present. As the variation of stresses over the cross-section is linear, three measuring points are sufficient to determine the stresses at any point. Here, four strain gages per measuring section are applied, thus giving spare information which can be used for control or will act as a safety in case the measurements from one gage are erroneous.

Furthermore, the instrumentation of the bridge model makes it possible to check the equilibrium of forces. For the vertical equilibrium shear forces are obtained from the slope of the moment curves along the girder. The vertical component of the cable forces can be calculated from the geometry of the system. When determining the moment curves it is assumed, that the strain gages are placed exactly at the midpoint section between the points of load transfer, and that all the load is transferred exactly at the point indicated by the centre

can be carried out for each load level in each of the seven tests. However, this would be rather tedious and of little interest. Some of the many possible calculations to check the behaviour of the bridge model can be found in *Vejrum* (1996).

LUSAS (1993): "LUSAS Theory Manual", *version 11, Finite Element Analysis Ltd., Surrey, United Kingdom.*

LUSAS (1993): "LUSAS User Manual", *version 11, Finite Element Analysis Ltd., Surrey, United Kingdom.*

Tanaka, H. (1992): "Wind Engineering", *Lecture Notes prepared for the Course at DTH, Copenhagen, Denmark.*

Thomsen, K. (1990): "Stålkonstruktioner, Massive Dragere", (in Danish), *4th ed., Polyteknisk Forlag, Lyngby.*

Timoshenko, S. P. and Gere, J. M. (1961): "Theory of elastic stability", *2nd ed., McGraw-Hill Book Company, Inc., New York.*

Traberg, S. (1987): "Bærende Konstruktioner Grundkursus 2, Matematisk Elasticitetsteori, Noter" (in Danish), *Department of Structural Engineering, Technical University of Denmark.*

Vacharajittiphan, P., Woolcock, S. T. and Trahair, N. S. (1974): "Effect of In-Plane Deformation on Lateral Buckling", *Journal of Structural Mechanics, vol. 3, n. 1, pp. 29-60.*

Vejdirektoratet (1984): "8.10.01 Broteknik, Belastninger, Beregnings- og belastningsregler for vejbroer" (in Danish), *Vejdirektoratet, Vejregeludvalget.*

Vejrum, T. (1996): "Model Test on Narrow, Cable Supported Bridge. Plane and Spatial Cable Systems" (in Danish), *Constructional and Workshop Drawings, Log Books I - IV and Personal Notes I - IV, deposited at the Department of Structural Engineering and Materials, Technical University of Denmark.*

Walther, R., Houriet, B., Isler, W. and Moïa, P. (1985): "Ponts Haubanés" (in French), *Presses Polytechniques Romandes, Lausanne, Switzerland.*

NOMENCLATURE

Roman

A	cross sectional area
	cross sectional area of prototype girder
A_{ac}	cross sectional area of anchor cable
A_c	cross sectional area of a stay cable
A_{in} , A_{out}	cross sectional area of inwards and outwards leaning cable, respectively
A_{pylon}	cross sectional area of prototype pylon
a	lateral distance between the two anchor zones at the pylon top ("pylon width")
	length of a fan
a_m	half the main span length
a_s	side span length
b	lateral distance between the two anchor zones at the pylon top ("pylon width")
	width of model girder
C	compressive force
C_0	compressive force, initial stage
C_{cb}	compressive normal force in cross beam in pylon
C_p	compressive normal force in pylon leg
c	length
d	distance
	distance between cable anchorage sections at girder (parallel to bridge axis)
	depth of prototype girder
dA_{in} , dA_{out} , dQ_{in} , dQ_{out} , dT_{in} , dT_{out} , $dT_{in,\ g+u}$, $dT_{out,\ g+u}$, $dT_{in,\ u}$, $dT_{out,\ u}$, dV_{in} , dV_{out} :	
	derivatives, see basic term
E	modulus of elasticity
E_{eq}	equivalent modulus of elasticity

E_t	tangent modulus of elasticity
F	force
F_0	force, initial stage
G	dead load
G_{in} , G_{out}	weight of inwards and outwards leaning cable, respectively
g	dead load of girder and bridge equipment (uniformly distributed)
h	height of pylon above deck
	depth of model girder
h_p	total pylon height above ground
I	moment of inertia
I_{lat}	moment of inertia of prototype girder, lateral bending
I_{tor}	moment of inertia of prototype girder, torsion
I_{vert}	moment of inertia of prototype girder, vertical bending
$I_{pylon,\ lat}$	moment of inertia of prototype pylon, bending in lateral direction of bridge
$I_{pylon,\ long}$	moment of inertia of prototype pylon, bending in longitudinal direction of bridge
$I_{pylon,\ tor}$	moment of inertia of prototype pylon, torsion
i	summation variable
K_E	scaling factor on elastic modulus
K_k	scaling factor on spring stiffness
K_l	scaling factor on length
K_ε	scaling factor on strain
K_σ	scaling factor on stress
k, k_s	spring stiffness
k_l	lateral spring stiffness
	elastic support of pylon top provided by anchor cables, longitudinal direction of bridge
k_v	vertical spring stiffness
l	length
l_{ac}	length of anchor cable

l_c	length of a stay cable
l_{in} , l_{out}	length of inwards and outwards leaning cable, respectively
$l_{in,\,l}$, $l_{out,\,l}$	projection of cable length, inwards and outwards leaning cable, respectively
l_s	characteristic length of compression member
M	bending moment
M_{lat}, M_{vert}	bending moment, lateral and vertical plane, respectively
M_{tor}	torsional moment
N	normal force
N_{cr}	critical compressive normal force
$N_{p,\,i}$	normal force between cable anchorage section (i-1) and (i) due to load p
P, P_{vert}	vertical load
P_{lat}	lateral load
p	traffic load (uniformly distributed)
Q	vertical load
Q_{ac}	quantity of steel in anchor cable
Q_{cb}	quantity of steel in cross beam in pylon
Q_{in} , Q_{out}	quantity of steel in inwards and outwards leaning cable, respectively
Q_p	quantity of steel in pylon leg
q	wind pressure
	vertical load (uniformly distributed)
r	price ratio
$S_{lat,\,i}$	safety factor at i'th cable anchorage section, lateral buckling
$S_{vert,\,i}$	safety factor at i'th cable anchorage section, vertical buckling
T_{ac}	cable force in anchor cable
$T_{ac,\,p}$	cable force in anchor cable due to traffic in main span
$T_{ac,\,u}$	cable force in anchor cable due to wind
T_{in} , T_{out}	cable force in inwards and outwards leaning cable, respectively
$T_{in,\,g+u}$, $T_{out,\,g+u}$	cable force due to dead and wind loads in inwards and outwards leaning cable, respectively
$T_{in,\,u}$, $T_{out,\,u}$	cable force due to wind load in inwards and outwards leaning cable,

	respectively
t	thickness
t_{in} , t_{out}	projection of cable force in inwards and outwards leaning cable, respectively
U	wind load
u	wind load (uniformly distributed)
V_{ac}	volume of anchor cable
V_{in} , V_{out}	volume of inwards and outwards leaning cable, respectively
v	wind speed
w	width of prototype girder
x	distance parallel to bridge axis

Greek

α_{in} , α_{out}	vertical inclination of inwards and outwards leaning cables, respectively
β	angle
δ, $\delta_{x, c}$	displacement
$\delta_{l, ac}$	lateral displacement due to anchor cables
$\delta_{l, c}$	lateral displacement due to stay cables
$\delta_{v, ac}$	vertical displacement due to anchor cables
$\delta_{v, c}$	vertical displacement due to stay cables
δ_{v}	vertical displacement
$\delta_{x, ac}$	displacement of pylon top due to anchor cables
ε	strain
ε_{N}	strain due to normal force
$\varepsilon_{N, err}$, $\varepsilon_{lat, err}$, $\varepsilon_{vert, err}$	errors on strain
ε_{ac}	strain in anchor cable
$\varepsilon_{ac, p}$	strain in anchor cable due to traffic
$\varepsilon_{ac, u}$	strain in anchor cable due to wind
$\varepsilon_{c, p}$	strain in stay cable due to traffic
$\varepsilon_{c, u}$	strain in stay cable due to wind

ε_{lat}	strain due to lateral bending
$\varepsilon_{q,\,i}$	strain in i'th stay cable due to load q
ε_{vert}	strain due to vertical bending
η	angle
κ_{tor}	uniformly distributed twist
λ	lateral distance between cable anchorages at girder
ν	Poisson's ratio
ρ	density
ρ_c	density of steel in cables
ρ_p	density of steel in pylon
σ	stress
σ_c	limiting stress in cables
σ_g	dead load stress in cables
σ_p	limiting stress for steel in pylon
θ	angle
τ_{max}	maximum shear stress
φ	rotation angle
φ_{in} , φ_{out}	lateral inclination of inwards and outwards leaning cable, respectively

Section	Outwards leaning cables [mm^2]	Inwards leaning cables [mm^2]
m1	569	416
m2	585	427
m3	614	447
m4	656	475
m5	709	511
m6	771	553
m7	840	601
m8	916	652
m9	997	706
m10	1083	766
m11	1173	846
m12	1267	927
m13	1365	962
m14	1466	1033
m15	1572	1107
m16	1682	1184
m17	1795	1260
m18	1913	1309
m19	2034	1392
m20	2237	1614
s1	569	416
s2	585	427
s3	614	447
s4	656	475
s5	709	511
s6	771	553
s7	840	601
s8	916	652
s9	997	706
s10	1083	766
s11	1118	806
s12	1463	1071
Anchor cables (four cables)	14365	10641
Total quantity of cable steel	695 tons	

Table A1 *Cable dimensions for spatial cable system a).*

Section	Outwards leaning cables [mm^2]	Inwards leaning cables [mm^2]
m1	1002	-
m2	-	986
m3	1226	-
m4	-	1075
m5	1319	-
m6	-	1239
m7	1582	-
m8	-	1441
m9	1897	-
m10	-	1675
m11	2248	-
m12	-	1946
m13	2643	-
m14	-	2205
m15	3080	-
m16	-	2511
m17	3584	-
m18	-	2712
m19	3916	-
m20	-	3668
s1	1002	-
s2	-	986
s3	1126	-
s4	-	1075
s5	1319	-
s6	-	1239
s7	1582	-
s8	-	1441
s9	1897	-
s10	-	1704
s11	2082	-
s12	-	2470
Anchor cables (two cables)	24859	-
Total quantity of cable steel	698 tons	

Table A2 *Cable dimensions for spatial cable system b).*

Section	Outwards leaning cables [mm^2]	Inwards leaning cables [mm^2]
m1	1033	957
m2	1063	983
m3	1113	1022
m4	1203	1100
m5	1276	1172
m6	1414	1286
m7	1521	1387
m8	1646	1473
m9	1835	1657
m10	1980	1784
m11	2098	1830
m12	2483	2173
m13	2291	2038
m14	2997	2467
m15	2705	2502
m16	3177	2474
m17	3769	3313
m18	2662	2061
m19	4966	3856
m20	3488	3525
s1	1033	957
s2	1063	983
s3	1113	1022
s4	1203	1100
s5	1276	1172
s6	1414	1286
s7	1521	1387
s8	1646	1473
s9	1949	1775
s10	1670	1507
s11	2560	2132
s12	2379	2075
Anchor cables (two cables)	24983	-
Total quantity of cable steel	699 tons	

Table A3 *Cable dimensions for spatial cable system c).*

Section	Outwards leaning cables [mm^2]	Inwards leaning cables [mm^2]
m1	984	-
m2	1011	-
m3	1062	-
m4	1135	-
m5	1226	-
m6	1332	-
m7	1451	-
m8	1581	-
m9	1720	-
m10	1867	-
m11	2023	-
m12	2185	-
m13	2354	-
m14	2529	-
m15	2714	-
m16	2906	-
m17	3099	-
m18	3274	-
m19	3446	-
m20	3877	-
s1	984	-
s2	1011	-
s3	1062	-
s4	1135	-
s5	1226	-
s6	1332	-
s7	1451	-
s8	1581	-
s9	1722	-
s10	1873	-
s11	1916	-
s12	2574	-
Anchor cables (two cables)	24863	-
Total quantity of cable steel	698 tons	

Table A4 *Cable dimensions for spatial cable system d).*

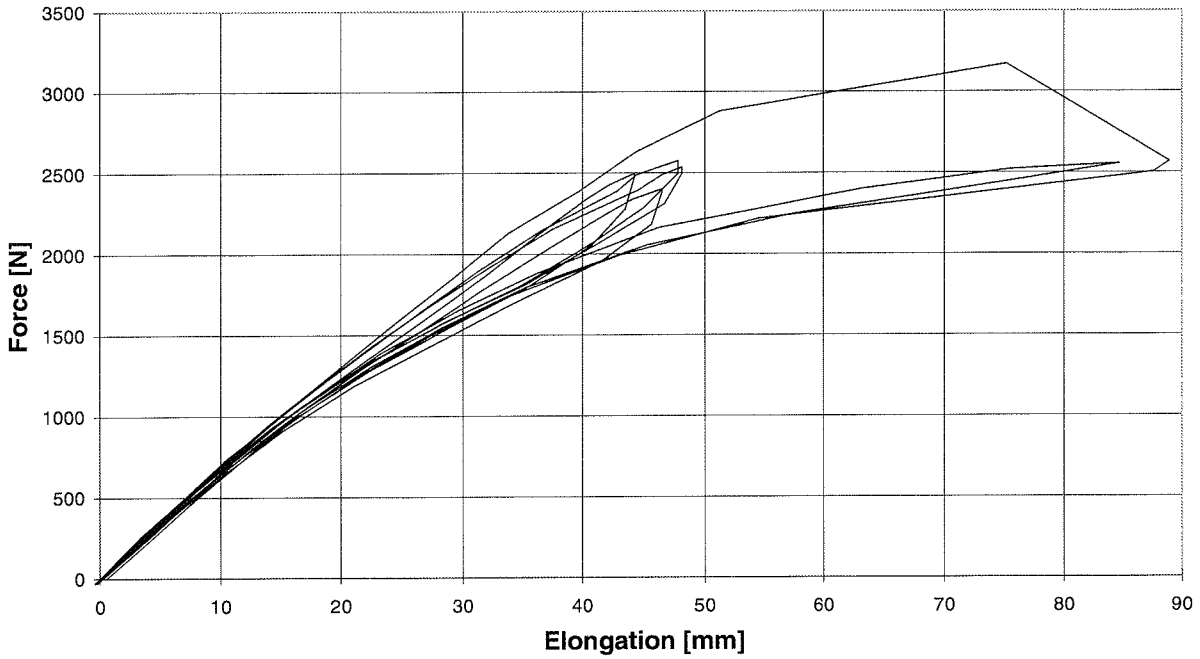

Figure B1 *Calibration of spring 1a.*

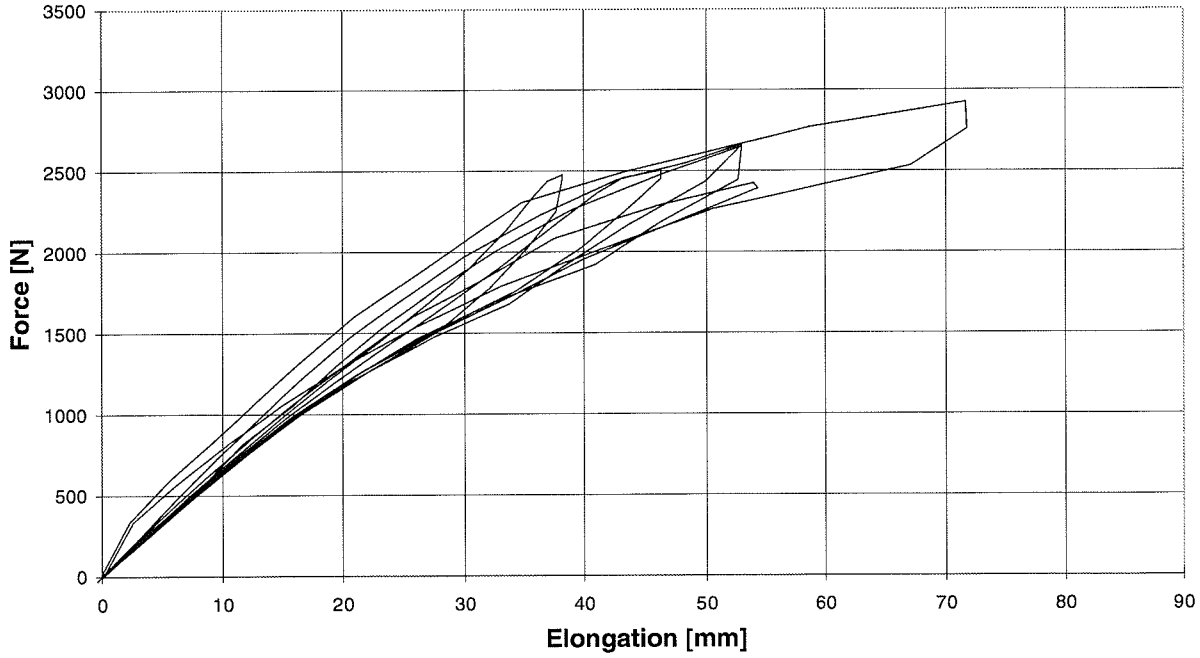

Figure B2 *Calibration of spring 1b.*

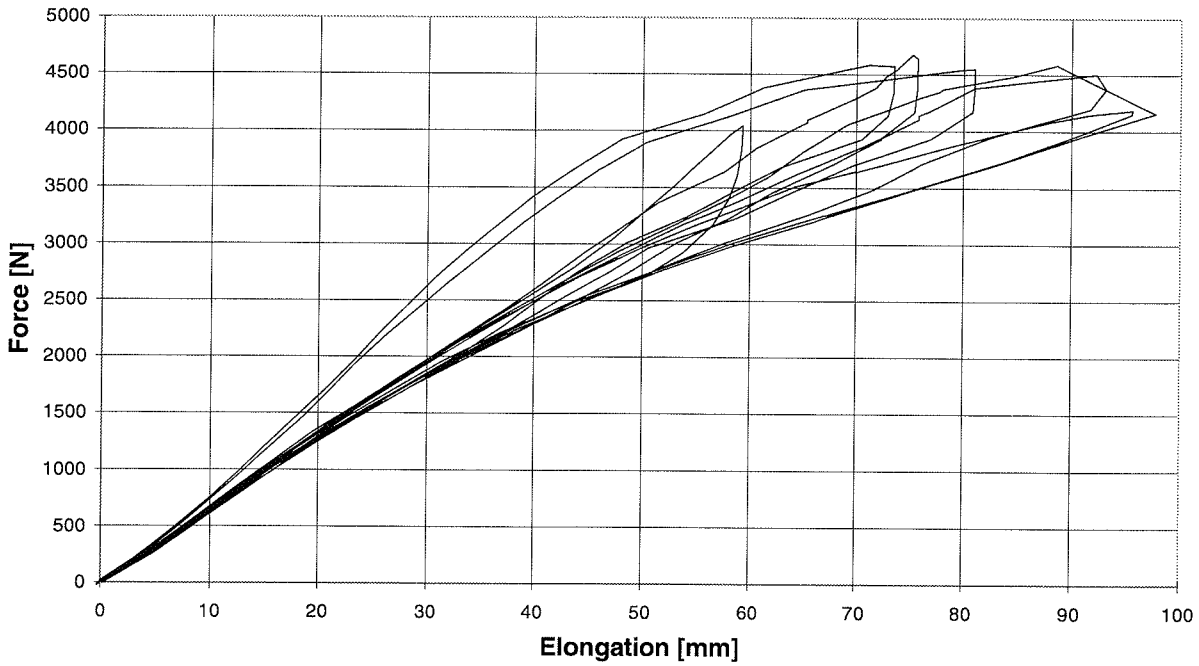

Figure B3 *Calibration of spring 2/3a.*

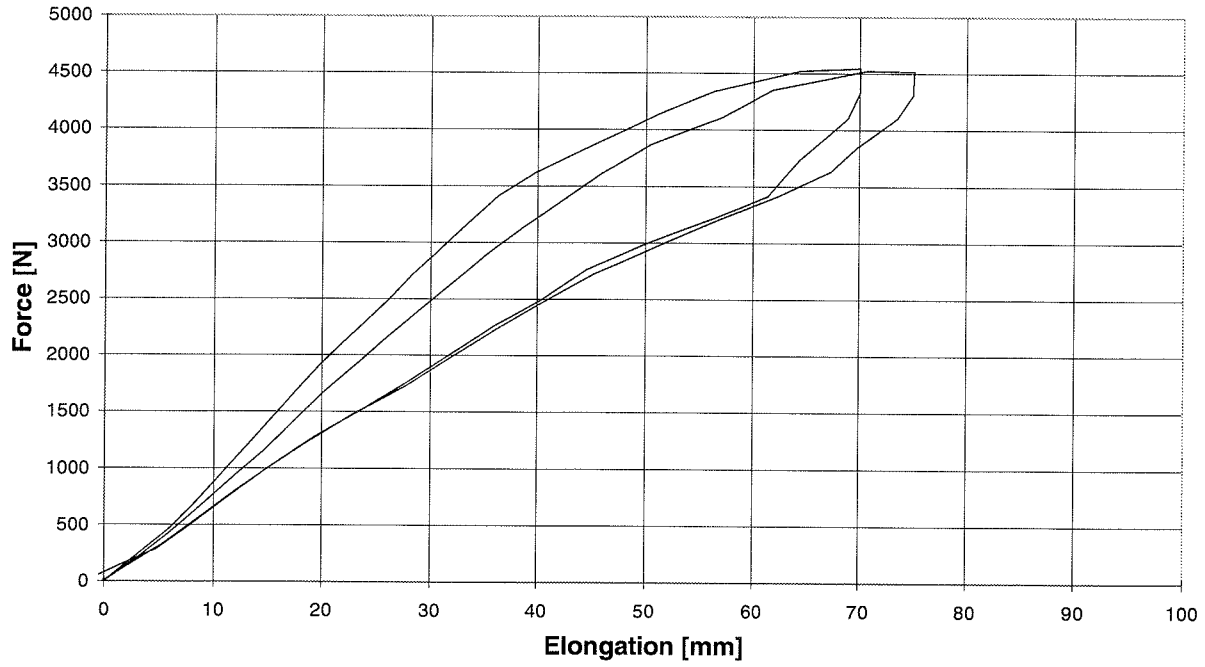

Figure B4 *Calibration of spring 2/3b.*

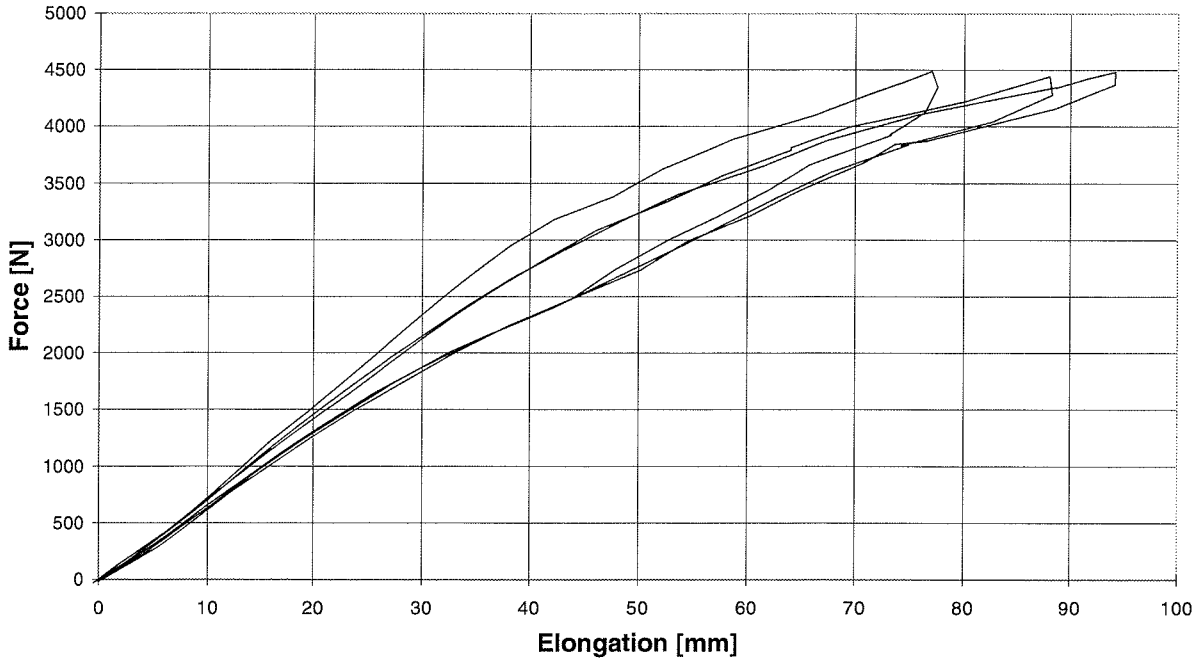

Figure B5 *Calibration of spring 2/3c.*

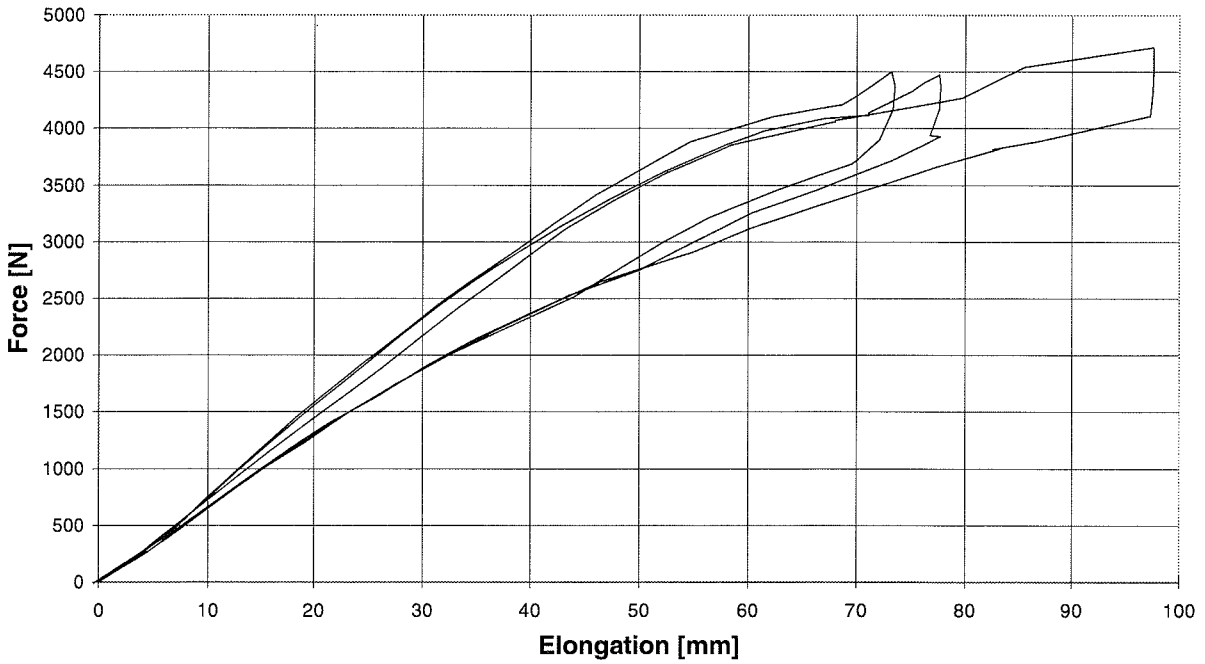

Figure B6 *Calibration of spring 2/3d.*

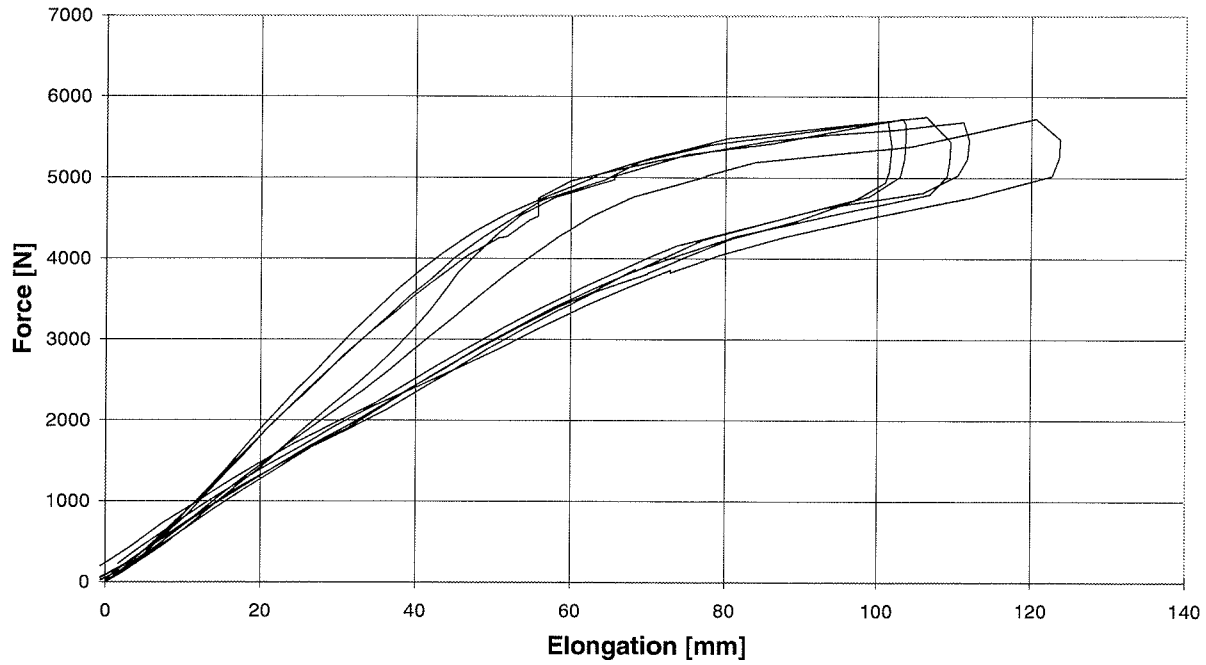

Figure B7 *Calibration of spring 4a.*

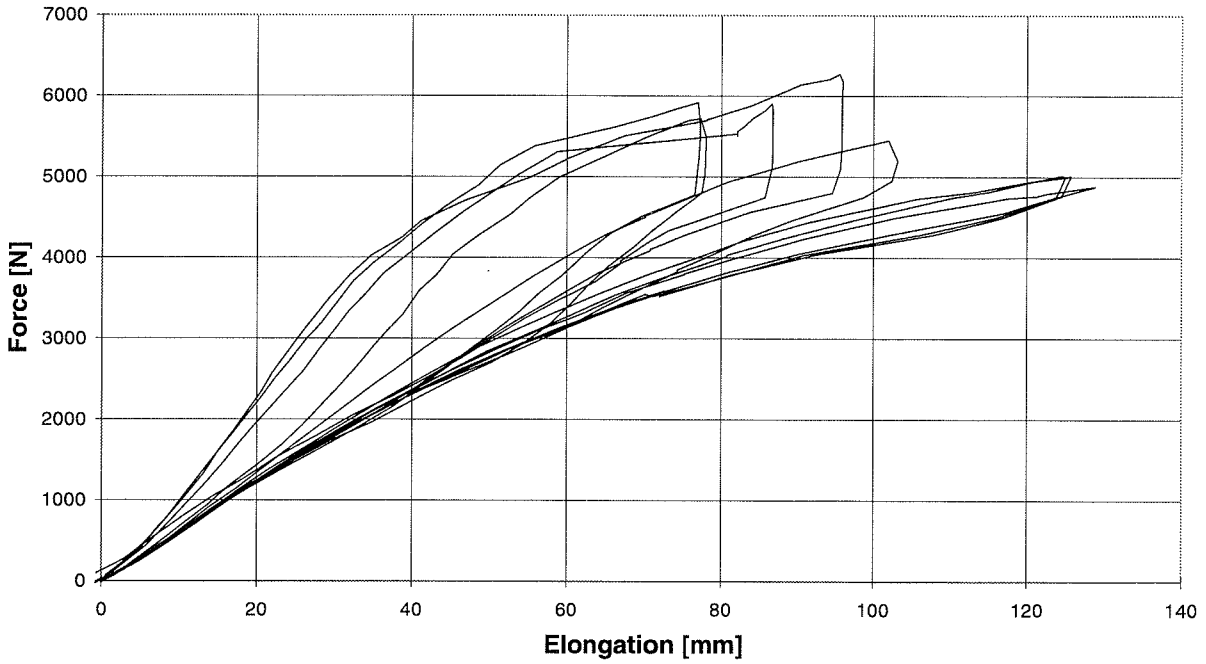

Figure B8 *Calibration of spring 4b.*

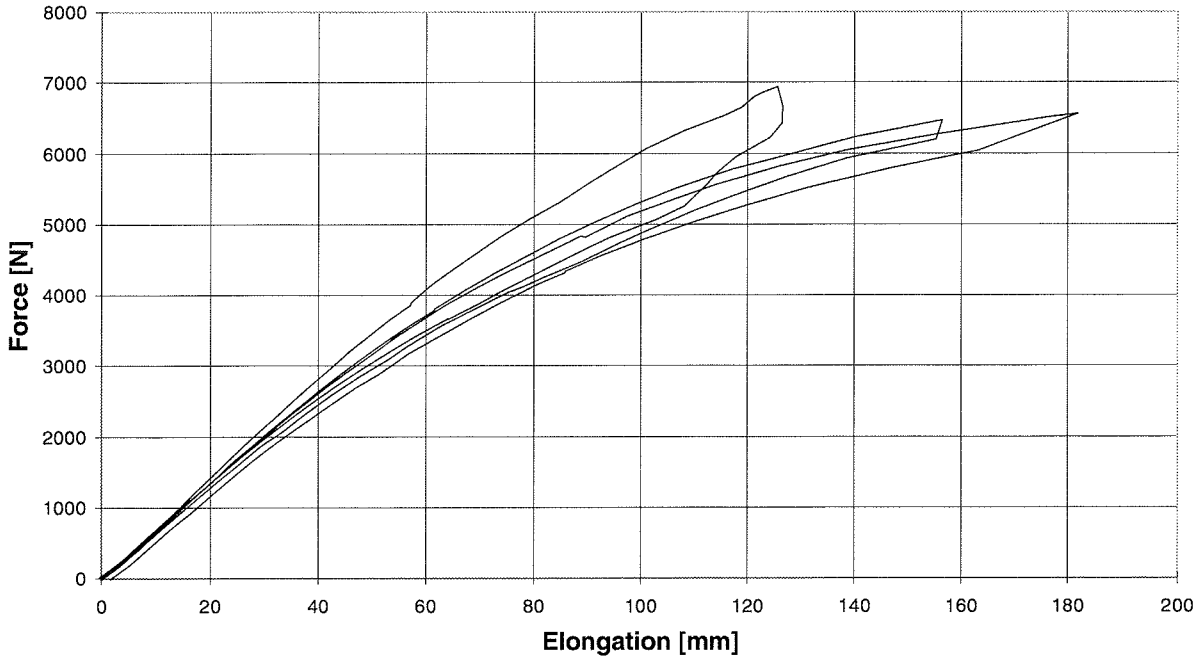

Figure B9 *Calibration of spring 5a.*

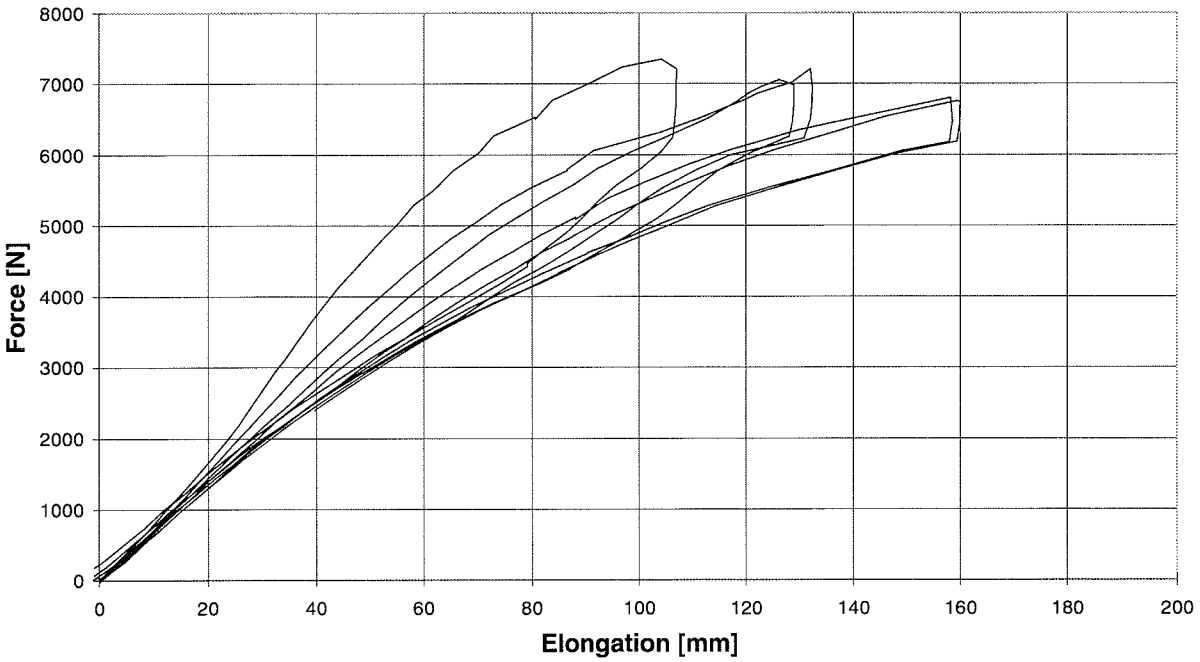

Figure B10 *Calibration of spring 5b.*

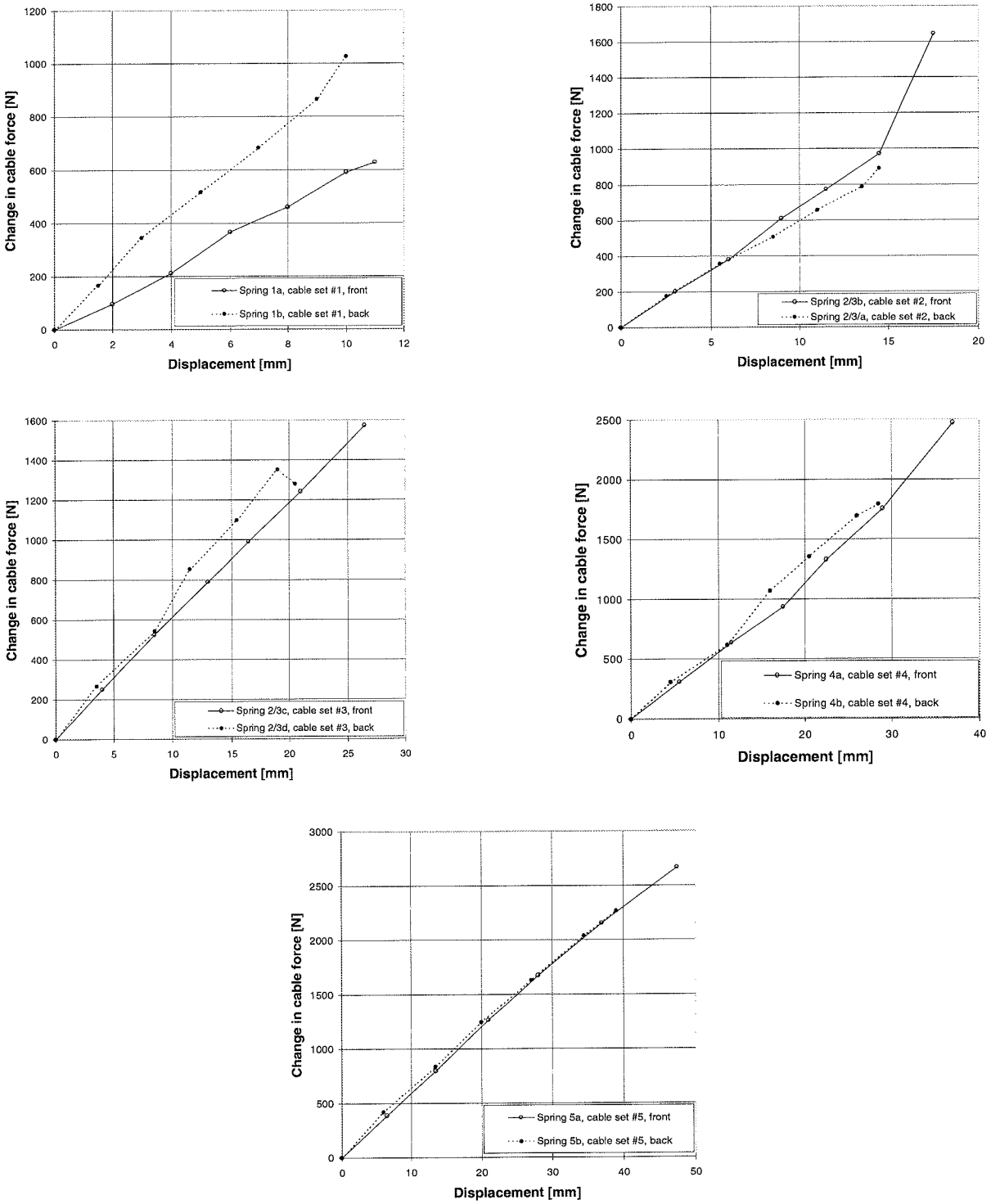

Figure C1 *Comparison of in situ spring responses in a cable set. Test I: Plane system, laterally free.*

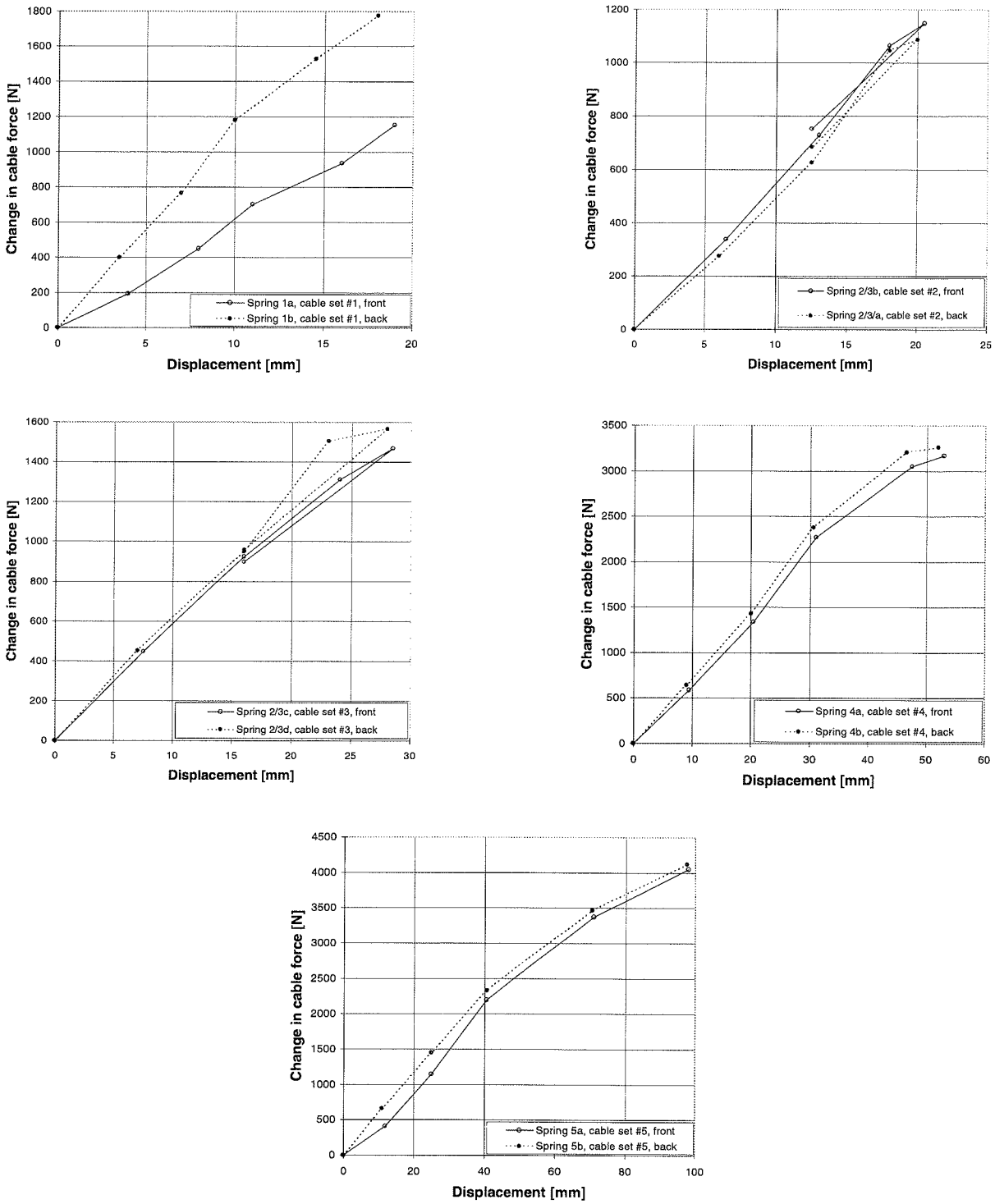

Figure C2 *Comparison of in situ spring responses in a cable set. Test II: Plane system, laterally restrained.*

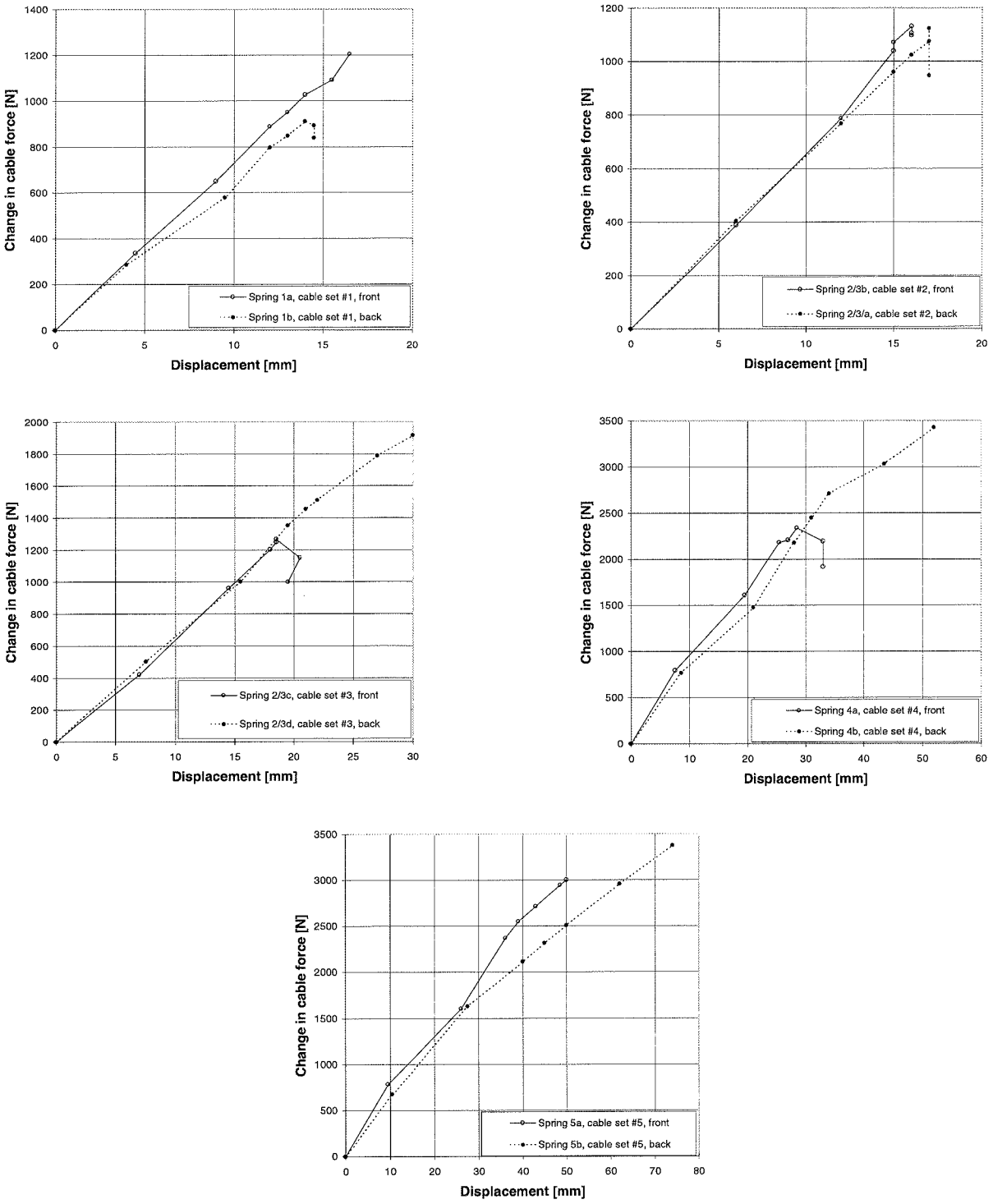

Figure C3 *Comparison of in situ spring responses in a cable set. Test III: Spatial system, a = 35 cm.*

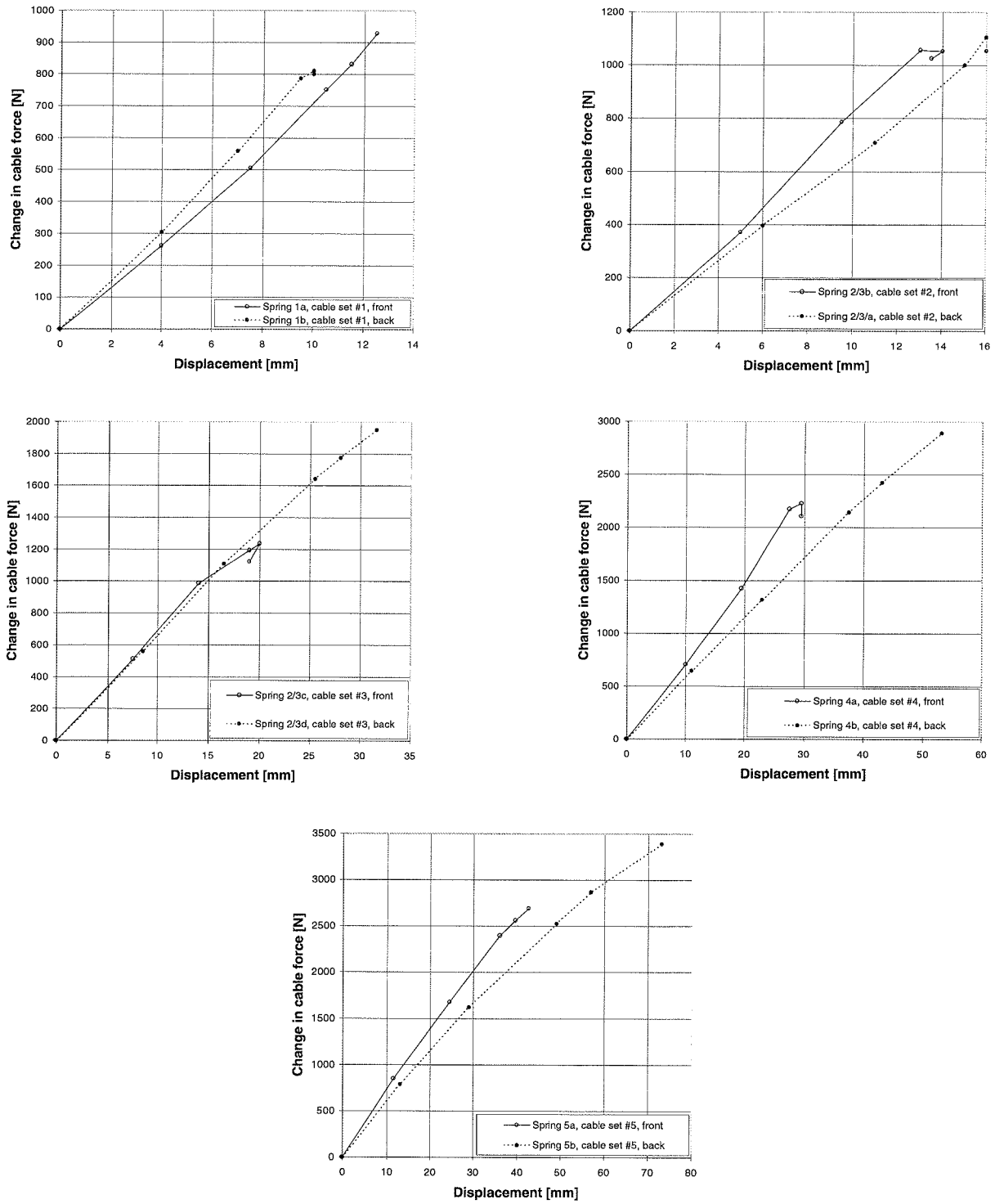

Figure C4 *Comparison of in situ spring responses in a cable set. Test IV: Spatial system, a = 45 cm.*

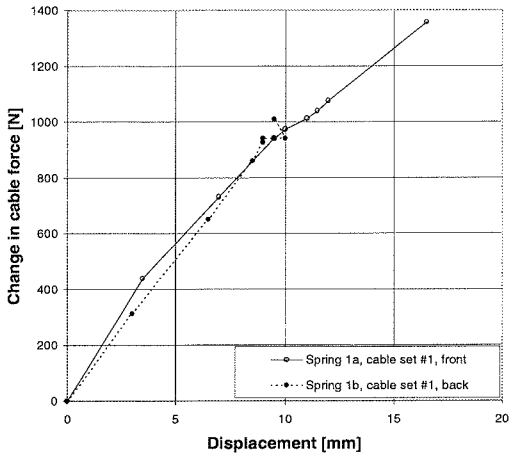

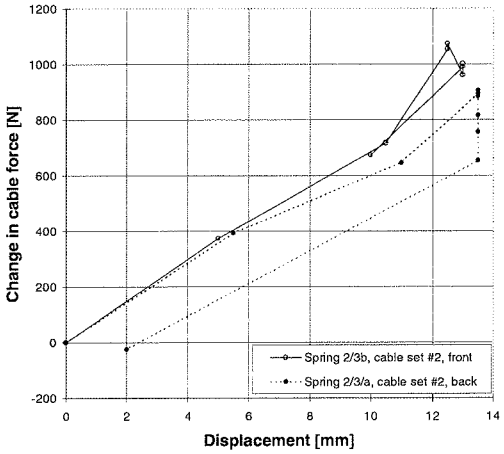

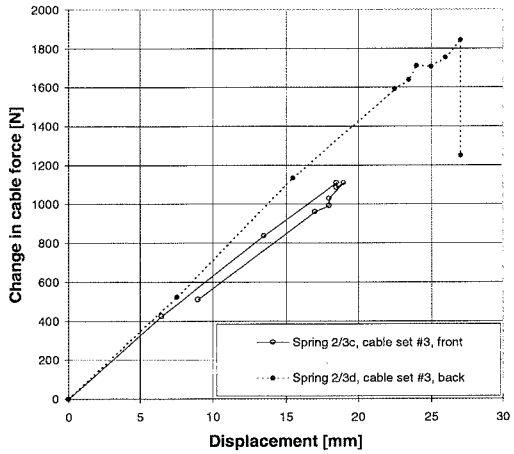

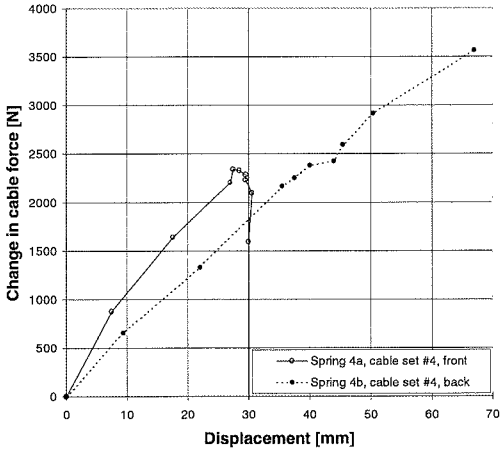

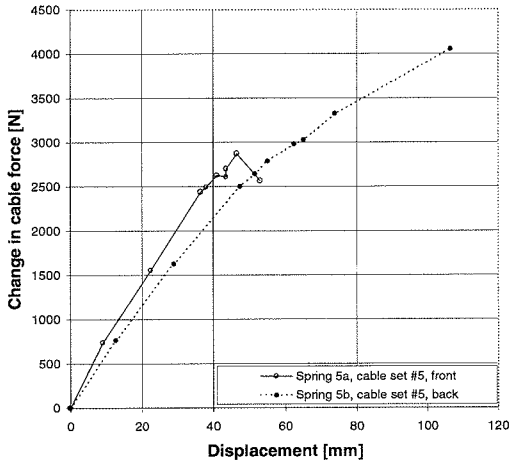

Figure C5 *Comparison of in situ spring responses in a cable set. Test V: Spatial system, a = 55 cm.*

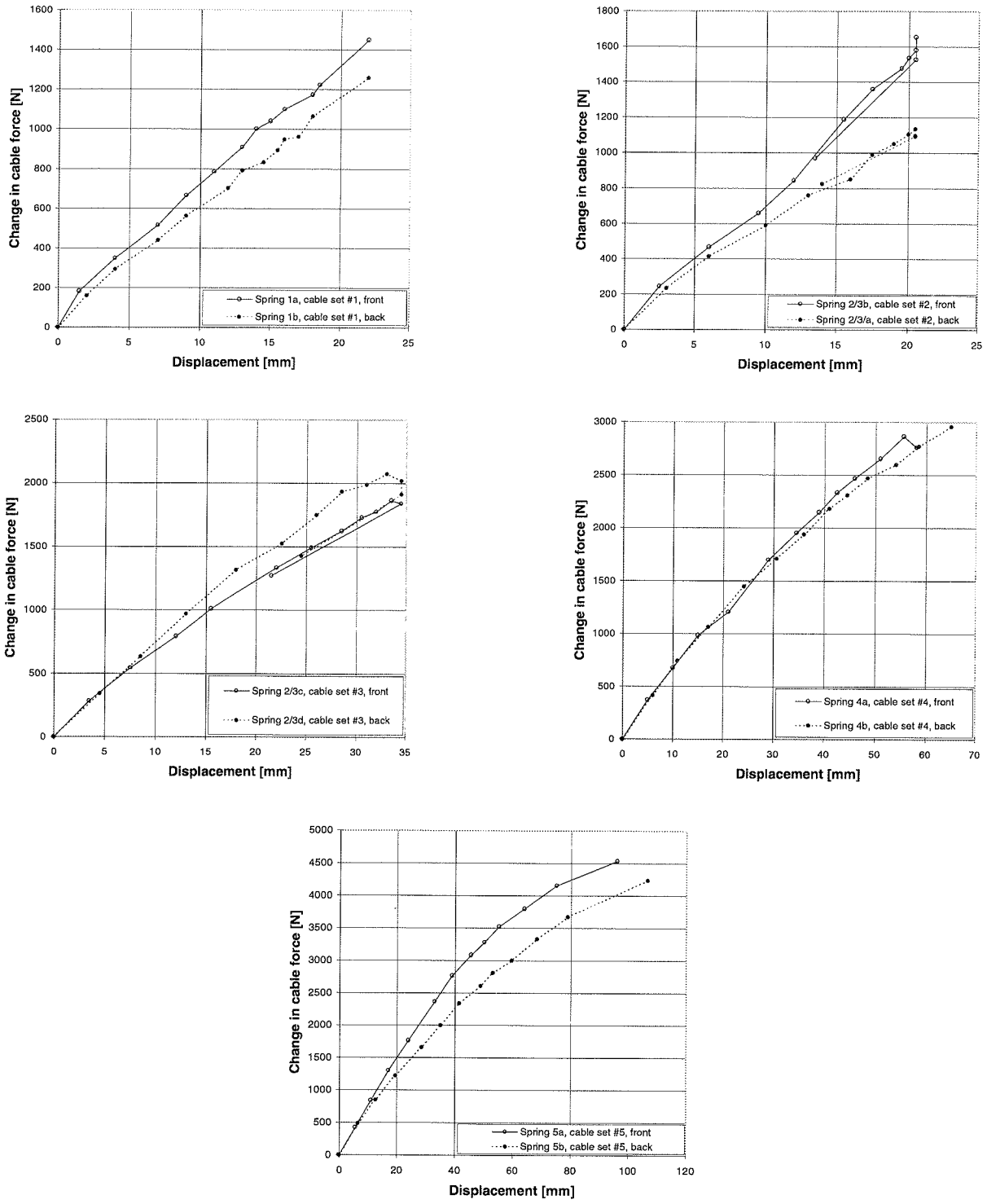

Figure C6 *Comparison of in situ spring response in a cable set. Test VI: Plane system, laterally restrained.*

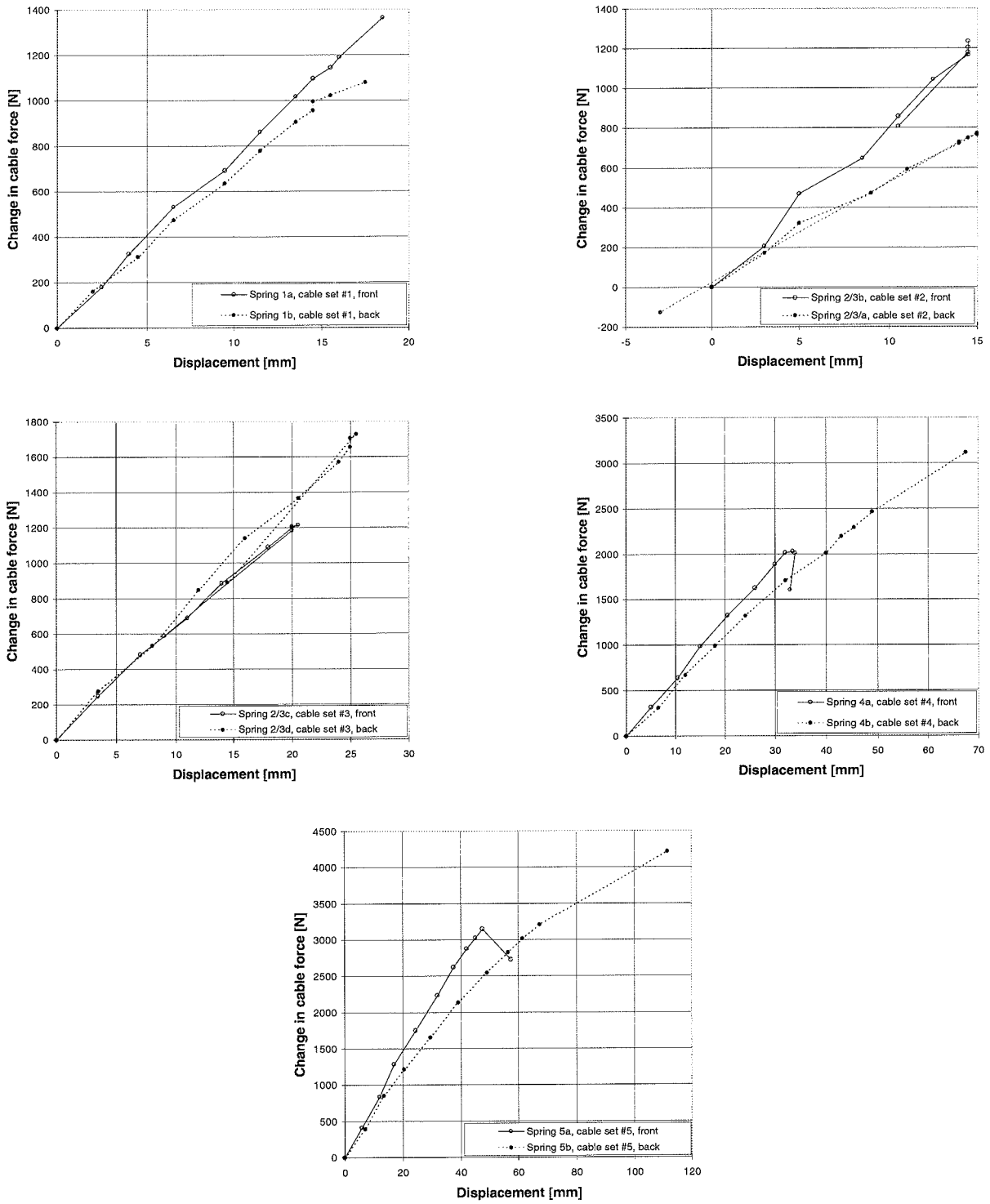

Figure C7 *Comparison of in situ responses in a cable set. Test VII: Spatial system, a = 75 cm.*

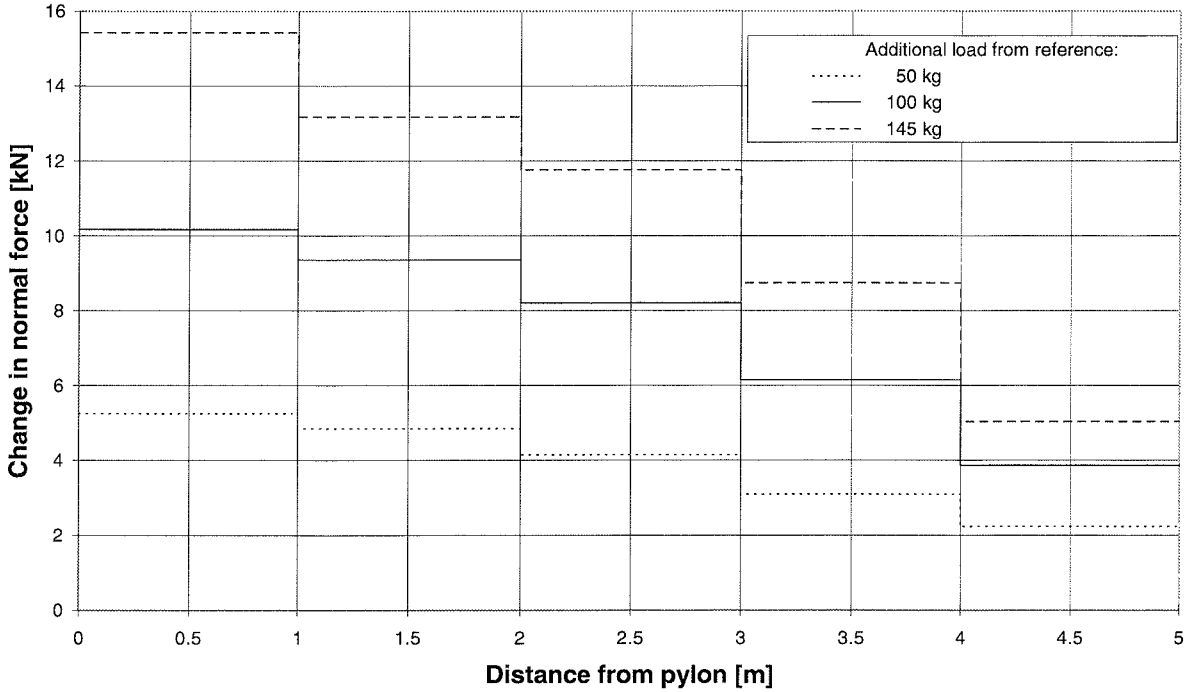

Figure D1 *Normal force distribution at selected load levels. Test I: Plane system, laterally free.*

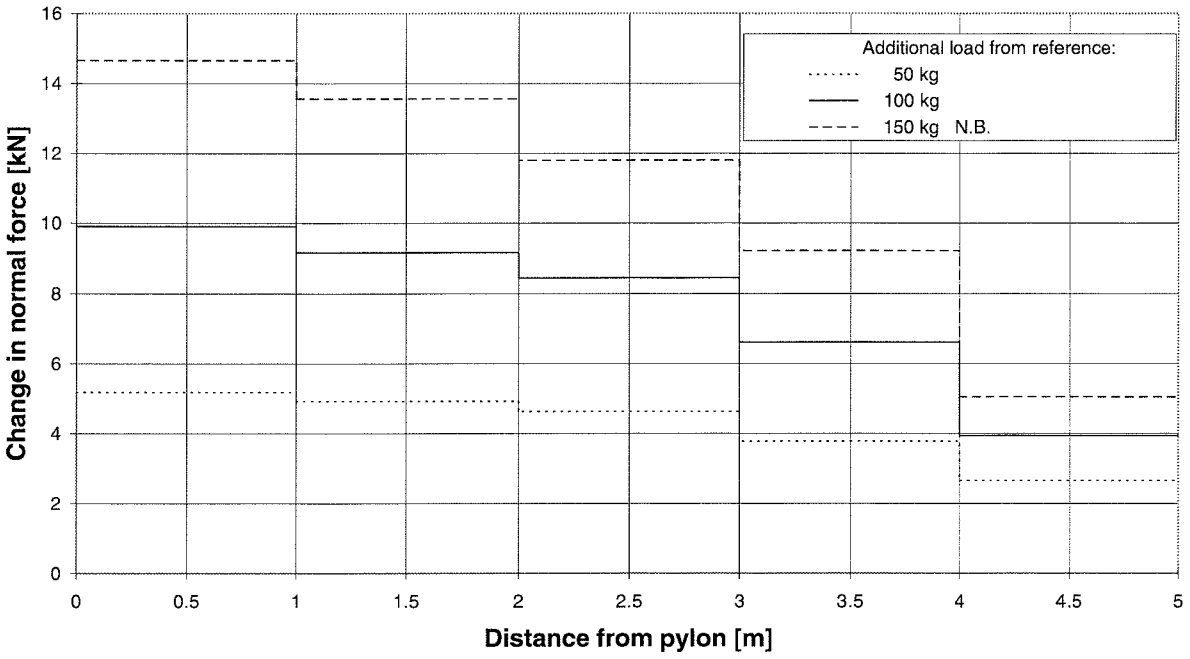

Figure D2 *Normal force distribution at selected load levels. Test II: Plane system, laterally restrained.*

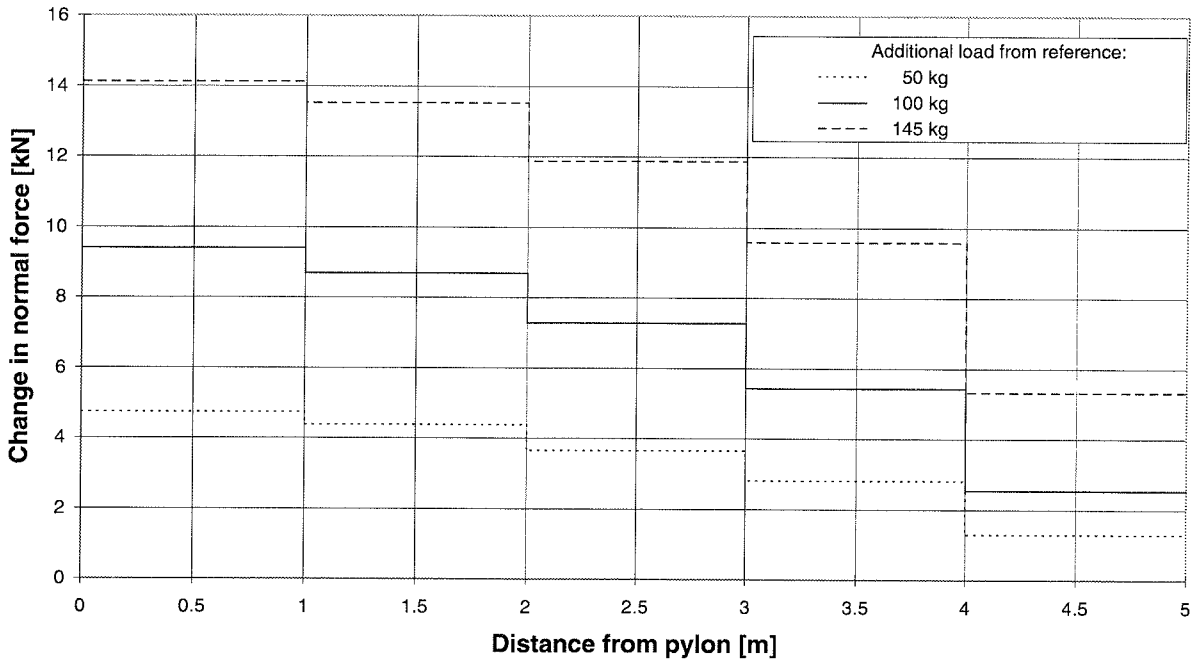

Figure D3 *Normal force distribution at selected load levels. Test III: Spatial system, a = 35 cm.*

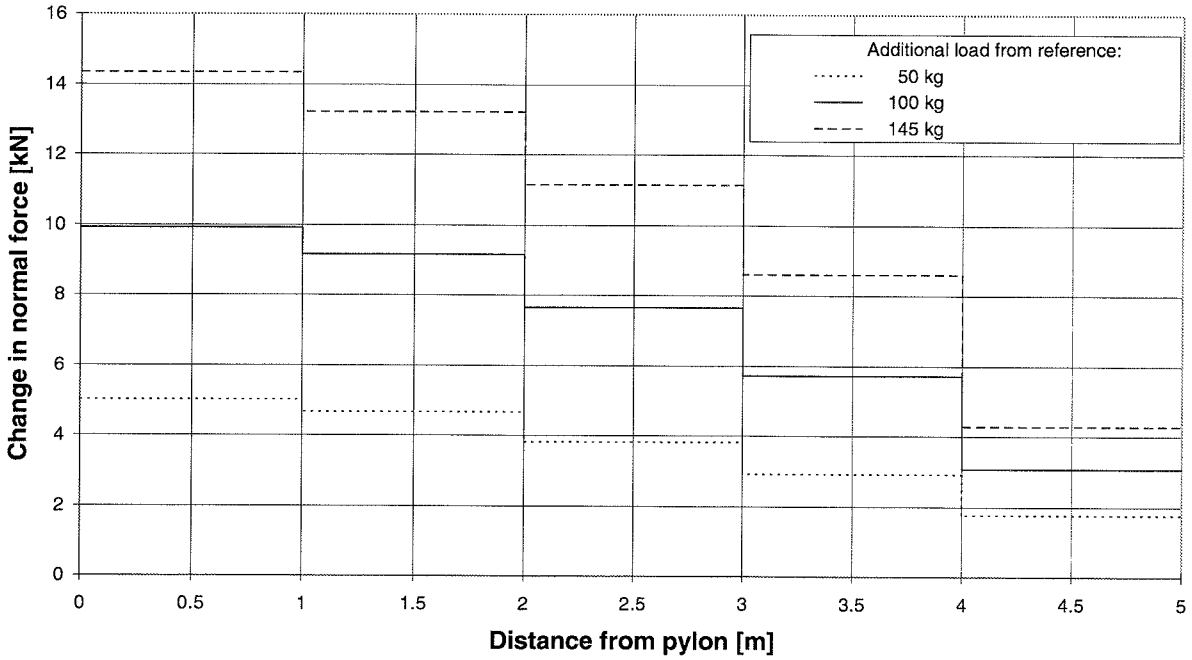

Figure D4 *Normal force distribution at selected load levels. Test IV: Spatial system, a = 45 cm.*

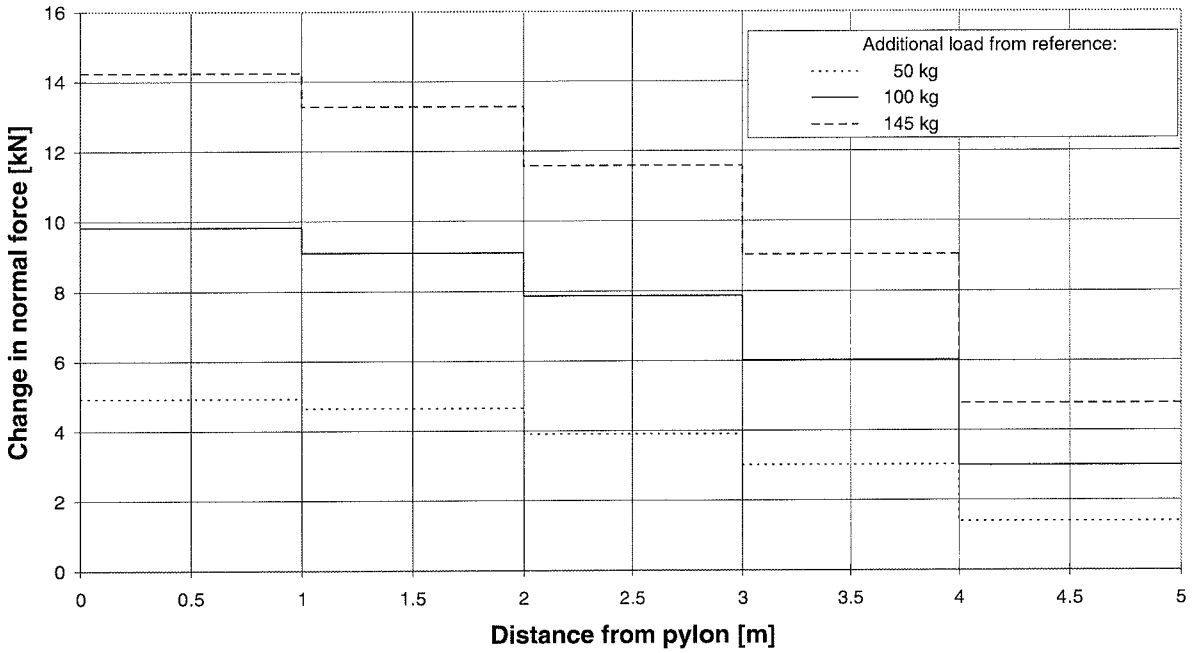

Figure D5 *Normal force distribution at selected load levels. Test V: Spatial system, a = 55 cm.*

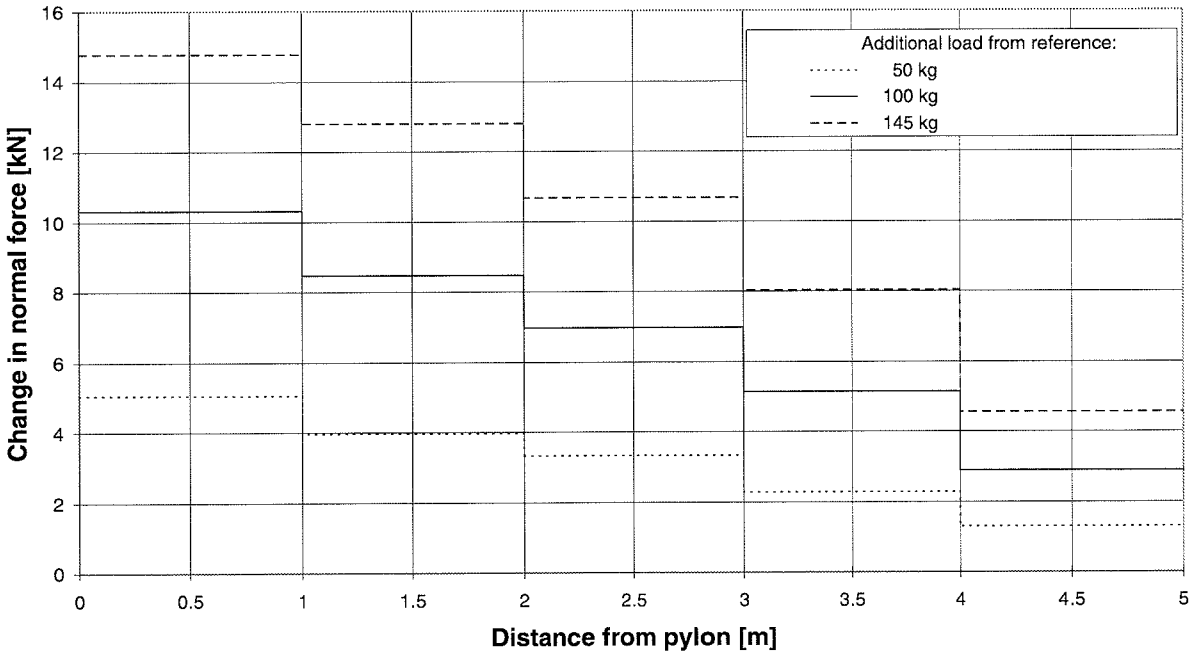

Figure D6 *Normal force distribution at selected load levels. Test VI: Plane system, laterally restrained.*

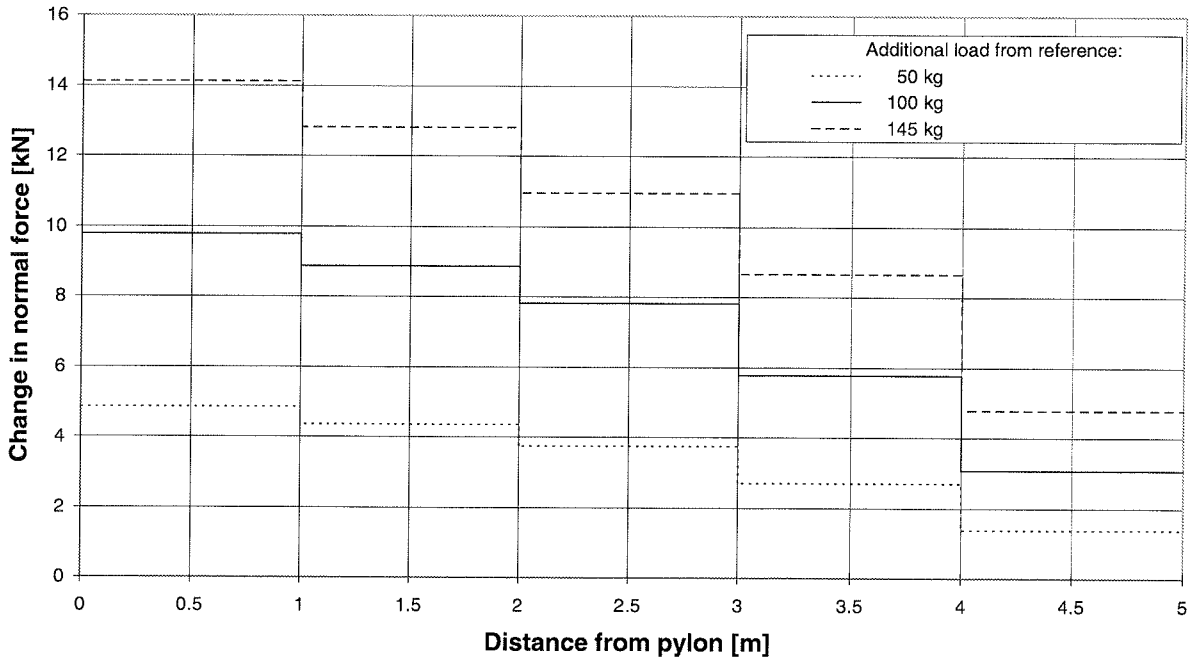

Figure D7 *Normal force distribution at selected load levels. Test VII: Spatial system, a = 75 cm.*

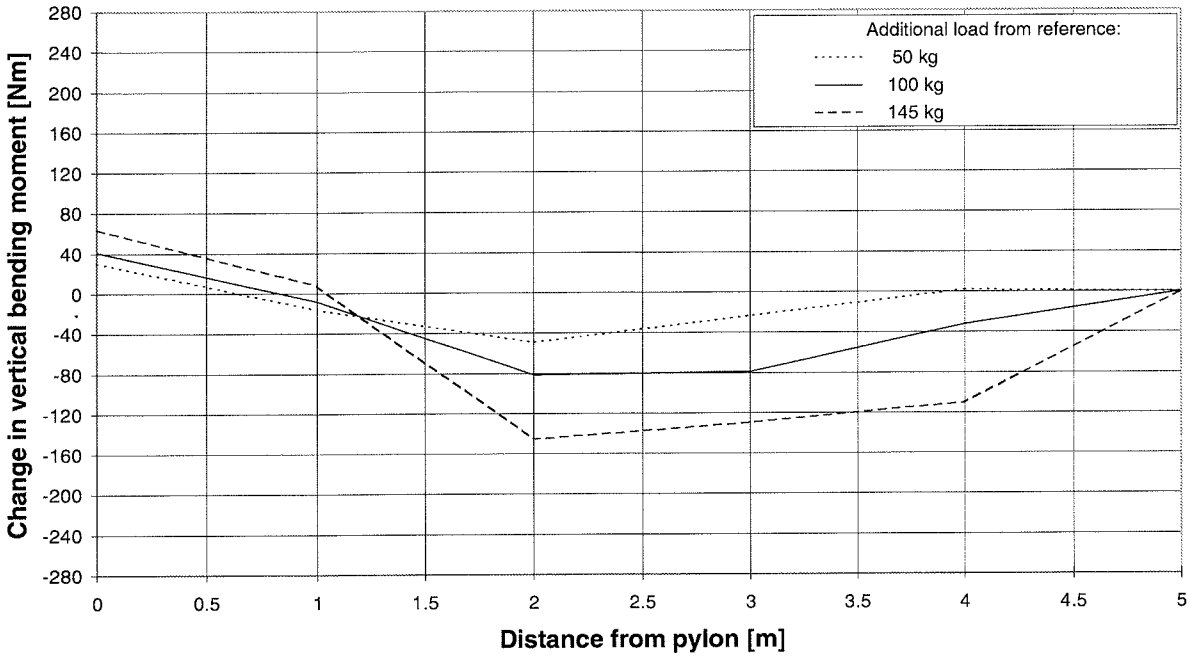

Figure E1 *Vertical bending moment distribution at selected load levels. Test I: Plane system, laterally free.*

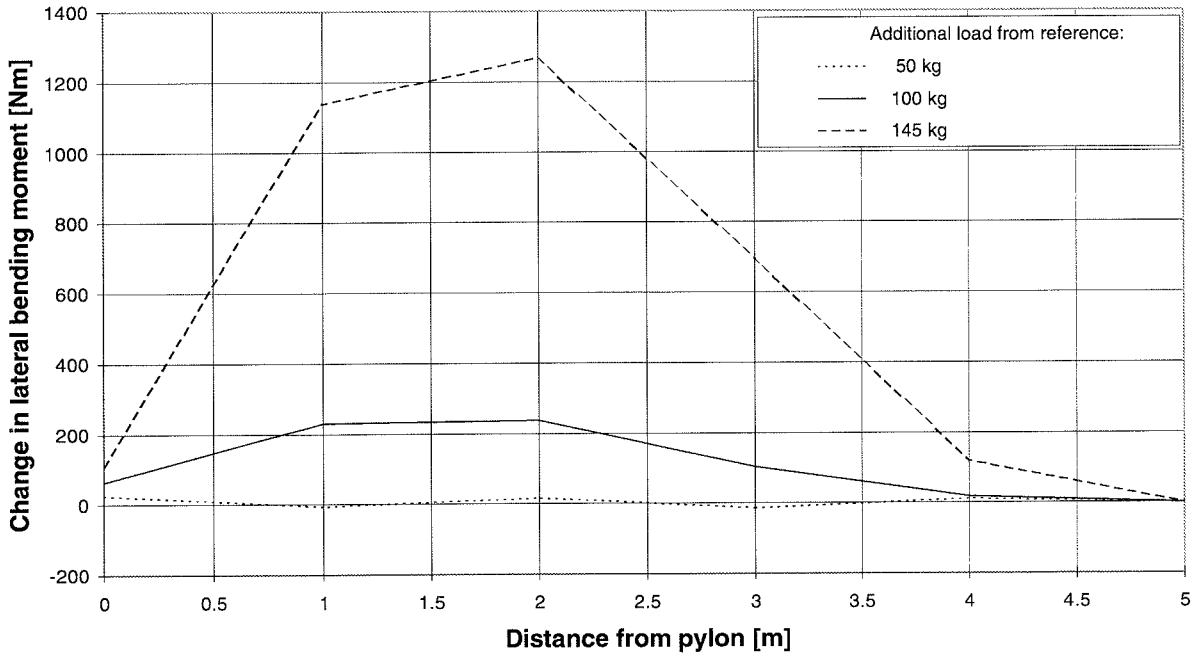

Figure E2 *Lateral bending moment distribution at selected load levels. Test I: Plane system, lateraly free.*

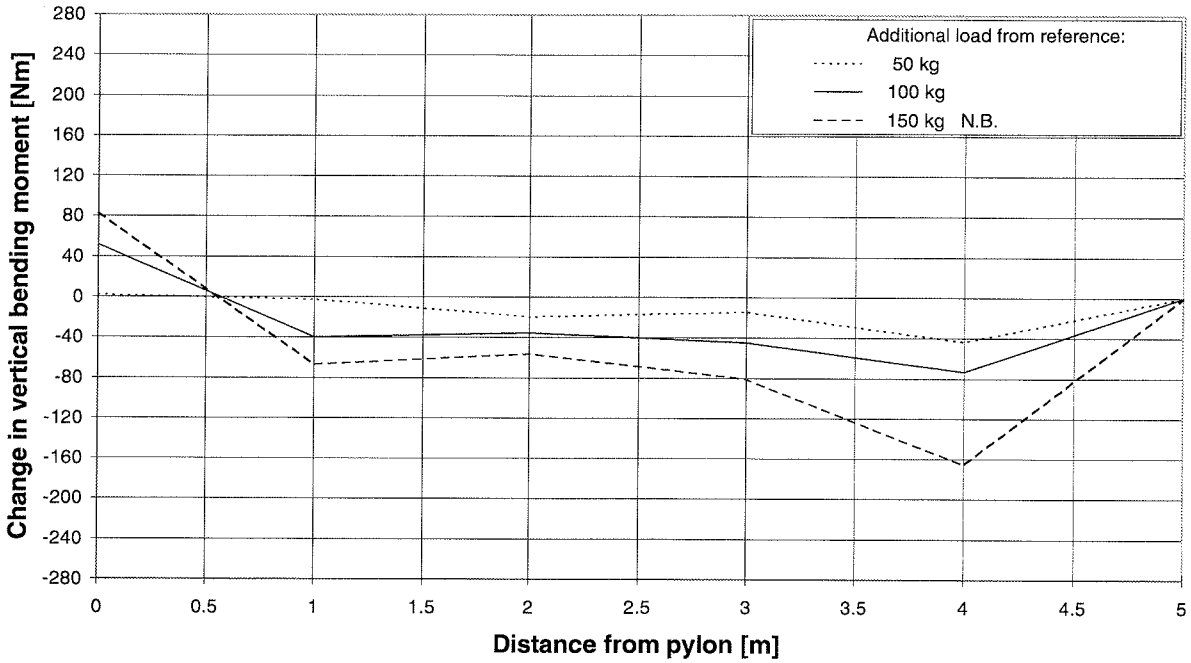

Figure E3 *Vertical bending moment distribution at selected load levels. Test II: Plane system, laterally restrained.*

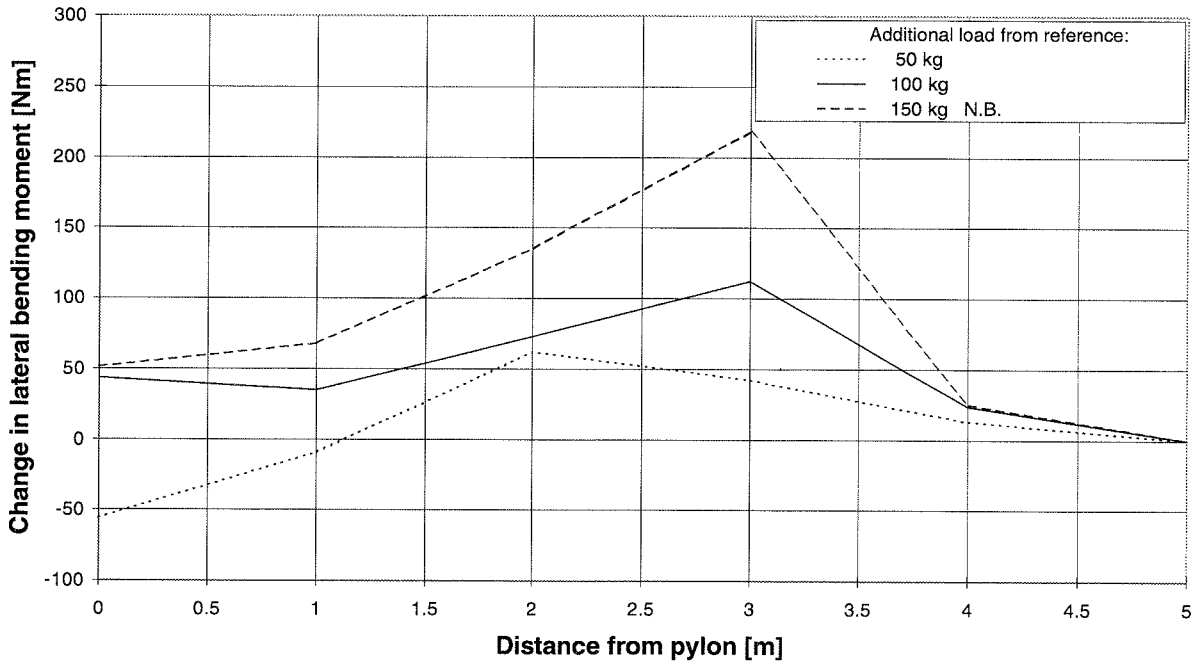

Figure E4 *Lateral bending moment distribution at selected load levels. Test II: Plane system, laterally restrained.*

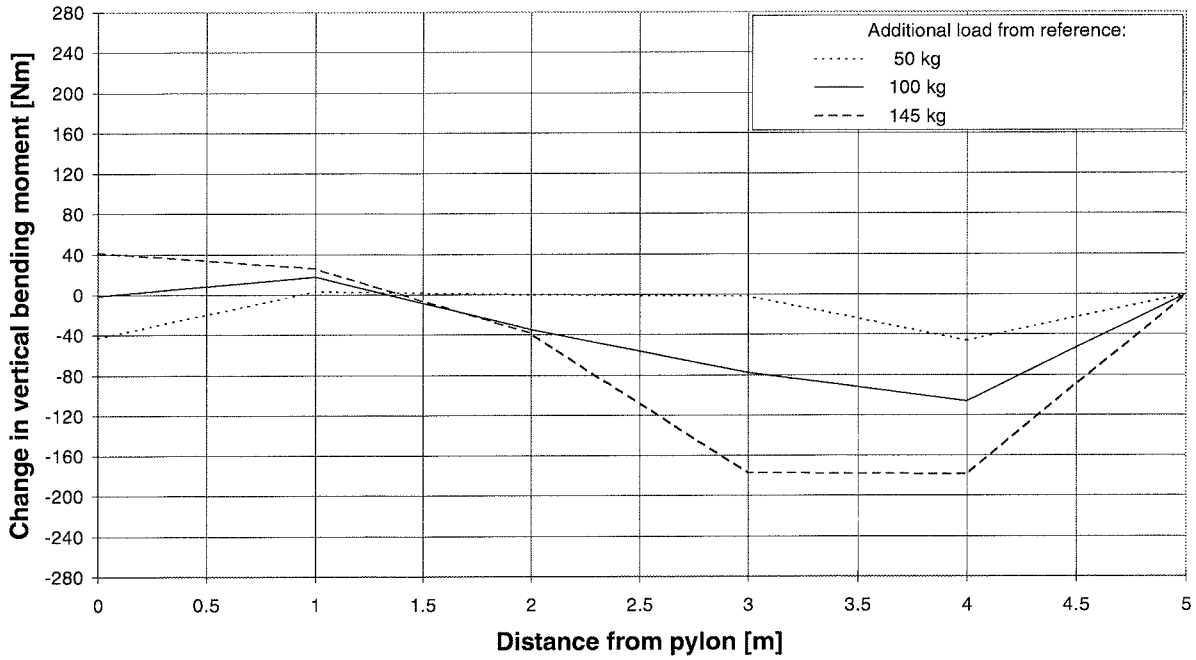

Figure E5 *Vertical bending moment distribution at selected load levels. Test III: Spatial system, a = 35 cm.*

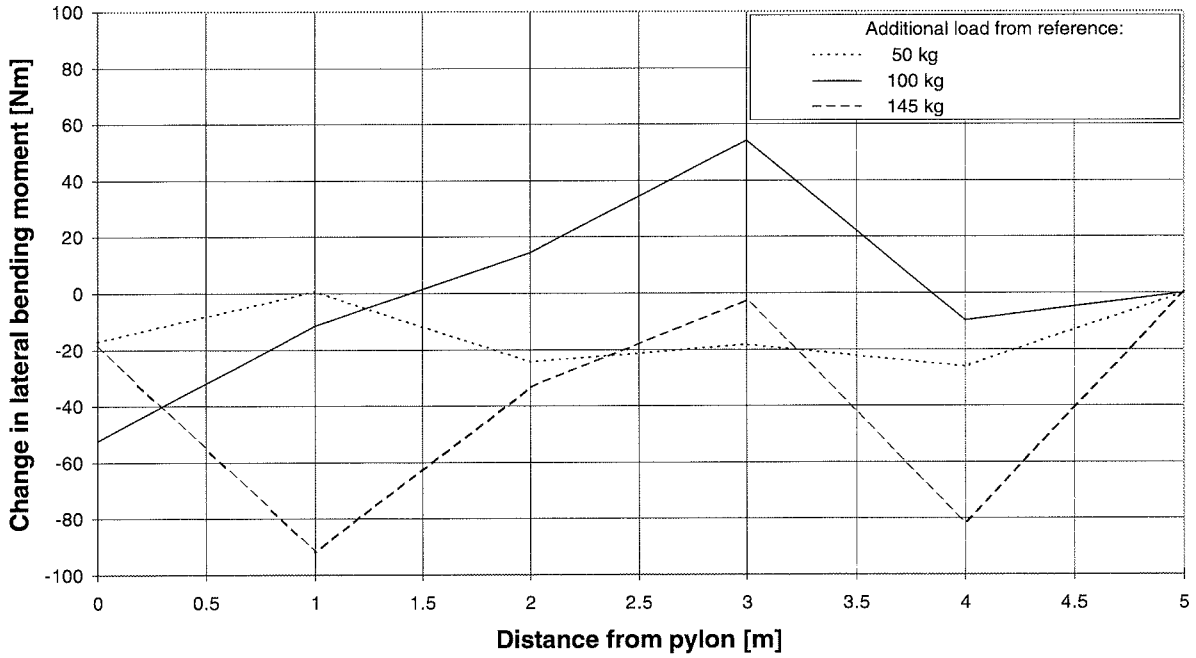

Figure E6 *Lateral bending moment distribution at selected load levels. Test III: Spatial system, a = 35 cm.*

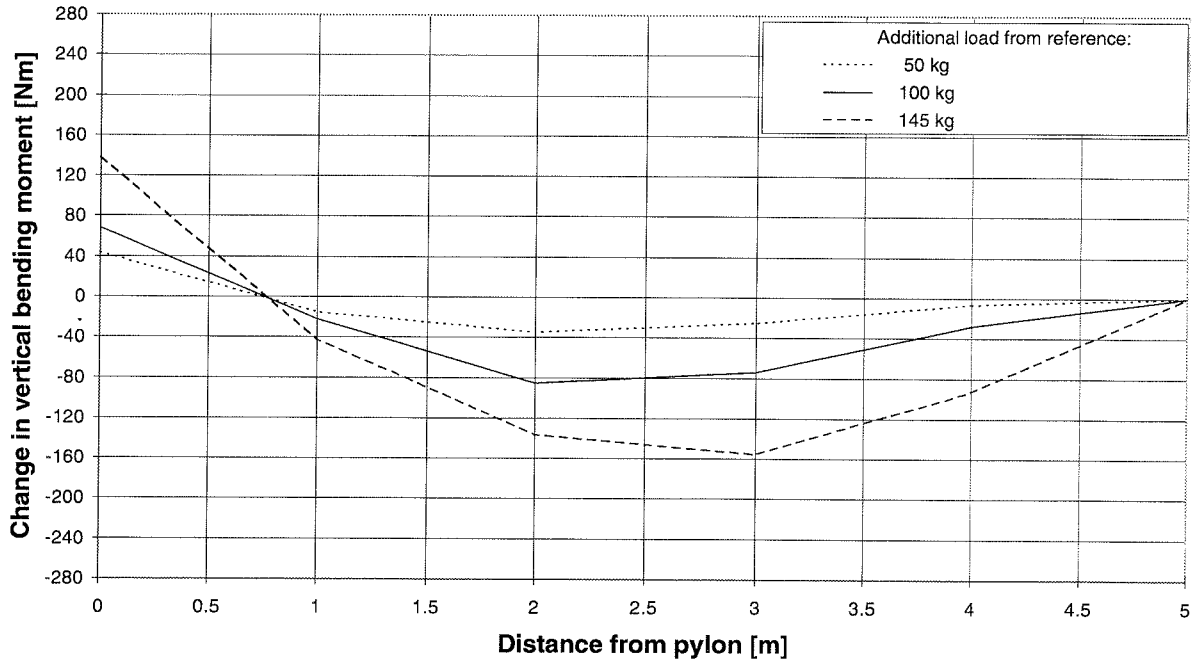

Figure E7 *Vertical bending moment distribution at selected load levels. Test IV: Spatial system, a = 45 cm.*

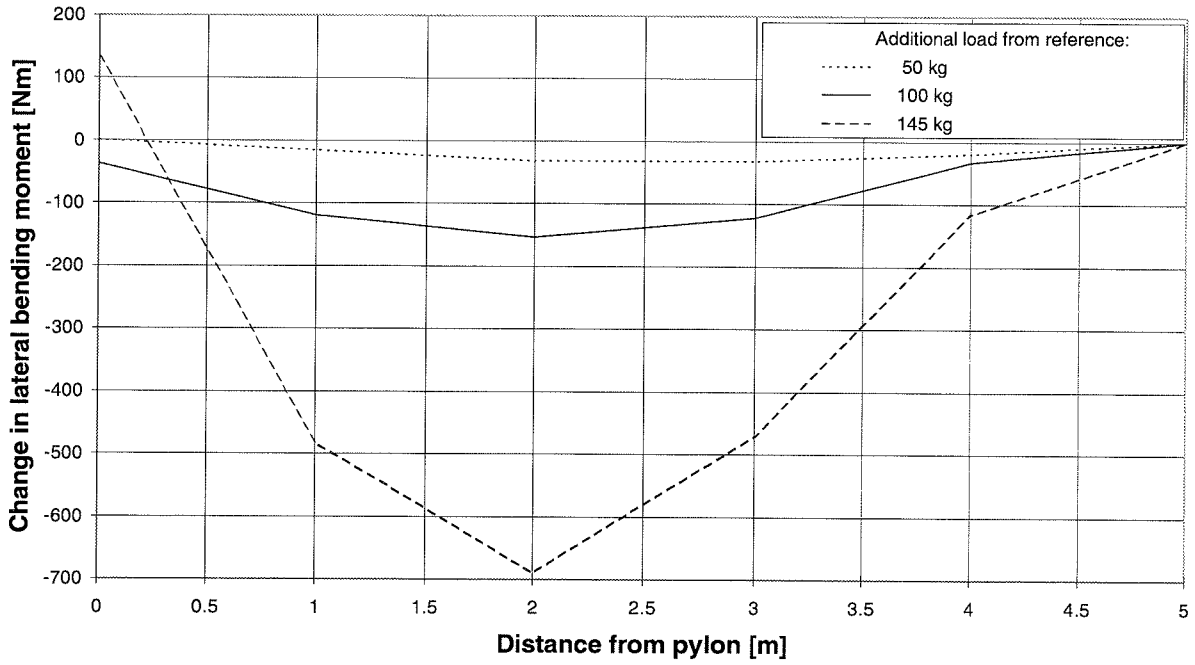

Figure E8 *Lateral bending moment distribution at selected load levels. Test IV: Spatial system, a = 45 cm.*

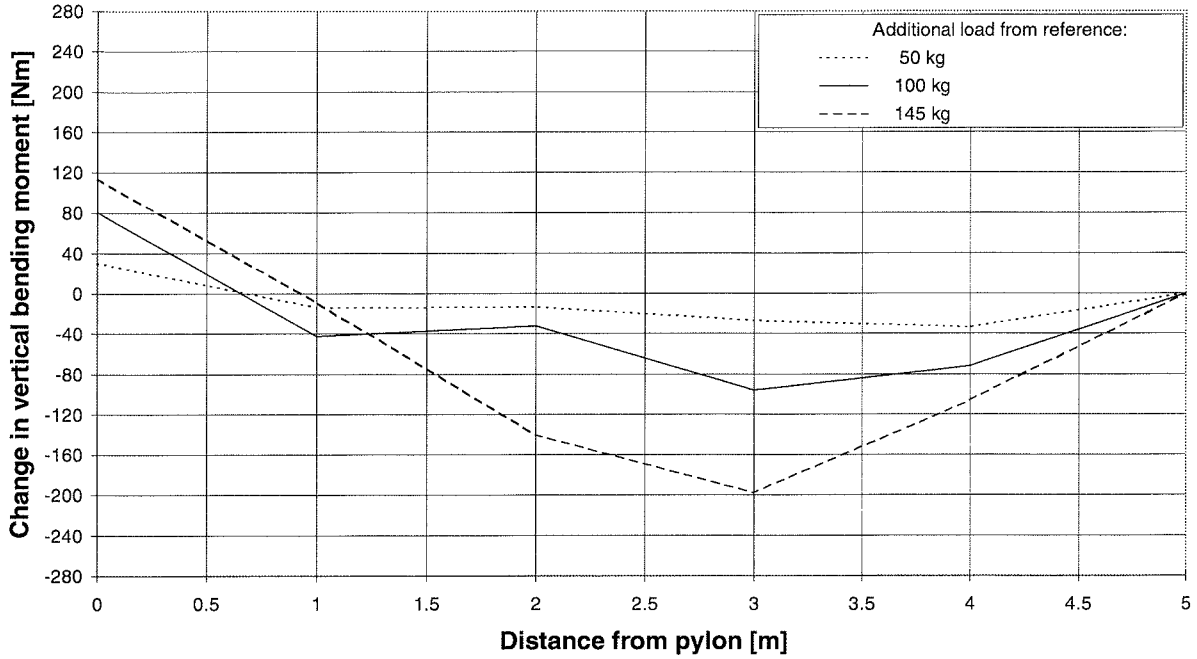

Figure E9 *Vertical bending moment distribution at selected load levels. Test V: Spatial system, a = 55 cm.*

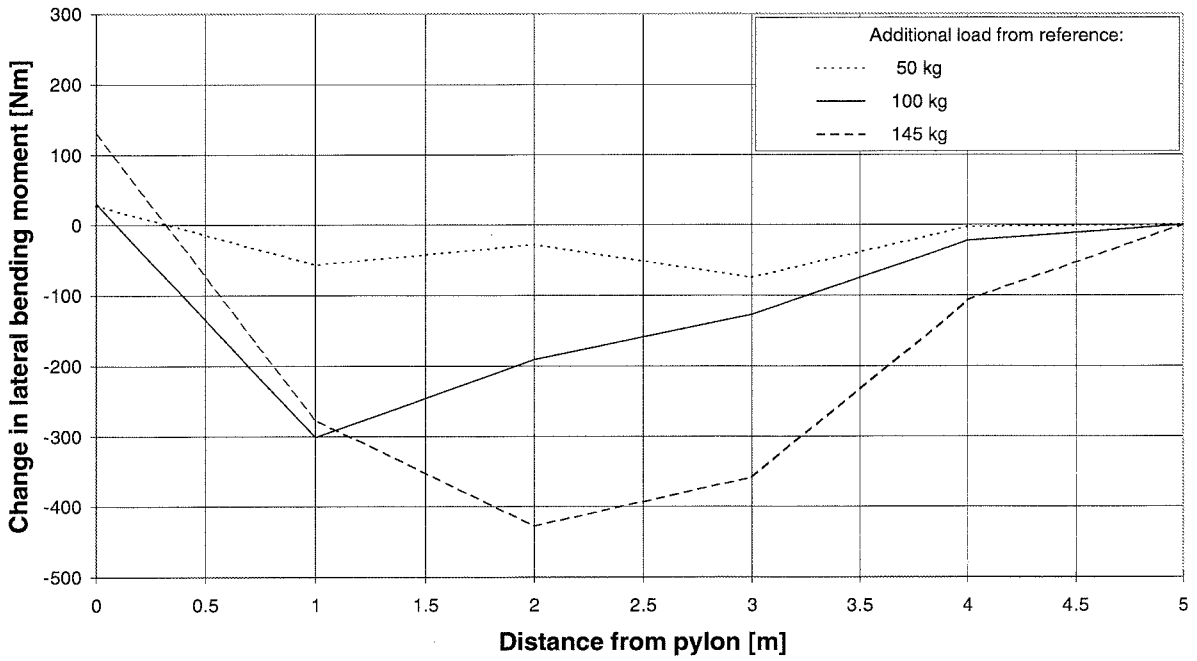

Figure E10 *Lateral bending moment distribution at selected load levels. Test V: Spatial system, a = 55 cm.*

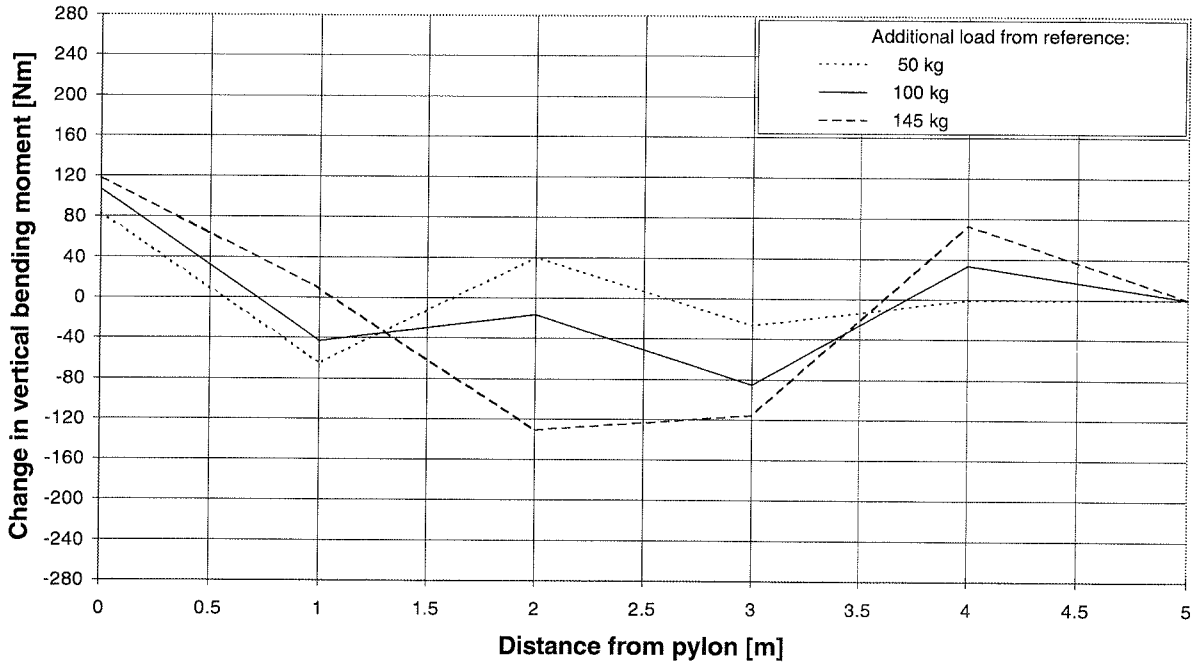

Figure E11 *Vertical bending moment distribution at selected load levels. Test VI: Plane system, laterally restrained.*

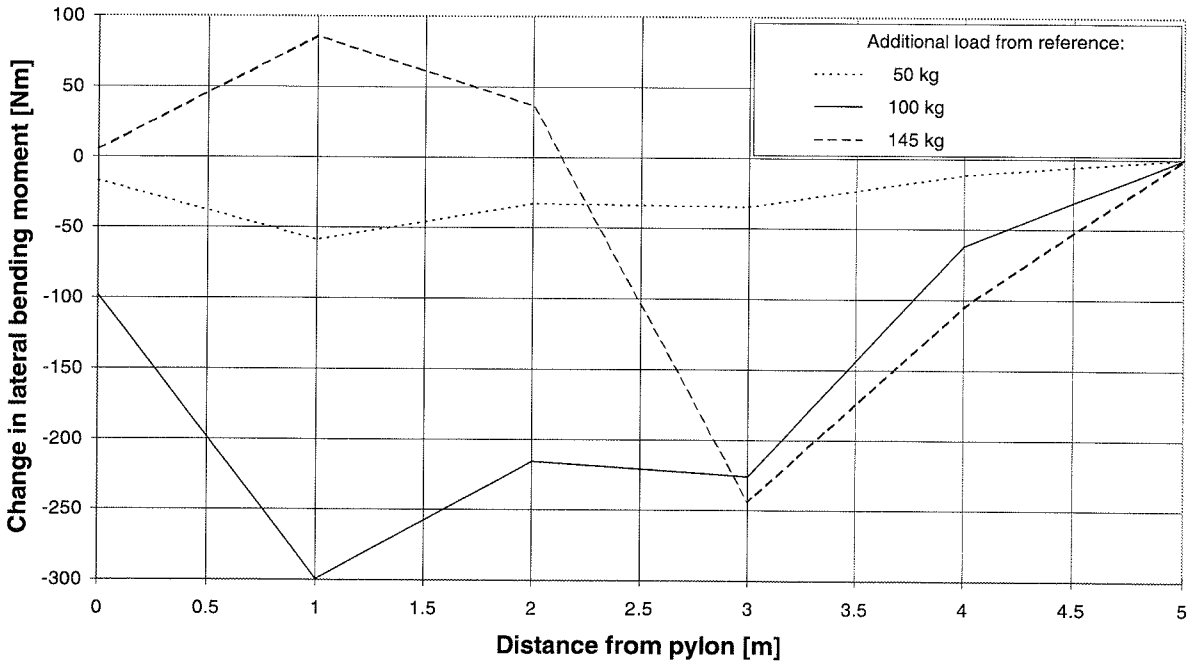

Figure E12 *Lateral bending moment distribution at selected load levels. Test VI: Plane system, laterally restrained.*

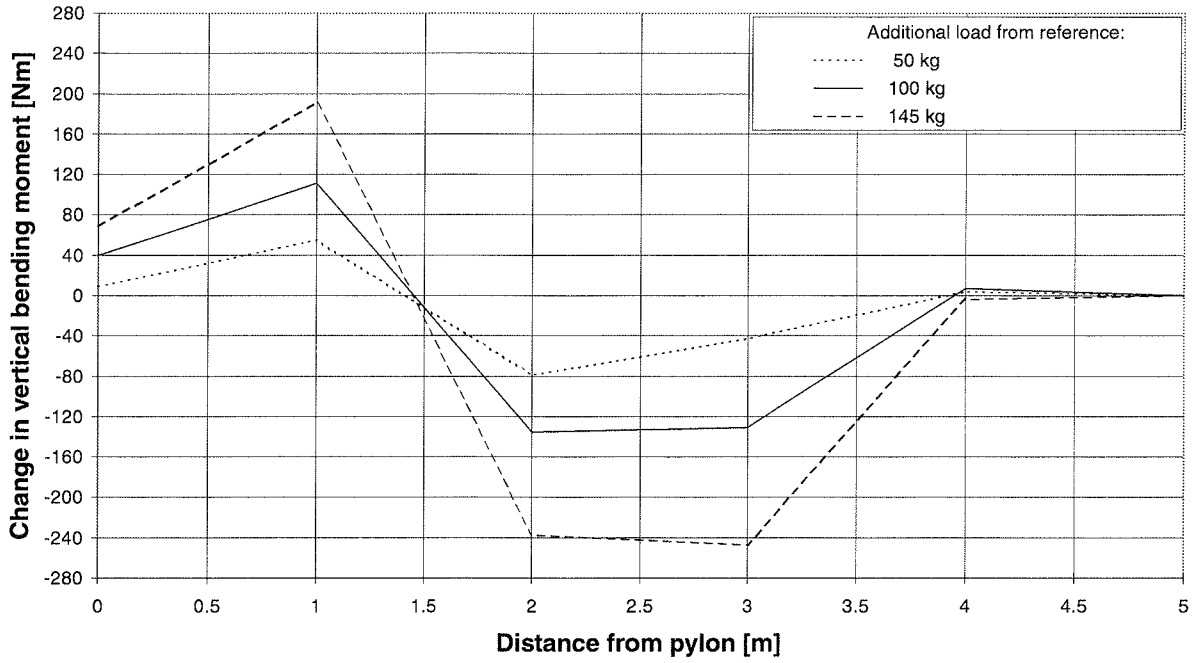

Figure E13 *Vertical bending moment distribution at selected load levels. Test VII: Spatial system, a = 75 cm.*

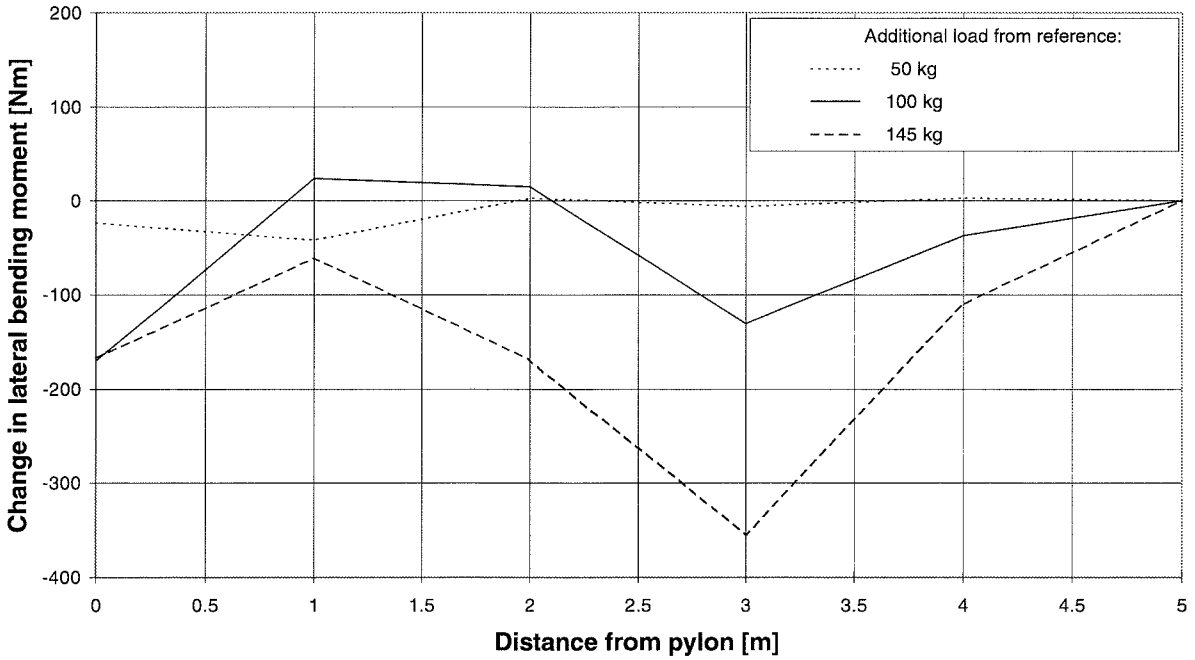

Figure E14 *Lateral bending moment distribution at selected load levels. Test VII: Spatial system, a = 75 cm.*

Effect of large in-plane and out-of-plane deformations on buckling:

The following analysis is an expansion of expressions found in *Vacharajittiphan et al.* (1974), where in-plane deformation (i.e. in the plane of loading) is taken into account in the analysis of lateral buckling. In the following we derive corresponding expressions where also out-of-plane deformation is accounted for. These out-of-plane deflections can for instance be due to an unsymmetrical system with respect to stiffnesses, like it was found in the bridge models. We follow the same procedure as in *Vacharajittiphan et al.* (1974) and use the same notation. The terms used are explained in the text or shown on the figures.

The deformations before and after buckling are shown in Fig. F1.

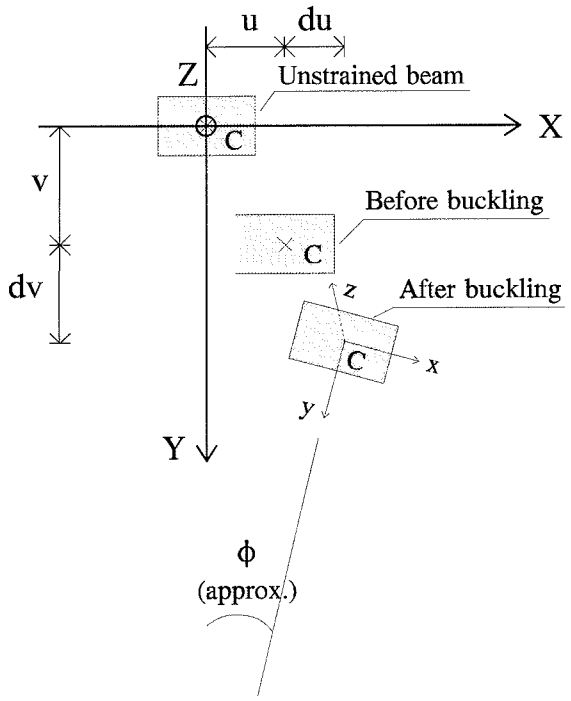

Figure F1 *Beam displacements before and after buckling viewed in the Z axis direction.*

The relationship between the moment and torsional resultants M_x, M_y, M_z acting about the final local axes x, y, z and those acting about the initial axes X, Y, Z can be expressed as:

$$\begin{Bmatrix} M_x \\ M_y \\ M_z \end{Bmatrix} = \left[T_R\right] \begin{Bmatrix} M_X \\ M_Y \\ M_Z \end{Bmatrix} \tag{1}$$

The elements of the rotation matrix $[T_R]$ are identical with the direction cosines which relate the orientations of the x, y, z and X, Y, Z axis systems, so that

$$\left[T_R\right] = \begin{bmatrix} l_x & m_x & n_x \\ l_y & m_y & n_y \\ l_z & m_z & n_z \end{bmatrix} \tag{2}$$

where l, m, n are the direction cosines of the final axes relative to the initial axes.

In the following we identify the elements in $[T_R]$ taking into account both in-plane and out-of-plane deformation. We consider a set of axes x_0, y_0, z_0 parallel to the initial axes X, Y, Z, respectively. The x_0, y_0, z_0 axes have their origin at the centre of gravity of a displaced cross-section of the beam. The local x, y, z axes also have their origin at the centre of gravity of the displaced cross-section of the beam. The x and y axes are the local principal axes, while z is tangential to the deformed beam axis.

The relative orientations between the X, Y, Z and x, y, z directions can be described by three independent rotations α, β and ϕ as shown in Fig. F2 - F4.

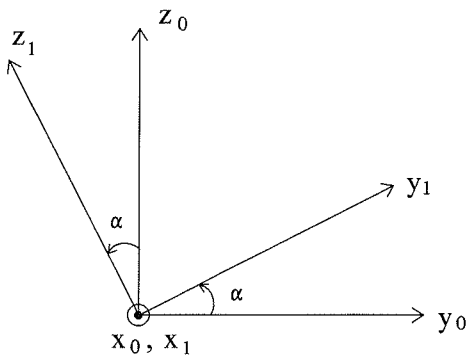

$$\begin{Bmatrix} x_1 \\ y_1 \\ z_1 \end{Bmatrix} = \begin{bmatrix} 1 & 0 & 0 \\ 0 & \cos\alpha & \sin\alpha \\ 0 & -\sin\alpha & \cos\alpha \end{bmatrix} \begin{Bmatrix} x_0 \\ y_0 \\ z_0 \end{Bmatrix} \quad (3)$$

Figure F2 *Rotation* α *about* x_0 *axis.*

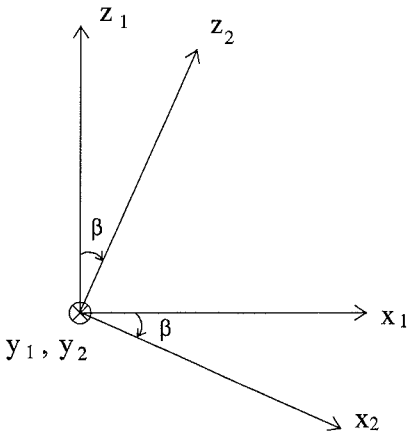

$$\begin{Bmatrix} x_2 \\ y_2 \\ z_2 \end{Bmatrix} = \begin{bmatrix} \cos\beta & 0 & -\sin\beta \\ 0 & 1 & 0 \\ \sin\beta & 0 & \cos\beta \end{bmatrix} \begin{Bmatrix} x_1 \\ y_1 \\ z_1 \end{Bmatrix} \quad (4)$$

Figure F3 *Rotation* β *about* y_1 *axis.*

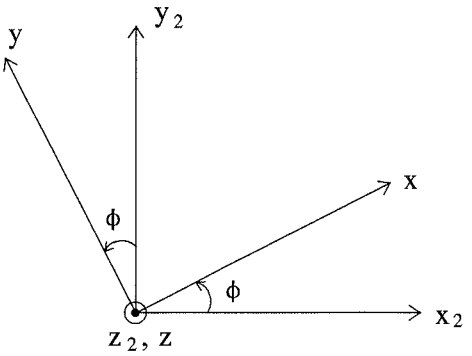

$$\begin{Bmatrix} x \\ y \\ z \end{Bmatrix} = \begin{bmatrix} \cos\phi & \sin\phi & 0 \\ -\sin\phi & \cos\phi & 0 \\ 0 & 0 & 1 \end{bmatrix} \begin{Bmatrix} x_2 \\ y_2 \\ z_2 \end{Bmatrix} \quad (5)$$

Figure F4 *Rotation* ϕ *about* z_2 *axis.*

By matrix multiplication we can determine the rotation matrix $[T_R]$:

$$[T_R] = \begin{bmatrix} \cos\beta \cdot\cos\phi & \sin\alpha \cdot\sin\beta \cdot\cos\phi + \cos\alpha \cdot\sin\phi & -\cos\alpha \cdot\sin\beta \cdot\cos\phi + \sin\alpha \cdot\sin\phi \\ -\cos\beta \cdot\sin\phi & -\sin\alpha \cdot\sin\beta \cdot\sin\phi + \cos\alpha \cdot\cos\phi & \cos\alpha \cdot\sin\beta \cdot\sin\phi + \sin\alpha \cdot\cos\phi \\ \sin\beta & -\sin\alpha \cdot\cos\beta & \cos\alpha \cdot\cos\beta \end{bmatrix} \tag{6}$$

The rotations α and β can be related to the slopes $v' = dv/dz$ and $u' = du/dz$ of the displaced beam axis, see Fig. F5.

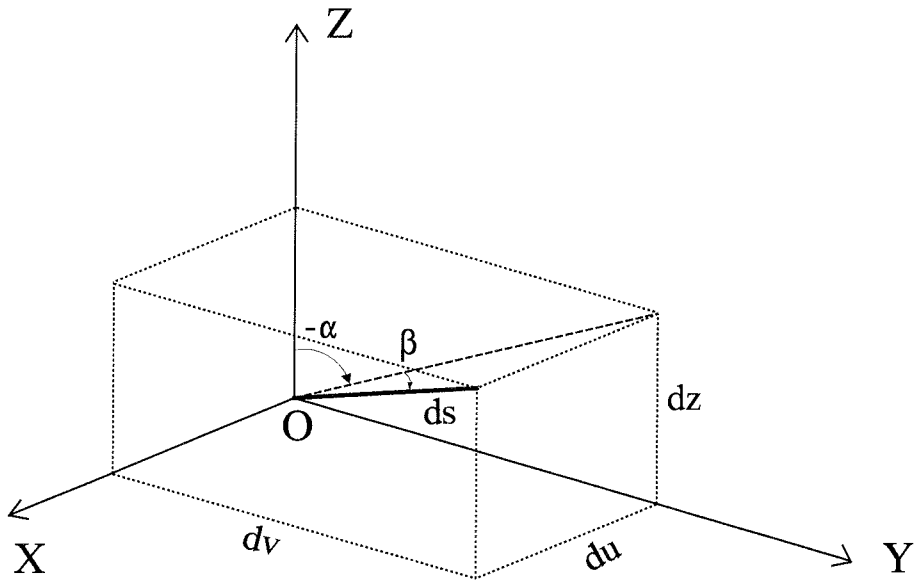

Figure F5 *Member projections on X, Y, Z axes.*

The in-plane slope v' and the out-of-plane slope u' are small but finite. The rotation matrix, $[T_R]$, can be evaluated in terms of the twist ϕ, and of the derivatives v', v'', u' and u'' of the in-plane and the out-of-plane deformations, dv and du. Terms involving small quantities with orders higher than 2 are consistently left out.

The in-plane deformation dv results in a rotation $-\alpha$ about the x_0-axis, see Fig. F2 and F5.

Using Taylor expansion trigonometric functions are replaced by the displacement derivative, v':

$$\sin(-\alpha) = -\sin\alpha \sim -\alpha - \frac{(-\alpha)^3}{3!} + \ldots \sim -\alpha \quad \Rightarrow \quad \sin\alpha \sim -v' \tag{7}$$

$$\cos(-\alpha) = \cos\alpha \sim 1 - \frac{\alpha^2}{2!} \ldots \sim 1 - \frac{1}{2}(v')^2 \tag{8}$$

The out-of-plane deformation du results in a rotation β about the y_1-axis, see Fig. F3 and F5, where β can be evaluated as follows:

$$\tan\beta \sim \beta + \frac{\beta^3}{3} + \ldots \sim \beta = \frac{du}{\sqrt{dz^2+dv^2}} = \frac{u'}{\sqrt{1+(v')^2}} \tag{9}$$

Using Taylor expansion for the denominator and small values of v', β can be expressed on the following form:

$$\beta \sim u'\left(1 - \frac{1}{2}(v')^2\right) \tag{10}$$

Now the trigonometric functions of β can be replaced by:

$$\sin\beta \sim \beta - \frac{\beta^3}{3!} + \ldots \sim \beta \sim u'\left(1 - \frac{1}{2}(v')^2\right) \tag{11}$$

$$\cos\beta \sim 1 - \frac{\beta^2}{2!} + \ldots \sim 1 - \frac{1}{2}\left[u'\left(1 - \frac{1}{2}(v')^2\right)\right]^2 \sim 1 - \frac{1}{2}(u')^2 \tag{12}$$

Finally the twist ϕ about the z_2- axis (see Fig. F4) assuming $\phi \ll 1$ gives us:

$$\sin\phi \sim \phi - \frac{\phi^3}{3!} + \ldots \sim \phi \tag{13}$$

$$\cos\phi \sim 1 - \frac{\phi^2}{2!} + \ldots \sim 1 \tag{14}$$

Referring to Eq. (6) we now identify the elements in $[T_R]$. Products involving terms with orders higher than 2 are consistently left out:

$$\left[T_R\right] = \begin{bmatrix} 1 - \frac{1}{2}(u')^2 & \phi - u'v' & -u' - v'\phi \\ -\phi & 1 - \frac{1}{2}(v')^2 & -v' \\ u' & v' & 1 - \frac{1}{2}(v')^2 - \frac{1}{2}(u')^2 \end{bmatrix} \tag{15}$$

Expressions for the curvatures κ_x, κ_y and the twist, τ, can be obtained considering the rate of change of the direction cosines along the length of a member, see for instance *Love* (1944):

$$\kappa_x = l_z \frac{dl_y}{ds} + m_z \frac{dm_y}{ds} + n_z \frac{dn_y}{ds} \tag{16a}$$

$$\kappa_y = l_x \frac{dl_z}{ds} + m_x \frac{dm_z}{ds} + n_x \frac{dn_z}{ds} \tag{16b}$$

$$\tau = l_y \frac{dl_x}{ds} + m_y \frac{dm_x}{ds} + n_y \frac{dn_x}{ds} \tag{16c}$$

where differentiation is made with respect to the distance s along the deformed beam axis. For small but finite values of v′ and u′ the differential operator d/ds can be replaced by:

$$\frac{d}{ds} = \frac{1}{\sqrt{1 + (v')^2 + (u')^2}} \frac{d}{dz} \sim \left(1 - \frac{1}{2}(v')^2 - \frac{1}{2}(u')^2\right) \frac{d}{dz} \tag{17}$$

where we have used Taylor expansion for a function of two variables.

Using Eq. (17) on the rotation matrix as expressed through Eq. (15), Eq. (16) can be written:

$$\kappa_x = -v'' - u'\phi' \tag{18a}$$

$$\kappa_y = u'' + v''\phi \tag{18b}$$

$$\tau = \phi' - u'v'' \tag{18c}$$

still omitting products involving terms with orders higher than 2.

The differential equations describing equilibrium of a member of doubly symmetric cross-section under the action of bending and torsional moments are:

$$EI_x\kappa_x = M_x \tag{19a}$$

$$EI_y\kappa_y = M_y \tag{19b}$$

$$\left(GJ + Zr_0^2\right)\tau = M_z \tag{19c}$$

where EI_x and EI_y are the bending stiffnesses and GJ the torsional stiffness. The term Zr_0^2 in the torsion equation is the increase in the torsional stiffness due to tensile axial force Z occurring when the member has a twist τ. The polar radius of gyration is r_0^2. The term in the torsion equation related to warping has been left out because its contribution is insignificant in relation to a solid cross-section like the one used for the girder in the bridge model tests, see for instance *Thomsen* (1990).

Combining Eq. (1), Eq. (15) and Eq. (18) together with Eq. (19), the governing differential equations become:

$$-EI_x\left(v'' + u'\phi'\right) = \left(1 - \frac{1}{2}(u')^2\right) M_X + \left(\phi - u'v'\right) M_Y + \left(-u' - v'\phi\right) M_Z \tag{20a}$$

$$EI_y\left(u'' + v''\phi\right) = -\phi\, M_X + \left(1 - \frac{1}{2}(v')^2\right) M_Y - v'\, M_Z \tag{20b}$$

$$\left(GJ + Zr_0^2\right)\left(\phi' - v''u'\right) = u'\,M_X + v'\,M_Y + \left(1 - \frac{1}{2}(v')^2 - \frac{1}{2}(u')^2\right) M_Z \quad (20c)$$

For comparison we now list the expressions derived in *Vacharajittiphan et al.* (1974) and discuss the points where they differ from the expressions derived in the present study, where both large in-plane and out-of-plane deformations are taken into account.

If only large in-plane deformation prior to buckling is considered, the governing differential equations according to *Vacharajittiphan et al.* (1974) become:

$$-EI_x\,v'' = M_X \quad (21a)$$

$$EI_y\left(u'' + v''\phi\right) = -\phi\,M_X + M_Y - v'\,M_Z \quad (21b)$$

$$\left(GJ + Zr_0^2\right)\left(\phi' - v''u'\right) = u'\,M_X + v'\,M_Y + M_Z \quad (21c)$$

again omitting the term related to warping in the torsion equation, Eq. (21c).

When out-of-plane bending and twist prior to buckling are neglected, the corresponding moments M_Y and M_Z do not appear in the differential equation governing the pre-buckling behaviour, Eq. (21a). Furthermore, in the initial stage of buckling M_Y and M_Z can be considered as small but finite, thus certain products involving small quantities can be omitted from the differential equations Eq. (21b) and Eq. (21c), compared to Eq. (20b) and Eq. (20c).

Neglecting out-of-plane bending and twist prior to buckling, Eq. (21a) can be solved for the in-plane deflection v and its higher derivatives. Subsequently the solution of the in-plane equation, Eq. (21a), can be substituted into the remaining two differential equations Eq. (21b) and Eq. (21c), which govern the flexural-torsional buckling of the member.

When also large out-of-plane deformation is taken into account, all three deformational variables v, u and ϕ occur in all three governing differential equations. We will not go further

into detail here with regard to solving the differential equations in Eq. (20) since this becomes quite complicated for a static system like our bridge models.